Schriftenreihe

**DES INSTITUTES FÜR
GRUNDBAU UND BODENMECHANIK
DER RUHR-UNIVERSITÄT BOCHUM**

Herausgeber: Th. Triantafyllidis

Heft 34

EXTENDED HYPOPLASTIC MODELS FOR SOILS

**by
Andrzej Niemunis**

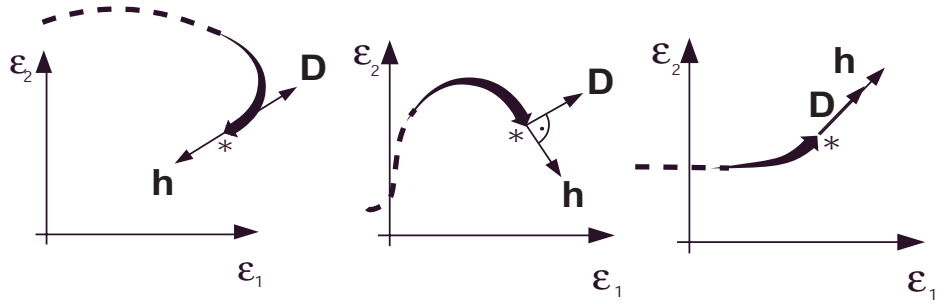

Bochum 2003

ISSN 1439-9342

Preface of the editor

The present work is a highlight of the outstanding work which started in Karlsruhe and was completed from 1999 up to date at our Institute here in Bochum. The author has paid a special attention to the deficiencies of the hypoplastic formulation originated by the Karlsruhe group and his intention is to provide solutions and/or improvements of the hypoplastic formalism in a positive manner keeping at the same time the key features of the model and his applications to the boundary value problems in soil mechanics.

There are different hypoplastic formulations like CLoE (Grenoble) or endochronic theories in addition to the model developed in Karlsruhe. The author in his work tried to bridge the gap between those formulations and succeeded in several ways. It turned out that the hypoplastic formulations of the Karlsruhe group to be a special case of the more general endochronic theory. Furthermore, the consequent removal of the existing deficiencies of the so called reference model led to a better coincidence between the Grenoble and Karlsruhe formalism. The introduction and extension of a correct bounding surface for the general case leads to a better description of pore-pressure build-up during undrained cyclic shearing and to a limitation of excessive ratcheting. Improvements had been made on the correct variation of the differential stiffness and to the influence of density changes as a the smooth transition from the dense to loose state is now postulated without to introduce different set of constants. Additional improvements refer to the long-term deformation including creep in a visco-hypoplastic formulation and to cumulative effects during cyclic loading. The extensions refer also to solvability, the positivness of the second order work leading to novel findings about the equivalence of controllability and the positivness of the second order work as well as to a novel criterion for localized bifurcation.

The present work deals not only with extensions of hypoplastic formulations but also on cumulative effects due to cyclic loading for a very large number of cycles with a proposed semi-explicit model. This model includes the influence of strain amplitude number of cycles, mean stress, stress ratio, void ratio e and the polarization of the strain. The form of the functions describing all these effects are derived from experimental observations based on a large series of triaxial cyclic tests carried out in Bochum.

The findings are well promising and open new fields for modelling the densification and

liquefaction behaviour of cyclic loaded soils.

The outstanding work which covers a great variety of problems as they could be mentioned in this short preface can be regarded as a thesaurus and encouragement for further work in the wide field of soil mechanics which still has to be done.

Th. Triantafyllidis

Author's preface to the Bochum edition

In summer 2003 professor Triantafyllidis kindly offered me an opportunity to print a revised version of my habilitation thesis at the Institute of Foundation Engineering and Soil Mechanics in Bochum. I was really grateful for this proposition, because several sections of the original work could be thought over again, supplemented or improved. The first version of this text appeared in January 2003 as publication number 34 of the series 'Monografie' of Gdańsk University of Technology (Politechnika Gdańska, monografia 34). By coincidence the Bochum edition appears with the same number, i.e. as 'Heft 34'. The following sections have been modified

- Section 2.5: added discussion on dilatancy of the reference hypoplastic model
- Section 3.2.1: added formulation of the reference hypoplastic model in terms of isomorphic variables p^+ and q^+
- Section 4.3.4: For the coincidence of bounding and yield surfaces the rotation of stiffness L has been corrected and extended to full tensorial form. I am obliged to professor R.Brannon and professor H.Xiao for help with this generalization.
- Section 4.3.6 is added. It explains why and how the shear stiffness in the reference hypoplastic model should be increased.
- Section 4.4 has been updated. I am indebted to Mr T. Wichtmann for valuable suggestions and for providing interesting experimental data from cyclic tests carried out at the Institute of Foundation Engineering and Soil Mechanics of the Ruhr-University in Bochum.

Apart form these major modifications also several minor changes have been made. No part of the original text was abridged or removed unless it was incorrect.

Andrzej Niemunis
Bochum, 30.6.2003

Author's preface to the Gdańsk edition

This treatise deals with the constitutive modeling in soil mechanics within the framework of hypoplasticity[1]. A considerable part of the text has been written during my stay (1991-1995) at the Institute of Soil and Rock Mechanics (IBF) in Karlsruhe from where the hypoplasticity originates. I continued this research at the Geotechnical Department of the Technical University of Gdańsk in the period (1996-1998) and later during my stay at the Institute for Foundation Engineering and Soil Mechanics at the Ruhr-University Bochum. I would like to express my gratitude to the head-teachers of the above institutes, professors E. Dembicki, G. Gudehus and Th. Triantafyllidis for their interest in my research subject and for their support and encouragement.

Hypoplasticity is an inelastic (dissipative) and incrementally nonlinear constitutive model which requires neither a yield surface nor a decomposition of strain rate into elastic and plastic portions. Its framework was first given by Kolymbas (1977) although similar models were also investigated independently by Illiushin (1954), Rivlin and Pipkin (1965), Valanis (1971) (endochronic models), Bazant (1978), Chambon (1981) and Darve (1982). In the eighties D. Kolymbas successfully developed his model benefiting from the contributions from the Karlsruhe research group, especially of G. Gudehus, W. Wu, Z. Sikora, M. Topolnicki and M. Ziegler. W. Wu and D. Kolymbas suggested the name 'hypoplastic' for all models with a tangential stiffness being a continuous function of the strain rate. The family of such models is considered less restrictive than the elasto-plasticity, which justifies the prefix hypo-.

In the early nineties the hypoplastic model was frequently verified and modified by the collective effort of G. Gudehus, D. Kolymbas and the IBF-newcomers: P. v.Wolffersdorff, E. Bauer, I. Herle, H. Hügel, J. Tejchman, V. Osinov and myself. A significant progress in the theoretical investigations and in the applications of the model for boundary value problems was achieved. In this treatise I take the opportunity to report on my contribution to this development and on some works in which I participated.

[1]In the literature the term hypoplasticity is used for *Karlsruhe*-hypoplasticity, *CLoE*-hypoplasticity and *Dafalias*-hypoplasticity. The first meaning applies here.

Due to the growing popularity of hypoplasticity and its numerous applications on one hand, and still existing shortcomings on the other hand, the theoretical investigation of the model is being continued. The web sites:
`http://info.uibk.ac.at/c/c8/c813/res/hypopl.html` and
`http://wwwrz.rz.uni-karlsruhe.de/~gn25/ibf/_hypoplastizitaet/index.html`.
report about the current development.

Appreciations: the opportunity of this research work followed from the cooperation agreement between the Technical University of Karlsruhe and my home Technical University of Gdańsk. I appreciate greatly the support of the authorities of these institutions, especially of Prof. E. Dembicki. My special thanks are dedicated to Prof. G. Gudehus and to Prof. D. Kolymbas for their guidance during my research work in Karlsruhe. I am also deeply obliged to Prof. Z. Mróz from the Institute of the Fundamental Technological Research in Warsaw for his support. During my stay in Bochum I enjoyed a great help of Prof. Th. Trianrafyllidis for which I am deeply obliged.

I am indebted to the members of IBF staff in Karlsruhe, especially to Mrs Schwab, Mrs Horzel, to G.Huber, E. Bösinger T. Manzaridis and J. Benkel for their patience with me, and to my colleges E. Bauer, I. Herle, H. Hügel, Ch. Karcher, S. Krieg, K.Nübel, T. Theile, P. von Wolffersdorff and Wu Wei. At this place I would also like to thank to my colleges in Gdańsk: M. Topolnicki, Z. Sikora, A. Bolt, B. Zadroga, J. Tejchman, G. Horodecki, J. Świniański, T. Brzozowski and in Bochum: T. Wichtmann Th. Sonntag and T. Maier with whom I cooperated closely during the final period of this work.

The financial support of the Deutsche Forschungsgemeinschaft and of Rheinbraun AG is also grateful acknowledged.

Last but not least, would like to thank my family and all my friends who motivated me to bring this study to the end.

Andrzej Niemunis

Contents

Chapter 1

Introduction

1.1 Motivation

Hypoplasticity is an incrementally nonlinear constitutive theory of granular materials. It is able to describe dissipative behaviour, plastic flow and nonlinear effects within the yield surface with a single tensorial equation. Early versions of the hypoplastic constitutive model, in spite of their simplicity, performed quite well in element tests and could be successfully implemented to a finite element (FE) program. The advantages of hypoplasticity over elastoplastic formulations follow from its nonlinearity which facilitates spontaneous localization of deformation, an ever-present phenomenon in particular in soil. Due to the absence of elasticity the phenomena of dilatancy and contractancy could be correctly reproduced. However, the first hypoplastic models had certain defects. For example, they allowed far too high stress ratios during some loading programs (lack of bounding surface), generated a much too high build-up of pore pressure during undrained cyclic shearing (exaggerated cyclic liquefaction) and led to a too fast accumulation of strain during small stress cycles (excessive ratcheting). The differential stiffness tensor was assumed to be a function of stress and current strain rate only (path-independent). The description of the influence of density changes (called pyknotropy) was oversimplified: dense and loose sand needed different sets of constants and no transition from dense to loose state was provided. The viscous part of an early model failed to predict the correct direction(!) of oedometric creep, if creep was preceded by an unloading.

These shortcomings manifested themselves in advanced applications of the model. For example, predictions of the long-term deformation involving creep were inaccurate. The performance of early hypoplastic models was also unsatisfactory in FE-calculation with cyclic loading. Hypoplastic predictions of subsidance in the vicinity of deep open-pit mining areas also turned out insufficiently precise. In order to overcome these and similar problems several *extensions* to hypoplasticity were urgently needed.

A geotechnical engineer may ask whether a sophisticated constitutive model is necessary for his practical decisions and what degree of complexity is reasonable for the problem faced. A systematic discussion of practical needs in geotechnical engineering was recently presented by Simpson [222]. The dilemma cannot be completely solved, however, constitutive models presented in this treatise are surely attractive due to their reliability and versatility. Recommendations of practice like "75% of settlement in organic soils occur after the construction period" are purely empirical and are therefore of limited applicability. Although both recommendations of practice and a constitutive model may be based on the same empirical knowledge, the numerical model expresses this knowledge in a precise mechanical and mathematical language, so that it can be more easily adapted to non-typical problems. Moreover, computations become inexpensive nowadays so one can be optimistic about the further applications of sophisticated constitutive equations. Due to the rapid development of computational systems and availability of good finite element programs, the perspectives of solving even complex geotechnical boundary-value problems are very promising. Effective FE codes with procedures dedicated to soil mechanics are widely available, as an open source code, e.g. `http://www.tochnog.com`, `http://www.bh.com/companions/fem/`, or in the commercial field of finite element programs ANSYS, PATRAN, ABAQUS, MARC, DIANA or PLAXIS. Most of them accept a constitutive description provided by the user, which is a good prospect for the development of hypoplasticity.

Summing up, usage of sophisticated constitutive models is nowadays affordable and geotechnical engineers can benefit from huge resources of available software. The FE-results can clearly support the conventional design methods but the quality of the constitutive theory is of crucial importance in this context. Proposing extensions to hypoplasticity at the expense of its simplicity seems therefore eligible.

1.2 Scope

Several hypoplastic models and several extensions are discussed in the following chapters. The hypoplastic model proposed by v. Wolffersdorff [265], see Section 2.5, is chosen as reference, i.e. it is the base for all extensions. In Section 2.2 a few earlier versions are shortly mentioned to give some idea of the development and to explain the origin of tensorial equation (2.29) which is characteristic for this family of models. In the same chapter the concepts of hypoplastic yield surface and bounding surface are discussed because they provide an intuitive understanding of how hypoplasticity works. In order to explain the meaning of the linear and the nonlinear (or relaxation) term a short introduction to the so-called response envelopes [68] is given. Already in the problem of the bounding surface

the concept of response envelope proves useful. Since the reference model implements the critical state concept, a short discussion of this subject has been given in Section 2.4.

In Chapter 3 the problems of solvability, positiveness of second-order work, asymptotic behaviour and localized bifurcation within the framework of hypoplasticity are dealt with. A novel finding about the equivalence of the positiveness of second-order work and the mixed controllability with respect to composite variables (like Roscoe's p, q) is presented. Moreover, analytical expressions for the second-order work surface and a novel criterion for localized bifurcation are derived.

The extensions are proposed in modular and optional form and some of them may be combined. For example, a novel state variable called intergranular strain has been implemented to hypoplasticity and to visco-hypoplasticity, but it can easily be 'switched off' by an appropriate choice of material parameters. Although some extensions are exclusively related to hypoplasticity, some points may be of more general interest. Numerical aspects of the proposed extensions have been examined and commented. Most of the proposed concepts have been successfully implemented and tested in FE codes. There is not enough place here for a detailed discussion of the performance of extended hypoplastic versions in the BVPs, the reader is referred to publications cited in text.

Some emphasis is given to the problem of long term settlement due to creep (Section 4.2) and due to cumulative effects during cyclic loading (Section 4.1 and Section 4.4). Cohesive soils have been discussed in the framework of a visco-hypoplastic model (Section 4.2) which departs rather strongly from original hypoplasticity.

The first section in chapter 'Extensions' describes an additional strain-like state variable (intergranular strain). It is used to memorize the recent deformation history and allows for increased stiffness in the range of small alternating deformations. The detailed presentation includes aspects of determination of material constants. On the theoretical side the problem of solvability is discussed. Next, the limit void ratios proposed in the reference model are critically discussed. A modified densification limit is proposed.

The second section in chapter 'Extension' is devoted to visco-hypoplasticity. It starts from a simple one-dimensional version for samples under oedometric conditions. Next, the visco-hypoplastic model is generalized to the three-dimensional case. Several details concerning the K_0 value and the determination of parameters are presented. The implementation of intergranular strain is worked out.

The decomposition of the stress rate into linear and nonlinear parts, evident in equation (2.29), is commonly used in hypoplasticity. Unfortunately this decomposition makes the model difficult to modify and to understand. In particular, the model may seem obscure

to readers accustomed to elastoplasticity. In Section 4.3 the hypoplastic equation has been rewritten in terms of alternative variables: linear stiffness, direction of plastic flow and degree of nonlinearity, see Eq. (4.138). This simple rearrangement of the hypoplastic equation provides flexibility which is necessary in some more radical modifications. For example, an improved, monotonous distribution of nonlinearity (with a minimum on the hydrostatic axis) and the 'limit surface consistency' (coincidence of the yield and bounding surface) could be achieved. Moreover, using the novel variables a hypoplastic model with an improved description of undrained response could easily be formulated. Even the implementation of an anisotropic dilatancy (without changes in the yield surface) turned out to be straightforward (Section 4.3.5).

Section 4.4 covers the implementation of a so-called explicit formula for cyclic accumulation. Cumulative effects are described as a monotonic process based on a single fatigue-like parameter. Some shortcomings of existing explicit models have been removed in the proposed semi-explicit model. The process of adaptation of the material fabric to cyclic loading (characterized by the polarization of the amplitude and by the average stress obliquity) is proposed to be described using two novel state variables.

Section 4.5 is devoted to partly saturated soils. Two general cases are considered: a mixture of water and small air bubbles fills completely the pores between the grains, and a pore water network coexists with the system of interconnected air channels between grains. In the first case a formula for compressible water/air mixture is proposed and implemented to the visco-hypoplastic model for clay. In the second case an expression of the capillary pressure proposed by Gudehus [71] is implemented to the reference model and used for silt. The applicability of the effective stress concept in the second case is discussed.

For the convenience of the reader some more complicated tensorial expressions are supplemented by short MATHEMATICA[1] packages. Some longer ones can be found in
`http://www.gub.ruhr-uni-bochum.de/mitarbeiter/andrzej_niemunis.htm`.
Most of author's publications (full text) are also available from this web site. The respective citations are marked with www.AN .

1.3 Notation and continuum framework

This is Section 1.3. Hypoplasticity is a phenomenological model. This means that its equations have not been *derived* from fundamental laws of physics but rather *invented*,

[1] Algebra program from Wolfram Research, see `www.wolfram.com`

basing on experimental data and keeping relevant principles of physics in mind. Hypoplasticity describes the behaviour of soil in terms of macro-variables like stress or void ratio treating soil as a continuum, without detailed description of movement of individual particles and so it is a macro-mechanical approach. In the micro-mechanics one traces locations of individual particles, their contact forces etc. [40, 237, 238]. A comparison between these approaches is possible applying averaging formulae, e.g. [124]) for stress $T_{ij} = \sum_{contacts}(f_i r_j)/V$ and for the deformation gradient $F_{ij} = \sum_{contacts}(\Delta r_i h_j)/V$. In the first definition the contact forces f_i are multiplied by the vectors r_j connecting the centres of the neighbouring grains and averaged over an arbitrary volume V around the point of consideration. In the second definition h_j are so-called polygon vectors. In the recent time the micro-mechanical approach enjoys much attention of physicists, e.g. [140], [88], `www.granular.com, www.ica1.uni-stuttgart.de/~lui/`. However, for practical geotechnical engineering problems the micro-mechanical analysis is nowadays not feasible (except perhaps for simulation of small samples up to 10^5 grains) because the description of individual contacts between particles requires huge computer capacities. Nevertheless, calculations on the microscopic level may provide valuable explanation of some phenomena observed on the macro-level.

In this text, granular materials are treated as simple materials in the sense of Truesdell and Noll [243], that is, the stress at a given point depends on the deformation history at this point only. Moreover, only the *first* spatial gradient of velocity enters our constitutive equations. The last limitation is dropped in the so-called gradient theories. Studies of polar and gradient continuum in connection with hypoplasticity can be found in the publications of Tejchman e.g. [235], Bauer [12], Huang [97], or Maier [142].

The constitutive models are formulated by means of 'material properties' and 'state variables'. A material property is a quantity that does not change during the processes of interest. Practically, soil properties should not vary over any mechanical process with the stress path in a range from several to several thousands kPa carried out at the usual void ratios, temperatures etc. Some apparently constant material parameters may actually change due to biological, chemical or thermal processes and mechanical aging [16]. Each time we should reconsider if our material constants are adequate to the particular problem met. Here, we regard purely mechanical processes within a relatively short period of time considering aging and chemical or thermal effects negligible (except for viscous effects).

State variables are material characteristics which refer to a particular time instant. They may evolve in a mechanical process and a description of such evolution must be a part of the constitutive model. Such evolution equations accompany the conventional stress-strain relations. If a deformation process causes no further changes in state variables, a residual or asymptotic state is reached. The most popular state variable in soil mechanics

is the density expressed as void ratio e, the specific volume $1+e$ or as an equivalent (preconsolidation) pressure.

We restrict our attention to *isotropic* granular materials , i.e. no material constant depends on the choice of the coordinate system. This means that the material has no inherent anisotropy and no directions are initially distinguished. Inherent anisotropy would be of use if soil was an assemblage of, say, plates or needles with a preferred orientation. We admit, however, an *induced* anisotropy caused by a process of deformation or/and by a stress path. Such anisotropy can be described by evolving tensorial state variables. All material constants and all constitutive equations are assumed to be isotropic but the tensorial state variables may contribute to (incrementally) anisotropic response. Briefly speaking, we preserve an isotropic material but allow for anisotropic states.

In our macro-description notions of continuum mechanics like stress or stretching may be applied. We argue that the dimensions of a soil volume under consideration are usually much larger than the size of a singular grain (or clay particle) so that the spatial distribution of contact forces is unimportant. This approach makes the well established theory of continuum mechanics available to geotechnical applications. In most practical cases this simplified model works sufficiently well.

The notation of the classical books on continuum mechanics [143, 243] is adopted. Both tensorial and index notations will be used. A fixed orthogonal Cartesian coordinate system with unit vectors $\{\mathbf{e}_1, \mathbf{e}_2, \mathbf{e}_3\}$ is used throughout the text. A repeated (dummy) index in a product indicates summation over this index taking values of 1, 2 and 3. A tensorial equation with one or two free (not-repeated) indices can be seen as a system of three or nine scalar equations, respectively. A comma preceding an index (e.g. $v_{i,j} = \partial v_i/\partial x_j$) indicates the the spatial gradient with respect to this index. We will also use Kronecker's symbol $\delta_{ij} = 1$ for $i = j$ and zero otherwise, and the permutation symbol $e_{ijk} = 1$ if $\{i, j, k\} \subset \{\{1, 2, 3\}, \{2, 3, 1\}, \{3, 1, 2\}\}$ and $e_{ijk} = -1$ if $\{i, j, k\} \subset \{\{1, 3, 2\}, \{2, 1, 3\}, \{3, 2, 1\}\}$ and otherwise $e_{ijk} = 0$.

Vectors and second-order tensors are distinguished by bold typeface, for example $\mathbf{N}, \mathbf{T}, \mathbf{v}$. Fourth order tensors are written in sans serif font (e.g. L). The symbol $\cdot$ denotes multiplication with one dummy index (single contraction), e.g. the scalar product of two vectors can be written as $\mathbf{a} \cdot \mathbf{b} = a_k b_k$. In tensorial expressions, multiplication with two dummy indices (double contraction) is denoted with a colon, e.g. $\mathbf{A} : \mathbf{B} = \operatorname{tr}(\mathbf{A} \cdot \mathbf{B}^T) = A_{ij} B_{ij}$, wherein $\operatorname{tr} \mathbf{X} = X_{kk}$ reads trace of a tensor. In some cases a slightly different multiplication $\mathbf{A} \cdot\cdot \mathbf{B} = \operatorname{tr}(\mathbf{A} \cdot \mathbf{B}) = A_{ij} B_{ji}$ can be used. We introduce fourth order unit tensor $I_{ijkl} = \frac{1}{2}(\delta_{ik}\delta_{jl} + \delta_{il}\delta_{jk})$. It is the symmetric part of the product $\delta_{ik}\delta_{jl}$ and thus provides 'minor symmetries' with respect to swapping of i, j or of k, l. The tensor I associates to

every second-order tensor its symmetric part. I is singular (yields zero for every skew symmetric tensor) but for symmetric argument $\mathbf{X}$ we have $\mathbf{X} = \mathsf{I} : \mathbf{X}$ and $\mathsf{I}^{-1} = \mathsf{I}$. A tensor raised to a power, like $\mathbf{T}^n$, can be written out as a sequence of $n-1$ multiplications $\mathbf{T} \cdot \mathbf{T} \cdot \ldots \mathbf{T}$. The brackets $\| \ \|$ denote the Euclidean norm, i.e. $\|\mathbf{v}\| = \sqrt{v_i v_i}$ or $\|\mathbf{T}\| = \sqrt{\mathbf{T} : \mathbf{T}}$. The definition of Mc Cauley brackets $< \cdot >$ reads $< x >= (x + |x|)/2$ and the double square brackets $[\![x]\!] = x^+ - x^-$ denote a jump of x over a discontinuity line. The deviatoric part of a tensor is denoted by an asterisk, e.g. $\mathbf{T}^* = \mathbf{T} - \frac{1}{3}\ \mathbf{1}\mathrm{tr}\,\mathbf{T}$, wherein $(\ \mathbf{1})_{ij} = \delta_{ij}$ holds. The expression $()_{ij}$ is an operator extracting the component (i,j) from the tensorial expression in brackets, for example $(\mathbf{T} \cdot \mathbf{T})_{ij} = T_{ik}T_{kj}$. Dyadic multiplication is written *without* $\otimes$, e.g. $(\mathbf{ab})_{ij} = a_i b_j$ or $(\mathbf{T}\ \mathbf{1})_{ijkl} = T_{ij}\delta_{kl}$. Note that $\mathbf{1}\ \mathbf{1} \neq \mathsf{I}$, i.e. in general $\delta_{ij}\delta_{kl} \neq I_{ijkl}$ holds. The symbol $\times$ denotes vector multiplication, for example $(\mathbf{a} \times \mathbf{b})_i = e_{ijk}a_j b_k$. Proportional tensors are denoted by tilde, e.g. $\mathbf{T} \sim \mathbf{D}$. The components of diagonal matrices (with zero off-diagonal components) are written as diag[, ,], for example $\mathbf{1} =$ diag$[1,1,1]$. Normalized tensors are denoted by arrow, for example $\vec{\mathbf{D}} = \mathbf{D}/\|\mathbf{D}\|$ with $\vec{\mathbf{0}} = \mathbf{0}$. The sign convention of general mechanics with *tension positive* is obeyed. Detailed information on the tensorial manipulations can be found for example in [19, 143].

The motion $\mathbf{x} = \mathbf{x}(\mathbf{X}, t)$ of a body can be thought of as a sequence of its configurations in time. The configuration is a location occupied by the body (i.e. coordinates of its points) at a particular time t. A single and fixed in space, rectangular coordinate system defined by a triad of orthogonal unit vectors $\{\mathbf{e}_1, \mathbf{e}_2, \mathbf{e}_3\}$ is used throughout this text to describe both, the reference position $\mathbf{X}$ of the material points and the current position $\mathbf{x}(\mathbf{X}, t)$ of these points at time t. The material points are identified by their positions $\mathbf{X}$ in the reference configuration. Each material point of the body obtains in this way its 'name' $\mathbf{X}$. Using the Lagrangian description of motion we are interested in quantities associated with a chosen (fixed) material point $\mathbf{X}$, for example velocity $\dot{\mathbf{x}}(\mathbf{X}, t)$, density $\rho(\mathbf{X}, t)$, and not with a certain position in space $\mathbf{x}$. We may find the inverse relation $\mathbf{X}(\mathbf{x}, t)$ and represent the above mentioned quantities *of material particles* as functions of spatial variables, here $\dot{\mathbf{x}}(\mathbf{X}(\mathbf{x}, t), t) = \mathbf{v}(\mathbf{x}, t)$ and $\rho(\mathbf{X}(\mathbf{x}, t), t))$, remembering, however that they are attributed to a material particle currently passing through $\mathbf{x}$ rather than of the position vector $\mathbf{x}$ as such. A superposed dot over a quantity denotes the *material* time derivative, i.e. the time derivative calculated at $\mathbf{X}$ held constant, e.g. $\dot{\mathbf{x}} = \partial\mathbf{x}(\mathbf{X}, t)/\partial t$. The symbol $\dot{\mathbf{x}}(\mathbf{X}, t)$ denotes the velocity of a particle $\mathbf{X} = \text{const}$ (a function of its referential position) whereas $\mathbf{v}(\mathbf{x}, t)$ expresses the same particle velocity in terms of the current position $\mathbf{x}$ of $\mathbf{X} = \text{const}$ i.e. $\mathbf{v}(\mathbf{x}, t) = \dot{\mathbf{x}}(\mathbf{X}(\mathbf{x}, t), t)$. The material time derivative (expressed in terms of $\mathbf{x}$ or $\mathbf{X}$) should be distinguished from the time derivative with $\mathbf{x}$ held constant. This distinction is important even if the current configuration is treated as the referential one, which is

evident considering a function $\rho(\mathbf{x},t)=\rho(\mathbf{x}(\mathbf{X},t),t)$

$$\dot{\rho}=\left.\frac{\partial\rho(\mathbf{x}(\mathbf{X},t),t)}{\partial t}\right|_{\mathbf{X}}=\left.\frac{\partial\rho(\mathbf{x},t)}{\partial t}\right|_{\mathbf{x}}+\left.\frac{\partial\rho(\mathbf{x},t)}{\partial\mathbf{x}}\right|_{t}\cdot\left.\frac{\partial\mathbf{x}(\mathbf{X},t)}{\partial t}\right|_{\mathbf{X}}, \tag{1.1}$$

wherein $|_{\mathbf{X}}$ means 'at constant $\mathbf{x}$. Even at the time instant t for which $\mathbf{x}=\mathbf{X}$ the material rate $\dot{\rho}$ may differ from the spatial rate $\partial\rho(\mathbf{x},t)/\partial t|_{\mathbf{x}=\text{const}}$ if the body is moving and if the distribution of ρ is inhomogeneous.

In mechanics of elastic solids one introduces the notion of *deformation* as a change in the shape of a body with respect to the undeformed (stress-free) configuration. It is physically justified by the ability of solid to remember this unique stress-free configuration which is recovered after the loads are removed. However, the notion of "stress-free" or "undeformed" state is controversial in soil mechanics. Neither the initial nor the stress-free configuration can be objectively chosen. In granular materials *no reference configuration seems to be distinguished by nature.* One may, of course, choose the reference configuration *arbitrarily* (for example, an initial one) and call it 'undeformed', however, the strain calculated with respect to such configuration has consistently an arbitrary but no *physical* meaning for the soil. However, for a construction founded on soil the initial configuration[2] is of importance because later settlements may cause internal forces and endanger serviceability. A unique configuration of soil could be thought of only in a limited incremental sense, for infinitesimally small loads applied on the top the referential K_0-state, say, but even in such case purely reversible soil response is disputable. In this text no referential configuration is introduced. For this reason variables like the gradient of deformation

$$\mathbf{F}=\partial\mathbf{x}/\partial\mathbf{X}, \tag{1.2}$$

the strain

$$\epsilon_{ij}=\frac{1}{2}\ln\left(\frac{\partial x_i}{\partial X_k}\frac{\partial x_j}{\partial X_k}\right), \tag{1.3}$$

or the first Piola-Kirchhoff stress should not appear in the constitutive model for soils although these notions are widely used for presentation of results.

Without a reference configuration the best choice left is to consider the current configuration as the referential one, obtaining the special case with $\mathbf{x}=\mathbf{X}$ and $F_{ij}=\delta_{ij}$ but $\dot{F}_{ij}\neq 0$. The spatial gradient $(\mathbf{L})_{ij}=v_{i,j}$ of velocity v_i can be decomposed into symmetric and skew symmetric part

$$L_{ij}=\dot{F}_{ij}=\frac{\partial v_i(\mathbf{x},t)}{\partial x_j}\quad\text{with}\quad D_{ij}=\frac{1}{2}\left(v_{i,j}+v_{j,i}\right)\quad\text{and}\quad W_{ij}=\frac{1}{2}\left(v_{i,j}-v_{j,i}\right) \tag{1.4}$$

[2] A time instant when the construction was placed in its nominal position or when it became statically undetermined may be chosen to be 'initial'.

i.e. into stretching $\mathbf{D}$ and vorticity (spin) $\mathbf{W}$. In an FE calculation, within a single increment we consider finite rotations only. In such increment from the 'undeformed' configuration at time t to an unknown configuration at $t + \Delta t$ the deformation gradient $\mathbf{F} = \mathbf{R} \cdot \mathbf{U}$ is decomposed to the orthogonal rotation tensor $\mathbf{R}$ to the symmetric right stretch tensor $\mathbf{U}$. We assume small strains and small distortions so $\mathbf{U}$ is not very much different from $\mathbf{1}$.

The motion of a body cannot be deduced from the boundary conditions making use of the general principles of conservation of momentum and its moment. These conservation principles must be supplemented by material-specific relations, because evidently the deformation depends on the substance (material) the body is made of. The material specific constitutive model iterrelates stress and strain. In general, stress is a functional of strain history but it is often more practical to postulate a rate-type equation between stress and strain and to provide evolution equations for auxiliary state variables which account for the deformation history. Therefore it is not necessary to memorize the deformation path as such. In the referential hypoplasticity the constitutive equations interrelate rates of stress and deformation and the state variables are the density (void ratio) and the stress itself.

The constitutive models should obey the following axioms known as *principles of rational continuum mechanics*:

- *principle of determinism* – the stress results from the *preceding* deformation of the body,
- *principle of local action* – the deformation outside an arbitrarily small neighbourhood of a point can be disregarded for determination of the stress at this point,
- *principle of material frame-indifference* – any two inertial[3] observers must measure the same stress at a point.
- *principle of equipresence* – all independent state variables should formally enter all constitutive equations unless their absence is proven or if it contradicts a physical or mathematical principle
- *principle of fading memory* – events from older sections of deformation history have less impact on the current mechanical response of the body than the recent ones.

Of course, the constitutive equations must not violate any general principle of conservation of mass, momentum, moment of momentum, energy or the principles of thermodynamics.

[3]'Inertial' means having no acceleration with respect to fixed stars

From the axiom of frame-indifference one can conclude that since two observers may use shifted time measures, the time t cannot appear explicitly in constitutive equations (sometimes called *principle of autonomy*).

Throughout this text the effective Cauchy stress (true stress) $\mathbf{T}$ ascribed to a given material point $\mathbf{X}$ is used. This tensor interrelates the traction (stress vector) $\mathbf{t}$ that is an averaged force acting between soil particles on the wavy cross-section along an oriented surface element $\mathbf{l}\mathrm{d}a$ with the direction $\mathbf{l}$ of this element. The quantities $\mathrm{d}a$, $\mathbf{l}$ and $\mathbf{t}$ are measured at the current time t. This relation is linear $\mathbf{t} = \mathbf{T} \cdot \mathbf{l}$ and known as Cauchy's stress theorem. Note that $\mathbf{T}$ is the partial stress in the solid phase[4] and the total stress is denoted as $\mathbf{T}^{\mathrm{tot}}$. This partial stress $\mathbf{T}$ is a functional of the deformation history $\mathbf{D}(t)$ provided the solid particles are incompressible in the bulk and direction independent. The partial stress $\mathbf{T}$ is often called 'effective stress' because both strength and deformation of the soil skeleton depend solely on its value[5]. We assume that the stress is calculated as if the material was dry and that thermal, chemical and electrical effects can be disregarded (are already included in $\mathbf{T}$).

From the principle of material frame indifference (objectivity) follows that the material time derivative of Cauchy stress $\dot{\mathbf{T}}$ being sensitive to the rigid angular rotation of the body (with respect to our fixed 'background' coordinate system $\{\mathbf{e}_1, \mathbf{e}_2, \mathbf{e}_3\}$) is not a suitable rate for the constitutive modeling. The stretching tensor $\mathbf{D}$, however, can be shown to be independent of the rigid rotation. A suitable (co-rotational) measure of stress rate can be found if we associate the stress tensor components $T^{\boxplus}_{ab}$ with an orthogonal coordinate system defined by unit vectors $\{\mathbf{r}_1, \mathbf{r}_2, \mathbf{r}_3\}$ embedded in the deformable material in such way that they follow the rotation of the body but remain insensitive to the stretching. We have $\mathbf{r}_i = \mathbf{R} \cdot \mathbf{e}_i$ and

$$\mathbf{T} = T_{ij}\mathbf{e}_i\mathbf{e}_j = T^{\boxplus}_{ab}\mathbf{r}_a\mathbf{r}_b \ . \tag{1.5}$$

For example, during a rigid rotation $\mathbf{F} = \mathbf{R}$ of the stressed body (inclusive rotation of all boundary conditions) the components $T^{\boxplus}_{ab}$ at a given material point do not change but the components T_{ij} do. Let us choose a momentaneous embedded coordinate system $\{\mathbf{r}_1, \mathbf{r}_2, \mathbf{r}_3\}$ such that $\mathbf{F} = \mathbf{R} = \mathbf{1}$, so $\mathbf{r}_i = \mathbf{e}_i$ and $\dot{\mathbf{r}}_i = \mathbf{W} \cdot \mathbf{e}_i$ (if the triad $\{\mathbf{r}_1, \mathbf{r}_2, \mathbf{r}_3\}$ was embedded in material then $\dot{\mathbf{r}}_i = \mathbf{L} \cdot \mathbf{e}_i$ would hold). The material time derivative of (1.5)

[4] It is often denoted by $\mathbf{T}', \mathbf{T}_s$ or $\boldsymbol{\sigma}'$ in the literature.

[5] We may usually neglect the compressibility of individual grains due to the increase of pore pressure, otherwise see [128]

is

$$\begin{aligned}\dot{\mathbf{T}} &= \dot{T}^{\boxplus}_{ab}\mathbf{r}_a\mathbf{r}_b + T_{ab}\dot{\mathbf{r}}_a\mathbf{r}_b + T_{ab}\mathbf{r}_a\dot{\mathbf{r}}_b \quad \text{sum over } a,b \qquad (1.6)\\ &= \mathring{\mathbf{T}} + T_{ab}\mathbf{W}\cdot\mathbf{r}_a\mathbf{r}_b + T_{ab}\mathbf{r}_a\mathbf{W}\cdot\mathbf{r}_b = \mathring{\mathbf{T}} + \mathbf{W}\cdot\mathbf{r}_a\mathbf{r}_b T_{ab} + T_{ab}\mathbf{r}_a\mathbf{r}_b\cdot\mathbf{W}^T \quad \text{or}\\ \mathring{\mathbf{T}} &= \dot{\mathbf{T}} + \mathbf{T}\cdot\mathbf{W} - \mathbf{W}\cdot\mathbf{T} \qquad (1.7)\end{aligned}$$

This objective measure $\mathring{\mathbf{T}}$ of stress rate is known as the Zaremba-Jaumann rate. Note that only $\mathring{\mathbf{T}}$ is material-specific and the expression $\mathbf{T}\cdot\mathbf{W} - \mathbf{W}\cdot\mathbf{T}$ in (1.7) is caused by the rigid body rotation and it is independent of the material. Similar objective rates are also used for all tensorial variables used in the constitutive model, for example, for the *intergranular strain* [172] www.AN , see also Section 4.1.

The Jaumann stress rate is sometimes criticized for causing artificial oscillation of stress during shearing. For example, during simple shearing with $F_{12} > 100\%$ a slow oscillation become visible (with a period of $F_{12} = 2\pi\%$) [42, 43]. The alternative, oscillation-free formulations by Green and Naghdi [66] or recently by Bruhns [25] require, however, a fixed (for example stress free) reference configuration which, as already mentioned, is controversial for soils. The Jaumann rate works equally well as the one by Green and Naghdi in the 'unrotated' reference configuration [23].

In our so-called *referential description* [223] (p.108) any configuration can be arbitrarily chosen to be the referential one and the response of the constitutive model should not depend on this choice. The Jaumann rate is widely used in soil mechanics and deformations above 100% are rarely needed, and if so, then they appear in localized zones where a polar continuum framework is more appropriate [97, 159, 234, 235].

The total strain is used for presentation purposes only. Time integration of the strain rate referred to the current configuration leads to the logarithmic strain (1.3). The advantage of this strain measure is the exact evaluation of volume changes via $\operatorname{tr}\boldsymbol{\epsilon}$ and insensitivity of $\boldsymbol{\epsilon}$ to rigid rotation, see illustrative examples in [167] www.AN .

We assume that soil has a *simple skeleton* [81] defined as an assemblage of grains or other solid particles with no macro-pores (pores with diameters greater than the mean grain size) between them. Extremely loose deposits (usually wet and collapsible, supported by capillary forces or cementation) in which such macro-pores may exist require a special treatment which is outside the scope of this work. Neither soil skeletons with clumps and honeycombs are accounted for. Grains themselves are assumed permanent (no grain crushing). It is assumed that osmotic pressure is inherently built into the effective stress concept, and in the absence of environmental changes need not be reconsidered. A deformation under homogeneous boundary conditions is assumed homogeneous, without spatial

fluctuation of strain and shear localization patterns. Such simplification is disputable as argued in Section 3.5.2.

Chapter 2

Framework

Hypoplasticity belongs to the group of path-dependent and rate-independent constitutive models. This means that the sequence of deformation increments has an influence on accumulated stresses but the duration of the deformation processes or individual increments is insignificant. Therefore, speaking of 'time integration' or 'time derivative', we do not necessarily mean the actually elapsed time but a time-like (monotonously increasing) parameter that merely indicates the sequence of events. Exception is made for the visco-elastic or visco-plastic models in which the true time scale must be used.

The sequence of applied boundary changes is important for stress and deformation and thus the theoretical description cannot consider solely the initial and the current configurations. The evolution of deformation is known as the strain path: $\boldsymbol{\epsilon}(\tau)$ or $\mathbf{F}(\tau)$ with $0 \leq \tau \leq t$. Using path dependent or history dependent models we must provide information about the whole deformation process because the final stress $\mathbf{T}^t$ is not just a function of the current deformation gradient $\mathbf{F}^t$ but, formally speaking, a functional $\mathbf{T}^t = \Im(\mathbf{F}(\tau))$ of its evolution [243] up to the current time t. Instead of formulating functionals we often prefer to write the rate-type equations $\mathring{\mathbf{T}} = \mathring{\mathbf{T}}(\mathbf{D})$. Such approach is numerically more convenient and rate relation is better exposed to direct experimental measurements. The information about the recent deformation history, however, is not ignored. It is partly available from suitably chosen state variables, including the stress itself. Since a unique relation $\mathbf{T}^t(\mathbf{F}^t)$ cannot exist in general, independently of the strain path, one says that hypoplastic or elastoplastic models are not integrable. Of course, this is not true for all constitutive models used in soil mechanics.

2.1 Integrability of different models

Judging by the integrability we may classify different soil models [136, 243] into the following groups:

1. **Hyperelasticity**. If the material is hyperelastic (= *Green-elastic*), both stress and energy are integrable and are recovered upon any closed strain circuit i.e. none of them can be accumulated. This can be expressed by the following conditions

$$\oint E_{ijkl}\mathrm{d}\epsilon_{kl} = \text{acc. stress} = 0, \quad \text{and} \quad \oint T_{ij}\mathrm{d}\epsilon_{ij} = \text{acc. energy} = 0, \tag{2.1}$$

wherein E_{ijkl} denotes the tangential stiffness. The relation between stretching $\mathbf{D}$ and stress rate $\mathring{\mathbf{T}}$ is linear but E_{ijkl} is not necessarily constant (it may be a function of state parameters, stress and strain). Hyperelastic stress - strain relations are usually derived from an elastic potential $W(\mathbf{T})$ or its complementary potential $\bar{W}(\boldsymbol{\epsilon}) = \mathbf{T}(\boldsymbol{\epsilon}) : \boldsymbol{\epsilon} - W(\mathbf{T}(\boldsymbol{\epsilon}))$ by partial differentiation

$$\mathbf{T} = \frac{\partial \bar{W}(\boldsymbol{\epsilon})}{\partial \boldsymbol{\epsilon}} \quad \text{or} \quad \boldsymbol{\epsilon} = \frac{\partial W(\mathbf{T})}{\partial \mathbf{T}} \tag{2.2}$$

From the existence of the elastic potential (energy is a function of stress only, the stress path is unimportant) follows a unique relationship between stress and strain (therefore also path independent): A critical review of several hyperelastic models for soils is given in [169, 170] www.AN .

2. **Elasticity**. In the so-called *Cauchy-elastic* material the stress is recovered after any closed strain circuit. The energy $\oint \mathbf{T} : \mathbf{D}\mathrm{d}t \neq 0$ need not be preserved.

$$\oint E_{ijkl}\mathrm{d}\epsilon_{kl} = \text{acc. stress} = 0, \quad \text{and} \quad \oint T_{ij}\mathrm{d}\epsilon_{ij} = \text{acc. energy} \neq 0. \tag{2.3}$$

We postulate a one-to-one (invertible) stress-strain dependence $\mathbf{T}(\boldsymbol{\epsilon})$ and therefore the resulting (after time differentiation) tangential stress-strain relation $\mathring{\mathbf{T}} = \mathsf{E} : \mathbf{D}$ is, of course, both invertible and integrable. Although the function $\mathbf{T}(\boldsymbol{\epsilon})$ is traditionally written in a seemingly linear form

$$\mathbf{T} = \mathsf{E}^s : \boldsymbol{\epsilon} \quad \text{or} \quad \boldsymbol{\epsilon} = \mathsf{C}^s : \mathbf{T}, \tag{2.4}$$

with the secant stiffness E^s or secant compliance C^s, this function need not be linear. In soil mechanics E^s and C^s depend strongly on stress. The tangent compliance is obtained from the following time differentiation

$$D_{ij} = \frac{\mathrm{d}\epsilon_{ij}}{\mathrm{d}t} = \frac{\partial (C^s_{ijkl} T_{kl})}{\partial T_{mn}} \cdot \frac{\mathrm{d}T_{mn}}{\mathrm{d}t} = \overbrace{\left(C^s_{ijmn} + \frac{\partial C^s_{ijkl}(\mathbf{T})}{\partial T_{mn}} T_{kl} \right)}^{=C_{ijmn}} \mathring{T}_{mn} \tag{2.5}$$

An accumulation or dissipation of energy over a closed circuit is possible since the elastic potential function $W(\mathbf{T})$ or $\bar{W}(\boldsymbol{\epsilon})$ does not exist. Some examples of Cauchy-elastic soil models are presented in [169, 170] www.AN . The energy which may

be extracted with repeated closed strain circuits can give rise to a discussion on thermodynamic admissibility of such models. The extraction of mechanical energy must be accompanied by cooling of the body, but such direct transfer of heat into mechanical work (with no losses) is known as perpetuum mobile of the second kind. Additional mechanisms for dissipation of energy should therefore be implemented. If Cauchy-elasticity satisfied a postulate by Ilyushin

$$\oint \mathbf{T} : \mathrm{d}\boldsymbol{\epsilon} \geq 0 \qquad \text{for all cycles,} \tag{2.6}$$

wherein $\mathbf{T}$ and $\boldsymbol{\epsilon}$ are work-conjugate, then it would imply (hyper)elasticity in the sense of Green (with $\oint \mathbf{T} : \mathrm{d}\boldsymbol{\epsilon} = 0$), see [93].

3. **Hypoelasticity**. In geomechanics, differentially (incrementally) elastic stress-strain relations are very popular. They are used for both elastic and elastoplastic modeling. The stress rate and the strain rate are related by a linear tangent stiffness matrix E.

$$\mathring{\mathbf{T}} = \mathsf{E} : \mathbf{D}. \tag{2.7}$$

This stiffness E is a directly postulated function of stress, void ratio and other state variables. In solid mechanics such approach is called hypoelasticity or sometimes *Truesdell-type* elasticity. Models described by (2.7) are called incrementally linear because in general, one cannot guarantee the existence of a unique (one-to-one) integrated relation $\mathbf{T}(\boldsymbol{\epsilon})$, not to speak of its linearity. The elastic potential $W(\boldsymbol{\epsilon})$ is also absent. Therefore a closed strain circuit can be found for which

$$\oint E_{ijkl}\mathrm{d}\epsilon_{kl} = \text{acc. stress} \neq 0, \quad \text{and} \quad \oint T_{ij}\mathrm{d}\epsilon_{ij} = \text{acc. energy} \neq 0, \tag{2.8}$$

i.e. neither stress nor energy are recovered. They both are path-dependent functionals[1]. For example, the well known hypoelastic pressure-dependent model:

$$\mathsf{E} = \lambda\ \mathbf{1}\ \mathbf{1} + 2\mu\ \ \mathsf{I} \quad \text{with} \quad \lambda = \frac{(-\mathrm{tr}\,\mathbf{T}/\kappa)\nu}{(1+\nu)(1-2\nu)} \quad \text{and} \quad \mu = \frac{(-\mathrm{tr}\,\mathbf{T}/\kappa)}{2(1+\nu)}$$

is obtained from isotropic elasticity replacing Young modulus with the stress function $-\mathrm{tr}\,\mathbf{T}/\kappa$ (with the swell index κ and at the Poisson ratio $\nu = \text{const}$). From the theoretical standpoint, similar models are controversial because they allow for energy extraction and accumulation of stress, see e.g. discussion by Hueckel and Drescher [101].

[1]Some models [50, 205, 226] use a combination of two hypoelastic equations one for loading and one for unloading. However, such bi-hypoelastic formulations have some serious defects as discussed by Mróz [156] or by Gudehus [68].

4. **Hyperplasticity (elastoplasticity)**. An elastoplastic model can be formulated as a system of two constitutive relations: an elastic one is restricted to stresses within the yield surface $f(\mathbf{T},\dots) < 0$ and a bilinear one applies to stresses on a yield surface $f(\mathbf{T},\dots) = 0$. The latter has to guarantee that the stress path remains inside a predefined elastic region $f(\mathbf{T},\dots) < 0$ or on its boundary. The equation system can be written as follows

$$\mathring{\mathbf{T}} = \mathsf{E} : \mathbf{D} - \frac{1}{g^{ep}} \boldsymbol{\lambda}^p < \boldsymbol{\lambda} : \mathbf{D} > \quad \text{for} \quad f(\mathbf{T},\dots) = 0 \tag{2.9}$$

$$\mathring{\mathbf{T}} = \mathsf{E} : \mathbf{D} \quad \text{for} \quad f(\mathbf{T},\dots) < 0, \tag{2.10}$$

wherein $\boldsymbol{\lambda}^p$, $\boldsymbol{\lambda}$ and g^{ep} are functions of state. Two linear relations $\mathring{\mathbf{T}} = \mathsf{E}^{ep} : \mathbf{D}$ and $\mathring{\mathbf{T}} = \mathsf{E} : \mathbf{D}$ follow from the bilinear form (2.9) for 'loading' $\boldsymbol{\lambda} : \mathbf{D} > 0$ and 'unloading' $\boldsymbol{\lambda} : \mathbf{D} < 0$, respectively. Evidently, equations (2.9) and (2.10) give identical responses for neutral loading $\boldsymbol{\lambda} : \mathbf{D} = 0$. In order to introduce the well-known notions of plastic flow rule $\vec{\mathbf{n}}_g$, loading direction $\vec{\mathbf{n}}_f$ (normal to the yield surface $\mathbf{n}_f = (\partial f/\partial \mathbf{T})$) and hardening modulus K (controls the evolution if the yield surface) we substitute $\boldsymbol{\lambda}^p = \mathsf{E} : \vec{\mathbf{n}}_g$, $\boldsymbol{\lambda} = \vec{\mathbf{n}}_f : \mathsf{E}$ and $g^{ep} = K + \vec{\mathbf{n}}_f : \mathsf{E} : \vec{\mathbf{n}}_g$.

Generally neither stress nor energy can be recovered during a strain circuit that has 'touched' the yield surface, i.e. if loading has occurred. An extended study of the elastoplasticity theory can be found in a recent textbook of Lubarda [139].

5. **Hypoplasticity**. Neither stress nor energy is recovered after *any* strain circle. The stress - strain relation is incrementally nonlinear for all stresses and all directions of stretching. It cannot be linearized for a specially chosen sector of directions of strain rates $\mathbf{D}$, as is the case in elastoplastic models. Note that only few vertex-type elastoplastic models are similarly nonlinear, for example the one by Christoffersen and Hutchinson [35]. Most vertex-type elastoplastic models are based on multiple mechanisms [144] and are piecewise linear [7].

The nonlinearity of the hypoplastic stiffness becomes evident from a simple example. Let us consider a broad class of hypoplastic constitutive equations defined by (2.29). By factoring out $\mathbf{D}$ one obtains

$$\mathring{\mathbf{T}} = \mathsf{E}(\vec{\mathbf{D}}) : \mathbf{D} = \left[\mathsf{L} + \mathbf{N}\vec{\mathbf{D}}\right] : \mathbf{D}, \tag{2.11}$$

and the term in the square brackets in (2.11) represents the tangential stiffness tensor, which is incrementally nonlinear, i.e. dependent on the direction of stretching $\vec{\mathbf{D}}$. Note, still referring to (2.29), that *any* infinitesimally small strain cycle with a double amplitude leads to an accumulation of stress $\oint \mathbf{N}\|\mathbf{D}\|\mathrm{d}t$.

6. **Visco-elasticity** belongs to the group of *rheological* models in which elastic stiffness is coupled with Newtonian viscosity (viscous fluid with $\mathbf{T}^* = \eta \mathbf{D}^*$ [224]). Different couplings may be considered. In this group of models the accumulation of stress is time dependent (relaxation) and occurs *irrespectively* of whether a strain circle is applied or not. Under stress-controlled conditions creep-like deformation (accumulation of strain) is obtained. The consideration of real time is essential, so at least one material constant must be related to time. Usually it is a so-called fluidity parameter (reference creep rate) or its reciprocal value called characteristic time. The direction of creep is normally assumed to be purely deviatoric and parallel to the current deviatoric stress. On account of linearity, effects of stress increments at different time points can be conveniently superimposed using hereditary integrals. This property has contributed to the popularity of visco-elastic models.

7. **Visco-plasticity** couples plasticity and viscosity effects in series. Viscous and plastic cumulative effects are superposed. The accumulation of stress may occur at the absence of a strain loop (time dependent relaxation) but differently to visco-elasticity a strain loop may decisively influence this process. Plastic and viscous deformations are often treated collectively, i.e. the total strain rate is decomposed into two parts

$$\mathbf{D} = \mathbf{D}^e + \mathbf{D}^{vis}, \tag{2.12}$$

   e.g. [1, 184, 282]. The essential difference between a visco-plastic and a visco-elastic model follows from the fact that in the former one the intensity of $\mathbf{D}^{vis}$ is strongly dependent on a so-called *overstress*, i.e. on the distance between the current stress $\mathbf{T}$ and a yield surface $f(\mathbf{T}, \dots) = 0$. Not only the yield surface but also the flow rule $\mathbf{D}^{vis} \sim \vec{\mathbf{n}}_g$ is adopted from plasticity. which clearly indicates the origin of this group of models. If all three strain rate components (elastic + plastic + viscous) are treated separately

$$\mathbf{D} = \mathbf{D}^e + \mathbf{D}^p + \mathbf{D}^{vis} \tag{2.13}$$

   we call the model visco-elasto-plastic, e.g. [21,41]. Consider two tests: a monotonous and a cyclic one with the same average $\vec{\mathbf{n}}_g$ and with the same overstress. Visco-elasto-plastic models can account for the length of the strain path during the cyclic process. According to visco-plastic models the accumulation after both tests is identical. The influence of the frequency of cyclic loading on cumulative effects was reported e.g. by Matsui [147].

8. **Visco-hypoplasticity** is a combination of viscous and hypoplastic models. Such models for clays are discussed in detail in Section 4.2 and in [165] www.AN . These

'hybrids' use the hypoplastic linear part and a hypoplastic flow rule (for direction of creep) on one hand and Norton's rule for the intensity of creep with reference to the explicitly defined yield function ported from the modified Cam-clay model on the other hand. In many aspects visco-plasticity and visco-hypoplasticity are similar. The latter, however, needs neither of the above mentioned decompositions ($\mathbf{D} = \mathbf{D}^e + \mathbf{D}^{vis}$ or $\mathbf{D} = \mathbf{D}^e + \mathbf{D}^p + \mathbf{D}^{vis}$) to be explicitly defined. This was achieved by a subtle expedient, namely, in order to evaluate the overstress we use the *equivalent* pressure (similarly as defined by Hvorslev [103]) and not the *preconsolidation* pressure, see Section 4.2. Actually $\mathbf{D}^{vis}$ is a secondary state variable (a function of $\mathbf{T}$ and e) introduced merely to ease the explanation of the model.

2.2 Basic equations of hypoplasticity

The requirement of smooth differentiability of a constitutive relation $\mathring{\mathbf{T}} = \mathbf{H}(\mathbf{T}, \mathbf{D})$ with respect to all $\mathbf{D} \neq \mathbf{0}$ has been proposed in [271] to be a formal definition of hypoplasticity. This definition provides little insight into the essence of hypoplasticity and needs some translation. Therefore we discuss the aspect of smooth differentiability later in this section and start with a less formal description.

It is commonly recognized that for geomaterials (as well as for polycrystals) the assumption of bilinear response proposed in elastoplastic models is inexact and in particular obstructs the appearance of shear bands, unless the flow rule is strongly nonassociative. Hypoplasticity is perhaps the simplest dissipative constitutive theory that goes beyond the bilinear or piecewise linear incremental response. It is incrementally nonlinear (the tangential stiffness depends on $\vec{\mathbf{D}}$) and it needs neither a yield surface nor a strain rate decomposition into plastic and elastic portions. The advantage of the model lies in its smooth response upon change of the direction of loading and in the reduced stiffness for "loading to the side", which is in particular desired to facilitate the localization of deformation. The pioneer of hypoplasticity, Kolymbas [119], introduced his model as an alternative to elastoplasticity. He wrote:

"Elastoplasticity, or equivalently, hyperplasticity is a conjunction of elasticity and plasticity. A distinction between loading and unloading is established by means of so-called yield surface and the strains are subdivided into elastic and plastic parts[2]*. Hypoplasticity is here understood as an alternative to the classical theory of elasto-plasticity (. . .) It includes all plastic (i.e. path dependent and dissipative) constitutive models which do not use any yield surface. Hypoplastic models use equations of the so-called rate type (equally such*

[2]This point is somewhat controversial. Strictly speaking, in elastoplasticity there is no need for decomposition of strains into plastic and elastic part. The plastic deformation is *not an obligatory* state variable, cf. Petryk [193]. Actually there is a *possibility* but not a *necessity* of defining the plastic strain rate $\mathbf{D}^p = \mathbf{D} - \mathsf{E}^{-1} : \mathring{\mathbf{T}}$ wherein E is the elastic stiffness.

equations could be called incremental or evolution equations) with the following general form

$$\mathring{\mathbf{T}} = \mathbf{H}(\mathbf{T}, \mathbf{D}, \dots),$$

where $\mathring{\mathbf{T}}$ *is the co-rotated rate of the actual (Cauchy) stress* $\mathbf{T}$ *and* $\mathbf{D}$ *is the deformation rate. The tensorial function* $\mathbf{H}(\mathbf{T}, \mathbf{D}, \dots)$ *must be non-linear with respect to* $\mathbf{D}$ *in order to describe dissipative behaviour.*

After this general presentation we proceed with the definition [219, 271] based on differentiability. It consists of the following requirements:

- The material model is simple, i.e. the stress at a material point $\mathbf{X}$ depends only on the strain history of $\mathbf{X}$. This, of course, refers also to elastoplasticity.
- Both hypoplastic and elastoplastic descriptions are usually rate independent. Let $\mathbf{T} = \mathbf{T}(\mathbf{F}(t)) = \mathbf{T}(\mathbf{F}(s(t)))$ denote the stress as a functional of the deformation gradient history. If the time t is replaced by *any* monotonically increasing function $s(t)$ the value of the functional will not change.
- There exists a *single*[3] function $\mathbf{H}$, such that

$$\mathring{\mathbf{T}} = \mathbf{H}(\mathbf{T}, \mathbf{D}, \dots). \tag{2.14}$$

- The function $\mathbf{H}(\mathbf{T}, \mathbf{D})$ is, as already mentioned, continuously differentiable with respect to all $\mathbf{D} \neq \mathbf{0}$. Considering the class of equations defined by (2.29) we have $\partial\mathring{\mathbf{T}}/\partial\mathbf{D} = \mathsf{L} + \mathbf{N}\mathbf{D}/\|\mathbf{D}\|$ which is undetermined[4] for $\mathbf{D} = \mathbf{0}$ only. The above condition is not satisfied by piecewise linear materials. In elastoplasticity two limits of the tangential stiffness $\partial\mathring{\mathbf{T}}/\partial\mathbf{D}$ exist for the neutral direction of stretching namely, $\partial\mathring{\mathbf{T}}/\partial\mathbf{D} = \mathsf{E}$ for $\boldsymbol{\lambda} : \mathbf{D} \to 0^-$, i.e. if we come from the unloading regime , and E^{ep} for $\boldsymbol{\lambda} : \mathbf{D} \to 0^+$, i.e. if we come from the active loading side. Although the usual continuity condition $\mathsf{E} : \mathbf{D} = \mathsf{E}^{ep} : \mathbf{D}$ guarantees the continuity of stress $\mathring{\mathbf{T}}(\mathbf{D})$, a jump $\mathsf{E} - \mathsf{E}^{ep} \neq \mathbf{0}$ of stiffness across the neutral stretching direction is possible.

[3] Apparently elastoplasticity needs at least two distinct functions: ($\mathring{\mathbf{T}} = \mathsf{E}^{ep} : \mathbf{D}$ for loading $\boldsymbol{\lambda} : \mathbf{D} \geq 0$ and $\mathring{\mathbf{T}} = \mathsf{E} : \mathbf{D}$ for unloading $\boldsymbol{\lambda} : \mathbf{D} \leq 0$) whereas hypoplasticity uses only one function. This 'difference' is not essential and can be abated substituting $< \boldsymbol{\lambda} : \mathbf{D} >= \frac{1}{2}(1 + \boldsymbol{\lambda} : \mathbf{D}/|\boldsymbol{\lambda} : \mathbf{D}|)$ into (2.9) and postulating a vanishingly small elastic locus and a continuous field of hardening moduli, like in the INS model by Mróz [158].

[4] In bilinear elastoplasticity we have $\partial\mathring{\mathbf{T}}/\partial\mathbf{D} = \mathsf{E} - \dfrac{1}{g}\boldsymbol{\lambda}^p\boldsymbol{\lambda}$ for $\boldsymbol{\lambda} : \mathbf{D} > 0$ and $\partial\mathring{\mathbf{T}}/\partial\mathbf{D} = \mathsf{E}$ for $\boldsymbol{\lambda} : \mathbf{D} < 0$. For $\boldsymbol{\lambda} : \mathbf{D} = 0$ (which contains the special case $\mathbf{D} = \mathbf{0}$) the derivative $\partial\mathring{\mathbf{T}}/\partial\mathbf{D}$ is not unique. From the aspect of differentiability, hypoplasticity is therefore more demanding ($\mathring{\mathbf{T}}$ must be differentiable with respect to all $\mathbf{D} \neq \mathbf{0}$) than elastoplasticity ($\mathring{\mathbf{T}}$ must be differentiable with respect to all $\mathbf{D}$ such that $\mathbf{D} : \boldsymbol{\lambda} \neq 0$). From this point of view the prefix 'hypo-' is somewhat misleading because the theory is more restrictive.

In order to obtain a rate independent constitutive equation the stress rate function $\mathbf{H}(\mathbf{T}, \mathbf{D})$ must be a positive homogeneous function of the first degree in $\mathbf{D}$ so that

$$\mathbf{H}(\mathbf{T}, \lambda^2\mathbf{D}) = \lambda^2\mathbf{H}(\mathbf{T}, \mathbf{D}), \tag{2.15}$$

where λ^2 is a positive multiplier. Since the hypoplastic response is nonlinear, we cannot assume superposition, i.e.

$$\mathbf{H}(\mathbf{T}, \lambda_1\mathbf{D}^{(1)} + \lambda_2\mathbf{D}^{(2)}) \neq \lambda_1\mathbf{H}(\mathbf{T}, \mathbf{D}^{(1)}) + \lambda_2\mathbf{H}(\mathbf{T}, \mathbf{D}^{(2)}) \tag{2.16}$$

unless $\mathbf{D}^{(2)} = \lambda^2\mathbf{D}^{(1)}$. By the requirement of objectivity, the function $\mathbf{H}(\mathbf{T}, \mathbf{D})$ must be isotropic (independent of the frame of reference) [243]. The most general representation of an isotropic tensor-valued function [258] of two tensorial symmetric arguments is

$$\begin{aligned} \mathring{\mathbf{T}} &= \phi_0\mathbf{1} + \phi_1\mathbf{T} + \phi_2\mathbf{D} + \phi_3\mathbf{T}^2 + \phi_4\mathbf{D}^2 + \phi_5(\mathbf{T}\cdot\mathbf{D} + \mathbf{D}\cdot\mathbf{T}) \\ &+ \phi_6(\mathbf{T}^2\cdot\mathbf{D} + \mathbf{D}\cdot\mathbf{T}^2) + \phi_7(\mathbf{T}\cdot\mathbf{D}^2 + \mathbf{D}^2\cdot\mathbf{T}) \\ &+ \phi_8(\mathbf{T}^2\cdot\mathbf{D}^2 + \mathbf{D}^2\cdot\mathbf{T}^2), \end{aligned} \tag{2.17}$$

where coefficients ϕ_i are functions of the invariants of $\mathbf{T}$ and $\mathbf{D}$ (also joint invariants):

$$\begin{aligned} \phi_i \;= \phi_i(\;& \mathrm{tr}\mathbf{T}, \mathrm{tr}\mathbf{T}^2, \mathrm{tr}\mathbf{T}^3, \mathrm{tr}\mathbf{D}, \mathrm{tr}\mathbf{D}^2, \mathrm{tr}\mathbf{D}^3, \\ & \mathrm{tr}(\mathbf{T}\cdot\mathbf{D}), \mathrm{tr}(\mathbf{T}^2\cdot\mathbf{D}), \mathrm{tr}(\mathbf{T}\cdot\mathbf{D}^2), \mathrm{tr}(\mathbf{T}^2\cdot\mathbf{D}^2) \;\;) \end{aligned} \tag{2.18}$$

The representation theorem yields plenty of possibilities, so one needs several additional restrictions and assumptions. The original hypoplastic model was formulated by trial and error using so-called candidate functions. A candidate is defined as a linear combination of several terms (called generators) picked up from (2.17), for example [117]

$$\mathring{\mathbf{T}} = C_1\frac{1}{2}(\mathbf{T}\cdot\mathbf{D} + \mathbf{D}\cdot\mathbf{T}) + C_2\ \mathbf{1}\mathbf{T}:\mathbf{D} + C_3\mathbf{T}\|\mathbf{D}\| + C_4\frac{\mathbf{T}\cdot\mathbf{T}}{\mathrm{tr}\,\mathbf{T}}\|\mathbf{D}\| \tag{2.19}$$

with material constants (here $C_1 \ldots C_4$). A sophisticated system for automatic calibration and for testing of such candidates has been developed [118]. In this heuristic approach, the verification of candidate functions $\mathbf{H}(\mathbf{T}, \mathbf{D})$ becomes an essential task. Since the seventies testing procedures have been systematically developed. At this place, a brief review of the requirements imposed on a candidate is possibly of some interest.

Let us start with a method of visualization of tangential stiffness with so-called response envelopes proposed in the seventies by Gudehus [68] and by Lewin [133] (for compliance). Roughly speaking a response envelope is a polar diagram of stiffness plotted for different directions of stretching. It enables comparative studies of various rate independent models. Usually stress states with cylindrical symmetry are considered. We start by choosing an initial stress $\mathbf{T}_0$ on the Rendulic plane $-\sqrt{2}\ T_2, -T_1$. The stress envelope is obtained

as a plot of the final stresses calculated with normalized strain probes $\mathrm{diag}[D_1, D_2, D_2]\Delta t$ (with $\|\mathbf{D}\|\Delta t = \text{const}$ or with $\|\mathbf{D}\| = 1$) applied in different directions. The scaling parameter Δt can be arbitrarily chosen, i.e. the size of the response envelope is of no importance.

A constitutive model may be seen as a mapping that carries a circle plotted in the $-\sqrt{2}\ D_2, -D_1$ space, Fig. 2.1 left, to the stress space where it becomes an ellipse, Fig. 2.1 right. The analytical equation of a response envelope at $\mathbf{T}_0$ obtained from strain increments $\mathbf{D}\Delta t$ of constant length $\|\mathbf{D}\|\Delta t = r_{\mathbf{D}} = \text{const}$ is simply

$$o(\mathbf{T}) \equiv \mathbf{D} : \mathbf{D}\Delta t^2 - r_{\mathbf{D}}^2 = 0 \tag{2.20}$$

wherein $\mathbf{D}$ is expressed as a function of the stress via stress rate $\mathring{\mathbf{T}} = (\mathbf{T} - \mathbf{T}_0)/\Delta t$. For hypoplastic models given by (2.29) the expression for $o(\mathbf{T})$ is

$$o(\mathbf{T}) \equiv \|\mathsf{L}^{-1} : (\mathbf{T} - \mathbf{T}_0 - \mathbf{N} r_{\mathbf{D}})\|^2 - r_{\mathbf{D}}^2 = 0 \tag{2.21}$$

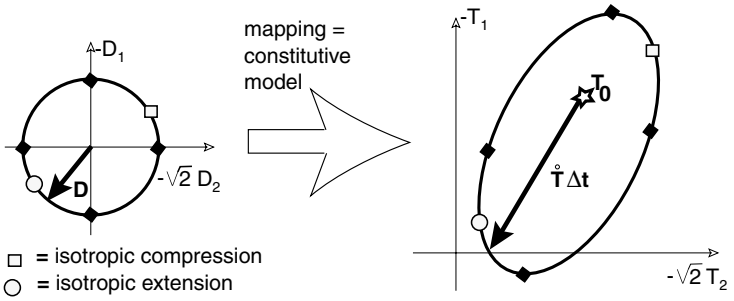

Figure 2.1: For the axially symmetric case the constitutive equation $\mathring{\mathbf{T}}(\mathbf{D})$ can be interpreted as a mapping that carries a circle (left) in the strain rate space into the stress rate space where it becomes an ellipse (right). The circle corresponds to unit strain probes $\|\mathbf{D}\|\Delta t = \text{const}$. A good idea is to superpose the original stress $\mathbf{T}_0$ by the stress increments $\mathring{\mathbf{T}}\Delta t$ (right) and to plot several such response envelopes in the same diagram as shown in Fig. 2.4. The strain and stress rate are not parallel, $\mathring{\mathbf{T}}(\mathbf{D}) \nsim \mathbf{D}$, so the mapping is not just a 'radial scaling' of the strain rate

Having applied strain-probes at $\mathbf{T}_0$ we may choose the next stress and repeat the construction from this stress using the same Δt. For example, a diagram obtained in this way is shown in Fig. 2.4. The starting points are denoted with crosses (+). In some cases an analogous mapping into the stress *rate* space is useful. For example, such rate-type response envelope can be obtained expressing condition $\mathbf{D} : \mathbf{D} - 1 = 0$ in terms of stress rate calculated from (2.29):

$$o(\mathring{\mathbf{T}}) \equiv \|\mathsf{L}^{-1} : (\mathring{\mathbf{T}} - \mathbf{N})\| - 1 = 0 \tag{2.22}$$

A complementary mapping of unit stress-rate-probes into the strain space [133] is rarely used because it requires inversion of $\mathbf{H}(\mathbf{T}, \mathbf{D})$ which is not always possible. Such complementary mapping has been used by Bardet [7] for comparison of different incrementally

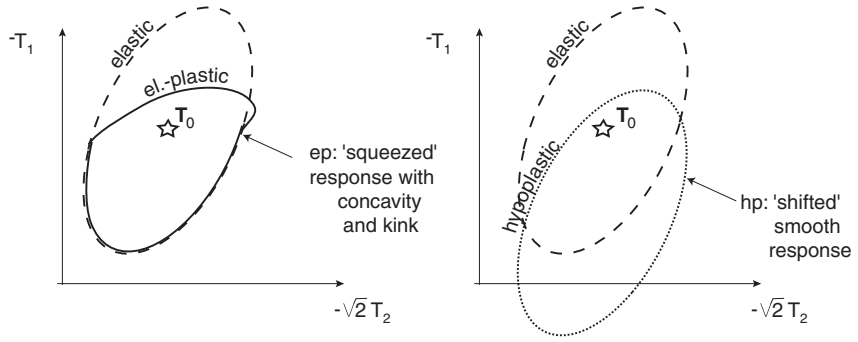

Figure 2.2: Typical response envelopes generated by hypoplasticity and elastoplasticity for unit strain increments applied at $\mathbf{T}_0$. The envelopes are obtained by 'shifting' or 'squeezing' of the elastic response envelope (dashed line), respectively. The elastoplastic envelope is concave and has a kink

nonlinear materials. Recently Doanh [53] revealed an interesting anomaly of the hypoplastic model in complementary plots. This is shown in Fig. 3.1. Collections of response envelopes in stress space for different constitutive laws can be found in [55, 68, 117, 265, 266]. The response envelope of the first two terms in (2.19), (the linear part of the hypoplastic model) can be shown [68] to be an ellipse with the initial stress $\mathbf{T}_0$ in the middle. The response envelope of the last two terms in (2.19) (the so-called nonlinear part) may be more complicated. Let us consider the most important family of hypoplastic models given by Eq. (2.29). The response of the nonlinear part $\mathbf{N}\|\mathbf{D}\|$ is, in such case, particularly simple. It is a point shifted from the origin $\mathbf{T}$ by $\mathbf{N}\|\mathbf{D}\|\Delta t$. These partial responses can be added and their sum is an ellipse shifted with respect to the original stress $\mathbf{T}_0$ by $\mathbf{N}\|\mathbf{D}\|\Delta t$. Note that elasto-plastic constitutive models generate somewhat awkward responses if compared with the well shaped hypoplastic ellipses, see Fig. 2.2.

The *smoothness* and convexity of the response envelope is regarded as an advantage of hypoplasticity. Smooth contours may indeed seem credible, although to the author's knowledge no concrete advantages of the convexity have been demonstrated. It has not been shown either, that such a shape results from any fundamental principle of mechanics. In passing, let us comment that the conditions of smoothness and convexity can be imposed on elastoplastic models. It can be done [162] www.AN by choosing a direction of $\overset{\circ}{\mathbf{T}}{}^{r} = -\mathsf{E}^e : \mathbf{D}^p$ to lie along the principal axis of the elastic response envelope, see Fig. 2.3. This approach can be also applied to vertex plasticity.

Having this possibility of graphic presentations of stiffness plots candidate functions could be more easily tested. A significant restriction on the generators in $\mathbf{H}(\mathbf{T}, \mathbf{D})$ came from experimental observations in true triaxial apparatus by Goldscheider [62]. He discovered that all proportional strain paths starting from the nearly stress free and undisturbed

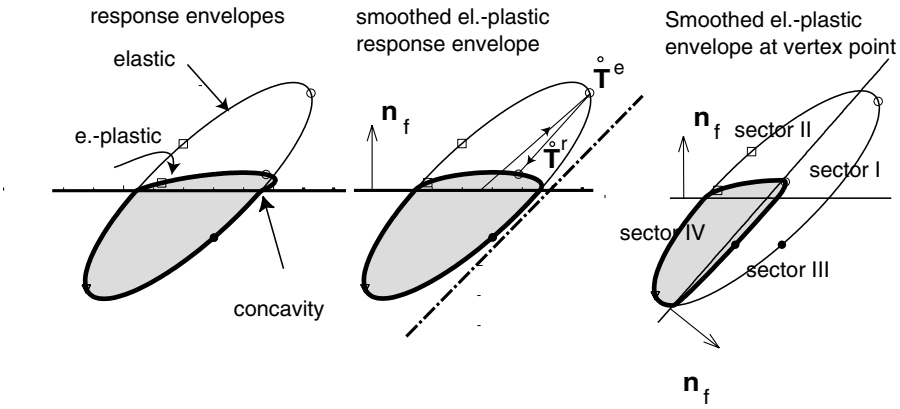

Figure 2.3: If the direction of loading $\mathbf{n}_f$ is related to the direction of plastic flow $\mathbf{n}_g$ by $\mathbf{n}_g \sim \mathsf{E}^e : \mathbf{n}_g$ (with elastic stiffness E^e) then $\mathring{\mathbf{T}}^r = \mathsf{E}^e : \mathbf{D}^p$ is parallel to the dash-dotted line and the elastoplastic response envelope can be shown [162] to be smooth. In order to satisfy this condition either elastic stiffness must be modified or the directions $\mathbf{n}_f$ or/and $\mathbf{n}_g$ must be rotated. Smooth response envelopes can also be obtained for the vertex-type elastoplasticity

state resulted in nearly proportional stress paths. By this observation Kolymbas [116] concluded that the function $\mathbf{H}(\mathbf{T}, \mathbf{D})$ has to be positively homogeneous with respect to $\mathbf{T}$, i.e.

$$\mathbf{H}(\lambda\mathbf{T}, \mathbf{D}) = \lambda^n \mathbf{H}(\mathbf{T}, \mathbf{D}), \tag{2.23}$$

where λ is an arbitrary positive scalar and n denotes the degree of homogeneity. This point is discussed in more detail in Section 3.4. The tangential stiffness in (2.23) is proportional to the n-th power of stress and vanishes for $\mathbf{T} = \mathbf{0}$. The value $n = 1$ was[5] used in early versions of hypoplasticity.

Numerous restrictions on candidates $\mathbf{H}(\mathbf{T}, \mathbf{D})$ arise from the fact that the space of accessible stresses must be confined, and the nonlinear function $\mathbf{H}(\mathbf{T}, \mathbf{D})$ should imply some counterpart of a yield condition. At first, it is not self evident that equations like (2.19) or generally (2.29) may reproduce the phenomenon of perfect plastic flow understood as

$$\mathring{\mathbf{T}}(\mathbf{D}) = \mathbf{0} \text{ for a certain } \mathbf{D} \neq \mathbf{0}. \tag{2.24}$$

Using the response envelopes, we may easily illustrate, how the concept of perfect plastic flow has been implemented into the hypoplastic model, see Fig. 2.4. The essential operation is to increase of the shift of the ellipse towards the hydrostatic axis as the stress obliquity $\mathbf{T}^*/\mathrm{tr}\,\mathbf{T}$ approaches the limit value denoted by the double line (the hypoplastic

[5] In the meanwhile, the requirement of the first order homogeneity of $\mathbf{H}$ with respect to stress turned out [71] to be inexact for sands. However, it is still considered to be an acceptable approximation for clays. For example, this homogeneity is preserved in the visco-hypoplastic model presented in Section 4.2.

yield surface). At the yield limit $\mathbf{T}_y$, this shift must be so large that the response envelope passes through the original stress $\mathbf{T}_y$. Then, a direction $\mathbf{D}$ can be found for which $\mathring{\mathbf{T}} = \mathbf{0}$ (see Section 2.3.1 for the derivation of this direction). Continuation of this specific deformation is called hypoplastic flow. Due to the homogeneity of $\mathbf{H}(\mathbf{T}, \mathbf{D})$ with respect to stress, all stresses proportional to $\mathbf{T}_y$ will have the same property. They constitute thus a conical yield surface in the principal stress space. Some examples of the hypoplastic yield surface $y(\mathbf{T})$ plotted on the deviatoric plane $\mathrm{tr}\,\mathbf{T} = \text{const.}$ are presented in Fig. 2.7 and 2.11.

Several candidate functions by Kolymbas and Wu [117,266] turned out to generate a yield surface similar to the one proposed by Lade [127]

$$F_L(\mathbf{T}) \equiv \frac{(I_1)^3}{I_3} - \text{const} = 0. \tag{2.25}$$

The model by Wolffersdorff [265, 265] generates the yield surface identical with the one originally proposed by Matsuoka and Nakai [148, 150]

$$y_{M-N}(\mathbf{T}) \equiv -\frac{I_1 I_2}{I_3} + \frac{9 - \sin^2\varphi_c}{-1 + \sin^2\varphi_c} = 0, \tag{2.26}$$

wherein $I_1 = \mathrm{tr}\,\mathbf{T}$, $I_2 = \frac{1}{2}\left[\mathbf{T} : \mathbf{T} - (I_1)^2\right]$ and $I_3 = \det(\mathbf{T}) = e_{ijk} T_{i1} T_{j2} T_{k3}$ are the stress invariants.

In the caption of Fig. 2.4 the problem of permeability of the yield surface has been mentioned. Contrary to elastoplastic yield surfaces the hypoplastic yield surface can be surpassed! Some stress paths may penetrate through it going outwards through the shaded areas where the response envelopes are bulging out of the yield surface. This effect is *not* a counterpart of the elasto-plastic hardening. The hypoplastic yield surface is 'leaky', so there is a need for a true *bounding surface* that would encompass all attainable stress states in the model. This problem will be discussed in detail in several sections later on. Due to the deficient bounding surface generated by the constitutive model (2.19) an alternative candidate function has been proposed by Wu [266]

$$\mathring{\mathbf{T}} = C_1(\mathrm{tr}\,\mathbf{T})\mathbf{D} + C_2\frac{\mathbf{T} : \mathbf{D}}{\mathrm{tr}\,\mathbf{T}}\mathbf{T} + C_3\frac{\mathbf{T}\cdot\mathbf{T}}{\mathrm{tr}\,\mathbf{T}}\|\mathbf{D}\| + C_4\frac{\mathbf{T}^*\cdot\mathbf{T}^*}{\mathrm{tr}\,\mathbf{T}}\|\mathbf{D}\|. \tag{2.27}$$

This version with material constants $\mathrm{C}_1 = -106.5$, $\mathrm{C}_2 = -801.5$, $\mathrm{C}_3 = -797.1$, $\mathrm{C}_4 = 1077.7$ reproduces fairly well the behaviour of dense Karlsruhe sand [269].

The respective expression for tangential stiffness at a given stress $\mathbf{T}$ is

$$\frac{\partial\mathring{\mathbf{T}}}{\partial\mathbf{D}} = \mathsf{E}^{hp} = C_1\mathrm{tr}\,\mathbf{T}\ \ \mathsf{I} + C_2\frac{\mathbf{T}\mathbf{T}}{\mathrm{tr}\,\mathbf{T}} + C_3\frac{\mathbf{T}\cdot\mathbf{T}\vec{\mathbf{D}}}{\mathrm{tr}\,\mathbf{T}} + C_4\frac{\mathbf{T}^*\cdot\mathbf{T}^*\vec{\mathbf{D}}}{\mathrm{tr}\,\mathbf{T}} \tag{2.28}$$

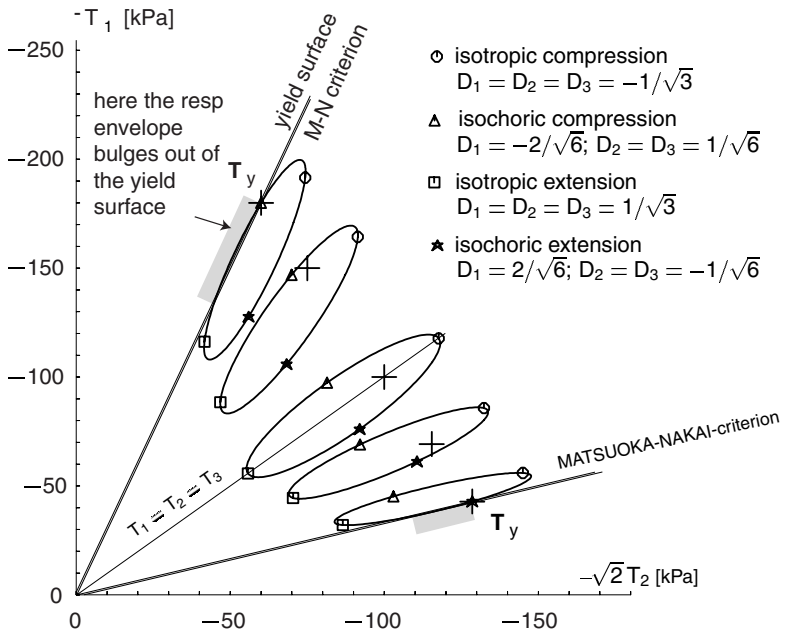

Figure 2.4: The response envelopes plotted for the reference model described in Section 2.5 The shift of the response envelope with respect to the initial stress $\mathbf{T}_0$ (denoted by +) increases with deviatoric stress and is directed towards the hydrostatic axis $T_1 = T_2 = T_3$. If $\mathbf{T}_0$ lies on the yield surface ($\mathbf{T}_0 = \mathbf{T}_y$) this shift is so large that the response envelope passes through the initial stress. Note that fragments of response envelopes plotted from $\mathbf{T}_y$ lie in the shadowed zone, i.e. slightly outside the yield surface (and it is not caused by scaling factor Δ t). Consistently, some stress paths can surpass the yield surface moving towards the shaded zone. It is controversial if this should be admitted. Beyond the yield surface the shifted the response envelope lies off the initial stress. The stress strain relation cannot be inverted any more, i.e. the function $\mathbf{D}(\mathring{\mathbf{T}})$ does not exist. This is discussed in Section 2.3.2

Note that the hypoplastic tangential stiffness is nonsymmetric. As already discussed it is *continuously* dependent on the direction $\vec{\mathbf{D}}$ of the applied strain rate.

Using response envelopes Wu [266] demonstrated graphically that the earlier nonlinear terms with $\mathbf{D} \cdot \mathbf{D}/\|\mathbf{D}\|$ or with $\|\mathbf{D}^*\|$ in place of $\|\mathbf{D}\|$ may lead to 'heart'-shaped or '8'-shaped contours which are unacceptable. Self-intersection of the contour implies loss of invertibility, i.e. no unique function $\mathbf{D}(\mathring{\mathbf{T}})$ exists. For this reason the development of hypoplastic models in the nineties was focused on the following general form

$$\boxed{\mathring{\mathbf{T}} = \mathsf{L} : \mathbf{D} + \mathbf{N}\|\mathbf{D}\|} \tag{2.29}$$

wherein L is a fourth order tensor and $\mathbf{N}$ is a second-order tensor, and both of them are functions of stress. Everywhere in this text we assume that L is positive definite and can always be inverted. In many cases analytical inversion is possible. For example, using (2.28) we obtain L in the form

$$L_{ijkl} = C_1 \mathrm{tr}\,\mathbf{T}\left[I_{ijkl} + C_2/C_1 \frac{T_{ij}T_{kl}}{(\mathrm{tr}\,\mathbf{T})^2}\right] \tag{2.30}$$

which can be analytically inverted

$$L^{-1}_{ijkl} = \frac{1}{C_1 \mathrm{tr}\,\mathbf{T}} \left[I_{ijkl} - \frac{C_2 T_{ij} T_{kl}}{C_1 (\mathrm{tr}\,\mathbf{T})^2 + C_2 \mathbf{T} : \mathbf{T}} \right] \tag{2.31}$$

using the Sherman-Morisson formula[6].

In hypoplasticity the notions of loading and unloading need not be explicitly defined, because the appropriate modification of stiffness follows automatically from the nonlinear term $\mathbf{N}\|\mathbf{D}\|$. Informally, loading and unloading can be understood as advancing towards or running away from the yield surface, respectively. The nonlinear part $\mathbf{N}\|\mathbf{D}\|$ is active for both loading and unloading .

At the end of this introductory presentation we consider the performance of a one-dimensional hypoplastic model within the stress range $-T_y < T < T_y$. Equation (2.29) can be rewritten in form

$$\dot{T} = LD + N|D| \quad \text{with} \quad 0 < -N \leq L \tag{2.32}$$

or equivalently

$$\begin{aligned} \dot{T} &= (L - N)D \qquad \text{for } D < 0 \\ \dot{T} &= (L + N)D \qquad \text{for } D > 0 \end{aligned} \tag{2.33}$$

Let us choose $0 < L = \text{const}$. The term N is a partial stiffness that increases or decreases the basic term L for a given T, depending on the direction of D. For the case $T > 0$ loading corresponds to $D > 0$ and N should be negative, in order to make the corresponding stiffness $L + N$ smaller than the one for unloading $(= L - N)$. By analogous argument N should be positive for $T < 0$. The quantity N can be seen as one half of the difference between the stiffness for loading and for unloading.

Let us now implement a yield surface by increasing the nonlinear term as the stress approaches the limit value T_y. We may simply choose $N = -LT/T_y$. By this expedient

$$\dot{T}\Big|_{T=T_y, D>0} = \dot{T}\Big|_{T=-T_y, D<0} = LD - LT/T_y|D| = 0, \tag{2.34}$$

so the hypoplastic yield surface $y(T) \equiv T^2 - T_y^2 = 0$ will not be surpassed (if the strain increments are sufficiently small). The model can be improved choosing more suitable expressions for $L(T)$ and $N(T)$, e.g. $N = -\mathrm{sign}(T)\ L\ (T/T_y)^n$ as examined with the following MATHEMATICA script

[6] for a given square nonsingular matrix $[\mathbf{A}]$ and a dyad $\{\mathbf{u}\}\{\mathbf{v}\}^T$ the identity $([\mathbf{A}] + \{\mathbf{u}\}\{\mathbf{v}\}^T)^{-1} = [\mathbf{A}]^{-1} - ([\mathbf{A}]^{-1}\{\mathbf{u}\}\{\mathbf{v}\}^T[\mathbf{A}]^{-1})/(1 + \{\mathbf{v}\}^T[\mathbf{A}]^{-1}\{\mathbf{u}\})$ holds provided the matrix and the dyad have the same size and $1 + \{\mathbf{v}\}^T[\mathbf{A}]^{-1}\{\mathbf{u}\} \neq 0$

```
dT = Compile[{LL, maxT, T, de, {expo, _Integer}},
      Module[{a}, LL de - LL *Sign[T]*Abs[T/maxT]^expo*Abs[de]]];
plot1d[LL_, maxT_, expo_, deps_, maxtime_] :=
Module[{t=0, dt=maxtime/1000, eps=Table[0,{i,0,1001}],T=Table[0,{i,0,1001}]},
        Do[{t+=dt; T[[i+1]]=T[[i]] + dT[LL,maxT,T[[i]],deps[t], expo]*dt;
            eps[[i + 1]] = eps[[i]] + deps[t] dt},   {i, 1, 1000}];
      ListPlot[Transpose[{eps, T}]];];
drate[t_] :=  Which[t<3.5,1, t>=3.5 && t<4,-1, t>=4 && t<10,1,  t>=10,-1];
DisplayTogether[ plot1d[1, 1, 6, drate, 20] ,  plot1d[1, 1, 6, drate, 20]]
```

The results for $n = 1$ and $n = 6$ are presented in Fig. 2.5. Note that increasing n we may obtain at the limit an elastoplastic model.

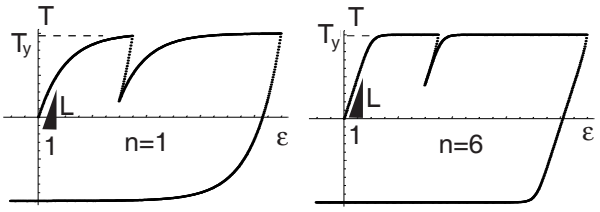

Figure 2.5: Yielding $\dot{T} = 0$ corresponds to $T = T_y$ or to $|L^{-1}N| = 1$, the initial stiffness is given by L and exponent n can be used to create a suitable transition between elastic and plastic behaviour

Some similarities between hypoplastic and elastoplastic one-dimensional models follow from the comparison between (2.33) and the elastoplastic relations:

$$\mathring{T} = \begin{cases} E^{ep} : D & \text{for } TD > 0 \text{ and } T^2 - T_y^2 = 0 \\ E : D & \text{for } TD < 0 \text{ or } T^2 - T_y^2 < 0 \end{cases}, \tag{2.35}$$

wherein $TD > 0$ corresponds to loading. The stiffnesses $E^{ep} = 0$ and E correspond to the elasto-plastic and the elastic response, respectively. The elastoplastic nonlinearity vanishes immediately if $T^2 - T_y^2 < 0$, whereas the hypoplastic term N decreases gradually with $T \to 0$.

A generalized one-dimensional hypoplastic overlay model is discussed further in the context of the endochronic theory, see Section 4.3.7, and more elaborate elastoplastic models with various types of hardening can be found in most books on plasticity, for instance in [220].

If the applied strain rate $\mathbf{D}$ is coaxial with the stress $\mathbf{T}$ (parallel eigenvectors of $\mathbf{D}$ and $\mathbf{T}$ or equivalently $\mathbf{D} \cdot \mathbf{T} = \mathbf{T} \cdot \mathbf{D}$) the hypoplastic model can be conveniently studied in the matrix form because the generated stress rate $\mathring{\mathbf{T}}$ is coaxial with both $\mathbf{T}$ and $\mathbf{D}$ (property of isotropic tensorial functions).

$$\begin{Bmatrix} \mathring{T}_1 \\ \mathring{T}_2 \\ \mathring{T}_3 \end{Bmatrix} = \left(\begin{bmatrix} L_{11} & L_{12} & L_{13} \\ L_{21} & L_{22} & L_{23} \\ L_{31} & L_{32} & L_{33} \end{bmatrix} + \begin{bmatrix} N_1\vec{D}_1 & N_1\vec{D}_2 & N_1\vec{D}_3 \\ N_2\vec{D}_1 & N_2\vec{D}_2 & N_2\vec{D}_3 \\ N_3\vec{D}_1 & N_3\vec{D}_2 & N_3\vec{D}_3 \end{bmatrix} \right) \begin{Bmatrix} D_1 \\ D_2 \\ D_3 \end{Bmatrix}. \tag{2.36}$$

Similar matrix expressions can be formulated for the general case of non-coaxial $\mathbf{T}$ and $\mathbf{D}$, see Section 3.1 and for the triaxial case, i.e. for the $p-q$ space, see Section 3.2.1.

As a final remark let us emphasize that hypoplasticity as proposed by Kolymbas should not be mixed up with the Dafalias' [44] hypoplastic model. The latter one is actually an extended elastoplastic model, in which the *direction* of plastic strain rate depends on the stress rate[7].

2.3 Yield surface and bounding surface

Early hypoplastic models were formulated heuristically, exploring different tensorial polynomials (by trial and error) rather than by following set rules.

At the beginning, candidate functions were simply subjected to various strain (or stress) paths followed in computer simulations. Plots (nicknamed hedgehogs, Fig. 2.6 upper left-hand diagram) of stress paths starting from a common stress $\mathbf{T}_0$ and corresponding to different $\mathbf{D}$ = const gained much popularity [117]. Also the shapes of the response envelopes for different stress states were carefully studied. Later, it appeared useful to establish some analytical tests, with which the candidate functions could be confronted. The most important among these tests concerned the existence and correct shape of the yield surface $y(\mathbf{T}) = 0$ and the bounding surface $b(\mathbf{T}) = 0$.

2.3.1 Yield surface

The yield condition can be found substituting $\mathring{\mathbf{T}} = \mathbf{0}$ into (2.29). From $\mathsf{L} : (\mathbf{D} + \mathsf{L}^{-1} : \mathbf{N}\|\mathbf{D}\|) = \mathbf{0}$ follows that $\mathring{\mathbf{T}} = \mathbf{0}$ is satisfied trivially by $\mathbf{D} = \mathbf{0}$, and by

$$\vec{\mathbf{D}} = -\mathsf{L}^{-1} : \mathbf{N} \tag{2.37}$$

Equation (2.37) imposes a condition on stress, which can be revealed by elimination of $\vec{\mathbf{D}}$ from (2.37). Taking the norm of both sides of (2.37) we obtain

$$y(\mathbf{T}) \equiv \|\mathsf{L}^{-1} : \mathbf{N}\| - 1 = 0\,. \tag{2.38}$$

[7]Strictly speaking, the Kolymbas' hypoplastic model would not be regarded by Dafalias as 'hypoplastic' because the direction of the irreversible strain accumulation in an infinitesimally small closed stress circuit turns out to be proportional to $-\mathsf{L}^{-1} : \mathbf{N}$, which may be found applying $\pm\mathring{\mathbf{T}}$ to (3.12), see Section 3.1.1. This result does not depend on the direction (polarization) of the applied stress circuit. From the opposite point of view Dafalias' 'hypoplastic' model with switch functions between various strain-rate sectors cannot be recognized as hypoplastic in the current context. Switch functions violate the criterion of continuous differential ($\partial\mathring{\mathbf{T}}/\partial\mathbf{D}$) mentioned at the beginning of this section. Actually, the early endochronic theory of Valanis [246,249,250] the model of Darve [49] or of Chambon [39] stand much closer to the here discussed formulation than the Dafalias' 'hypoplasticity'. Although endochronic and hypoplastic models are of different origin, their rate equations are very similar.

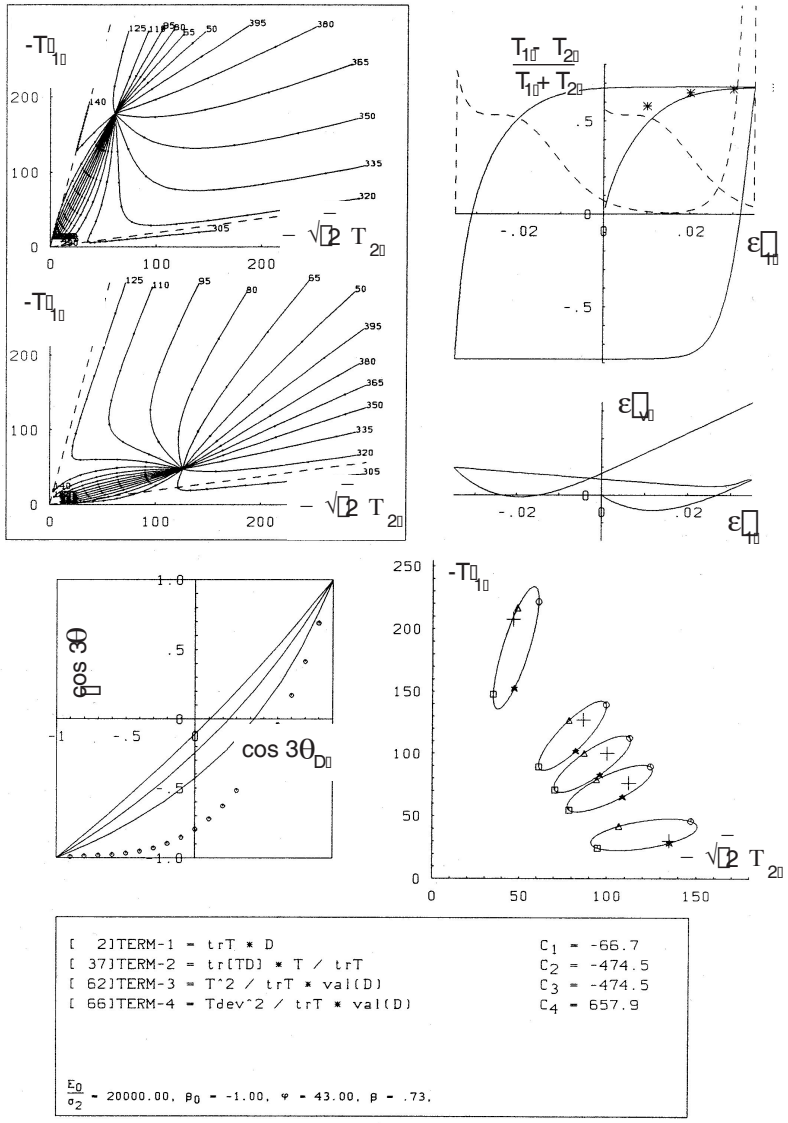

Figure 2.6: Quality certificate for a candidate function. The combination of tensorial terms and set of parameters are listed below. Two 'hedgehogs', cyclic shear response, deviatoric flow rule plot (proposed by Goldscheider [62]) and five response envelopes are presented. The angle $\theta = \pi/3 - \theta^{Lode}$ is related to the well known Lode angle $\theta^{Lode} = \frac{1}{3}\arccos\left(-\frac{3}{2}\sqrt{3}J_3/J_2^{3/2}\right)$ with $J_2 = \frac{1}{2}\|\mathbf{T}^*\|$ and $J_3 = \det(\mathbf{T}^*)$, see Fig. 2.16. The angle θ_D is identical with θ but refers to the direction of flow $\mathbf{D}$ and not to stress. If $\mathbf{D}$ and $\mathbf{T}$ were proportional the diagram would be a straight diagonal line

This stress function is, roughly speaking, a counterpart of the yield criterion in elastoplasticity [117, 266]. It is convenient to introduce the tensorial function

$$\mathbf{B} = \mathsf{L}^{-1} : \mathbf{N} \,. \tag{2.39}$$

We may write $\mathring{\mathbf{T}} = \mathsf{L} : (\mathbf{D} + \mathbf{B}\|\mathbf{D}\|)$ and $y(\mathbf{T}) \equiv \|\mathbf{B}\| - 1 = 0$. A kind of flow rule is given by (2.37), i.e. by $\vec{\mathbf{D}} = -\mathbf{B}$. The flow rule can be extended in hypoplasticity to stresses inside the 'yield surface' (with $\|\mathbf{B}\| < 1$) by writing $\vec{\mathbf{D}} = -\vec{\mathbf{B}}$. If $\|\mathbf{B}\| = 1$ and $\mathbf{D} \sim -\mathbf{B}$ then $\mathring{\mathbf{T}} = \mathbf{0}$ and perfectly plastic deformation occurs. Note that direction of this perfectly plastic flow $-\vec{\mathbf{B}}$ is a function of stress $\mathbf{T}$ only, similarly as the flow rule for $\mathbf{D}^p \sim \mathbf{n}_g(\mathbf{T})$ in elastoplasticity. However, the strain rate decomposition into plastic and elastic parts, analogously to

$$\mathbf{D} = \mathbf{D}^e + \mathbf{D}^p = (\mathsf{I} - \mathbf{n}_g\mathbf{n}_f : \mathsf{E}) : \mathbf{D} + (\mathbf{n}_g\mathbf{n}_f : \mathsf{E}) : \mathbf{D} \tag{2.40}$$

(with loading direction $\mathbf{n}_f$) makes little sense in hypoplasticity because in the view of incremental nonlinearity (2.16) a superposition of stress rates does not work.

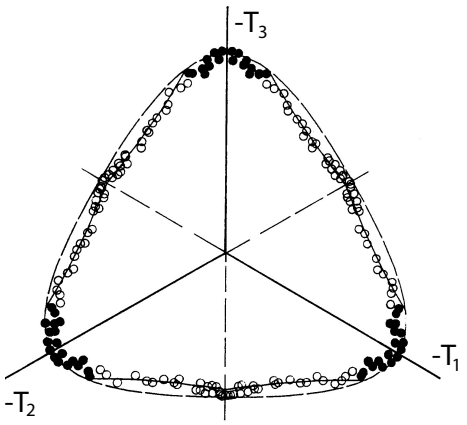

Figure 2.7: Hypoplastic yield surface compared to experimental (5 times mirrored) results by Goldscheider [62]. Since the diagram is mirrored a full experimental surface could reveal an anisotropy [194]

The existence of the surface (2.38) is not automatically assured by the form of (2.29). This existence must be demonstrated for each candidate function and for each set of material parameters. A considerable work (mostly by trial and error) has been invested to find a candidate function for which the yield surface (2.38) would resemble the Coulomb pyramid, see Fig. 2.7.

We have shown that pure hypoplastic flow (2.37) requires that stress satisfies (2.38) and that the applied strain rate is appropriate, i.e. $\mathbf{D} \sim -\mathbf{B}$. Apparently, the hypoplastic yield surface and the hypoplastic flow rule (equations (2.38) and (2.37)) emerge as *by-products* of the constitutive equation. In the hypoplastic community this fact was regarded advantageous or at least elegant [119], compared to the yield surface and to the flow rule prescribed a priori in elastoplasticity. It turns out however, that the explicit formulation is more convenient, at least at the stage of formulation and modification of a model. The explicit approach has been de facto adapted to hypoplasticity by Wolffersdorff [265] and by Bauer [11]. The generalized hypoplasticity as presented in Section 4.3 continues this line of thought.

Perusal of equations (2.37) and (2.38) reveals that the flow rule is 'non-associative', because $\dfrac{\partial\|\mathbf{B}\|-1}{\partial\mathbf{T}}$ need not be parallel to $-\mathbf{B}$, see for example Fig. 2.11. This has been shown by Niemunis [162] www.AN and Wu and Niemunis [272, 274]. Plotting contours perpendicularly to the direction of $\mathbf{B}$ Wu and Niemunis [273] obtained surfaces similar to plastic potential surface $g(\mathbf{T})=0$ sometimes used to calculate $\mathbf{n}_g=(\partial g(\mathbf{T})/\partial\mathbf{T})$, see Fig. 2.8. In the early hypoplastic models the flow direction $-\vec{\mathbf{B}}$, being a by-product of the hypoplastic equation, could hardly be adjusted to experimental data. In particular, it was not possible to achieve purely deviatoric flow rule on the yield surface $y(\mathbf{T})=0$, which is an important feature for description of the critical state, see Section 2.4.

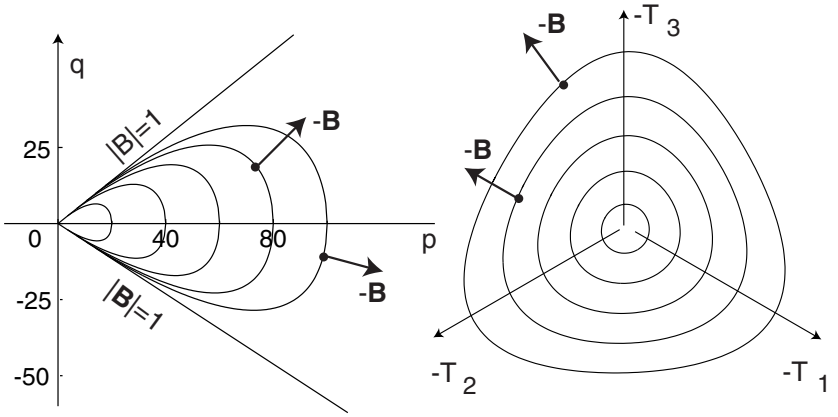

Figure 2.8: Hypoplastic potential surfaces. The tensors $-\mathbf{B}$ are outward normals (depicted as arrows) to these contours

In order to compare hypoplasticity with elastoplasticity Wu and Niemunis [273] defined a hypoplastic dissipation function $\mathbf{T}:\mathbf{D}^p$ defining the plastic strain rate $\mathbf{D}^p$ to be a portion of the strain amplitude that is accumulated after an infinitesimally small stress loop. However, such plastic strain rate is somewhat artificial in hypoplasticity. This idea has not been further developed.

2.3.2 Bounding surface

As already mentioned, some stress paths may surpass the hypoplastic yield surface. This can actually be concluded from Fig. 2.4, where fragments of the response envelopes bulge slightly out of the yield surface towards the shadowed areas.

Such paths can be constructed in a systematic manner maximizing the mobilized friction angle. Alternatively, a suitably formulated 'random walk' algorithm can reveal the possibility of surpassing $y(\mathbf{T})$. Numerical investigations of this problem demonstrated that *all* examined candidate functions allowed the stress path to overstep the yield surface and in some extreme cases a specially contrived stress path was practically unrestricted. Thus,

the existence of the hypoplastic yield surface does not guarantee yet that the attainable stresses are bounded, contrary to intuitive expectation. It can be shown that computations of the constitutive response beyond $y(\mathbf{T})$ are fraught with numerical difficulties like loss of invertibility and negative definite stiffness, see Section 3.1.

As we know, all stress paths should be bounded and therefore existence of a bounding surface $b(\mathbf{T}) = 0$ that encompasses all attainable stresses has been postulated. It should lie outside and be possibly close to the yield surface or preferably coincide with it. Due to the stress homogeneity of $\mathbf{H}(\mathbf{T}, \mathbf{D})$ the bounding surface, if it exists, is expected to have a conical form.

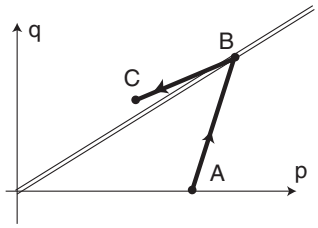

Figure 2.9: Experimental stress path going beyond the yield surface

Using the language of response envelopes the situation beyond $y(\mathbf{T})$ is as follows: the shift $\mathbf{N}\|\mathbf{D}\|\Delta t$ of the ellipse is greater than its radius $\|\mathsf{L} : \mathbf{D}\|\Delta t$ parallel to this shift. Therefore the initial stress lies *outside* of the response ellipse, see Fig. 2.10-left. This, however, does not preclude existence of a stress rate that would still increase the stress obliquity for which the shift $\mathbf{N}\|\mathbf{D}\|\Delta t$ can be even larger. Note also that for the stress increment $\mathring{\mathbf{T}}_A$ no corresponding strain rate exists and for $\mathring{\mathbf{T}}_B$ two rates are possible (Fig. 2.10 left). Only for specially (tangentially to the ellipse) chosen stress rates $\mathring{\mathbf{T}}_C$ the strain response can be uniquely determined. A similar situation can be observed for elastoplastic softening (Fig. 2.10 right).

The possibility of a stress path going beyond the yield surface was advocated experimentally [266, 272, 274]. Consider a drained triaxial test, as shown in Fig. 2.9, with a sample at the initial isotropic stress (A). The sample is vertically loaded, as usual, until the peak strength (B) is reached. Then an unconventional loading programme is applied. Both pressure p and deviatoric stress q are simultaneously decreased but in such way that the mobilized friction angle (stress obliquity) is slightly increased (C). Such increase could indeed be observed experimentally and interpreted as the stress path goes beyond the yield surface. The latter is assumed to be a straight line (0B) in the $p - q$ diagram.

This interpretation of the observed effect is controversial. The increase of the value of the mobilized friction angle can alternatively be ascribed to the sudden change of the direction of deformation which may cause a transitory increase of stiffness and strength[8]. Another explanation of the experimental observation may be related to the dependence of the peak friction angle on the void ratio (initially overlooked because early hypoplastic

[8]This effect of recent strain history can be described by an extended hypoplastic model, see Section 4.1

equations disregarded the influence of void ratio changes). A *relative* void ratio [71] is defined by

$$r_e = \frac{e - e_d(p)}{e_c(p) - e_d(p)} \tag{2.41}$$

wherein $e_d(p)$ denotes the smallest possible void ratio at a given pressure p, and $e_c(p)$ is the *critical* void ratio for which neither dilatancy nor contractancy prevails during shearing, see the following Section 2.4. Reduction of pressure p on the path BC at practically constant void ratio e causes a decrease of r_e and thus an increase of strength. Briefly, the experimentally observed drift from the radial unloading path along the yield surface may occur due to the fact that the actual stiffness and the yield state are not homogeneous functions of stress.

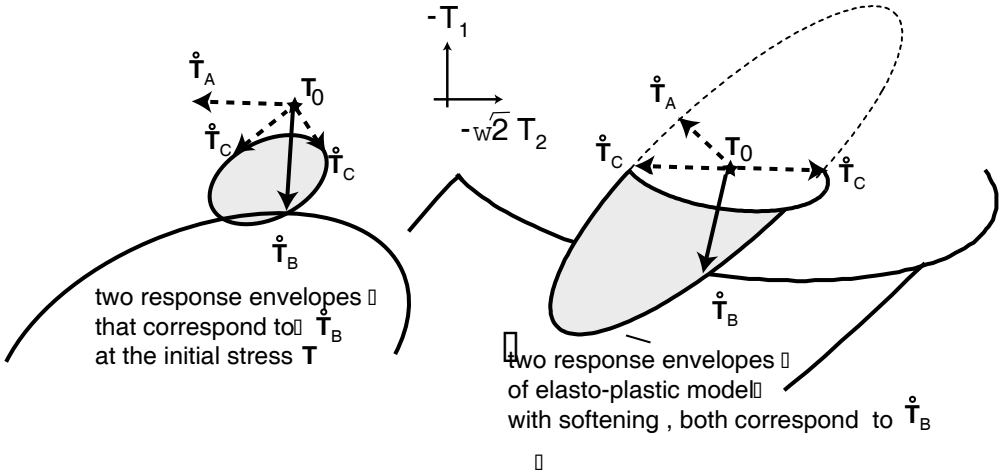

Figure 2.10: Left: two hypoplastic response envelopes plotted at $\mathbf{T}_0$ beyond the yield surface. Two different strain rates $\mathbf{D}$ return the same stress increment $\mathring{\mathbf{T}}_B$. Right: elastoplastic response envelope obtained with negative hardening modulus K. For comparison, the hypothetical elastic response envelope is presented with a dashed line. In both models we may have the following cases: for $\mathring{\mathbf{T}}_A$ no corresponding strain rate can be found; for $\mathring{\mathbf{T}}_B$ two strain rates exist (two response envelopes are passing through $\mathbf{T} + \mathring{\mathbf{T}}_B \Delta t$); for $\mathring{\mathbf{T}}_C$ the strain response can be unique (special case). Note also that the elastoplastic response envelope is concave and intersects itself

A theoretical criterion and a numerical procedure of investigation of the bounding surface have been formulated by Wu and Niemunis [274]. Suppose there exists a bounding surface $b(\mathbf{T}) = 0$ and it is an isotropic function of stress. Consider the stress $\mathbf{T}_b$ lying on the bounding surface so that $b(\mathbf{T}_b) = 0$. It is convenient to consider the principal components of $\mathbf{T}_b$ by choosing a coordinate system aligned with the respective eigenvectors in the stress space. The tensor normal to the bounding surface at $\mathbf{T}_b$ (and directed outwards)

$$\mathbf{Z} = \left.\frac{\partial b(\mathbf{T})}{\partial \mathbf{T}}\right|_{\mathbf{T}=\mathbf{T}_b}, \tag{2.42}$$

must be diagonal in this case. A true bounding surface cannot be surpassed so the stress rate $\mathring{\mathbf{T}}$ calculated for any $\mathbf{D}$ at $\mathbf{T}_b$ must be directed to the interior of the bounding surface, viz.

$$\mathbf{Z} : \mathring{\mathbf{T}} \leq 0. \tag{2.43}$$

Since all off-diagonal components of $\mathbf{Z}$ are zero we multiply only the diagonal components of $\mathring{\mathbf{T}}$ with $\mathbf{Z}$. Therefore, without loss of generality, only stress rates coaxial with stress need to be considered. According to inequality (2.43) we may seek for a direction of $\mathring{\mathbf{T}}$ such that

$$\max \left(\mathbf{Z} : \mathring{\mathbf{T}} \right)_{\mathbf{T}=\mathbf{T}_b} = 0. \tag{2.44}$$

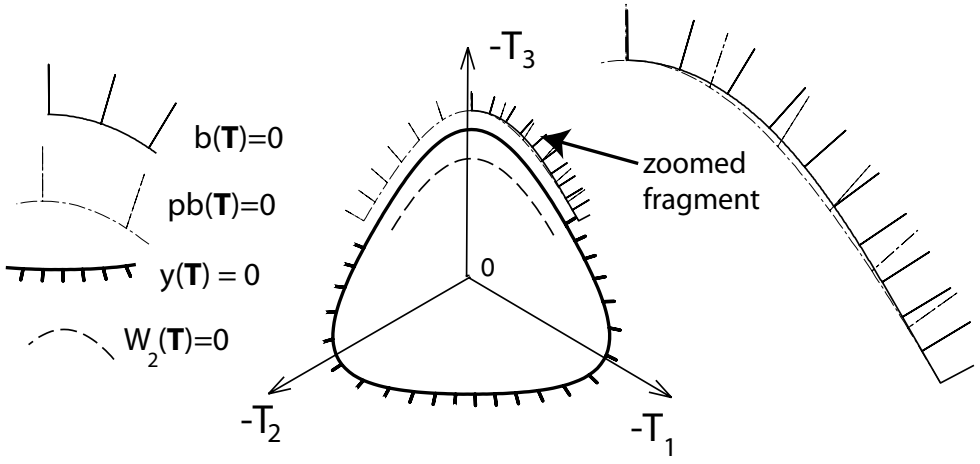

Figure 2.11: Cross-section of the yield surface $y(\mathbf{T}) = 0$ and the bounding surface $b(\mathbf{T}) = 0$ with the deviatoric plane. For comparison the pseudo-bounding surface $pb(\mathbf{T}) = 0$, cf. Equation (2.50), and vanishing second-order work surface $W_2(\mathbf{T}) \equiv \mathring{\mathbf{T}} : \mathbf{D} = 0$ are also presented. The short lines going to the outside of the bounding surface are plotted as normals to the response envelopes at their outermost points. These directions turn out to be perpendicular to $b(\mathbf{T}) = 0$ so the response envelopes must lie inside $b(\mathbf{T}) = 0$. On the pseudo bounding surface the (pseudo) outermost point of a response envelope is assumed to satisfy $\mathring{\mathbf{T}} = \lambda \mathbf{T}$. The short lines protruding from $pb(\mathbf{T}) = 0$ are perpendicular to the response envelope but not to $pb(\mathbf{T}) = 0$. The short lines going to the outside of the yield surface denote the flow direction $-\mathbf{B}$. These lines are not perpendicular to the yield surface (non-associative flow rule)

Formulating this problem in terms of $\mathbf{D}$ and requiring $\|\mathbf{D}\| = 1$ we obtain a target function $\mathbf{Z} : (\mathsf{L} : \mathbf{D} + \mathbf{N}\|\mathbf{D}\|) + \lambda(\|\mathbf{D}\| - 1)$ with maximum for $\lambda = 0$ and for

$$\mathbf{D}_{\max} \sim \mathbf{Z} : \mathsf{L}\,. \tag{2.45}$$

Substituting this result to (2.29) and to (2.44) we obtain a condition for stress

$$\boxed{\|\mathbf{Z} : \mathsf{L}\| = -\mathbf{Z} : \mathbf{N}.} \tag{2.46}$$

Note that $\mathbf{Z} : \mathbf{N} < 0$ holds. Since the normal direction $\mathbf{Z}$ is unknown, the criterion (2.46) alone is not sufficient to determine the bounding surface. If the stress $\mathbf{T}_b$ lies on the

bounding surface then due to stress homogeneity the proportional stresses $\lambda^2\mathbf{T}_b$ also do. Thus $b(\mathbf{T}) = 0$ must be a conical surface with the vertex at the origin of the stress space. From this fact we infer the orthogonality

$$\mathbf{T}_b : \mathbf{Z} = 0 \tag{2.47}$$

which can serve as the required additional criterion to determine $b(\mathbf{T}) = 0$. Summing up, stress $\mathbf{T}_b$ lies on the bounding surface if the following system of three equations:

$$\begin{cases} \|\mathbf{Z} : \mathsf{L}\| = -\mathbf{Z} : \mathbf{N} \\ \mathbf{T}_b : \mathbf{Z} = 0 \\ \|\mathbf{Z}\| = 1 \end{cases} \tag{2.48}$$

has a unique real solution for $\mathbf{Z} = \text{diag}[Z_1, Z_2, Z_3]$. Graphically, Fig. 2.12, cone B generated by normals to the planes tangential to the response envelope must be tangential to the plane π_2 normal to $\mathbf{0T}$.

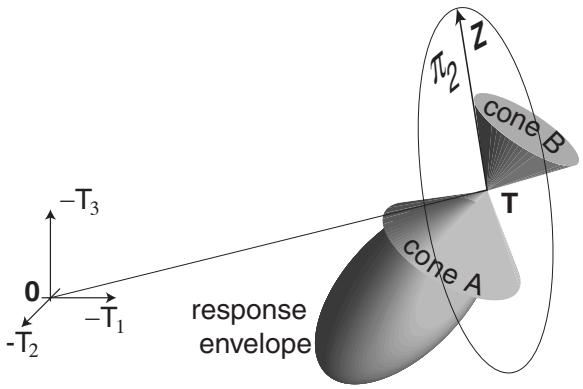

Figure 2.12: Planes passing through $\mathbf{T}$ and tangential to the response envelope form cone A. Their normals $\mathbf{Z}$ generate cone B expressed by (2.46). Plane π_2 perpendicular to $\mathbf{0} - \mathbf{T}$ is described by (2.47)

With the MATHEMATICA script we may test the solvability of the above system. The example below refers to the reference model presented in Section 2.5 .

```
getF[Tin_] :=
  Module[{tanpsi = 0, tanpsi2, cos3theta = 1, TT = {0, 0, 0}, TD = {0, 0, 0},F},
    TT = Tin/(Tin[[1]] + Tin[[2]] + Tin[[3]] );
    TD = TT - {1, 1, 1}*(TT[[1]] + TT[[2]] + TT[[3]])/3;
    tanpsi = Sqrt[3*(TD.TD)];
    tanpsi2 = tanpsi*tanpsi;
    cos3theta =
    If[tanpsi != 0, -Sqrt[6](TD[[1]]^3 + TD[[2]]^3 + TD[[3]]^3)*((TD.TD)^(-1.5)), 0];
     F = Sqrt[tanpsi2/8+(2-tanpsi2)/(2+Sqrt[2]*tanpsi*cos3theta)]-tanpsi/(2*Sqrt[2])
   ]
geta[figrad_] :=
    Module[{sfi,a},sfi=Sin[figrad*Pi/180];a=Sqrt[3] (3-sfi) /( 2 Sqrt[2] sfi)
    ]
TT = {-3.9, -1, -1}
TT = TT /(TT[[1]] + TT[[2]] + TT[[3]] )
```

```
TD  = TT - {1, 1, 1} *( TT[[1]] + TT[[2]] + TT[[3]])/3;
a = N[geta[30]];
eF = getF[TT];
LL = N[ eF* IdentityMatrix[3] + a*a* Outer[Times, TT, TT] ];
NN = N[ Simplify[a*eF*(TT + TD)]];
zz = Array[z, {3}];
sol = Solve[{ Sqrt[zz.((LL.LL).zz)] == -zz.NN , zz.TT == 0, zz.zz == 1},
             {zz[[1]], zz[[2]], zz[[3]]} ]
```

For the special case $T_2 = T_3$ the respective partial derivatives Z_2 and Z_3 are also equal, which allows us to find a stress on the surface $b(\mathbf{T}) = 0$ from

$$\begin{cases} \mathbf{T}_b - \mathbf{1}\dfrac{\mathbf{T}_b : \mathbf{T}_b}{\operatorname{tr} \mathbf{T}_b} &= \mathbf{Z} \\ \|\mathbf{Z} : \mathsf{L}\| &= -\mathbf{Z} : \mathbf{N} \end{cases} \tag{2.49}$$

see Fig 2.13. We may use this solution as a starting point for numerical (incremental) determination of bounding surface. As already mentioned, without loss of generality the whole calculation can be performed using diagonal tensors only. Deviatoric cross-sections of the bounding surface $b(\mathbf{T})$, the yield surface $y(\mathbf{T})$ and two other surfaces discussed elsewhere is presented in Fig. 2.11.

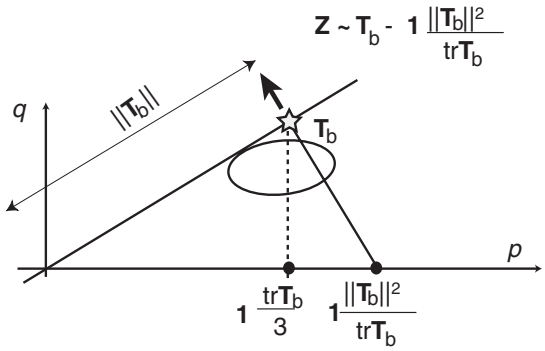

Figure 2.13: Direction of $\mathbf{Z}$ for an axially symmetric stress state

The response *ellipsoid* $o(\mathbf{T}) = 0$ plotted in a three-dimensional diagram for $\mathbf{T}_b$ is tangential to the bounding surface (from the inside) but their touching point does not necessarily lie on the line $\mathbf{0T}_b$, as shown in Fig. 2.14(top).

Another method [119, 219] for evaluation of $b(\mathbf{T})$ was proposed in the early nineties. It was based on the following much simpler criterion: the stress $\mathbf{T}$ was said to lie on the bounding surface if the equation

$$\alpha \cdot \mathbf{T} = \mathring{\mathbf{T}} \quad \text{with} \quad \|\mathbf{D}\| = 1 \tag{2.50}$$

had exactly one solution α. However, careful inspection revealed that this criterion is applicable for axially symmetric states only. For general stress states it is insufficient and generates a *pseudo*-bounding surface.

In Figure 2.14 the yield surface, bounding surface and two response envelopes are presented in 3-d space. It can be seen that the pseudo bounding surface can be surpassed because a fragment of the response envelope lies outside of this surface (dashed line).

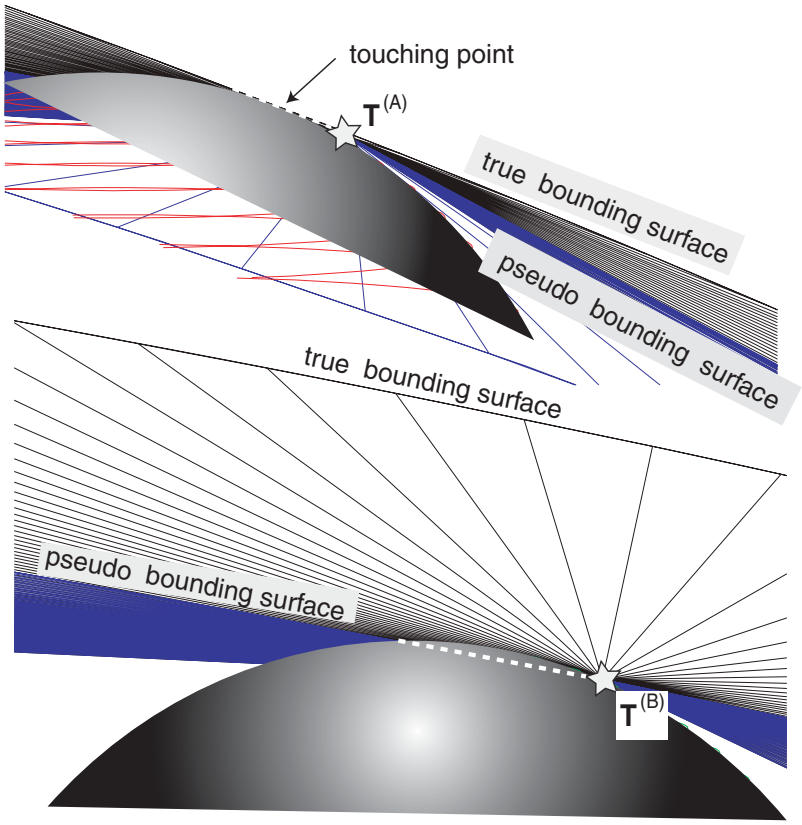

Figure 2.14: Parts of two response envelopes for stress $\mathbf{T}^{(A)}$ on the true bounding surface (above), and for $\mathbf{T}^{(B)}$ on the pseudo bounding surface (below) as seen by the observers situated exactly on the respective **0T**-lines and looking towards the origin of the coordinate system. The bounding surface and the pseudo bounding surface are marked by radial lines going out from the origin of the stress space. The fragments of the response ellipsoids (shadowed spherical surfaces) are calculated for the initial stresses (denoted by star) that is lying on the true bounding surface (upper view) and on the pseudo bounding surface (lower view). It can be seen that a part of the response ellipsoid lies beyond the pseudo bounding surface (lower picture) whereas the upper response ellipsoid is tangential to the true bounding surface from the inside

Bearing in mind problems with invertibility beyond the yield surface (see also Section 3.1.1) one may postulate the bounding surface to be identical with the yield surface, i.e. $y(\mathbf{T}) = b(\mathbf{T})$. This so-called hypoplastic consistency or limit surface consistency condition [32,39,51] is an important difference between the hypoplastic constitutive model CLoE, developed in Grenoble, and the here discussed Karlsruhe version. In the latter such consistency is not obligatory.

In the language of response envelopes the limit surface consistency means that the response ellipse for $\mathbf{T}_y$ must be tangent to the *yield* surface. If the initial stress $\mathbf{T}_y$ lies on the yield

surface it must also be the (only) point where the ellipse and the yield surface touch each other. The outer normal directions of these surfaces must therefore be parallel. With the abbreviations $B_{ij} = L^{-1}_{ijkl} N_{kl}$ and $B'_{ijkl} = (\partial B_{ij}/\partial T_{kl})$ the direction in the stress space, outer normal to $y(\mathbf{T})$, is

$$\frac{\partial y(\mathbf{T})}{\partial T_{ij}} = \frac{1}{\|\mathbf{B}\|} B_{kl} B'_{klij} \tag{2.51}$$

If the equation of the bounding surface is supposed to be identical with (2.38), i.e. with $y(\mathbf{T}) \equiv \|\mathbf{B}\| - 1 = 0$ then the response envelope should be tangential to this surface. The touching point corresponds to $\mathring{\mathbf{T}} = \mathbf{0}$ i.e. to $\mathbf{D} \sim -\mathsf{L}^{-1} : \mathbf{N}$. Differentiation of $o(\mathring{\mathbf{T}})$ given by (2.22) with respect to $\mathring{\mathbf{T}}$ at $\mathring{\mathbf{T}} = \mathbf{0}$ gives the direction

$$\left.\frac{\partial o(\mathring{\mathbf{T}})}{\partial \mathring{\mathbf{T}}}\right|_{\mathring{\mathbf{T}}=\mathbf{0}} = -2\mathbf{B} : \mathsf{L}^{-1} \tag{2.52}$$

of the outer normal to the response envelope. If we align the axes of the stress rate space with the ones of the stress space, then the direction normal to $o(\mathring{\mathbf{T}})$ should be parallel to the direction normal to $y(\mathbf{T})$, i.e.

$$\boxed{B_{ij} L^{-1}_{ijmn} = \lambda B_{ij} B'_{ijmn}.} \tag{2.53}$$

Under this condition the bounding surface and the yield surface can coincide. λ is a proportionality factor. In Section 4.3.4, we demonstrate how to achieve the coincidence of $y(\mathbf{T})$ and $b(\mathbf{T})$ introducing a small modification of the linear part of the constitutive equation.

2.4 Implementation of the critical state

Early versions of the hypoplastic model were independent of the void ratio e. Equation (2.27) was used with different sets of material constants $C_1, \ldots, C_4$ for loose and for dense sand. In order to

- take into account changes in e during a mechanical process
- cover a broader range of densities and stresses
- constitute a framework for usage of general material constants (pressure and density independent)

several comprehensive hypoplastic models have been proposed by Wu, Gudehus and Bauer [10, 11, 71, 268, 270]. The constants $C_1, \ldots, C_4$ became functions of the void ratio. This was done keeping C_1/C_2 and C_3/C_4 constant and introducing a product of two new functions $f_s(\operatorname{tr}\mathbf{T}, e)$ and $f_d(\operatorname{tr}\mathbf{T}, e)$. They collectively describe the barotropy (=stress level dependence) and the pycnotropy (=density dependence) of the hypoplastic stiffness. Function $f_s(\operatorname{tr}\mathbf{T}, e)$ consists of two sub-factors (introduced for reasons of convenience)

$$f_s(\operatorname{tr}\mathbf{T}, e) = f_e(\operatorname{tr}\mathbf{T}, e) f_b(\operatorname{tr}\mathbf{T}) \tag{2.54}$$

and expresses the overall increase of stiffness during proportional, in particular isotropic, loading, see Section 2.5.1. The function $f_d(\operatorname{tr}\mathbf{T}, e)$ expresses the shear-induced dilatancy and substitutes the Casagrande's [29] critical state (CS) concept established by Roscoe and Burland [206] and by Schofield and Wroth [217] in form of the critical state soil mechanics (CSSM). It postulates that for a given stress level $p = -\frac{1}{3}\operatorname{tr}\mathbf{T}$ a unique critical void ratio $e_c(p)$, and a unique deviatoric stress[9] $q = \sqrt{\frac{3}{2}}\|\mathbf{T}^*\|$ exist, for which perfectly plastic isochoric flow ($\mathbf{D} \neq \mathbf{0}, \mathring{\mathbf{T}} = \mathbf{0}, \operatorname{tr}\mathbf{D} = 0$) is possible. Plotting such states in $p-q-e$ space one obtains the critical state line (CSL). The projections of this line onto $p-q$ and $p-e$ planes are also referred to as CSLs. In view of (2.37) and (2.38) the hypoplastic model (2.29) satisfies the CS requirements if $\operatorname{tr}\mathbf{B} = 0$ and $\|\mathbf{B}\| = 1$ occur simultaneously for $e = e_c$. The critical void ratio e_c is not a material constant but a function of the mean stress. For clays, and approximately also for sands, this function decreases linearly with $\ln p$, as it is shown in $e-\ln(p/p_0)$ diagram in Fig. 2.15. The function $e_c(p)$ needs, of course, some material constants but we defer the definition of $e_c(p)$ until Section 2.5. The most important fact about the CS is that the functions $e_c(p)$ and $q = M_C p$ describe states (i.e. combinations (p, q, e)) which are intrinsically preferred by the material during monotonic shearing. If the monotonic shear deformation is homogeneous and sufficiently large then the critical state is asymptotically reached. Thus dense sands with $e < e_c$ tend to dilation $\dot{e} > 0$ ($\dot{p} > 0$), and loose sands $e > e_c$ tend to contraction $\dot{e} < 0$ ($\dot{p} < 0$) during deviatoric loading under isobaric $p = \text{const.}$ (isochoric $e = \text{const.}$) conditions. In both cases the current state (p, q, e) tends towards the CSL. Under isochoric conditions the void ratio is constant so the current state (p, q, e)) tends towards the CSL by means of increasing or decreasing the mean effective stress p for dense and loose sand, respectively, see Fig. 2.15. These processes are overlaid by an increase of q and manifest themselves as climbing up or sliding down (softening, liquefaction) of the stress path along the Coulomb line. Let us remark that experimental determination of CS is rather difficult because it requires considerable shear deformations during which inhomogeneities of deformation (onset of

[9] Let us assume a fixed Lode's angle here, say isotropic compression with $\theta^{Lode} = 0$ and $q = M_c p = \frac{6\sin\varphi_c}{2-\sin\varphi_c} p$. An anisotropic critical void void has been implemented to hypoplasticity in [168].

shear bands) are unavoidable.

In the stress space, the CSL corresponding to the yield condition $\|\mathbf{B}\| - 1 = 0$ at $e = e_c$ is called the residual strength criterion. For initially dense soils the peak strength precedes a much lower residual strength which is approached as the soil dilates.

The dilatancy means a shear-volumetric coupling. Let a state of soil (a point in the $p - q - e$ space, Fig. 2.15) be moving towards the CSL during isochoric shearing, i.e. $e - e_c(p) \to 0$ and $q - M_C p \to 0$. This purely deviatoric deformation generates not only a shear stress but also $\dot{p} \neq 0$. Conversely, isobaric shearing generates both shape and volume changes, i.e. $\operatorname{tr}\mathbf{D} = \dot{e}/(1+e) \neq 0$. With isotropic linear elasticity and Roscoe's variables (see also Section 3.2) $p = -\frac{1}{3}(T_1 + 2T_2)$, $q = -(T_1 - T_2)$, $\dot{\epsilon}_\mathrm{v} = -(D_1 + 2D_2)$, $\dot{\epsilon}_q = -\frac{2}{3}(D_1 - D_2)$ we would have

$$\begin{Bmatrix} \dot{p} \\ \dot{q} \end{Bmatrix} = \begin{bmatrix} K & 0 \\ 0 & 3G \end{bmatrix} \begin{Bmatrix} \dot{\epsilon}_\mathrm{v} \\ \dot{\epsilon}_q \end{Bmatrix} \tag{2.55}$$

wherein the elastic moduli are $K = \frac{1}{3}E/(1-2\nu)$ and $G = \frac{1}{2}E/(1+\nu)$. Zero off-diagonal terms preclude a cross-coupling, i.e. no dilatancy/contractancy $\dot{\epsilon}_\mathrm{v}$ during isobaric shearing (with $\dot{p} = 0$) and no pressure changes during isochoric shearing (with $\dot{\epsilon}_\mathrm{v} = 0$) is possible.

Traditionally, the residual effective stresses obtained in undrained tests are said to lie on the steady state (SS) line. It has been experimentally shown that SS and CS coincide [17] so indeed a unique CS (asymptotic state) exists for both drained and undrained shear tests. This is in accordance with CSSM. It is a simplifying *assumption*, however, that a unique CS holds for all directions of shear deformation at a common e or p. The experimental tests show, for example, that the triaxial compression and extension tests lead to slightly different critical p, e values. The strains necessary to reach the CS may be very large and thus the results may be blurred by the localization of deformation in shear bands, as demonstrated by Desrues *et al.* [52]. Generally, the CS concept could be enriched by consideration of

- the influence of the intermediate principal stress [280],
- the influence of fabric [245, 283],
- the quasi steady state QSS (implementation of the PTL),

especially if natural spatial fluctuations of state variables are disregarded. Recent findings on the fabric effects in soil behaviour have been collected in the textbook by Oda and Iwashita [183].

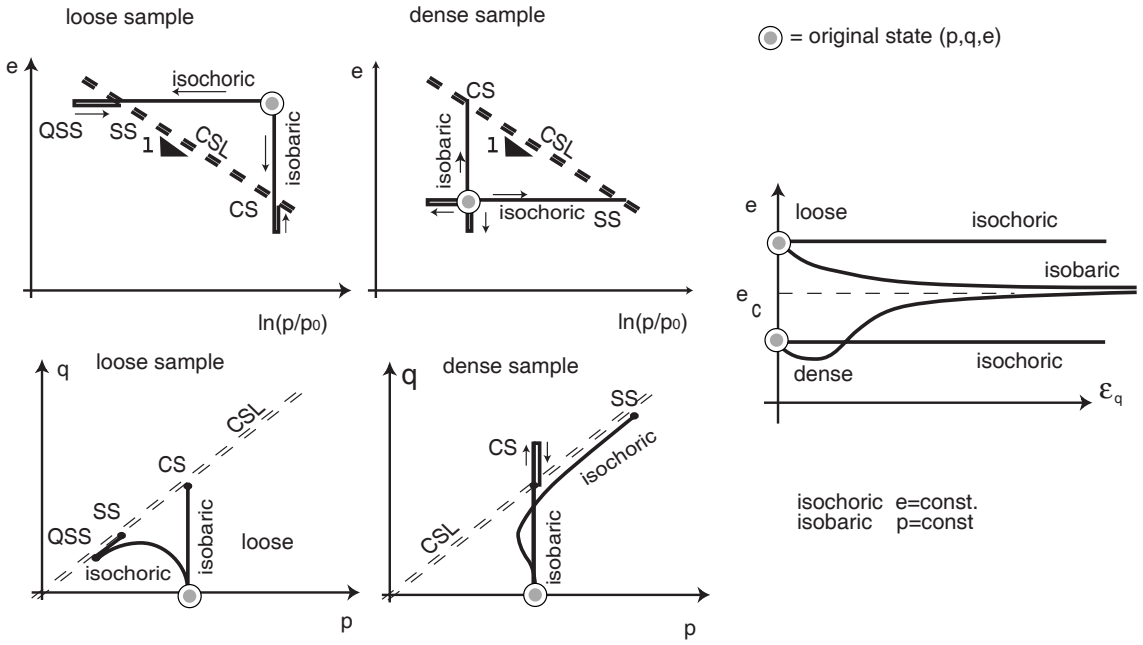

Figure 2.15: The critical state line is an attractor for various kinds of shearing monotonous ϵ_q. The states below the critical line are relatively dense and tend to dilation if sheared. The states above CSL are relatively loose and spontaneously tend to compaction. Under isochoric shearing an increase or a decrease of the mean effective pressure p is observed, respectively. To be exact we notice that the evolution is not monotonic. Stress paths for undrained loose samples reveal the phenomenon of the so-called quasi steady state (QSS). These states are observed to lie on the so-called phase transformation line (PTL) similar to CSL. These phenomena are rather subtle, strongly anisotropic and depend on sample preparation [283]. According to Gudehus they may be related to localization of deformation or dispersion of grains of different size. Dafalias [45] suggests that below PTL dominates sliding of grains and beyond PTL dominates rolling. Some recent discrete element tests indicate a continuous decrease of contacts per grain (coordination number) beyond PTL

By assumption, for $e = e_c$ we have $f_d(e, \mathbf{T}) = 1$ and for this case the CS condition $\operatorname{tr}\mathbf{B} = 0$ and $\|\mathbf{B}\| = 1$ imposes a constraint on the material constants in (2.29), in particular on $C_1, \ldots, C_4$ in (2.27). This enabled Bauer [11] to formulate the following simple expression:

$$\mathring{\mathbf{T}} = f_s \left[\overbrace{(\hat{a}^2 \mathsf{I} + \hat{\mathbf{T}}\hat{\mathbf{T}})}^{=\hat{\mathsf{L}}} : \mathbf{D} + f_d \overbrace{\hat{a}\,(\hat{\mathbf{T}} + \hat{\mathbf{T}}^*)}^{=\hat{\mathbf{N}}} \|\mathbf{D}\| \right] \tag{2.56}$$

wherein $f_s = f_s(\operatorname{tr}\mathbf{T}, e)$ and $f_d = f_d(\operatorname{tr}\mathbf{T}, e)$ are the new functions ($f_d = 1$ for $e = e_c$) and

$$\hat{\mathbf{T}} = \mathbf{T}/\operatorname{tr}\mathbf{T} \quad \text{and} \quad \hat{\mathbf{T}}^* = \hat{\mathbf{T}} - \frac{1}{3}\mathbf{1} \tag{2.57}$$

are called the dimensionless stress and the dimensionless stress deviator, respectively. In (2.56) the quantities which are functions of $\hat{\mathbf{T}}$ are denoted with hat ($\hat{}$) for clarity. The function $\hat{a}(\hat{\mathbf{T}}) > 0$ is discussed in the following. We show that it can be used to define

a hypoplastic yield surface $y(\mathbf{T}) = 0$. The pleasant properties of the form (2.56) (with $f_d = 1$) are:

- the yield condition $\|\hat{\mathsf{L}}^{-1} : \hat{\mathbf{N}}\| - 1 = 0$ is equivalent to $\hat{a}(\hat{\mathbf{T}}) - \|\hat{\mathbf{T}}^*\| = 0$ so the equation of the critical yield surface (for $f_d = 1$) is simply

$$y(\mathbf{T}) \equiv \hat{a}(\hat{\mathbf{T}}) - \|\hat{\mathbf{T}}^*\| = 0 \tag{2.58}$$

- for $y(\hat{\mathbf{T}}) = \hat{a}(\hat{\mathbf{T}}) - \|\hat{\mathbf{T}}^*\| = 0$ the direction of flow is purely deviatoric: $\vec{\mathbf{D}} = -\hat{\mathsf{L}}^{-1} : \hat{\mathbf{N}} = -\frac{1}{a}\hat{\mathbf{T}}^*$, so $\operatorname{tr}(-\hat{\mathsf{L}}^{-1} : \hat{\mathbf{N}}) = 0$

The first property can be proven writing out $y(\mathbf{T}) \equiv \|\hat{\mathsf{L}}^{-1} : \hat{\mathbf{N}}\| - 1 = 0$. We substitute

$$\hat{\mathsf{L}}^{-1} = \frac{1}{\hat{a}^2}\left(\mathsf{I} - \frac{\hat{\mathbf{T}}\hat{\mathbf{T}}}{\hat{a}^2 + \hat{\mathbf{T}} : \hat{\mathbf{T}}}\right) \quad \text{and} \quad \hat{\mathbf{N}} = \hat{a}(\hat{\mathbf{T}} + \hat{\mathbf{T}}^*) \tag{2.59}$$

and solve (2.38) for $\hat{a}$, for example with MATHEMATICA

```
(* abbreviations: t=T , d= T^* , s = T+T^* , ss = s:s  etc. *)
y = Expand[(1/a (s - t st/(a^2 + tt)) )^2 - 1] /. {s^2-> ss,  t^2->  tt, s t-> st};
y1 = y /. { st -> 2 dd + 1/3, ss -> 1/3 + 4 dd , tt -> dd + 1/3, td -> dd };
Solve[y1 == 0, a]           (* Out[] a = Sqrt[dd] and five other solutions*)
```

The second property follows directly by substituting $\hat{a}^2 = \hat{\mathbf{T}}^* : \hat{\mathbf{T}}^* (= \hat{\mathbf{T}} : \hat{\mathbf{T}}^*)$ into $\operatorname{tr}(\hat{\mathsf{L}}^{-1} : \hat{\mathbf{N}})$.

A suitable expression for $\hat{a}(\hat{\mathbf{T}})$ that conforms with a desired shape of the yield surface can be easily derived comparing $y(\mathbf{T})$ with (2.58). Bauer [11] implemented in this way, e.g., the yield surface of van Eekelen [58] choosing

$$\hat{a} = \sqrt{\frac{8}{3}}\frac{\sin\varphi_c}{3 + \sin\varphi_c}\left[1 + \sqrt{\frac{8}{3}}\|\hat{\mathbf{T}}^*\|\,(1 - \cos(3\theta))\right]^{-1} \tag{2.60}$$

with $\cos(3\theta)$ given in (2.67), and v.Wolffersdorff [265] implemented the surface of Matsuoka and Nakai [148, 150], as shown in Section 2.5.

Contrary to earlier hypoplastic models, the formulation (2.56) incorporates *predefined* yield surface $y(\mathbf{T}) = 0$ and a predefined flow rule. The formal hypoplastic structure (2.29) is preserved and it is just a matter of convenience whether the rate equation (2.29) is used to find $y(\mathbf{T}) = 0$ or this yield surface is assumed prior to a particular expression for (2.29). For $f_d = 1$ the CS condition $\operatorname{tr}\mathbf{B} = 0$ is satisfied everywhere along the intersection line of the cone $\|\mathbf{B}\| = 1$ with the current deviatoric plane $p = \text{const}$. The barotropy factor f_s influences neither the yield surface nor the flow rule.

2.5 Reference model

The hypoplastic constitutive model formulated by Wolffersdorff [262, 265] is taken as reference in the following chapters. It has the usual form (2.29) supplemented by a scalar function $f_d(\mathrm{tr}\,\mathbf{T}, e)$, as originally proposed by Gudehus [71]:

$$\mathring{\mathbf{T}} = \mathsf{L} : \mathbf{D} + f_d \mathbf{N} \|\mathbf{D}\| \,. \tag{2.61}$$

The expressions for L and $\mathbf{N}$ satisfy the following two conditions at $f_d = 1$:

- the yield surface $y(\mathbf{T})$ is identical with the one formulated by Matsuoka and Nakai [148]

$$y_{M-N}(\mathbf{T}) \equiv -\frac{I_1 I_2}{I_3} - \frac{9 - \sin^2\varphi_c}{1 - \sin^2\varphi_c} = 0 \tag{2.62}$$

  with stress invariants $I_1 = \mathrm{tr}\,\mathbf{T}$, $I_2 = \frac{1}{2}\left[\|\mathbf{T}\|^2 - (I_1)^2\right]$ and $I_3 = \det(\mathbf{T})$.

- the flow direction on the yield surface $y(\mathbf{T})$ is purely deviatoric, i.e. $\mathrm{tr}\,\mathbf{B} = 0$

These conditions enable a description of the critical states, as it was already outlined in Section 2.4.

The mathematical representation of $\mathsf{L}(\mathbf{T}, e)$ and $\mathbf{N}(\mathbf{T}, e)$ is the following:

$$\mathsf{L} = \frac{f_b\, f_e}{\hat{\mathbf{T}} : \hat{\mathbf{T}}} a^2 \left(\left(\frac{F}{a}\right)^2 \mathsf{I} + \hat{\mathbf{T}}\hat{\mathbf{T}} \right) = \frac{f_b\, f_e}{\hat{\mathbf{T}} : \hat{\mathbf{T}}} \hat{\mathsf{L}} \,, \tag{2.63}$$

$$\mathbf{N} = \frac{f_b\, f_e}{\hat{\mathbf{T}} : \hat{\mathbf{T}}} a^2 \left(\frac{F}{a}\right) \left(\hat{\mathbf{T}} + \hat{\mathbf{T}}^* \right) = \frac{f_b\, f_e}{\hat{\mathbf{T}} : \hat{\mathbf{T}}} \hat{\mathbf{N}}, \tag{2.64}$$

$$a = \frac{\sqrt{3}(3 - \sin\varphi_c)}{2\sqrt{2}\sin\varphi_c} \,, \tag{2.65}$$

$$F = \sqrt{\frac{1}{8}\tan^2\psi + \frac{2 - \tan^2\psi}{2 + \sqrt{2}\tan\psi\cos 3\theta}} - \frac{1}{2\sqrt{2}}\tan\psi \,, \tag{2.66}$$

$$\tan\psi = \sqrt{3}\|\hat{\mathbf{T}}^*\| \quad , \quad \cos 3\theta = -\sqrt{6}\,\frac{\mathrm{tr}\,(\hat{\mathbf{T}}^* \cdot \hat{\mathbf{T}}^* \cdot \hat{\mathbf{T}}^*)}{\left[\hat{\mathbf{T}}^* : \hat{\mathbf{T}}^*\right]^{3/2}} \quad . \tag{2.67}$$

with $I_{ijkl} = \frac{1}{2}(\delta_{ik}\delta_{jl} + \delta_{il}\delta_{jk})$ and $(\hat{\mathbf{T}}\hat{\mathbf{T}})_{ijkl} = \hat{T}_{ij}\hat{T}_{kl}$. The form of equations (2.63) and (2.64) is slightly rearranged with respect to the original texts by Wolffersdorff [262, 265] in order to emphasize the similarity with (2.56). Obviously, the function $\hat{a}(\hat{\mathbf{T}})$ from the previous Section corresponds to the present F/a. The current a is a material constant

depending on the residual friction angle φ_c. The term $1/(\hat{\mathbf{T}} : \hat{\mathbf{T}})$ decreases with the stress obliquity $\hat{\mathbf{T}}$, which makes the overall stiffness smaller with ab approach to the yield surface. This factor reaches its maximum $1/(\hat{\mathbf{T}} : \hat{\mathbf{T}}) = 3$ for the isotropic case $\hat{T}_{ij} = \frac{1}{3}\delta_{ij}$.

The function (2.67) for θ is formally identical with the well known function of Lode's angle

$$\theta^{Lode} = \frac{1}{3}\arccos\left(-\frac{3}{2}\sqrt{3}J_3/J_2^{3/2}\right) \quad \text{with} \quad J_2 = \frac{1}{2}\|\mathbf{T}^*\| \quad \text{and} \quad J_3 = \det(\mathbf{T}^*) \tag{2.68}$$

however they take *different arguments*, namely $\mathbf{T}$ and $\hat{\mathbf{T}}$, respectively. Therefore the angle θ is *not* always identical with the Lode's angle:

- $\theta^{Lode} = \pi/3 - \theta$ if the stress components are negative (as assumed here and by Wolffersdorff)
- $\theta^{Lode} = \theta$ if the stress components are positive (tensile stress, not relevant for soils)

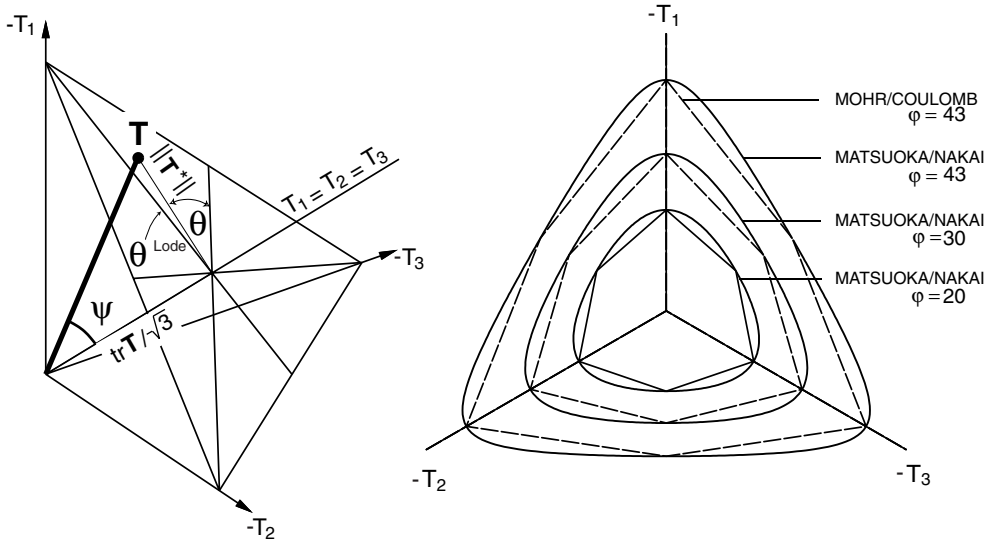

Figure 2.16: Explicit yield surfaces $y(\mathbf{T})$ by Matsouka and Nakai [148] coincides with the Mohr-Coulomb surfaces for triaxial compression and for triaxial extension only

The angles ψ and θ are shown in Fig. 2.16. For triaxial compression and for hydrostatic stresses $F = 1$. For triaxial extension the factor $F(\mathbf{T})$ decreases with the stress obliquity, viz.

$$F = \begin{cases} 1 & \text{if } q/p > 0 \\ 1 + q/(3p) & \text{if } q/p < 0 \end{cases}$$

A simpler method to fit the hypoplastic yield surface to the surface by Matsuoka Nakai is proposed in Section 4.3.

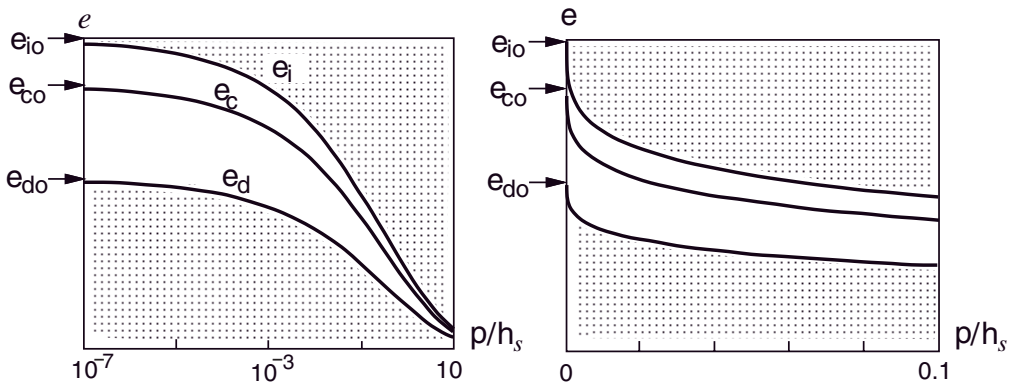

Figure 2.17: Decrease of the characteristic void ratios e_i, e_c and e_d with effective pressure $p = -\mathrm{tr}\,\mathbf{T}/3$ normalized by the granulate hardness h_s. Function (2.69) is plotted in logarithmic (left), and linear (right) p-scale

Finally, let us discuss the pycnotropy and barotropy functions. Gudehus [71] introduced three characteristic void ratio functions in his 'comprehensive' hypoplastic model:

- $e_i(p)$ describes the loosest possible state at a given pressure p. Such void ratios correspond to the isotropic compression starting from the minimum density;
- $e_c(p)$ denotes the critical void ratio discussed already in Section 2.4;
- $e_d(p)$ corresponds to maximum densification usually reached after cyclic shearing.

These functions are assumed to be affine to each other, namely, starting from different origins $e_{i0} > e_{c0} > e_{d0}$ (= material constants) at $\mathrm{tr}\,\mathbf{T} = 0$ they all decrease along with the same function $B(\mathrm{tr}\,\mathbf{T})$ proposed by Bauer [10]:

$$\frac{e_i}{e_{i0}} = \frac{e_c}{e_{c0}} = \frac{e_d}{e_{d0}} = \exp\left[-\left(\frac{-\mathrm{tr}\mathbf{T}}{h_s}\right)^n\right] = B(\mathrm{tr}\,\mathbf{T}). \tag{2.69}$$

The function $B(\mathrm{tr}\,\mathbf{T})$ contains two material constants:

- solid phase[10] hardness h_s
- exponent n

The function, say $e_c(\mathrm{tr}\,\mathbf{T})$, has finite limits e_{c0} and 0 for $\mathrm{tr}\,\mathbf{T} \to 0$ and $\mathrm{tr}\,\mathbf{T} \to -\infty$, respectively, whereas the conventional logarithmic compression curve is in this sense unrestricted. The characteristic void ratios e_i, e_c, e_d are supposed to describe three asymptotic

[10]Gudehus [76] proposed recently to use $B(\mathbf{T})$ as given in (2.69) also for clays. In this case h_s becomes argotropic (rate dependent) and the term 'hardness of the solid phase' seems more appropriate than 'granulate hardness' used in the past.

values (attractors) for isotropic compression, monotonic isochoric shearing and alternating shearing with $\dot{p} = 0$, respectively. The function $B(\operatorname{tr}\mathbf{T})$, in spite of having these nice limits (1 and 0), is not sufficiently precise to cover a large range of stress, so the parameters e_{c0}, n and h_s should be determined for a particular stress range of interest [81, 86], which is a common geotechnical practice anyway.

To be exact, the range of possible void ratios is not limited by the curves $e_i(p)$ from above and by $e_d(p)$ from below as shown in Fig. 2.17, this is merely the range of applicability of the reference hypoplastic model, beyond which the control is supposed to be passed to another constitutive relation. However, to author's knowledge, such relation has not been formulated yet. The curves $e_i(\operatorname{tr}\mathbf{T})$ and $e_d(\operatorname{tr}\mathbf{T})$ have been postulated a priori, i.e. differently to the yield or bounding surfaces, they do not follow from (2.61). Hypoplasticity admits that the evolving state $(e, \operatorname{tr}\mathbf{T})$ may leave the range of applicability of the model. This fact is numerically troublesome and a remedy is discussed in Section 4.3.8, see also [176] www.AN . Having the characteristic void ratios prescribed, two scalar factors for barotropy and pycnotropy f_e and f_d have been postulated [10, 71] and supplemented by another barotropy factor f_b that guarantees consistency of (2.61) with (2.69), see Subsection 2.5.1:

$$f_e(\operatorname{tr}\mathbf{T}, e) = \left(\frac{e_c}{e}\right)^{\beta} \quad , \tag{2.70}$$

$$f_d(\operatorname{tr}\mathbf{T}, e) = \left(\frac{e - e_d}{e_c - e_d}\right)^{\alpha} = r_e^{\alpha}, \tag{2.71}$$

$$f_b(\operatorname{tr}\mathbf{T}) = \left(\frac{e_{i0}}{e_{c0}}\right)^{\beta} \frac{h_s}{n} \frac{1 + e_i}{e_i} \left(\frac{-\operatorname{tr}\mathbf{T}}{h_s}\right)^{1-n} \left[3 + a^2 - a\sqrt{3}\left(\frac{e_{i0} - e_{d0}}{e_{c0} - e_{d0}}\right)^{\alpha}\right]^{-1} \tag{2.72}$$

r_e denotes the relative void ratio, see (2.41), and the new material constants are

- exponent α in $f_d()$
- exponent β in $f_e()$

The function $f_e(\operatorname{tr}\mathbf{T}, e)$ postulated in (2.70) is supposed to increase the overall stiffness for dense soils in comparison with loose ones at the same stress level independently of $\mathbf{D}$. The interpolation function $0 < f_d(\operatorname{tr}\mathbf{T}, e) < 1$ given in (2.71) affects the peak friction angle because now the yield surface reads

$$y(\mathbf{T}) \equiv f_d \, \|\mathbf{B}\| - 1 = 0 \,. \tag{2.73}$$

For $f_d = 0$, i.e. for $e = e_d$, the friction angle reaches the limit $\varphi = 90°$.

Small factors f_d increase the dilatancy at the peak stress. This deserves a short comment. For stresses $\mathbf{T}$ that lie on the yield surface, $y(\mathbf{T}) = 0$, the flow direction (for which $\mathring{\mathbf{T}} = \mathbf{0}$) is $\mathbf{D} \sim -\mathbf{B}$ and the dilatancy is

$$d(\mathbf{T}) = -\operatorname{tr}\mathbf{B}/\|\mathbf{B}^*\| \,. \tag{2.74}$$

with $\mathbf{B} = \mathsf{L}^{-1} : \mathbf{N} = \hat{\mathsf{L}}^{-1} : \hat{\mathbf{N}}$. Although the direction $\vec{\mathbf{B}}(\hat{\mathbf{T}})$ for a given stress ratio $\hat{\mathbf{T}}$ is not affected by f_d, one can reach higher stress ratios $\hat{\mathbf{T}}$ for smaller f_d and in this way the dilatancy at peak can become larger. In other words, the peak values of d increase as the the yield surface (=the peak stress ratio) is pushed outwards by small f_d in the model.

In a general case dilatancy is not restricted to the yield surface. For $y(\mathbf{T}) < 0$ we have to redefine d as the ratio of the volumetric strain rate to the deviatoric strain rate upon purely deviatoric stress paths. Since the plastic portion of the strain rate is not distinguished in hypoplasticity we use the total strain rates. In order to calculate the dilatancy we have to

1. inverse (2.61) to the form $\mathbf{D} = \mathbf{D}(\mathring{\mathbf{T}})$ using the method given in Subsection 3.1.1,
2. apply a purely deviatoric stress rate $\mathring{\mathbf{T}} = \mathring{\mathbf{T}}^*$
3. calculate $\mathbf{D}$ and finally $d = \operatorname{tr}\mathbf{D}/\|\mathbf{D}^*\|$

So defined dilatancy depends not only on stress but also on the direction of the deviatoric stress rate applied. For triaxial paths with $\operatorname{tr}\mathbf{T} = \text{const}$, only two such stress rates need to be considered, namely $\mathring{\mathbf{T}} = \mathring{\mathbf{T}}^* \sim \pm\,\operatorname{diag}(2, -1, -1)$. In Fig. 2.18 it is shown that the dilatancy calculated with the hypoplastic model fits relatively well the laboratory results.

In the reference hypoplastic model the dilatancy d depends on the void ratio, differently to the Rowe's postulate, cf. dilatancy theory in [207]. Also in some recently proposed elastoplastic models, e.g. [135], this assumption is left out.

The determination of the material constants appearing in functions f_e and f_d was presented by Bauer [10] and further researched by Herle [81, 86].

The last function $f_b(\operatorname{tr}\mathbf{T})$ of the reference model is given in (2.72). It enforces the consistency between the prediction of the model during isotropic compression and the curve e_i proposed by Gudehus and Bauer [10, 71]. Readers interested in (somewhat lengthy) derivation of (2.72) are referred to Subsection 2.5.1.

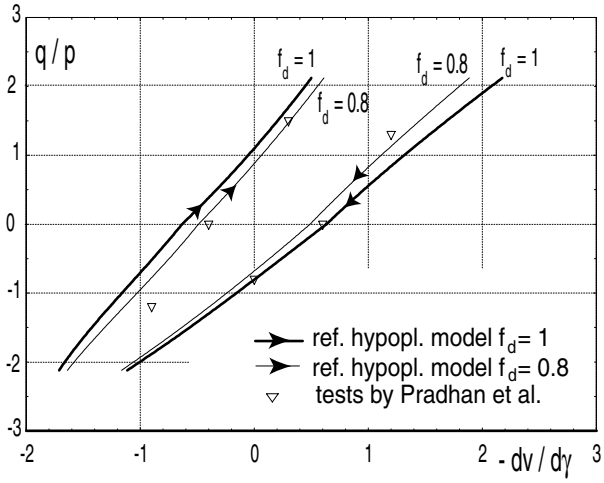

Figure 2.18: Dilatancy diagram obtained from the reference hypoplastic model with $f_d = 1$ and $f_d = 0.8$ and compared with experimental results [195] for dense sand. The experimental results for loose sands are very similar. In this figure the experimental points are calculated from *plastic* strain rates $\frac{\mathrm{d}v^p}{\mathrm{d}\gamma^p} \approx \frac{\mathrm{d}v}{\mathrm{d}\gamma} = \pm\sqrt{\frac{3}{2}d}$. In the hypoplastic calculation $\varphi = 27.7^\circ$ was set.

2.5.1 Barotropy factor f_b

As already mentioned, early versions of the hypoplastic constitutive model were formulated as first-order homogeneous functions of stress, i.e. $\mathbf{H}(\lambda\mathbf{T}, \mathbf{D}) = \lambda\mathbf{H}(\mathbf{T}, \mathbf{D})$, which implied that for $\mathbf{T} \to \mathbf{0}$ the stiffness vanished. Therefore, on one hand, too large strains were needed to approach a stress free state and on the other hand for extremely high pressures negative void ratio could be obtained. After Gudehus and Bauer [10,71] rewrote the hypoplastic equation in terms of dimensionless stress $\hat{\mathbf{T}} = \mathbf{T}/\mathrm{tr}\,\mathbf{T}$ and multiplied the obtained formula by a specially contrived function $f_b()$ these shortcomings were eliminated. It is evident that $B(\mathrm{tr}\,\mathbf{T})$ cannot be negative and for $-\mathrm{tr}\,\mathbf{T} \to 0$ stiffness vanishes slower than stress. Still, however, no stress path can depart from percolation limit $\mathbf{T} = \mathbf{0}$ unless exponent $n \geq 1$. Note that for $f_b = C_1 \mathrm{tr}\,\mathbf{T}\hat{\mathbf{T}} : \hat{\mathbf{T}}$ and for $F = f_e = 1$ the earlier version (2.27) (with restricted parameters) can be recovered.

Our present goal is to formulate a stress function $f_b(\mathrm{tr}\,\mathbf{T})$ that renders the hypoplastic model compatible with the postulated empirical compression curve

$$e \equiv e_i = e_{i0} \exp\left[-\left(\frac{3p}{h_s}\right)^n\right], \tag{2.75}$$

see Fig. 2.17. As already mentioned this curve describes the special case of isotropic compression passing through extremely loose states. It starts at the 'percolation limit' $p = 0$ and $e = e_{i0}$ and continues for $p > 0$ with $e > 0$ for $\mathrm{tr}\,\mathbf{T} \to \infty$. Moreover, at the limit $\mathrm{tr}\,\mathbf{T} \to 0$ the stiffness vanishes much slower than the stress.

For the special case of isotropic compression of a granulate in the loosest state $e = e_i$ we denote

$$f_{ei} = (e_c/e_i)^\beta = (e_{c0}/e_{i0})^\beta = \text{const.} \tag{2.76}$$

Let us derive a function $f_b(\operatorname{tr}\mathbf{T})$ consistent with Equation (2.75) for monotonic isotropic compression. We will write the relation between the rate of pressure $\dot{p}$ and the rate of the void ratio $\dot{e}$ using

$$\dot{p} = -\frac{1}{3}\delta_{ij}\mathring{T}_{ij}\,, \qquad \dot{e} = (1+e)D_{kl}\delta_{kl}\,, \tag{2.77}$$

$$D_{kl} = \frac{\dot{e}}{3(1+e)}\delta_{kl}\,, \quad \text{and} \quad \|\mathbf{D}\| = \frac{|\dot{e}|}{3(1+e)}\sqrt{3}\,. \tag{2.78}$$

The state of stress $\mathbf{T}$ remains isotropic so

$$\begin{aligned} T_{ij} = -p\delta_{ij}, \qquad \operatorname{tr}\mathbf{T} = -3p \qquad \hat{T}_{ij} = \frac{1}{\operatorname{tr}\mathbf{T}}T_{ij} = \frac{1}{3}\delta_{ij}, \\ \hat{T}^*_{ij} = \hat{T}_{ij} - \frac{1}{3}\delta_{ij} = 0 \quad \text{and} \quad \hat{\mathbf{T}} : \hat{\mathbf{T}} = \frac{1}{3}\frac{1}{3}\delta_{ij}\delta_{ij} = \frac{1}{3}\,. \end{aligned} \tag{2.79}$$

The constitutive equation for isotropic compression can be written in the following equivalent form

$$\begin{aligned} \dot{p} = -\frac{1}{3}\,\mathbf{1} : \mathring{\mathbf{T}} \;&=\; -\frac{1}{3}f_{ei}f_b\,(\,\mathbf{1} : \mathsf{L} : \mathbf{D} + f_{di}\,\mathbf{1} : \mathbf{N}\|\mathbf{D}\|)\,, \\ &=\; -\frac{1}{9(1+e)}f_{ei}f_b\left(L_{iikl}\delta_{kl}\dot{e} + f_{di}N_{ii}\sqrt{3}|\dot{e}|\right)\,, \\ &=\; -\frac{1}{9(1+e)}f_{ei}f_b\left(L_{iikk}\dot{e} + f_{di}N_{ii}\sqrt{3}|\dot{e}|\right)\,, \end{aligned} \tag{2.80}$$

wherein the value of f_{di} denotes the factor $f_d(e, \operatorname{tr}\mathbf{T})$ function calculated at $e = e_i$, i.e.

$$f_{di} = \left(\frac{e_{i0} - e_{d0}}{e_{c0} - e_{d0}}\right)^\alpha\,. \tag{2.81}$$

We calculate now the scalar quantity $L_{iikk} = \delta_{ij}L_{ijkl}\delta_{kl}$ for the reference model:

$$\begin{aligned} L_{iikk} \;&=\; \frac{1}{\hat{\mathbf{T}} : \hat{\mathbf{T}}}\mathbf{1} : \left(F^2\,\mathsf{I} + a^2\,\hat{\mathbf{T}}\hat{\mathbf{T}}\right) : \mathbf{1} = \frac{1}{1/3}\delta_{ij}\left(\delta_{ik}\delta_{jl} + a^2\frac{1}{3}\frac{1}{3}\delta_{ij}\delta_{kl}\right)\delta_{kl}\,, \\ L_{iikk} \;&=\; 3(3+a^2)\,. \end{aligned} \tag{2.82}$$

Note that due to the isotropic stress state we may substitute $F = 1$. Now we proceed similarly with $N_{ii} = \delta_{ij}N_{ij}$ keeping $F = 1$:

$$N_{ii} = \mathbf{1} : \mathbf{N} \;=\; \frac{Fa}{\hat{\mathbf{T}} : \hat{\mathbf{T}}}\mathbf{1} : \left(\hat{\mathbf{T}} + \hat{\mathbf{T}}^*\right) = \frac{a}{\frac{1}{3}}\delta_{ij}\hat{T}_{ij}3a\delta_{ij}\frac{1}{3}\delta_{ij} = 3a\,. \tag{2.83}$$

Finally we set the expressions for L_{iikk} and N_{ii} into the constitutive equation (2.80)

$$\dot{p} \;=\; -\frac{1}{9(1+e)} f_{ei} f_b \left(3(3+a^2)\dot{e} + f_{di} 3a\sqrt{3}|\dot{e}| \right) . \tag{2.84}$$

For isotropic compression with $\dot{e} < 0$

$$\dot{p} = -\left[\frac{1}{3(1+e)} f_b f_{ei} \left((3+a^2) - f_{di} a\sqrt{3} \right) \right] \dot{e} \, . \tag{2.85}$$

$$\tag{2.86}$$

Time differentiation of the compression curve (2.75) results in

$$\dot{e} \;=\; e_{i0} \exp\left[-\left(\frac{3p}{h_s} \right)^n \right] (-n) \left(\frac{3p}{h_s} \right)^{n-1} \frac{3}{h_s} \dot{p} = -\left(\frac{3p}{h_s} \right)^{n-1} \frac{3ne_i}{h_s} \dot{p}$$

or

$$\dot{p} = -\left(\frac{3p}{h_s} \right)^{1-n} \frac{h_s}{3ne_i} \dot{e} \tag{2.87}$$

which can be compared with final form (2.85) of the constitutive equation. From this comparison follows

$$f_b = \frac{1}{f_{ei}} \left(\frac{3p}{h_s} \right)^{1-n} \frac{3(1+e)h_s}{3ne_i} \left(3 + a^2 - f_{di} a\sqrt{3} \right)^{-1} . \tag{2.88}$$

Finally, substituting $e = e_i$ one obtains

$$f_b = \frac{1}{f_{ei}} \left(\frac{3p}{h_s} \right)^{1-n} \frac{3(1+e_i)h_s}{3ne_i} \left(3 + a^2 - f_{di} a\sqrt{3} \right)^{-1} , \tag{2.89}$$

which is identical with the expression (2.72) given in the previous subsection.

Chapter 3

Inspection

In this chapter we examine in some detail the following properties of the reference hypoplastic model: solvability , invertibility and mixed controllability of (2.29) using simple and composite components, second-order work, proportional paths, asymptotic behaviour and occurrence of localized bifurcation. These topics are of rather theoretical nature but sometimes a deeper insight may be helpful in formulation of new extensions of for a diagnosis of problems encountered numerically.

3.1 Solvability, invertibility and controllability

In laboratory experiment, soil samples may be loaded on the boundaries by application of prescribed displacements, tractions and pore pressure. Speaking of *element tests* we assume homogeneity of the stress and strain field throughout the sample. It is an open question, however, whether such assumption is justified and if the spatial fluctuation of the state variables should not be considered, e.g. choosing a fine FE discretization or treating such fluctuations as state variables. This subject is addressed shortly in Section 3.5.2. Here we start with an idealized situation of perfect uniformity of stress and deformation within a representative volume element. Of course, soils are full of spatial fluctuations with a complex nature, different characteristic lengths etc. so ignoring fluctuation in our mathematical description of field we use some *equivalent modeling* on the constitutive level, for example a back stress. With such artificial homogeneity we may conveniently simulate soil behaviour numerically, calculating evolution of state variables (stress, void ratio) for single material points and using interpolation functions. However, spatial fluctuations may be useful if one needs physical (measurable) interpretation of some state variables.

In numerical calculation we may distinguish stress or strain or mixed controlled tests depending on the components of rates $\mathring{\mathbf{T}}$ and $\mathbf{D}$ which are prescribed. In other words, we

follow a strain path or a stress path or a path in a mixed stress-strain space during the calculation.

In kinematically controlled numerical tests (i.e. with known $\mathbf{D}$) the material response $\mathring{\mathbf{T}}$ of (2.29) exists and is always unique. The question arises, for which states (2.29) can be inverted, i.e. be solved for strain rate $\mathbf{D}$ at a given stress rate $\mathring{\mathbf{T}}$. Further questions concern mixed control problems in which some components of $\mathbf{D}$ and the complementary components of $\mathring{\mathbf{T}}$ are given. These questions can also considered in terms of *composite variables*, for example Roscoe's variables p, q and D_v, D_q obtained from a linear combination of components of $\mathbf{D}$ and of $\mathring{\mathbf{T}}$ as shown in Section 3.2. The solvability problem of the constitutive equation for various combinations of prescribed rate components will also be revisited in the next chapters discussing extended versions of hypoplasticity.

In this section the matrix notation is used in which the components of 2-nd rank tensors are written in a from of 9×1 column matrix with the index $k = 1 \dots 9$ going with the pair (i, j) (tensorial indices) in the following sequence:

$$(1,1), (2,2), (3,3), (1,2), (2,1), (1,3), (3,1), (2,3), (3,2).$$

With this index convention the 4-th rank tensors $3 \times 3 \times 3 \times 3$ become 9×9 matrices. In particular we have:

$$\mathbf{1} = \{1,1,1,0,0,0,0,0,0\}^T , \qquad \mathbf{0} = \{0,0,0,0,0,0,0,0,0\}^T \tag{3.1}$$

$$\mathsf{I} = \begin{bmatrix} 1 & & & & & & & & \\ & 1 & & & & & & & \\ & & 1 & & & & & & \\ & & & \frac{1}{2} & \frac{1}{2} & & & & \\ & & & \frac{1}{2} & \frac{1}{2} & & & & \\ & & & & & \frac{1}{2} & \frac{1}{2} & & \\ & & & & & \frac{1}{2} & \frac{1}{2} & & \\ & & & & & & & \frac{1}{2} & \frac{1}{2} \\ & & & & & & & \frac{1}{2} & \frac{1}{2} \end{bmatrix}, \quad \mathsf{J} = \begin{bmatrix} 1 & & & & & & & & \\ & 1 & & & & & & & \\ & & 1 & & & & & & \\ & & & 1 & & & & & \\ & & & & 1 & & & & \\ & & & & & 1 & & & \\ & & & & & & 1 & & \\ & & & & & & & 1 & \\ & & & & & & & & 1 \end{bmatrix} \tag{3.2}$$

Matrices I and J correspond to two 4-th rank unit tensors: $I_{ijkl} = \frac{1}{2}(\delta_{ik}\delta_{jl} + \delta_{il}\delta_{jk})$ and $J_{ijkl} = \delta_{ik}\delta_{jl}$. The former one insures that in $\mathring{\mathbf{T}} = \mathsf{I}\mathbf{D}$ the output $\mathring{\mathbf{T}}$ is symmetric irrespectively of symmetry in $\mathbf{D}$ as mentioned already in Section 1.3. The 9×1 matrices are sometimes (informally) called 'vectors'. In this section we will write for example $\mathbf{T}^T\mathbf{T}$ and $\mathbf{T}\mathbf{T}^T$ instead of $\mathbf{T} : \mathbf{T}$ and $\mathbf{T}\mathbf{T}$, respectively.

Since the nonlinear part $\mathbf{N}(\mathbf{T})\|\mathbf{D}\|$ is an isotropic function of stress it is always coaxial with $\mathbf{T}$. Without loss of generality we choose the coordinate system to be parallel to the

principal stress directions. Doing so we obtain:

$$\begin{array}{rcl}
\{\mathbf{T}\} &=& [\ T_{11}\ \ T_{22}\ \ T_{33}\ \ 0\ \ 0\ \ 0\ \ 0\ \ 0\ \ 0\ ]^{\mathrm{T}} \\
\{\mathring{\mathbf{T}}\} &=& [\ \mathring{T}_{11}\ \ \mathring{T}_{22}\ \ \mathring{T}_{33}\ \ \mathring{T}_{12}\ \ \mathring{T}_{21}\ \ \mathring{T}_{13}\ \ \mathring{T}_{31}\ \ \mathring{T}_{23}\ \ \mathring{T}_{32}\ ]^{\mathrm{T}} \\
\{\mathbf{D}\} &=& [\ D_{11}\ \ D_{22}\ \ D_{33}\ \ D_{12}\ \ D_{21}\ \ D_{13}\ \ D_{31}\ \ D_{23}\ \ D_{32}\ ]^{\mathrm{T}} \\
\{\mathbf{N}\} &=& [\ N_{11}\ \ N_{22}\ \ N_{33}\ \ 0\ \ 0\ \ 0\ \ 0\ \ 0\ \ 0\ ]^{\mathrm{T}}
\end{array} \tag{3.3}$$

and

$$\mathsf{L} = \left[\begin{array}{ccc|cc|cc|cc}
L_{1111} & L_{1122} & L_{1133} & & & & & & \\
L_{2211} & L_{2222} & L_{2233} & & & & & & \\
L_{3311} & L_{3322} & L_{3333} & & & & & & \\
\hline
 & & & L_{1212} & L_{1221} & & & & \\
 & & & L_{2112} & L_{2121} & & & & \\
\hline
 & & & & & L_{1313} & L_{1331} & & \\
 & & & & & L_{3113} & L_{3131} & & \\
\hline
 & & & & & & & L_{2323} & L_{2332} \\
 & & & & & & & L_{3223} & L_{3232}
\end{array}\right] . \tag{3.4}$$

The off-diagonal components of $\mathbf{N}$ (i.e. components $N_4, \ldots N_9$) disappear since $\mathbf{N}(\mathbf{T})$ is an isotropic function. However, we must preserve the off-diagonal terms of $\mathbf{D}$ which are independent of $\mathbf{T}$. These components generate, of course, a stress rate $\mathring{\mathbf{T}}$ which is not necessarily diagonal.

Tensorial expressions were often derived and manipulated with (somewhat lengthy) MATHEMATICA script `nova.m` available from www.AN . It contains many useful simplifying rules and uses tensorial notation, for example `T[i,j]`. The results from `nova.m` can be conveniently translated to matrix notation with the following MATHEMATICA module:

```
transfer99[expression_]:= Module[ {reindex, ii, jj, i9,j9,a,ttQ,iQ,xrules},
ttQ[x_] := MemberQ[{T, D}, x];  (* declare your tensors here, e.g. T and  D*)
iQ[x_] := MemberQ[{1, 2, 3}, x];
i9 = {1,2,3,1,2,1,3,2,3}; j9 = {1,2,3,2,1,3,1,3,2}; a = Table[0, {9}, {9}];
For[ii=1 , ii < 10,  ii++, For[jj=1,jj<10,jj++ , a[[ii,jj]] =
    Evaluate[expression /. {i->i9[[ii]], j->j9[[ii]], k->i9[[jj]], l->j9[[jj]]} ]]] ;
xrules = {\[Delta][i_?iQ, i_?iQ] -> 1,
          \[Delta][i_?iQ, j_?iQ] /; Not[SameQ[i, j]] -> 0,
         tr[x_?ttQ] -> (x[1, 1] + x[2, 2] + x[3, 3]), x_tQ[i_iQ, i_iQ] -> x[i, i],
          x_?ttQ[i_?iQ, j_?iQ] /; Not[SameQ[i, j]] -> 0} ;
a //. xrules
]
(* for example: *) expr = F^2 (\[Delta][i,k] \[Delta][j,l] +
                               \[Delta][i,l] \[Delta][j,k] )/2 + a^2 T[i,j] T[k,l] ;
MatrixForm[transfer99[expr]]
```

For the reference model given by (2.63) and (2.64) we obtain:

$$\mathsf{L} = \frac{f_e f_b}{\hat{\mathbf{T}}^T \hat{\mathbf{T}}} \begin{bmatrix} F^2 + a^2\hat{T}_1^2 & a^2\hat{T}_1\hat{T}_2 & a^2\hat{T}_1\hat{T}_3 & 0 & 0 & 0 & 0 & 0 & 0 \\ a^2\hat{T}_1\hat{T}_2 & F^2 + a^2\hat{T}_2^2 & a^2\hat{T}_2\hat{T}_3 & 0 & 0 & 0 & 0 & 0 & 0 \\ a^2\hat{T}_1\hat{T}_3 & a^2\hat{T}_2\hat{T}_3 & F^2 + a^2\hat{T}_3^2 & 0 & 0 & 0 & 0 & 0 & 0 \\ 0 & 0 & 0 & \frac{F^2}{2} & \frac{F^2}{2} & 0 & 0 & 0 & 0 \\ 0 & 0 & 0 & \frac{F^2}{2} & \frac{F^2}{2} & 0 & 0 & 0 & 0 \\ 0 & 0 & 0 & 0 & 0 & \frac{F^2}{2} & \frac{F^2}{2} & 0 & 0 \\ 0 & 0 & 0 & 0 & 0 & \frac{F^2}{2} & \frac{F^2}{2} & 0 & 0 \\ 0 & 0 & 0 & 0 & 0 & 0 & 0 & \frac{F^2}{2} & \frac{F^2}{2} \\ 0 & 0 & 0 & 0 & 0 & 0 & 0 & \frac{F^2}{2} & \frac{F^2}{2} \end{bmatrix},$$

$$\mathbf{N} = \frac{f_e f_b F a}{\hat{\mathbf{T}}^T \hat{\mathbf{T}}} \begin{bmatrix} \hat{T}_1 + \hat{T}_1^* \\ \hat{T}_2 + \hat{T}_2^* \\ \hat{T}_3 + \hat{T}_3^* \\ 0 \\ 0 \\ 0 \\ 0 \\ 0 \\ 0 \end{bmatrix} \quad \text{and} \quad \mathring{\mathbf{T}} = \mathsf{L}\mathbf{D} + f_d \mathbf{N}\|\mathbf{D}\| \tag{3.5}$$

Examining the form of L in (3.4) we can easily discover that aligning the coordinate system parallel to the principal stress directions ($\mathbf{T}$ becomes diagonal) and choosing $\mathbf{D}$ coaxial with $\mathbf{T}$ (i.e. $\mathbf{D}$ has a diagonal form too) the stress rate $\mathring{\mathbf{T}}$ becomes also coaxial with both of them (has also a diagonal form). Under such restriction stress and strain paths may be described by diagonal components only, see Equation (2.36).

Since $\mathsf{L}(\mathbf{T})$ and $\mathbf{N}(\mathbf{T})$ are isotropic functions of stress they must have the same symmetry group as the stress itself. Thus, L and $\mathbf{N}$ must be orthotropic with respect to the principal axes of $\mathbf{T}$, as can be seen from (3.5).

The form (3.5) has the minor symmetries

$$L_{ijkl} = L_{ijlk} = L_{jikl} = L_{jilk}, \tag{3.6}$$

i.e. instead of $T_{12} = 2L_{1212} \cdot D_{12}$ we keep the tensorial expression $T_{12} = L_{1212} \cdot D_{12} + L_{1221} \cdot D_{21}$ wherein $L_{ijkl} = L_{ijlk}$ holds. The minor symmetries render L singular because it associates null tensor to every skew symmetric tensor. For symmetric argument $\mathbf{D}$ the stiffness L can be inverted. The analytical form of the inverse matrix and the eigenvalues and eigenvectors of L are presented later on, see Equation (3.33). Moreover, the linear

part of the reference model (2.61) has the major symmetry $L_{ijkl} = L_{klij}$. Note that contrary to some literature, e.g. Müllerschön [160], this symmetry does *not* necessarily imply that L originates from an elastic potential. In fact the symmetry is a necessary but not a sufficient condition for existence of an elastic potential. Implementation of an elastic potential would be a desirable improvement to the elastic part of the reference hypoplastic model. An appropriate potential stress function was proposed for example by Niemunis and Cudny [169] www.AN and critically compared with several existing formulations.

3.1.1 Inverse solution of hypoplastic equation

In matrix notation Equation (2.29) has an analogous form

$$\mathring{\mathbf{T}} = \mathsf{L}\mathbf{D} + f_d\mathbf{N}\|\mathbf{D}\| \quad \text{with} \quad \|\mathbf{D}\| = \sqrt{\mathbf{D}^T\mathbf{D}}\,. \tag{3.7}$$

Since f_d does not qualitatively affect the results presented in this section we assume for simplicity $f_d = 1$. Alternatively, we can think of $\mathbf{N}$ as containing f_d. Given a stress rate $\mathring{\mathbf{T}}$ we may try to solve Equation (3.7) for $\mathbf{D}$ using the method presented in [162] www.AN. First, let us find $x = \|\mathbf{D}\|$. Multiplying both sides of (3.7) with L^{-1} we obtain

$$\mathbf{D} = \mathsf{L}^{-1}\mathring{\mathbf{T}} - \mathsf{L}^{-1}\mathbf{N}\|\mathbf{D}\| = \mathbf{A} - \mathbf{B}\|\mathbf{D}\| \quad \text{with} \quad \mathbf{A} = \mathsf{L}^{-1}\mathring{\mathbf{T}} \quad \text{and} \quad \mathbf{B} = \mathsf{L}^{-1}\mathbf{N} \tag{3.8}$$

Next, we calculate the square of both sides

$$x^2 = \mathbf{D}^T\mathbf{D} = (\mathbf{A} - \mathbf{B}x)^T(\mathbf{A} - \mathbf{B}x) \tag{3.9}$$

which is a quadratic equation $ax^2 + bx + c = 0$ with respect to x with

$$\begin{cases} a = & \mathbf{B}^T\mathbf{B} - 1, \\ b = & -2\mathbf{A}^T\mathbf{B}, \\ c = & \mathbf{A}^T\mathbf{A} \end{cases} \tag{3.10}$$

The roots of the quadratic equation are

$$x_{1,2} = \frac{\mathbf{A}^T\mathbf{B}}{\mathbf{B}^T\mathbf{B} - 1} \pm \sqrt{\left(\frac{\mathbf{A}^T\mathbf{B}}{\mathbf{B}^T\mathbf{B} - 1}\right)^2 - \frac{\mathbf{A}^T\mathbf{A}}{\mathbf{B}^T\mathbf{B} - 1}}. \tag{3.11}$$

The unknown strain rate is

$$\mathbf{D} = \mathbf{A} - x\mathbf{B} \tag{3.12}$$

where

$$x = x_1 = \frac{\mathbf{A}^T\mathbf{B}}{\mathbf{B}^T\mathbf{B} - 1} + \sqrt{\left(\frac{\mathbf{A}^T\mathbf{B}}{\mathbf{B}^T\mathbf{B} - 1}\right)^2 - \frac{\mathbf{A}^T\mathbf{A}}{\mathbf{B}^T\mathbf{B} - 1}}, \tag{3.13}$$

because we take the positive root $x = \|\mathbf{D}\| \geq 0$ only.

Using the above algorithm Doanh [53] plotted the complementary envelopes and discovered their concavity for some early hypoplastic models. Here we use the following MATHEMATICA script in order to demonstrate that this concavity is present also in the referential model.

```
f=1; a=3.06186; t1 = 2/4; t2=1/4;
tt = {t1,t2,t2}; trt=t1+2*t2; td = {t1- trt/3, t2-trt/3, t2-trt/3};
LL = f^2 * IdentityMatrix[3] + a^2 Outer[Times, tt,tt] ; NN = f*a* (tt+td);
LL1= Simplify[Inverse[LL]]; BB= Simplify[LL1.NN]; denom=Simplify[BB.BB - 1];
getx[AA_] := Simplify[AA.BB/denom + Sqrt[(AA.BB/denom)^2 - AA.AA/denom] ]
dt2[t_] := Cos[t]/Sqrt[2]; dt1[t_] := Sin[t];
AA[t_]  := LL1.{dt1[t], dt2[t],dt2[t]}; dd[t_] := AA[t] -  getx[AA[t]] * BB;
ParametricPlot[{- Sqrt[2] dd[t][[2]],  -dd[t][[1]]   },  {t, 0, 2 Pi} ]
```

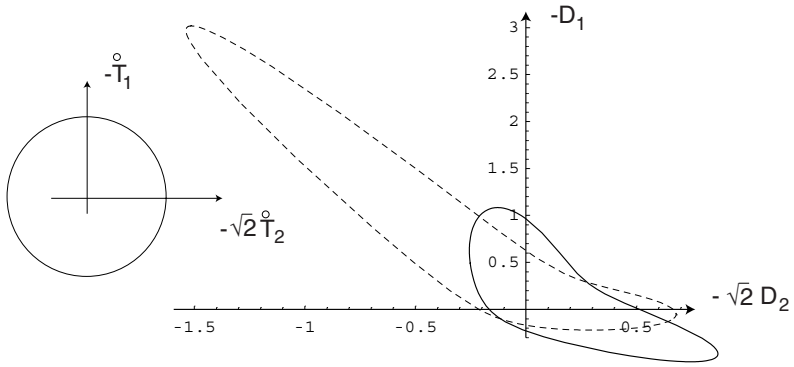

Figure 3.1: Complementary response envelopes obtained with (3.12) in strain space as a response to the unit stress rate in different directions. The continuous and the dashed envelopes are calculated for $\hat{\mathbf{T}} \sim$ diag$[1,1,1]$ and for $\hat{\mathbf{T}} \sim$ diag$[2,1,1]$, respectively. Contrary to the stress rate response envelope, the complementary envelope is concave

Condition of invertibility

Since $x = \|\mathbf{D}\| = \sqrt{\mathbf{D}^T\mathbf{D}}$ denotes the norm of a tensor it must be *nonnegative*. If two negative roots $x_1 < 0$ and $x_2 < 0$ are obtained from (3.9) none of them can be admitted, and if $x_1 > 0$ and $x_2 > 0$ both roots are allowed for, which renders the solution non-unique. Thus the inequality $x_1 \cdot x_2 \leq 0$ can be taken as a criterion of invertibility of (3.7). This condition is identical with $ac \leq 0$. Noting that $c > 0$ always holds and using (3.11) the condition of invertibility can be simplified to $a < 0$ or

$$\boxed{\mathbf{B}^T\mathbf{B} < 1 \quad \text{or} \quad (\mathsf{L}^{-1}\mathbf{N})^T(\mathsf{L}^{-1}\mathbf{N}) < 1} \tag{3.14}$$

For $f_d \neq 1$ we obtain an analogous inequality with $(1/f_d)^2$ on the right-hand side. Condition (3.14) is identical with the requirement that $\mathbf{T}$ should lie inside the yield surface $y(\mathbf{T}) = 0$ given in (2.38). This means that Equation (3.7) is invertible when the stress lies inside the response envelope, see Fig. 3.2, i.e. for stresses $y(\mathbf{T}) < 0$ inside the hypoplastic yield surface.

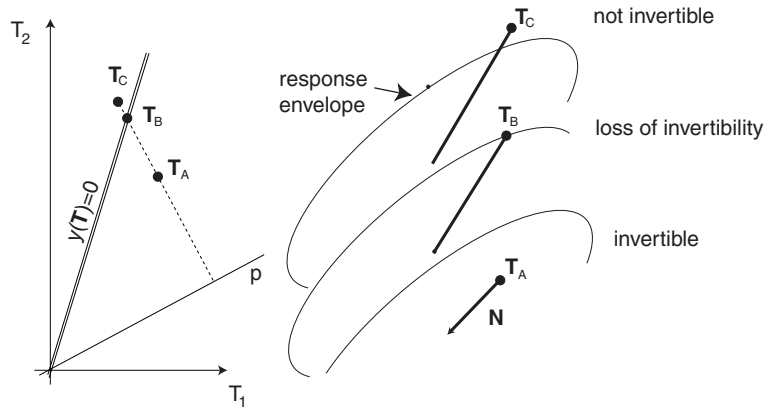

Figure 3.2: Invertibility condition (3.14) is satisfied unconditionally for stresses that lie inside the yield surface only

3.1.2 Mixed controlled tests

Let us solve the constitutive equation (3.7) for the case when several components of the stress rate $\mathring{\mathbf{T}}$ and the complementary components of the strain rate $\mathbf{D}$ are given and the remaining components in both vectors have to be calculated. If a stress rate component $\dot{T}_{ij}$ is unknown then the respective strain rate D_{ij} must be prescribed or vice versa. The known components are denoted with breve ($\breve{}$). For example, the oedometric test with the vertical stress and the lateral deformation (equal zero) prescribed is a mixed controlled element test. Another example is the drained triaxial test with the vertical displacement and horizontal stress prescribed.

The solution of mixed problems is required for 'true' (first class) predictions of element tests with a mixed control or with load-control. In first class numerical predictions we should prescribe the same variables which are controlled in the simulated laboratory test. Otherwise, taking *output* from the experiment (possibly blurred by inaccurate measurements or errors) as an *input* in the numerical calculation the results are less accurate. Further advantage of the mixed control becomes evident in simulations of tests during which some components of strain are not monitored at all. For example, in a triaxial apparatus the accurate lateral-strain measurement of a dry sample is very difficult and the data, if any, are not exact. In such case one can use a mixed controlled algorithm (with prescribed vertical strain and lateral pressure) to compare the development of the vertical stress with the one from the numerical simulation, e.g. [79].

Here it is demonstrated how to solve (3.7) for mixed control. The condition of solvability of such problem shown to be more restrictive than (3.14), i.e. for some stresses a mixed control problem cannot be uniquely solved although (3.7) can be inverted.

For *incrementally linear* constitutive relations $\mathring{\mathbf{T}} = \mathsf{E}\mathbf{D}$ the problem of mixed controlla-

bility was investigated by Nova and Imposimato [106, 180]. They were using generalized stress and strain components[1]. Having collected the unknown variables in sub-vectors $\mathbf{D}_1$, $\mathring{\mathbf{T}}_2$ and the prescribed ones in $\breve{\mathbf{D}}_2$, $\mathring{\breve{\mathbf{T}}}_1$ they examined solvability of the following block-matrix equation:

$$\left\{ \begin{array}{c} \mathring{\breve{\mathbf{T}}}_1 \\ \mathring{\mathbf{T}}_2 \end{array} \right\} = \left[\begin{array}{cc} \mathsf{E}_{11} & \mathsf{E}_{12} \\ \mathsf{E}_{21} & \mathsf{E}_{22} \end{array} \right] \left\{ \begin{array}{c} \mathbf{D}_1 \\ \breve{\mathbf{D}}_2 \end{array} \right\} \tag{3.15}$$

The dimensions of blocks (sub-matrices) $\mathsf{E}_{11}, \mathsf{E}_{12}, \mathsf{E}_{21}$ and E_{22} correspond, of course, to the size of vectors $\mathbf{D}_1$ and $\breve{\mathbf{D}}_2$. Although the solution

$$\mathbf{D}_1 = \mathsf{E}_{11}^{-1}(\mathring{\breve{\mathbf{T}}}_1 - \mathsf{E}_{12}\breve{\mathbf{D}}_2) \tag{3.16}$$

$$\mathring{\mathbf{T}}_2 = \mathsf{E}_{21}\mathsf{E}_{11}^{-1}(\mathring{\breve{\mathbf{T}}}_1 - \mathsf{E}_{12}\breve{\mathbf{D}}_2) + \mathsf{E}_{22}\breve{\mathbf{D}}_2 \tag{3.17}$$

is straightforward (similar to static condensation procedure), an interesting question arises concerning the general solvability condition of (3.15) when the matrix E is non-symmetric. Nova and Imposimato [106, 180] have shown that the solvability condition of (3.15) coincides with the requirement of the positive second-order work $W_2 = \mathring{\mathbf{T}}^T\mathbf{D} > 0$ for any rate $\mathbf{D}$.

For *incrementally nonlinear* case the above result does not hold. Therefore we investigate in some detail the solvability of Equation (3.7) under mix control. In hypoplastic context, the question of mixed controlled tests was recently addressed by Kolymbas [120]. For the selection of prescribed components he uses the partition matrices P and Q both of dimensions 9×9. They are padded with zeroes everywhere except for several diagonal components which correspond to the prescribed components and are equal to one. These unit diagonal components are chosen in such way that $\mathring{\breve{\mathbf{T}}}_1 = \mathsf{P}\mathring{\mathbf{T}}$ and $\breve{\mathbf{D}}_2 = \mathsf{Q}\mathbf{D}$ hold. Obviously P and Q are complementary in the sense that PQ is the 9×9 zero matrix and $\mathsf{P} + \mathsf{Q} = \mathsf{J}$. Obviously $\mathsf{QQ} = \mathsf{Q}$ and similarly $\mathsf{PP} = \mathsf{P}$ must hold. The controlling vector that contains all prescribed components is $\mathbf{X} = \mathsf{Q}\mathbf{D} + \mathsf{P}\mathring{\mathbf{T}}$ and the dependent variables consists of complementary components $\mathbf{Y} = \mathsf{Q}\mathring{\mathbf{T}} + \mathsf{P}\mathbf{D}$. Kolymbas [120] inverted these relations

$$\mathbf{D} = \mathsf{Q}\mathbf{X} + \mathsf{P}\mathbf{Y} \tag{3.18}$$

$$\mathring{\mathbf{T}} = \mathsf{P}\mathbf{X} + \mathsf{Q}\mathbf{Y}, \tag{3.19}$$

formulated the implicit form of hypoplastic equation

$$\mathbf{F}(\mathbf{X}, \mathbf{Y}) \equiv \overbrace{\mathsf{P}\mathbf{X} + \mathsf{Q}\mathbf{Y}}^{=\mathring{\mathbf{T}}} - \mathsf{L}(\overbrace{\mathsf{Q}\mathbf{X} + \mathsf{P}\mathbf{Y}}^{\mathbf{D}}) - \mathbf{N}\| \overbrace{\mathsf{Q}\mathbf{X} + \mathsf{P}\mathbf{Y}}^{\mathbf{D}} \| = \mathbf{0} \tag{3.20}$$

[1] Such 'composite components' are discussed further in this chapter.

and examined the uniqueness of the equivalent explicit function $\mathbf{Y}(\mathbf{X})$. Locally, in the small vicinity of $(\mathbf{X}_0, \mathbf{Y}_0)$ such explicit function exists and is unique if $\mathbf{F}(\mathbf{X}_0, \mathbf{Y}_0) = \mathbf{0}$ and if $\det[(\partial\mathbf{F}/\partial\mathbf{Y})] \neq \mathbf{0}$ at $(\mathbf{X}_0, \mathbf{Y}_0)$. This, however, does not guarantee the uniqueness of $\mathbf{Y}(\mathbf{X})$ at a given $\mathbf{X}_0$, which become obvious considering as a counter-example a scalar function $F(x, y) \equiv |y - x| - 1 = 0$. Kolymbas (private communication, 2001) argues that the above condition must be interpreted globally, meaning that $\det[(\partial\mathbf{F}/\partial\mathbf{Y})] \neq 0$ for any $(\mathbf{X}, \mathbf{Y})$. However, our scalar function $F(x, y) \equiv |y - x| - 1 = 0$ fulfills also this global condition everywhere except for the line $y = x$, where the derivative does not exist. Possibly one should postulate $F(\ )$ to have everywhere a continuous y-derivative but such requirement would rule out also the hypoplastic implicit equation (3.20) because the derivative $(\partial\mathbf{F}/\partial\mathbf{Y})$ of $\mathbf{F}(\mathbf{X}, \mathbf{Y})$ given by (3.20) is undetermined for $\mathsf{Q}\mathbf{X}+\mathsf{P}\mathbf{Y} = \mathbf{0}$ $(= \mathbf{D})$. The Kolymbas [120] approach seems therefore controversial and needs further clarification.

Here, we formulate an alternative criterion for solvability of mixed problems without introducing the partition matrices P and Q, remembering however that $\breve{\mathring{\mathbf{T}}}_1$, $\mathring{\mathbf{T}}_2$, $\mathbf{D}_1$ and $\breve{\mathbf{D}}_2$ are selected from $\mathring{\mathbf{T}}$ and from $\mathbf{D}$ in an arbitrary way and then grouped into vectors of smaller dimensions. The rearranged constitutive equation has the form:

$$\left\{ \begin{array}{c} \breve{\mathring{\mathbf{T}}}_1 \\ \mathring{\mathbf{T}}_2 \end{array} \right\} = \left[\begin{array}{cc} \mathsf{L}_{11} & \mathsf{L}_{12} \\ \mathsf{L}_{21} & \mathsf{L}_{22} \end{array} \right] \left\{ \begin{array}{c} \mathbf{D}_1 \\ \breve{\mathbf{D}}_2 \end{array} \right\} + f_d \left\{ \begin{array}{c} \mathbf{N}_1 \\ \mathbf{N}_2 \end{array} \right\} \sqrt{\left\{ \begin{array}{cc} \mathbf{D}_1^T & \breve{\mathbf{D}}_2^T \end{array} \right\} \left\{ \begin{array}{c} \mathbf{D}_1 \\ \breve{\mathbf{D}}_2 \end{array} \right\}} \tag{3.21}$$

It is a system of 9 nonlinear equations with 9 unknowns in sub-vectors $\mathring{\mathbf{T}}_2$ and $\mathbf{D}_1$. Fr simplicity we assume $f_d = 1$ (or f_d hidden in)

A convenient starting point is to find

$$x = \sqrt{\mathbf{D}^T\mathbf{D}} = \sqrt{\mathbf{D}_1^T\mathbf{D}_1 + \breve{\mathbf{D}}_2^T\breve{\mathbf{D}}_2} \tag{3.22}$$

With the abbreviation x Equation (3.21) reads as

$$\breve{\mathring{\mathbf{T}}}_1 = \mathsf{L}_{11}\mathbf{D}_1 + \mathsf{L}_{12}\breve{\mathbf{D}}_2 + \mathbf{N}_1 x \tag{3.23}$$

$$\mathring{\mathbf{T}}_2 = \mathsf{L}_{21}\mathbf{D}_1 + \mathsf{L}_{22}\breve{\mathbf{D}}_2 + \mathbf{N}_2 x \tag{3.24}$$

The sub-vector $\mathbf{D}_1$ can be calculated from (3.23)

$$\mathbf{D}_1 = \mathsf{L}_{11}^{-1}(\breve{\mathring{\mathbf{T}}}_1 - \mathsf{L}_{12}\breve{\mathbf{D}}_2 - \mathbf{N}_1 x) \tag{3.25}$$

Introducing the abbreviations

$$\mathbf{P} = \mathsf{L}_{11}^{-1}(\breve{\mathring{\mathbf{T}}}_1 - \mathsf{L}_{12}\breve{\mathbf{D}}_2) \tag{3.26}$$

$$\mathbf{Q} = \mathsf{L}_{11}^{-1}\mathbf{N}_1 \tag{3.27}$$

we may simplify (3.25) to the form

$$\mathbf{D}_1 = \mathbf{P} - \mathbf{Q}x. \tag{3.28}$$

Substitution of (3.28) in (3.22) results in

$$x^2 = (\mathbf{P} - \mathbf{Q}x)^T(\mathbf{P} - \mathbf{Q}x) + \breve{\mathbf{D}}_2^T\breve{\mathbf{D}}_2 \tag{3.29}$$

which is a quadratic equation

$$ax^2 + bx + c = 0 \tag{3.30}$$

with respect to x with the coefficients

$$\begin{cases} a = & \mathbf{Q}^T\mathbf{Q} - 1, \\ b = & -2\mathbf{P}^T\mathbf{Q} \\ c = & \mathbf{P}^T\mathbf{P} + \breve{\mathbf{D}}_2^T\breve{\mathbf{D}}_2 \end{cases} \tag{3.31}$$

The solution is completed by solving (3.30) for x and substituting x into (3.28) and (3.24) to obtain $\mathbf{D}_1$ and $\mathring{\mathbf{T}}_2$.

Condition of solvability

A positive unique real solution x can be determined from (3.30) if $x_1x_2 < 0$ i.e. if $ac < 0$ holds. Since c is always positive $ac < 0$ implies $a < 0$, i.e.

$$\|\mathbf{Q}\| = \|\mathsf{L}_{11}^{-1}\mathbf{N}_1\| < 1 \tag{3.32}$$

This condition is stronger than (3.14) because it refers to all possible *parts* of L and of $\mathbf{N}$. It is important to perform the calculation in the proper sequence: first L_{11} is extracted from L and $\mathbf{N}_1$ from $\mathbf{N}$ and then L_{11} is inverted and finally the multiplication L_{11}^{-1} by $\mathbf{N}_1$ takes place.

The condition (3.32) contains a combination of components of L and $\mathbf{N}$ that correspond to the components of the prescribed stress rate. The solvability of (3.21) must be guaranteed in a general case of any choice of prescribed rates (among stress-rate or strain-rate components). There are 62 possible combinations of prescribed stress components. Due to the obligatory symmetry of stress $T_{ij} = T_{ji}$ we have $\sum_{i=1}^{5}\binom{6}{i} = 62$ instead of $\sum_{i=1}^{8}\binom{9}{i} = 510$ combinations of components to be examined. The set of all combinations can be generated with the MATHEMATICA command:

```
<< DiscreteMath‘Combinatorica‘
Do[ xx[i] = Map[Flatten, KSubsets[{1,2,3,{4,5},{6,7},{8,9}},i]], {i,1,5}];
zz=Join[xx[1], xx[2], xx[3], xx[4], xx[5]]
```

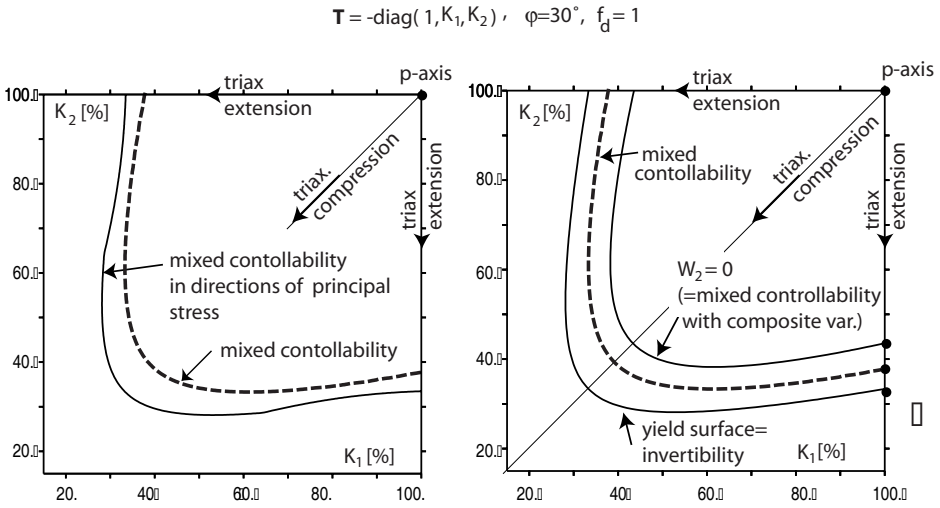

Figure 3.3: Comparison of invertibility and mixed controllability for the hypoplastic model of Wolffersdorff with $f_d = 1$ and $\mathbf{T} = -\mathrm{diag}(1, K_1, K_2)$

Note that shear components are grouped in pairs and must be chosen collectively. It can be shown that the maximum (over all 62 choices of components) of the norm $\|\mathsf{L}_{11}^{-1}\mathbf{N}_1\|$ depends on the choice of the coordinate system. In other words, it is not sufficient to examine the maximum of the norm $\|\mathsf{L}_{11}^{-1}\mathbf{N}_1\|$ choosing L_{11} and $\mathbf{N}_1$ from the matrices (3.5) being functions of principal stress components only. The maximum of the norm $\|\mathsf{L}_{11}^{-1}\mathbf{N}_1\|$ that enters the controllability condition (3.32) should be taken over all submatrices L_{11} and over all stresses including various 'equivalent' representations with the same eigenvalues but different (also off-diagonal) components.

The limits of controllability with and without coaxial $\mathbf{D}$ and $\mathbf{T}$ are shown in the left part of Fig. 3.3. The mixed controllability limit lies between the zero second-order work line $W_2 = 0$ and the yield (=invertibility) surface as shown in the right part of Fig. 3.3. The fact that the second-order work corresponds to the loss of mixed controllability with respect to composite variables will be explained in Section 3.2.3. In this illustration we have chosen the reference model (2.61) with the relations (2.63 - 2.67). For the examination of the value $\|\mathsf{L}_{11}^{-1}\mathbf{N}_1\|$ the multipliers f_e and $f_b/\|\hat{\mathbf{T}}\|^2$ are insignificant and may be set to unity, $f_e = f_b/\|\hat{\mathbf{T}}\|^2 = 1$. For simplicity we consider a special case $f_d = 1$ for which $\mathsf{L}_{11}^{-1}\mathbf{N}_1 = \hat{\mathsf{L}}_{11}^{-1}\hat{\mathbf{N}}_1$ holds but generalization of the result to $f_d \neq 1$ should be straightforward.

In (2.31) the analytical form of the inverse linear stiffness has been already used (see the corresponding footnote). For the reference model we have analogously

$$\hat{\mathsf{L}}^{-1} = \frac{1}{F^2}\left[\mathsf{I} - \frac{\hat{\mathbf{T}}\hat{\mathbf{T}}^T}{\left(\frac{F}{a}\right)^2 + \hat{\mathbf{T}}^T\hat{\mathbf{T}}}\right] \tag{3.33}$$

Now the same method is used to inverse the sub-matrix L_{11}. Let the sub-vector $\hat{\mathbf{T}}_1$ (of

dimensions 8×1 or shorter) contain these components of $\hat{\mathbf{T}}$ which correspond of the prescribed stress rate $\overset{\circ}{\hat{\mathbf{T}}}_1$. The deviatoric part can be calculated from $\hat{\mathbf{T}}_1^* = \hat{\mathbf{T}}_1 - \frac{1}{3}\,\mathbf{1}_1$, wherein $\mathbf{1}_1$ is an analogously selected part of unit vector $\mathbf{1}$ given in (3.1). Moreover I_{11} is defined to be a part of I extracted from (3.2) by choosing these rows and columns that correspond to the components of the prescribed stress rate $\overset{\circ}{\hat{\mathbf{T}}}_1$. Using this notation we obtain:

$$\hat{\mathsf{L}}_{11} = F^2\mathsf{I}_{11} + a^2\hat{\mathbf{T}}_1\hat{\mathbf{T}}_1^T \quad \text{and} \quad \hat{\mathbf{N}}_1 = Fa(\hat{\mathbf{T}}_1 + \hat{\mathbf{T}}_1^*) \tag{3.34}$$

and finally after inversion of L_{11}

$$\hat{\mathsf{L}}_{11}^{-1}\hat{\mathbf{N}}_1 = \frac{a}{F}\left(\hat{\mathbf{T}}_1 + \hat{\mathbf{T}}_1^* - \hat{\mathbf{T}}_1\frac{\hat{\mathbf{T}}_1^T(\hat{\mathbf{T}}_1 + \hat{\mathbf{T}}_1^*)}{\dfrac{F^2}{a^2} + \hat{\mathbf{T}}_1^T\hat{\mathbf{T}}_1}\right) \tag{3.35}$$

From the numerical results depicted in Fig 3.3 we may notice that the contollability of the hypoplastic model written in terms of principal stresses does not guarantee the contollability at the same stress expressed by components of a different coordinate system. Let us also notice that the mixed contollability of the hypoplastic equations does not depend on the *values* of the prescribed components of $\overset{\circ}{\hat{\mathbf{T}}}_1$ and $\breve{\mathbf{D}}_2$.

Calculations for the coaxial case were performed with MATHEMATICA script `controlab.m` and the general case with the FORTRAN program `fullcon.f90` both available from www.AN .

3.2 Composite components

In some cases it is convenient to discuss the hypoplastic constitutive model in terms of composite strain rate or stress rates. The most popular composite components are known as Roscoe's variables:

$$\dot{p} = -(\dot{T}_1 + \dot{T}_2 + \dot{T}_3)/3 \quad \text{and} \quad \dot{q} = -\dot{T}_1 + (\dot{T}_2 + \dot{T}_3)/2 \quad \text{with} \tag{3.36}$$

$$D_v = -(D_1 + D_2 + D_3) \quad \text{and} \quad D_q = -\frac{2}{3}D_1 + \frac{1}{3}(D_2 + D_3) \tag{3.37}$$

defined with principal stresses and strains for axially symmetric states. Generally, we admit any *linear* combination of strain rate components to be a composite strain rate, and analogously for the composite stress rate. No combinations of components of stress- *and* strain rates are allowed.

The definition of p and q reflect the manner in which a triaxial test is actually controlled. In conventional triaxial test we prescribe p and q rather than T_1 and $T_2 = T_3$. In undrained

triaxial compression test of a fully saturated soil sample we may prescribe vertical and lateral pressures (the components of the total stress $\mathbf{T}^{tot}$) but the pore pressure is usually a part of the material response and therefore the effective stress $\mathbf{T}$ cannot be directly controlled. Assuming incompressibility of water we control the volumetric strain rate ($D_v = 0$) and the difference $\dot{q} = -(\mathring{T}_1 - \mathring{T}_2) = -(\mathring{T}_1^{tot} - \mathring{T}_2^{tot})$ which is the deviatoric *effective* stress rate. The material response is observed through the complementary variables $\dot{p}$ (after subtraction of pore pressure) and D_q. We cannot treat the effective stress components as prescribed because they are influenced by the build-up of pore water pressure, i.e. by a part of material response which we do not control. In this case choosing the composite variables under a mixed control seems quite natural for numerical simulation.

Let us introduce a general stress rate measure[2] $\dot{\mathbf{t}} = \mathsf{M}\mathring{\mathbf{T}}$ wherein M is a non-singular matrix of constant coefficients. Such operation is sometimes called 'the regular linear substitution' or 'linear transformation' cf. [14] p.201. The corresponding strain rate is $\mathbf{d} = \mathsf{M}^{-T}\mathbf{D}$ so that the second-order work can be calculated analogously, viz.

$$W_2 = \mathring{\mathbf{T}}^T \mathbf{D} = \dot{\mathbf{t}}^T \mathbf{d}\,. \tag{3.38}$$

The following relations hold

$$\begin{array}{llll} \dot{\mathbf{t}} &= \mathsf{M}\mathring{\mathbf{T}} & \mathring{\mathbf{T}} &= \mathsf{M}^{-1}\dot{\mathbf{t}} \\ \mathbf{d} &= \mathsf{M}^{-T}\mathbf{D} & \mathbf{D} &= \mathsf{M}^{T}\mathbf{d} \end{array} \tag{3.39}$$

In general, the nonsingular matrix M is neither symmetric nor orthogonal. The substitution of $\mathring{\mathbf{T}} = \mathsf{M}^{-1}\dot{\mathbf{t}}$ and $\mathbf{D} = \mathsf{M}^{T}\mathbf{d}$ into the reference constitutive equation results in the following equation

$$\boxed{\dot{\mathbf{t}} = \bar{\mathsf{L}}\mathbf{d} + f_d \bar{\mathbf{N}}\sqrt{\mathbf{d}^T \mathsf{C}\ \mathbf{d}},} \tag{3.40}$$

with

$$\bar{\mathsf{L}} = \mathsf{M}\mathsf{L}\mathsf{M}^T, \qquad \bar{\mathbf{N}} = \mathsf{M}\mathbf{N}, \quad \text{and} \quad \mathsf{C} = \mathsf{M}\mathsf{M}^T. \tag{3.41}$$

One says that $\bar{\mathsf{L}}$ and L are congruent. The following example illustrates how an alternative system of variables can be defined. Let us consider the principal components of stress and strain only so that M has a size of 3×3 and all vectors - a size of 3×1.

$$\left\{\begin{array}{c} \dot{p} \\ \dot{q} \\ \dot{z} \end{array}\right\} = \left[\begin{array}{ccc} -1/3 & -1/3 & -1/3 \\ -1 & 1/2 & 1/2 \\ 0 & -1 & 1 \end{array}\right] \left\{\begin{array}{c} \mathring{T}_1 \\ \mathring{T}_2 \\ \mathring{T}_3 \end{array}\right\} \qquad \text{or briefly} \quad \dot{\mathbf{t}} = \mathsf{M}\mathring{\mathbf{T}} \tag{3.42}$$

[2]It should not to be mixed up with traction $\mathbf{t}$

$$\left\{\begin{array}{c} D_v \\ D_q \\ D_z \end{array}\right\} = \left[\begin{array}{ccc} -1 & -1 & -1 \\ -2/3 & 1/3 & 1/3 \\ 0 & -1/2 & 1/2 \end{array}\right] \left\{\begin{array}{c} D_1 \\ D_2 \\ D_3 \end{array}\right\} \qquad \text{or briefly} \quad \mathbf{d} = \mathsf{M}^{-T}\mathbf{D} \tag{3.43}$$

The stress rate component $\dot{z}$ is introduced to insure the one-to-one relation between the composite components and the basic set $\{\mathring{T}_1, \mathring{T}_2, \mathring{T}_3\}$ of stress variables. The strain rate D_z in $\mathbf{d}$ is the counterpart of $\dot{z}$. We could choose any linear combination of $\dot{T}_1$, $\dot{T}_2$, $\dot{T}_3$ as a definition of $\dot{z}$ provided M remains non-singular. Definition $\dot{z} = -\dot{T}_2 + \dot{T}_3$ may be conveniently used to impose the 'triaxial' symmetry $\dot{T}_2 = \dot{T}_3$ by setting $\dot{z} = 0$.

One may choose a special class of linear transformations requiring additionally, that M is an orthogonal matrix. Orthogonality implies $\mathsf{M}^{-T} = \mathsf{M}$ and $\mathsf{M}\mathsf{M}^T = \mathsf{C} = \mathsf{J}$. We have thus $W_2 = \mathring{\mathbf{T}}^T\mathbf{D} = \dot{\mathbf{t}}^T\mathbf{d}$ and additionally $\mathbf{D}^T\mathbf{D} = \mathbf{d}^T\mathbf{d}$ and $\mathring{\mathbf{T}}^T\mathring{\mathbf{T}} = \dot{\mathbf{t}}^T\dot{\mathbf{t}}$. For example, we could define 'normalized' (or isomorphic) Roscoe's variables:

$$\left\{\begin{array}{c} \dot{p}^+ \\ \dot{q}^+ \\ \dot{z}^+ \end{array}\right\} = \left[\begin{array}{ccc} -\frac{1}{3}\sqrt{3} & -\frac{1}{3}\sqrt{3} & -\frac{1}{3}\sqrt{3} \\ -2/\sqrt{6} & 1/\sqrt{6} & 1/\sqrt{6} \\ 0 & -1/\sqrt{2} & 1/\sqrt{2} \end{array}\right] \left\{\begin{array}{c} \mathring{T}_1 \\ \mathring{T}_2 \\ \mathring{T}_3 \end{array}\right\}$$

$$\left\{\begin{array}{c} D_v^+ \\ D_q^+ \\ D_z^+ \end{array}\right\} = \left[\begin{array}{ccc} -\frac{1}{3}\sqrt{3} & -\frac{1}{3}\sqrt{3} & -\frac{1}{3}\sqrt{3} \\ -2/\sqrt{6} & 1/\sqrt{6} & 1/\sqrt{6} \\ 0 & -1/\sqrt{2} & 1/\sqrt{2} \end{array}\right] \left\{\begin{array}{c} D_1 \\ D_2 \\ D_3 \end{array}\right\}$$

instead of ones defined in (3.42) and (3.43). An advantage of these 'normalized' variables is that C is equal to the unit matrix J. Such isomorphic variables would be perhaps chosen by a mathematician because

$$\mathring{\mathbf{T}}^T\mathring{\mathbf{T}} = (\dot{p}^+)^2 + (\dot{q}^+)^2 + (\dot{z}^+)^2 \quad \text{and} \quad \mathring{\mathbf{T}}^T\mathring{\mathbf{T}} = 3\dot{p}^2 + \frac{2}{3}\dot{q}^2 + 2\dot{z}^2 \neq \dot{p}^2 + \dot{q}^2 + \dot{z}^2 \tag{3.44}$$

The normal to the yield surface in stress space is *not* perpendicular to the contour of the yield surface in the $p-q$ plane but it is in the $p^+ - q^+$ plane. The following relations can be easily found

$$p^+ = \sqrt{3}p, \;\; q^+ = \sqrt{\frac{2}{3}}q, \;\; D_v^+ = \frac{1}{\sqrt{3}}D_v, \;\; D_q^+ = \sqrt{\frac{3}{2}}D_q$$

and the Coulomb yield condition $(T_{\max} - T_{\min})/(T_{\max} + T_{\min}) \leq \sin\varphi$ corresponds to inequalities

$$\frac{-2\sqrt{2}\sin\varphi}{3+\sin\varphi} \leq \eta^+ \leq \frac{2\sqrt{2}\sin\varphi}{3-\sin\varphi}$$

wherein $\eta^+ = q^+/p^+ = \frac{\sqrt{2}}{3}\eta$.

3.2.1 Reference model in $p-q$ and p^+-q^+ space

Before proceeding with contollability condition in terms of composite variables let us explicitly formulate the hypoplastic reference model in terms of Roscoe's and of isomorphic variables. The results of this simple exercise will be useful in the following sections. The transition matrix M that relates the principal components of stress and strain to the Roscoe variables has already been known from (3.42). The new rates $\dot{\mathbf{t}} = [\dot{p}, \dot{q}, \dot{z}]^T$ and $\mathbf{d} = [D_v, D_q, D_z]^T$ can be calculated form expressions analogous to (3.40) and (3.41)

$$\dot{\mathbf{t}} = \frac{f_b\, f_e}{\hat{\mathbf{T}}^T \hat{\mathbf{T}}} (\bar{\mathsf{L}}\mathbf{d} + f_d \bar{\mathbf{N}} \sqrt{\mathbf{d}^T \mathsf{C}\, \mathbf{d}},) \tag{3.45}$$

$$\bar{\mathsf{L}} = \mathsf{M}\, \hat{\mathsf{L}}\, \mathsf{M}^T, \quad \text{and} \quad \bar{\mathbf{N}} = \mathsf{M}\, \hat{\mathbf{N}}, \quad \text{and} \quad \mathsf{C} = \mathsf{M}\mathsf{M}^T. \tag{3.46}$$

to which we impose the symmetries $\dot{T}_2 \equiv \dot{T}_3$ and $D_2 \equiv D_3$ requiring $\dot{z} = -\dot{T}_2 + \dot{T}_3 \equiv 0$ and $D_z = -D_2 + D_3 \equiv 0$. The constitutive relationship in $p-q$ space can be now easily generated, for example with the following MATHEMATICA script

```
rulet = Solve[{-(t1+t2+t3)/3==p, -(t1-t3)==q, t2==t3},{t1,t2,t3}] [[1]]
ruletd = {td1-> t1-(t1+t2+t3)/3 , td2-> t2-(t1+t2+t3)/3, td3->t3-(t1+t2+t3)/3 }
mm = {{-1/3,-1/3,-1/3},{-1,1/2,1/2},{0,-1,1}}; trT = t1+t2+t3; tt= {t1,t2,t3}
LL= f^2 IdentityMatrix[3]+a^2/trT^2 Outer[Times,tt,tt]  /. rulet
nnaux =  f a fd/trT {t1+td1,t2+td2,t2+td2} /. ruletd; nn = nnaux /. rulet;
LLpq = mm.LL.Transpose[mm];     nnpq = mm.nn;    ccpq = mm.Transpose[mm];
```

This script calculates (3.46) and expresses stress in $\hat{\mathsf{L}}$ and $\hat{\mathbf{N}}$ by p and q. The resulting '$p-q$' version of the reference hypoplastic model has the matrix form

$$\begin{aligned}\begin{Bmatrix} \dot{p} \\ \dot{q} \end{Bmatrix} &= \frac{f_b\, f_e}{\frac{1}{3} + \frac{2}{27}\eta^2} \begin{bmatrix} \frac{a^2+3F^2}{9} & \frac{a^2}{9}\eta \\ \frac{a^2}{9}\eta & \frac{3F^2}{2} + \frac{a^2}{9}\eta^2 \end{bmatrix} \cdot \begin{Bmatrix} D_v \\ D_q \end{Bmatrix} + \\ &+ \frac{f_b\, f_e f_d}{\frac{1}{3} + \frac{2}{27}\eta^2} \cdot \frac{aF}{3} \begin{Bmatrix} -1 \\ -2\eta \end{Bmatrix} \sqrt{\begin{bmatrix} D_v & D_q \end{bmatrix} \cdot \begin{bmatrix} \frac{1}{3} & 0 \\ 0 & \frac{3}{2} \end{bmatrix} \cdot \begin{Bmatrix} D_v \\ D_q \end{Bmatrix}} \end{aligned} \tag{3.47}$$

wherein $\eta = q/p$. The components $D_z \equiv 0$ and $\dot{z} \equiv 0$ has been omitted in (3.48).

Analogous expressions can be derived for isomorphic variables. Eq. (2.66) becomes simply

$$F = \begin{cases} 1 & \text{if } \eta^+ > 0 \\ 1 + \eta^+/\sqrt{2} & \text{if } \eta^+ < 0 \end{cases}$$

and the hypoplastic model for $p^+ - q^+$ space has the form

$$\begin{aligned}\begin{Bmatrix} \dot{p^+} \\ \dot{q^+} \end{Bmatrix} &= \frac{f_b\, f_e}{\frac{1}{3}\left[1 + (\eta^+)^2\right]} \begin{bmatrix} F^2 + \frac{1}{3}a^2 & \frac{1}{3}a^2\eta^+ \\ \frac{1}{3}a^2\eta^+ & F^2 + \frac{1}{3}a^2(\eta^+)^2 \end{bmatrix} \cdot \begin{Bmatrix} D_v^+ \\ D_q^+ \end{Bmatrix} + \\ &+ \frac{f_b f_e f_d}{\frac{1}{3}\left[1 + (\eta^+)^2\right]} \cdot \frac{aF}{\sqrt{3}} \begin{Bmatrix} -1 \\ -2\eta^+ \end{Bmatrix} \sqrt{(D_v^+)^2 + (D_q^+)^2} \end{aligned} \tag{3.48}$$

wherein $\eta^+ = q^+/p^+$. Equation (3.48) is a good opportunity to determine the coefficient of earth pressure at rest K_0. Under oedometric conditions the only nonzero deformation component is $D_1 = -1$ so $D_v^+ = 1/\sqrt{3}$ and $D_q^+ = 2/\sqrt{6}$. We require $\dot{\eta}^+ = \eta^+$, i.e.

```
LL = {{1 + a^2/3, a^2 e/3 }, {a^2 e/3, 1 + a^2 e^2 /3}}; DD = {1/Sqrt[3], 2/Sqrt[6]};
Solve[((LL.DD)[[2]] - 2 a e fd /Sqrt[3] )/((LL.DD)[[1]] - a fd /Sqrt[3] ) ==    e, e]
```

It gives $\eta^+ = \sqrt{2}/(1 + af_d)$ which in terms of stress components results in $K_0 = \frac{af_d}{3+af_d}$

3.2.2 Inverse relation expressed in composite variables

We consider (3.40) with $f_d = 1$ leaving M unspecified. Suppose that the composite stress rate $\dot{\mathbf{t}}$ is given and we have to find the solution for $\mathbf{d}$. The inverse solution of (3.40) in terms of composite variables is similar to the one in terms of basic variables, see Section 3.1.1. Now, instead of $\mathbf{A}$ and $\mathbf{B}$ we define $\bar{\mathbf{A}} = \bar{\mathsf{L}}^{-1}\dot{\mathbf{t}}$ and $\bar{\mathbf{B}} = \bar{\mathsf{L}}^{-1}\bar{\mathbf{N}}$. The value $x = \sqrt{\mathbf{D}^T\mathbf{D}} = \sqrt{\mathbf{d}^T\mathsf{C}\,\mathbf{d}}$ can be calculated from the quadratic equation

$$ax^2 + bx + c = 0 \quad \text{with} \quad \begin{cases} a = & \bar{\mathbf{B}}^T\mathsf{C}\,\bar{\mathbf{B}} - 1, \\ b = & \bar{\mathbf{A}}^T\mathsf{C}\,\bar{\mathbf{B}} + \bar{\mathbf{B}}\mathsf{C}\,\bar{\mathbf{A}}^T, \\ c = & \bar{\mathbf{A}}^T\mathsf{C}\,\bar{\mathbf{A}}. \end{cases} \tag{3.49}$$

We take the positive root $x = (-b+\sqrt{b^2 - 4ac})/(2a)$ of the quadratic equation and obtain the final solution in form

$$\mathbf{d} = \bar{\mathbf{A}} - x\bar{\mathbf{B}} \tag{3.50}$$

Condition of invertibility

Obviously, the matrix $\mathsf{C} = \mathsf{M}\mathsf{M}^T$ is positive-definite so that $c > 0$ holds and the invertibility condition $ac < 0$ can be simplified to $a < 0$, i.e. to

$$\bar{\mathbf{B}}^T\mathsf{C}\,\bar{\mathbf{B}} < 1 \quad \text{or} \quad \|\mathsf{M}^T\bar{\mathbf{B}}\| < 1 \tag{3.51}$$

which can be further reduced to

$$\|\mathsf{M}^T(\mathsf{M}\mathsf{L}\mathsf{M}^T)^{-1}\mathsf{M}\mathbf{N}\| = \|\mathsf{M}^T\mathsf{M}^{-T}\mathsf{L}^{-1}\mathsf{M}^{-1}\mathsf{M}\mathbf{N}\| = \|\mathsf{L}^{-1}\mathbf{N}\| < 1 \tag{3.52}$$

This is identical with the condition (3.14). We conclude that invertibility is independent of the choice of composite variables. In the next subsection we show that it is not the case for mixed controlled problems.

3.2.3 Solution of mixed controlled problem in composite variables

Let us solve the hypoplastic equation assuming that several components of $\dot{\mathbf{t}}$ and the complementary components of $\mathbf{d}$ are known. For example, in undrained an load-controlled triaxial test we have $\dot{q} = 1$ and $D_v = 0$ and we try to find $\dot{p}$ and D_q. Again, we group the prescribed components into subvectors which are denoted with a breve ($\breve{}$). The rearranged constitutive equation may be written as

$$\begin{Bmatrix} \breve{\dot{\mathbf{t}}}_1 \\ \dot{\mathbf{t}}_2 \end{Bmatrix} = \begin{bmatrix} \bar{\mathsf{L}}_{11} & \bar{\mathsf{L}}_{12} \\ \bar{\mathsf{L}}_{21} & \bar{\mathsf{L}}_{22} \end{bmatrix} \begin{Bmatrix} \mathbf{d}_1 \\ \breve{\mathbf{d}}_2 \end{Bmatrix} + f_d \begin{Bmatrix} \bar{\mathbf{N}}_1 \\ \bar{\mathbf{N}}_2 \end{Bmatrix} \sqrt{\begin{Bmatrix} \mathbf{d}_1^T & \breve{\mathbf{d}}_2^T \end{Bmatrix} \begin{bmatrix} \mathsf{C}_{11} & \mathsf{C}_{12} \\ \mathsf{C}_{21} & \mathsf{C}_{22} \end{bmatrix} \begin{Bmatrix} \mathbf{d}_1 \\ \breve{\mathbf{d}}_2 \end{Bmatrix}} \tag{3.53}$$

It is a system of 9 nonlinear equations with 9 unknowns collected in subvectors $\dot{\mathbf{t}}_2$ and $\mathbf{d}_1$. We choose $f_d = 1$ for the sake of simplicity. The operation of selecting and grouping the prescribed and unknown components of rates can be accomplished by an appropriate choice of M divided into two rectangular blocks M_1 ($k \times 9$) and M_2 ($(9-k) \times 9$) so that

$$\begin{Bmatrix} \breve{\dot{\mathbf{t}}}_1 \\ \dot{\mathbf{t}}_2 \end{Bmatrix} = \begin{bmatrix} \mathsf{M}_1 \\ \mathsf{M}_2 \end{bmatrix} \left\{ \mathring{\mathbf{T}} \right\} \; ; \{\mathbf{D}\} = \begin{bmatrix} \mathsf{M}_1^T & \mathsf{M}_2^T \end{bmatrix} \begin{Bmatrix} \mathbf{d}_1 \\ \breve{\mathbf{d}}_2 \end{Bmatrix} \tag{3.54}$$

We obtain

$$\bar{\mathsf{L}} = \begin{bmatrix} \bar{\mathsf{L}}_{11} & \bar{\mathsf{L}}_{12} \\ \bar{\mathsf{L}}_{21} & \bar{\mathsf{L}}_{22} \end{bmatrix} = \left[\begin{array}{c|c} \mathsf{M}_1 \mathsf{L} \mathsf{M}_1^T & \mathsf{M}_1 \mathsf{L} \mathsf{M}_2^T \\ \hline \mathsf{M}_2 \mathsf{L} \mathsf{M}_1^T & \mathsf{M}_2 \mathsf{L} \mathsf{M}_2^T \end{array}\right], \quad \begin{Bmatrix} \bar{\mathbf{N}}_1 \\ \bar{\mathbf{N}}_2 \end{Bmatrix} = \begin{bmatrix} \mathsf{M}_1 \\ \mathsf{M}_2 \end{bmatrix} \{\mathbf{N}\} \tag{3.55}$$

and

$$\mathsf{C} = \begin{bmatrix} \mathsf{C}_{11} & \mathsf{C}_{12} \\ \mathsf{C}_{21} & \mathsf{C}_{22} \end{bmatrix} = \left[\begin{array}{c|c} \mathsf{M}_1 \mathsf{M}_1^T & \mathsf{M}_1 \mathsf{M}_2^T \\ \hline \mathsf{M}_2 \mathsf{M}_1^T & \mathsf{M}_2 \mathsf{M}_2^T \end{array}\right], \tag{3.56}$$

In order to find $x = \sqrt{\mathbf{D}^T \mathbf{D}} = \sqrt{\mathbf{d}^T \mathsf{C}\, \mathbf{d}}$ we decompose (3.53) into two equations

$$\breve{\dot{\mathbf{t}}}_1 \; = \; \bar{\mathsf{L}}_{11} \mathbf{d}_1 + \bar{\mathsf{L}}_{12} \breve{\mathbf{d}}_2 + \bar{\mathbf{N}}_1 x \tag{3.57}$$

$$\dot{\mathbf{t}}_2 \; = \; \bar{\mathsf{L}}_{21} \mathbf{d}_1 + \bar{\mathsf{L}}_{22} \breve{\mathbf{d}}_2 + \bar{\mathbf{N}}_2 x \tag{3.58}$$

and calculate

$$\mathbf{d}_1 = \bar{\mathsf{L}}_{11}^{-1} (\breve{\dot{\mathbf{t}}}_1 - \bar{\mathsf{L}}_{12} \breve{\mathbf{d}}_2 - \bar{\mathbf{N}}_1 x) \tag{3.59}$$

from the first one. Introducing auxiliary variables

$$\mathbf{P} = \; \bar{\mathsf{L}}_{11}^{-1} (\breve{\dot{\mathbf{t}}}_1 - \bar{\mathsf{L}}_{12} \breve{\mathbf{d}}_2) \tag{3.60}$$

$$\mathbf{Q} = \qquad \bar{\mathsf{L}}_{11}^{-1} \bar{\mathbf{N}}_1 \tag{3.61}$$

we may shorten (3.59) to the form

$$\mathbf{d}_1 = \mathbf{P} - \mathbf{Q}x. \tag{3.62}$$

Substitution of (3.62) in the definition of x results in

$$x^2 = \mathbf{d}_1^T \mathsf{C}_{11}\mathbf{d}_1 + \mathbf{d}_1^T \mathsf{C}_{12}\breve{\mathbf{d}}_2 + \breve{\mathbf{d}}_2^T \mathsf{C}_{21}\mathbf{d}_1 + \breve{\mathbf{d}}_2^T \mathsf{C}_{22}\breve{\mathbf{d}}_2 \tag{3.63}$$

which is a quadratic equation of the form

$$0 = \quad ax^2 + bx + c \quad \text{with} \tag{3.64}$$

$$a = \quad \mathbf{Q}^T \mathsf{C}_{11}\mathbf{Q} - 1, \tag{3.65}$$

$$b = -(\mathbf{P}^T \mathsf{C}_{11}\mathbf{Q} + \mathbf{Q}^T \mathsf{C}_{11}\mathbf{P}) - \mathbf{Q}^T \mathsf{C}_{12}\breve{\mathbf{d}}_2 - \breve{\mathbf{d}}_2^T \mathsf{C}_{21}\mathbf{Q}, \tag{3.66}$$

$$c = \quad \mathbf{P}^T \mathsf{C}_{11}\mathbf{P} + \mathbf{P}^T \mathsf{C}_{12}\breve{\mathbf{d}}_2 + \breve{\mathbf{d}}_2^T \mathsf{C}_{21}\mathbf{P} + \breve{\mathbf{d}}_2^T \mathsf{C}_{22}\breve{\mathbf{d}}_2 \tag{3.67}$$

We solve (3.64) taking for x the positive root. The solution is completed by substitution of x into (3.62) and (3.58) to obtain $\mathbf{d}_1$ and $\dot{\mathbf{t}}_2$.

Condition of mixed controllability

Real solutions of (3.64) exist if the radix $\Delta = b^2 - 4ac$ of (3.64) is positive. Moreover, a valid solution for x must be positive ($x > 0$) because x is the norm of the strain rate ($x = \sqrt{\mathbf{D}^T\mathbf{D}}$). If both roots x_1 and x_2 of (3.64) are positive then the solution is non-unique, if two roots are negative then the solution does not exist. Hence the condition of controllability can be written as $x_1 x_2 < 0$ or equivalently

$$ac < 0 \tag{3.68}$$

The expression for c given in (3.67) can be rewritten in a matrix form

$$c = \left\{ \mathbf{P}^T \;\; \breve{\mathbf{d}}_2^T \right\} \begin{bmatrix} \mathsf{C}_{11} & \mathsf{C}_{12} \\ \mathsf{C}_{21} & \mathsf{C}_{22} \end{bmatrix} \left\{ \begin{matrix} \mathbf{P} \\ \breve{\mathbf{d}}_2 \end{matrix} \right\} = \mathbf{x}^T \mathsf{C}\, \mathbf{x} = (\mathbf{x}^T \mathsf{M})(\mathsf{M}^T \mathbf{x}) > 0 \tag{3.69}$$

This form reveals the fact that c is always positive so the controllability condition can be simplified to

$$a < 0 \quad \text{or} \quad \mathbf{Q}^T \mathsf{C}_{11}\mathbf{Q} < 1 \quad \text{or} \quad \|\mathsf{M}_1^T(\mathsf{M}_1 \mathsf{L} \mathsf{M}_1^T)^{-1}(\mathsf{M}_1 \mathbf{N})\| < 1\,. \tag{3.70}$$

For the special case of orthogonal M:

$$\mathbf{Q}^T\mathbf{Q} < 1 \quad \text{or} \quad \|(\mathsf{M}_1 \mathsf{L} \mathsf{M}_1^T)^{-1}(\mathsf{M}_1 \mathbf{N})\| < 1 \tag{3.71}$$

Since inequality (3.68) implies $\Delta > 0$, it guarantees both existence and uniqueness of a real solution. From this condition we conclude that the solvability depends on stress via L and $\mathbf{N}$ and on the partial matrix M_1. The prescribed *values* in $\breve{\mathbf{t}}_1$ and $\breve{\mathbf{d}}_2$ are of no importance, which means that if the controllability is insured for $\breve{\mathbf{t}}_1$, $\breve{\mathbf{d}}_2$ it will be automatically insured if we increase say k-th component of $\breve{\mathbf{t}}_1$ by factor α (or equivalently if we multiply say k-th row of M_1 by α).

Mixed controllability and positiveness of the second-order work

The second order work

$$W_2 = \mathring{\mathbf{T}}^T\mathbf{D} \quad \text{with} \quad \mathring{\mathbf{T}} = \mathring{\mathbf{T}}(\mathbf{D}) \tag{3.72}$$

is discussed in the Section 3.3. Here, the equivalence of the condition $W_2 > 0$ with the mixed controllability condition in terms of composite variables is demonstrated.

First, we demonstrate that the negative second-order work implies loss of controllability. In order to prove this statement we show such M_1 that from $W_2 < 0$ follows a non-unique (if any) solution of the mixed problem. A unit $\mathbf{D}$ ($\|\mathbf{D}\| = 1$) is considered for which $W_2 < 0$. We may choose such orthogonal matrix M that rotates $\mathbf{D}$ to the following composite form $\mathbf{d} = \mathsf{M}^{-T}\mathbf{D} = \{-1, 0, 0, \ldots, 0\}^T$. i.e. with all components equal zero except for $d_1 = -1$. Since $\mathbf{D}^T\mathring{\mathbf{T}} = \mathbf{d}^T\dot{\mathbf{t}} < 0$ and $\|\mathbf{D}\| = 1$ after substitution $\mathbf{D} = \mathsf{M}^T\mathbf{d}$ we obtain

$$W_2 = \mathbf{D}^T\mathsf{L}\mathbf{D} + \mathbf{D}^T\mathbf{N}\|\mathbf{D}\| = \mathbf{d}^T\mathsf{M}\mathsf{L}\mathsf{M}^T\mathbf{d} + \mathbf{d}^T\mathsf{M}\mathbf{N} < 0 \tag{3.73}$$

Let M_1 be chosen to be the first row of M meaning that we prescribe the composite stress component t_1 that corresponds to d_1. Due to the special choice of $\mathbf{d}$ we may write

$$W_2 = d_1\mathsf{M}_1\mathsf{L}\mathsf{M}_1^T d_1 + d_1\mathsf{M}_1\mathbf{N} = \mathsf{M}_1\mathsf{L}\mathsf{M}_1^T - \mathsf{M}_1\mathbf{N} = \bar{L}_{11} - \bar{N}_1 < 0 \tag{3.74}$$

wherein $d_1 = -1$ was used. This further means that

$$(\mathsf{M}_1\mathsf{L}\mathsf{M}_1^T)^{-1}\mathsf{M}_1\mathbf{N} = \bar{N}_1/\bar{L}_{11} > 1 \tag{3.75}$$

because L is positive definite. Comparing the above inequality with (3.71) we have just shown that the negative second-order work implies loss of mixed controllability. In other words, controllability requirement is equally strong or stronger than the $W_2 > 0$ condition.

Second, we demonstrate that loss of controllability implies a negative second-order work. We assume that for a specially chosen orthogonal matrix M_1 we have detected loss of controllability, i.e., the condition (3.71) is violated and $\|\bar{\mathsf{L}}_{11}^{-1}\bar{\mathbf{N}}_1\| > 1$ is satisfied. This

condition can be shown to imply negative second-order work $W_2 = \mathbf{d}^T\dot{\mathbf{t}} < 0$ for $\mathbf{d}$ chosen in the form

$$\mathbf{d} = \left\{ \begin{array}{c} \mathbf{d}_1 \\ \mathbf{0} \end{array} \right\} \quad \text{with} \quad \mathbf{d}_1 = -\bar{\mathsf{L}}_{11}^{-1}\bar{\mathbf{N}}_1 \quad \text{and} \quad \|\mathbf{d}\| = \|\mathbf{d}_1\| > 1 \tag{3.76}$$

We rewrite:

$$\mathbf{d}^T\dot{\mathbf{t}} = \mathbf{d}_1^T\dot{\mathbf{t}}_1 = \mathbf{d}_1^T\bar{\mathsf{L}}_{11}\mathbf{d}_1 + \mathbf{d}_1^T\bar{\mathbf{N}}_1\|\mathbf{d}_1\| = \bar{\mathbf{N}}_1^T\bar{\mathsf{L}}_{11}^{-T}\bar{\mathbf{N}}_1(1 - \|\mathbf{d}_1\|). \tag{3.77}$$

Since the matrix L is positive-definite so $\bar{\mathsf{L}}$ and $\bar{\mathsf{L}}^{-T}$ are. Therefore the expression in brackets in (3.77) must be negative and we conclude that the second-order work must be negative. This means that the condition for vanishing of the second-order work is equally strong or stronger than the controllability requirement.

Summing up, we have demonstrated that the positive second-order work follows from the condition of controllability and vice versa. Therefore both conditions must be *equivalent*. This result can be interpreted graphically using the stress-strain diagram ϵ_x, t_x form Fig. 3.4. With reference to this figure, loss of controllability at the point B is apparent, if we prescribe all strain rate components except d_x and we intend to choose $\mathring{t}_x > 0$.

3.3 Second-order work W_2

On relevance to stability and uniqueness

We consider a state of a body under dead loads, i.e. tractions or body forces which do not change due to the movement of boundaries. The state of equilibrium may be regarded stable [91] if small transitory disturbances cause small displacements. The analysis of uniqueness and stability of a boundary value problem is related to the second-order effects and therefore stress and strain should be precisely work-conjugate[3]. One should distinguish between the product $W_2 = \mathbf{D}^T\mathring{\mathbf{T}}$ introduced in Section 3.2 and an exact second-order work per unit volume in the reference configuration required in the stability analysis. Even in the case, when the reference configuration is chosen to be the current one the difference may be of importance. The effects of interest are subtile and comparable with the change of boundary pressures due to the stretching of the loaded surface or with the work differences caused by the strain path curvatures over the small increment under consideration, [190, 193].

A better choice than $\mathring{\mathbf{T}}$ and $\mathbf{D}$ is to consider, for example, the rate of nominal (Piola) stress $\dot{\mathbf{T}}^P$ and the rate $\dot{\mathbf{F}}$ of the deformation gradient, both referred to the current configuration.

[3]Such conjugate pair could be the Kirchhoff stress $\mathbf{T}\det(\mathbf{F})$ based on the current configuration and the stretching $\mathbf{D}$ or the Piola stress $T_{iJ}^P = \det(\mathbf{F})T_{ik}F_{Jk}^{-1}$ and the rate of deformation gradient $\dot{F}_{iJ}$ both based on the current configuration.

Of course, in such case is $\mathbf{F} = \mathbf{1}$ and the Piola stress $\mathbf{T}^P$ is identical with the Cauchy stress $\mathbf{T}$, nevertheless their rates may differ. We choose these new variables because comparing alternative solutions of a BVP we must refer their energies to a common unit volume V (or a common unit mass). After Hill [90], stability condition is

$$\int_V \dot{T}^P_{iJ}\dot{F}_{iJ}\mathrm{d}V > 0 \tag{3.78}$$

wherein

$$\dot{F}_{iJ} = (D_{ik} + W_{ik})F_{kJ} \quad \text{and} \tag{3.79}$$

$$\dot{T}^P_{iJ} = \det(\mathbf{F})(\mathring{T}_{ik} + T_{ik}\mathrm{tr}\,(\mathbf{D}) + W_{iq}T_{qk} - T_{iq}D_{qk})F^{-1}_{Jk} \quad \text{with} \tag{3.80}$$

$$F^{-1}_{Ji} = F_{iJ} = \delta_{iJ} \tag{3.81}$$

This stability condition was applied already in the hypoplastic analysis of slope stability by Gudehus [69, 71] and Raju [201] and in a hypoplastic wave propagation problem by Osinov [186]. Note, however, that although the incremental work $T^P_{iJ}\mathrm{d}F_{iJ}$ is invariant, the second-order term appearing in the second place of expansion

$$T^P_{iJ}\mathrm{d}F_{iJ} \approx T^P_{iJ}\dot{F}_{iJ}\mathrm{d}t + \frac{1}{2}\dot{T}^P_{iJ}\dot{F}_{iJ}\mathrm{d}t\mathrm{d}t + \frac{1}{2}T^P_{iJ}\ddot{F}_{iJ}\mathrm{d}t\mathrm{d}t + \ldots \tag{3.82}$$

is *not* an objective concept [193] because $\dot{F}_{iJ}$ is not. Obviously the curvature of the incremental path expressed by $\ddot{F}_{iJ}$ is also of importance.

Solving an incremental mechanical problem we ask if two or more solutions may be developed from the current state called further the initial or the referential one. We are given a common reference geometry, here expressed by volume V and boundaries S_t and S_u for traction and displacements, respectively. Both alternative rate solutions must be compatible with the prescribed displacement rate $\breve{v}_i$ on S_u and with the rate of tractions $l_J\dot{T}^P_{iJ}$ per unit initial area of the boundary S_t. The vector $(\mathbf{l})_j = l_j$ is defined as unit vector outer normal to the boundary S_t on which tractions are prescribed. It is measured in the reference configuration. Moreover, the alternative solutions must be in equilibrium with the rate $\rho^0\dot{f}_i$ of the body force per unit initial volume, viz.

$$\dot{T}^P_{iJ,J} + \rho^0\dot{f}_i = 0 \tag{3.83}$$

We denote the difference between quantities $\bullet$ of two alternative solutions of a BVP by $\Delta\bullet$. For the existence of multiple velocity fields (bifurcation in velocities), $\Delta\mathbf{v} \neq \mathbf{0}$ we need

$$\begin{cases} \Delta\dot{F}_{iJ} & \neq 0 \text{ at least somewhere in } V \\ (\Delta\dot{T}^P_{iJ})_{,J} & = 0 \text{ everywhere in } V, \\ \Delta v_i & = 0 \text{ everywhere on } S_u \\ \Delta\dot{T}^P_{iJ}l_J & = 0 \text{ everywhere on } S_t \end{cases} \tag{3.84}$$

which using divergence theorem implies

$$\int\limits_{S_t+S_u} \Delta v_i \; \Delta \dot{T}^P_{iJ} l_J \; \mathrm{d}S = \int_V \Delta \dot{F}_{iJ} \;\; \Delta \dot{T}^P_{iJ} \; \mathrm{d}V = 0 \tag{3.85}$$

(but not vice versa). Performing logical negation of the implication:
$\{$ non-unique BVP solution$\}$ $\Rightarrow$ (3.85)
we obtain
$\{\int_V \Delta \dot{F}_{iJ} \;\; \Delta \dot{T}^P_{iJ} \; \mathrm{d}V \neq 0\} \Rightarrow$ $\{$ unique BVP solution $\}$
Hence

$$\int_V \Delta \dot{F}_{iJ} \Delta(\dot{T}^P_{ij}) > 0 \tag{3.86}$$

is a *sufficient* condition for uniqueness of a BVP solution.

The problems of stability and uniqueness are of general nature in continuum mechanics and has been addressed by many authors, e.g. by Drucker [57] and Hill [90, 92–94] or more recently by Petryk [190–193], Loret [138] and in the hypoplastic context by Chambon [31,31,32], Gudehus [69] and Sikora [219], to name only a few. Stability and uniqueness of geomaterials were intensively investigated by Darve [46–48] and by Vardoulakis [252–254]. For particular paths a negative second-order work may be experimentally observed in soils relatively early, as shown experimentally by Lade [127, 129].

An important application of the stability analysis in soils is the prediction of the spontaneous liquefaction, i.e. instabilities under isochoric condition. In this context a comparison of instability surfaces for referential hypoplastic model and an elasto-plastic model by di Prisco [197, 198] is presented by Herle [85].

In hypoplasticity, states with the negative second order work $W_2 = \mathring{T}_{ij} D_{ij}$ (if $\mathbf{D}$ is suitably chosen) can be encountered inside the yield surface, as shown in Fig. 2.11 and Fig. 3.12. For loose sand, with $e > e_c$ and increased nonlinear term (via $f_d > 1$), the stress surface $W_2 = 0$ can be reached at relatively small stress obliquity [85, 87] inside the W_2-surface presented in Fig. 3.12.

We have already discussed the second-order work in the context of controllability, see Section 3.2.3.

In the next subsections we provide an interpretation of the $W_2 < 0$ condition in the graphical language of response envelopes. A dynamic investigation of stability in the sense of Liapunov is performed for 1-D case in Subsection 4.1.1.

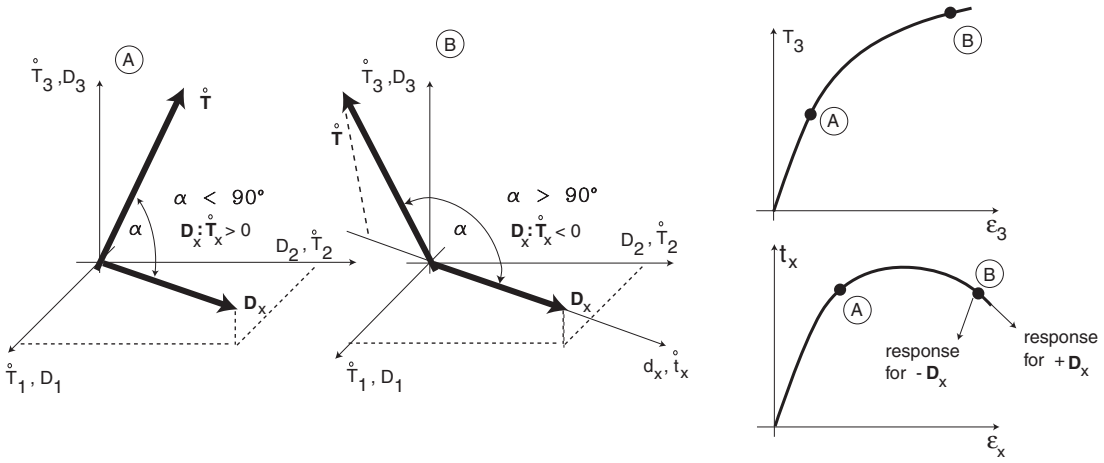

Figure 3.4: While loading with $\mathbf{D}_x$ we are passing through the states A and B. The second-order work is positive and negative with $\alpha < \pi/2$ and $\alpha > \pi/2$, respectively. The statement that the negative second-order work appears before the peak (e.g. [120]) must be carefully interpreted. Actually, softening ($\mathbf{D}^T\mathring{\mathbf{T}}(\mathbf{D}) < 0$) manifests itself as a falling curve in stress-strain diagram which can be demonstrated with suitably chosen composite variables $\dot{\mathbf{t}}$ and $\mathbf{d}$. Let the first components of such variables, denoted here by t_x and d_x, be chosen *along* the loading direction (here, we must find such M that $\mathbf{d} = \{1, 0, 0, \ldots, 0\}$ corresponds to $\mathbf{D}_x$). In stress-strain diagram with randomly chosen axes, here $\epsilon_3 - T_3$, the softening phenomenon $\mathring{\mathbf{T}} : \mathbf{D} < 0$ may indeed lie 'before the peak' whereas in $\epsilon_x - t_x$ diagram the point B lies already beyond the peak. Considering a state of material (and not a deformation process) $\mathbf{D}_x$ is not given and we look for a 'dangerous' strain rate for which $\mathbf{D}^T\mathring{\mathbf{T}}$ reaches minimum. If such product is negative our state lies already on the falling branch in certain diagram plotted with suitable composite variables

3.3.1 Negative W_2 interpreted with response envelopes

Usually the strain rates $\mathbf{D}$ and the corresponding stress rates $\mathring{\mathbf{T}}(\mathbf{D})$ form a sharp angle in a 9-dimensional stress rate - strain rate space with parallel axes of the corresponding components of $\mathring{\mathbf{T}}$ and $\mathbf{D}$, see Fig. 3.4. This means that inequality

$$\mathbf{D}^T\mathring{\mathbf{T}} = \mathbf{D}^T\mathsf{L}\ \mathbf{D} + \mathbf{D}^T\mathbf{N}\|\mathbf{D}\| > 0 \tag{3.87}$$

holds, for any strain rate $\mathbf{D}$ (we set $f_d = 1$ in this section too). Inequality (3.87) is interpreted as the angle between the stress rate and the strain rate being less than 90°, see Fig. 3.4. The tensor L is always positive definite but as the stress path approaches the limit surface we may find strain rates for which the absolute value of the product $\mathbf{D}^T\mathbf{N}\|\mathbf{D}\| < 0$ is greater than $\mathbf{D}^T\mathsf{L}\mathbf{D} > 0$ and (3.87) is not satisfied.

It is sufficient to consider (3.87) with L and $\mathbf{N}$ calculated from (3.5), i.e. using the principal stress components only. Moreover, we can restrict our discussion to the principal components of strain-rate only. This needs a short explanation. Let us find the stress state $\mathbf{T}$ for which the product (3.87) is positive for all $\mathbf{D}$ except for one which yields

$$\mathbf{D}^T\mathsf{L}\ \mathbf{D} + \mathbf{D}^T\mathbf{N}\|\mathbf{D}\| = 0 \tag{3.88}$$

Such stress is of interest here because it separates the positive and negative second-order work regions in the stress space. Let us search for the minimum of the l.h.s. of (3.88) under the additional condition $\|\mathbf{D}\| = 1$. Of course, assumption $\|\mathbf{D}\| = 1$ does not influence the sign of the discussed product (3.87).

We choose the coordinate system in such way that the stress tensor has a diagonal form, i.e. $\mathbf{T} = (T_{11}, T_{22}, T_{33}, 0, 0, \dots)^T$. The term $\mathbf{N}(\mathbf{T})$ is an isotropic tensorial function of $\mathbf{T}$ so it has also a diagonal form $\mathbf{N} = (N_{11}, N_{22}, N_{33}, 0, 0, \dots)^T$. We have assumed that L is a positive definite (and symmetric) matrix so the contribution from the off-diagonal components $\mathbf{D}^{\text{off}} = (0, 0, 0, D_{12}, D_{21}, D_{13} \dots)^T$ to the l.h.s. of (3.88) will be always positive because $\mathbf{N}^T\mathbf{D}^{\text{off}} = 0$ holds. Since we are looking for the minimum of the product $\mathbf{D}^T\mathring{\mathbf{T}}$ (over different $\mathbf{D}$-s) we may omit the always-positive contribution from the off-diagonal part of the strain rate $\mathbf{D}^{\text{off}}$ to (3.87) and restrict our discussion to the principal stresses and principal strain rates only, which means that $\mathbf{D}$ is coaxial with $\mathbf{T}$. In this situation the hypoplastic equation yields the stress rate $\mathring{\mathbf{T}}$ which is also coaxial with $\mathbf{D}$ and $\mathbf{T}$, see the matrix form (2.36). This simplifies greatly the numerical treatment of our problem.

Using the Lagrangian multiplier λ for the boundary condition $\|\mathbf{D}\| - 1$ we formulate the target function

$$F(\mathbf{D}, \lambda) = \mathbf{D}^T\mathsf{L}\,\mathbf{D} + \mathbf{D}^T\mathbf{N}\|\mathbf{D}\| + \lambda(\|\mathbf{D}\| - 1) \tag{3.89}$$

and search for its minimum with

$$\partial F/\partial \mathbf{D} \;=\; \mathbf{0} \tag{3.90}$$

$$\partial F/\partial \lambda \;=\; 0\,. \tag{3.91}$$

Moreover, this unknown minimum corresponds to the zero value of the target function $F(\mathbf{D}, \lambda) = 0$ so multiplying (3.90) by $\mathbf{D}$ and using $\|\mathbf{D}\| = 1$ we get $\lambda = 0$ and the resulting system of equations is

$$-2\mathsf{L}\mathbf{D} \;=\; (\mathbf{D}^T\mathbf{N})\mathbf{D} + \mathbf{N} \tag{3.92}$$

$$\|\mathbf{D}\| \;=\; 1 \tag{3.93}$$

Multiplying (3.92) by $\mathsf{L}^{-1} \cdot (\quad)$ and calculating of the norm of both sides we arrive at a system of two scalar equations

$$\|\mathsf{L}^{-1}(\mathbf{D}(\mathbf{N}^T\mathbf{D}) + \mathbf{N})\| \;=\; 2 \tag{3.94}$$

$$\|\mathbf{D}\| \;=\; 1 \tag{3.95}$$

which allows for a graphic interpretation in stress-rate space.

The construction of the response envelopes has been presented in Section 2.2 in (2.21) or in its rate form (2.22), see also Fig. 2.1. Here we choose the latter form, i.e. the

one plotted in the stress *rate* space. It is constituted by all stress rates $\mathring{\mathbf{T}}$ generated by the unit strain rate $\|\mathbf{D}\| = 1$. The equation of the hypoplastic response envelope is simply $\|\mathsf{L}^{-1}(\mathring{\mathbf{T}} - \mathbf{N})\| = 1$. For linear elastic material such response envelope would be $\|\mathsf{L}^{-1}\mathring{\mathbf{T}}\| = 1$.

Defining $\mathbf{x} = \mathbf{D}(\mathbf{N}^T\mathbf{D}) + \mathbf{N}$ and substituting it to (3.94) we obtain

$$\|\mathsf{L}^{-1}\mathbf{x}\| = 2 \tag{3.96}$$

which can be seen as an elastic response envelope of argument $\mathring{\mathbf{T}} = \mathbf{x} = \mathbf{D}(\mathbf{N}^T\mathbf{D}) + \mathbf{N}$ (the large ellipse in Fig. 3.5). Moreover, we may express (3.95) in terms of $\mathbf{x}$

$$(\mathbf{x} - 2\mathbf{N})^T(\mathbf{x} - \mathbf{N}) = 0 \tag{3.97}$$

which is equivalent to $(\mathbf{x}-\frac{3}{2}\mathbf{N})^T(\mathbf{x}-\frac{3}{2}\mathbf{N})-\frac{1}{4}\mathbf{N}^T\mathbf{N} = 0$ and corresponds to to the shadowed circle in Fig. 3.5 with the centre at $\mathbf{x} = \frac{3}{2}\mathbf{N}$ and the radius $\frac{1}{2}\|\mathbf{N}\|$. This simple conversion may be elegantly visualized in 2d case with MATHEMATICA:

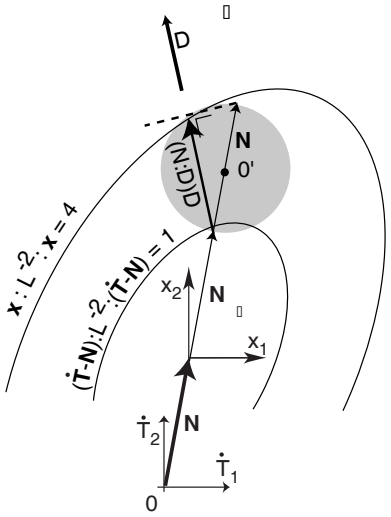

Figure 3.5: Geometrical construction of $W_2 > 0$ test in stress rate space: the shadowed circle (sphere) should lie inside the large ellipse

```
<< Graphics`ImplicitPlot`
ImplicitPlot[(x-1)(x-2)+(y-1)(y-2)==0,{x,-3,3}]
```

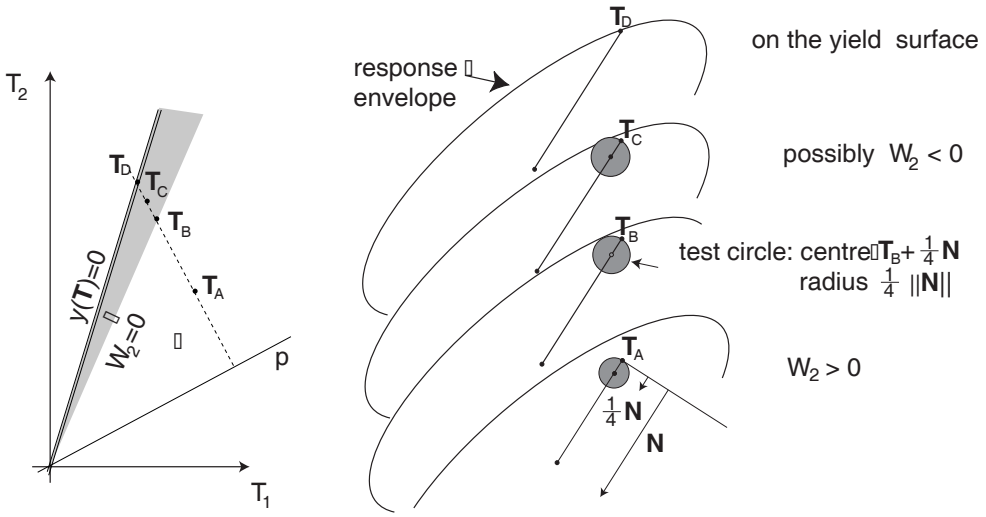

Figure 3.6: A possible occurrence of the negative second-order work can be detected drawing the *test circle* of radius $\frac{1}{4}\|\mathbf{N}\|$ with the centre at $\frac{3}{4}\mathbf{N}$ and looking for its intersection with the response envelope. At the stress state $\mathbf{T}_B$ (and above) a strain rate $\mathbf{D}$ exists for which $W_2 = 0$

Condition (3.94) is fulfilled if the large ellipse and the circle do not intersect, i.e. if the shortest distance between the ellipse $\|\mathsf{L}^{-1}\mathbf{x}\| = 2$ and the point $\mathbf{x} = \frac{3}{2}\mathbf{N}$ is larger than $\frac{1}{2}\|\mathbf{N}\|$.

In other words (scaling our result by half), condition (3.87) is satisfied if the whole sphere of radius $\frac{1}{4}\|\mathbf{N}\|$ with the centre at $\frac{3}{4}\mathbf{N}$ lies inside the response envelope $f_{env}(\overset{\circ}{\mathbf{T}}) \equiv \|\mathbf{D}(\overset{\circ}{\mathbf{T}})\| = 1$ in the stress rate space as shown in Fig. 3.6.

3.3.2 Analytical expression for the surface $W_2(\mathbf{T}) = 0$

Our present purpose is to find stresses for which $W_2(\mathbf{T}, \mathbf{D}) = 0$ has exactly one solution $\mathbf{D} \neq \mathbf{0}$. In other words, we are looking for a surface that separates stresses $\mathbf{T}$ with positive second-order work from the ones for which (3.87) for some $\mathbf{D}$ may be not satisfied. For simplicity we assume $f_d = 1$. Moreover, we set $f_b f_e/(\hat{\mathbf{T}}^T\hat{\mathbf{T}}) = 1$ because this multiplier does not affect the sign of the product in (3.87), anyway.

The calculation of the shortest distance from the point $\frac{3}{4}\mathbf{N}$ to the ellipsoid $o(\overset{\circ}{\mathbf{T}})$ leads to a 6-th order polynomial equation so the geometrical interpretation derived in the previous subsection is worth little or nothing in the analytical determination of the second-order work surface.

As argued in the previous subsection the second order work problem can be considered in principal stress space using coaxial strain rates $\mathbf{D} = \text{diag}[D_1, D_2, D_3]$ only. Unfortunately, even in this case the problem is quite complex. Formally, the task may seem straightforward: we have four nonlinear equations given in (3.92) and (3.93) from which three diagonal components of $\mathbf{D}$ might be eliminated. However, a direct solution of this problem is too complex to be managed by hand or using MATHEMATICA. A closed-form solution can be easier obtained if we notice that the $\hat{\mathsf{L}}$ given by (2.63) has a double eigenvalue.

In principal stress space we determine the eigenvalues of submatrix $\hat{\mathsf{L}}$ extracted from (3.5) as the 3×3 upper left-hand corner block. Consistently $\hat{\mathbf{N}}, \hat{\mathbf{T}}, \mathbf{D}$ have dimensions 3×1, like in (2.36). The eigenvalues of $\hat{\mathsf{L}}$ are then $\lambda_1 = \lambda_2 = F^2$ and $\lambda_3 = F^2 + a^2(\hat{T}_1^2 + \hat{T}_2^2 + \hat{T}_3^2)$ and the eigenvectors are $\{-\hat{T}_3, 0, \hat{T}_1\}$, $\{-\hat{T}_2, \hat{T}_1, 0\}$ and $\mathbf{v}^{(3)} = \{\hat{T}_1, \hat{T}_2, \hat{T}_3\}$, respectively. The double eigenvalue $\lambda_1 = \lambda_2$ implies that any vector perpendicular to $\mathbf{v}^{(3)}$ must be an eigenvector. We need a set of orthogonal eigenvectors so $\mathbf{v}^{(1)}$ may chosen arbitrarily and $\mathbf{v}^{(2)}$ is calculated with the Gram-Schmidt orthogonalization algorithm:

```
<< LinearAlgebra`Orthogonalization`
tt = {T1, T2, T3} ; LL =  F^2 * IdentityMatrix[3] + a^2 Outer[Times, tt, tt];
evs = Eigensystem[LL][[2]]
oevs = GramSchmidt[evs, Normalize->False]
```

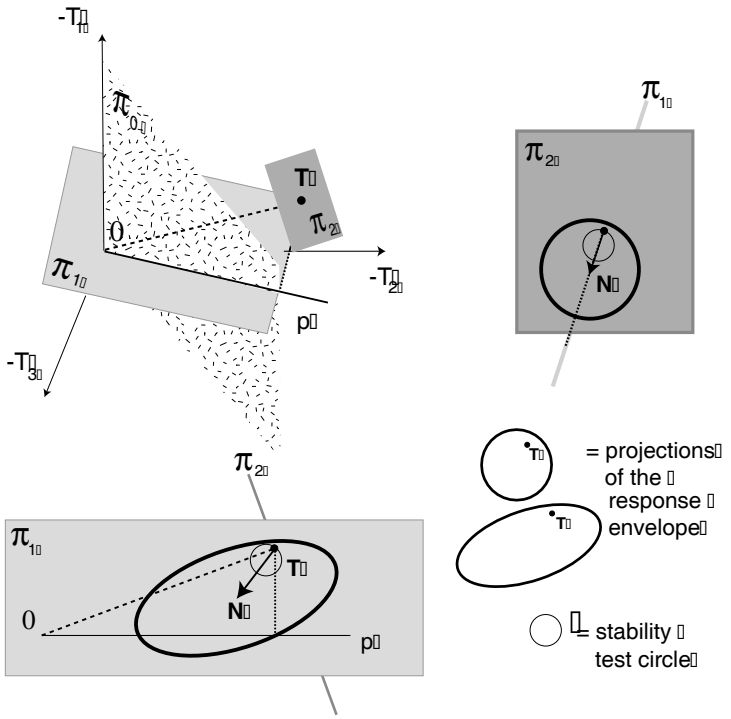

Figure 3.7: The cross-sections of the response envelope and the test sphere by different planes in stress space. The plane π_0 (Rendulic plane) corresponds to the condition $T_3 = T_2$. The plane π_1 contains the hydrostatic axis p and the current stress $\mathbf{T}$. The plane π_2 contains $\mathbf{T}$ and is perpendicular to the line $\mathbf{0} - \mathbf{T}$. Note that π_1 is not identical with the Rendulic plane and the plane π_2 is not identical with the deviatoric plane. The cross-section of the response envelope with the π_2 plane ($\pi_2 \perp \mathbf{T}$) gives a circle (not an ellipse) shifted along the $\mathbf{N} \sim (\mathbf{T} + \mathbf{T}^*)$. Since $\mathbf{N}$ lies on the π_1 plane so does the touching point of the test circle (sphere) and the response envelope

We choose $\mathbf{v}^{(1)}$ to lie on the plane π_1, see Fig. 3.7, that contains the hydrostatic axis p and the actual stress $\mathbf{T} \not\sim \mathbf{1}$.

After some manipulation we obtain three eigenvectors (not normalized): $\mathbf{v}^{(1)}$ and $\mathbf{v}^{(3)}$ lying the plane π_1 and $\mathbf{v}^{(2)}$ perpendicular to π_1, viz.

$$\mathbf{v}^{(1)} = \{\hat{T}_2^2 + \hat{T}_3^2 - \hat{T}_1(\hat{T}_2 + \hat{T}_3),\ \ \hat{T}_1^2 + \hat{T}_3^2 - \hat{T}_2(\hat{T}_1 + \hat{T}_3),\ \ \hat{T}_1^2 + \hat{T}_2^2 - \hat{T}_3(\hat{T}_2 + \hat{T}_1)\}^T \tag{3.98}$$

$$\mathbf{v}^{(2)} = \{-\hat{T}_2 + \hat{T}_3,\quad \hat{T}_1 - \hat{T}_3,\quad -\hat{T}_1 + \hat{T}_2\}^T \tag{3.99}$$

$$\mathbf{v}^{(3)} = \{\hat{T}_1, \hat{T}_2, \hat{T}_3\}^T . \tag{3.100}$$

Let us introduce another plane π_2 that passes through the current stress $\mathbf{T}$ and is perpendicular to the line $\mathbf{0T}$, see Fig. 3.7. For all strain rates $\mathbf{D}$ such that $\mathbf{D}^T\mathbf{T} = 0$ and $\|\mathbf{D}\| = 1$ the material response is

$$\mathring{\mathbf{T}} \sim (F^2\mathbf{D} + \hat{\mathbf{N}}) \tag{3.101}$$

which constitutes a circle shifted from $\mathbf{T}$ by $\mathbf{N}$ on the π_2 plane. From the interpretation presented in Section 3.3.1 follows that the test-sphere should be shifted from $\mathbf{T}$ by $\frac{1}{4}\mathbf{N}$ so

that the touching point of the response ellipsoid and the test-sphere must lie on the π_1 plane. We choose such composite stress-rate components that their coordinate axes lie parallel to $\vec{\mathbf{v}}^{(1)}, \vec{\mathbf{v}}^{(2)}, \vec{\mathbf{v}}^{(3)}$, i.e.

$$\left\{ \begin{array}{c} \dot{t}_1 \\ \dot{t}_2 \\ \dot{t}_3 \end{array} \right\} = \left[\begin{array}{ccc} \vec{v}_1^{(1)} & \vec{v}_2^{(1)} & \vec{v}_3^{(1)} \\ \vec{v}_1^{(2)} & \vec{v}_2^{(2)} & \vec{v}_3^{(2)} \\ \vec{v}_1^{(3)} & \vec{v}_2^{(3)} & \vec{v}_3^{(3)} \end{array} \right] \left\{ \begin{array}{c} \dot{T}_1 \\ \dot{T}_2 \\ \dot{T}_3 \end{array} \right\} \qquad \text{or briefly} \quad \dot{\mathbf{t}} = \mathsf{M}\mathring{\mathbf{T}} \tag{3.102}$$

with the conjugate strain rates

$$\mathbf{d} = \mathsf{M}^{-T}\mathbf{D} \tag{3.103}$$

The touching point of the ellipse and the test-sphere lies on the π_1 plane and so does the corresponding stress rate $\mathring{\mathbf{T}}^{\text{touch}}$. The corresponding strain rate $\mathbf{D}^{\text{touch}}$ satisfies the condition $(\mathbf{D}^{\text{touch}})^T\mathring{\mathbf{T}}^{\text{touch}} = 0$. It also lies on the π_1 plane, provided the axes T_1, T_2, T_3 are aligned with D_1, D_2, D_3 (and of course with $\mathring{T}_1, \mathring{T}_2, \mathring{T}_3$). This can be deduced from (3.101) and from the fact that $\mathbf{N}$ lies on π_1 too. This further means that

$$d_2^{\text{touch}} = 0 \quad \text{and} \quad \dot{t}_2^{\text{touch}} = 0 \tag{3.104}$$

must hold. Let us rewrite the constitutive model in terms of the composite variables $\dot{\mathbf{t}}$ and $\mathbf{d}$ applying the transformations (3.41). We may easily discover that C is the 3×3 identity matrix due to the orthogonality of M given in (3.102). Since M is composed of normalized eigenvectors of $\hat{\mathsf{L}}$ the new stiffness $\bar{\mathsf{L}} = \mathsf{M}\hat{\mathsf{L}}\mathsf{M}^T$ that interrelates the composite variables $\dot{\mathbf{t}}$ and $\mathbf{d}$ is diagonal:

$$\bar{\mathsf{L}} = \mathsf{M}\hat{\mathsf{L}}\mathsf{M}^T = \left[\begin{array}{ccc} F^2 & 0 & 0 \\ 0 & F^2 & 0 \\ 0 & 0 & F^2 + a^2\|\hat{\mathbf{T}}\|^2 \end{array} \right] \tag{3.105}$$

and $\bar{\mathbf{N}} = \mathsf{M}\hat{\mathbf{N}}$ has the form

$$\bar{\mathbf{N}} = \left\{ \begin{array}{c} -\frac{\sqrt{2}}{3}\, a\, F \sqrt{\frac{\left(\hat{T}_1^2+\hat{T}_2^2-\hat{T}_2\,\hat{T}_3+\hat{T}_3^2-\hat{T}_1\left(\hat{T}_2+\hat{T}_3\right)\right)}{\hat{T}_1^2+\hat{T}_2^2+\hat{T}_3^2}} \\ 0 \\ \frac{a\,F\left(\hat{T}_1\left(-1+6\,\hat{T}_1\right)+\hat{T}_2\left(-1+6\,\hat{T}_2\right)+\hat{T}_3\left(-1+6\,\hat{T}_3\right)\right)}{3\sqrt{\hat{T}_1^2+\hat{T}_2^2+\hat{T}_3^2}} \end{array} \right\} \tag{3.106}$$

with $\bar{N}_2 = 0$ as we could expect, judging form the fact that $\mathbf{N}$ lies on the π_1 plane. Finally we express (3.92) and (3.93) in terms of the composite variables $d_1, d_2 = 0$ and d_3 with $\bar{\mathsf{L}}$ and $\bar{\mathbf{N}}$ given by (3.105) and (3.106). We obtain three equations

$$\left\{ \begin{array}{c} 2\bar{L}_{11}d_1 + (d_1\bar{N}_1 + d_3\bar{N}_3)d_1 + \bar{N}_1 = 0 \\ 2\bar{L}_{33}d_3 + (d_1\bar{N}_1 + d_3\bar{N}_3)d_3 + \bar{N}_3 = 0 \\ d_1^2 + d_3^2 = 1 \end{array} \right. \tag{3.107}$$

which are much simpler than (3.92) and (3.93). Elimination of $\mathbf{d}$ from (3.107) with an aid of MATHEMATICA is straightforward

```
nn = Array[n,2]; dd=Array[d,2]; LL=DiagonalMatrix[{L[1,1],L[2,2]}];zero={0,0};
eqs = { 2 LL.dd + dd (nn.dd) + nn == zero, dd.dd == 1};
FullSimplify[Eliminate[eqs, {d[1], d[2]}]]
```

This leads to an analytical expression of the second-order work surface as a function of stress:

$$\begin{aligned} W_2(\mathbf{T}) \equiv \bar{N}_3^2 [\ & 16\bar{L}_{11}^4 - 32\bar{L}_{11}^3\bar{L}_{33} + 3\bar{N}_1^4 + 3\bar{N}_1^2\bar{N}_3^2 + \bar{N}_3^4 + 2\bar{L}_{11}\bar{L}_{33}\left(4\bar{L}_{33}^2 + 19\bar{N}_1^2 - 4\bar{N}_3^2\right) \\ & -\bar{L}_{33}^2\left(20\bar{N}_1^2 + \bar{N}_3^2\right) + 4\bar{L}_{11}^2\left(2\bar{L}_{33}^2 - 5\bar{N}_1^2 + 2\bar{N}_3^2\right)] \\ - \quad & \left[\bar{L}_{11}^2 - \bar{N}_1^2\right]\left[4\bar{L}_{33}\left(-\bar{L}_{11} + \bar{L}_{33}\right) + \bar{N}_1^2\right]^2 = 0 \end{aligned} \tag{3.108}$$

The functions f_e and f_b (cf. (2.56) or (2.63) do not influence the above result but f_d does. The solution for $f_d \neq 1$ is identical (3.108) but one has to replace $\bar{N}_1$ and $\bar{N}_3$ with $f_d\bar{N}_1$ and $f_d\bar{N}_3$, respectively. It can be seen from Fig. 3.8 and Fig. 3.3 that the negative second-order work is encountered prior to the yield surface.

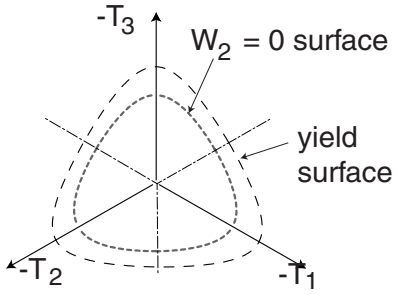

Figure 3.8: $W_2 = 0$ condition on the deviatoric plane

A similar situation is known from elastoplastic models, see Equation (2.9), with a non-associative flow rule $\vec{\mathbf{n}}_g \neq \vec{\mathbf{n}}_f$, and a non-symmetric stiffness

$$\mathsf{E}^{ep} = \mathsf{E} - \frac{\mathsf{E} : \vec{\mathbf{n}}_g\vec{\mathbf{n}}_f : \mathsf{E}}{K + \vec{\mathbf{n}}_g : \mathsf{E} : \vec{\mathbf{n}}_f},$$

i.e. $(\mathsf{E}^{ep})^T \neq \mathsf{E}^{ep}$ or $E^{ep}_{klij} \neq E^{ep}_{ijkl}$. The vanishing second-order work

$$D_{ij}E^{ep}_{ijkl}D_{kl} = \frac{1}{2}D_{ij}[E^{ep}_{ijkl} + E^{ep}_{klij}]\ D_{kl} = 0 \tag{3.109}$$

implicates that the smallest eigenvalue of $(\mathsf{E}^{ep})^{\text{symm}}$ vanishes but, according to Bromwich bounds, symmetrization can only widen the spectrum of real[4] eigenvalues so (3.109) does not necessarily imply $\det(\mathsf{E}^{ep}) = 0$, i.e. it does not allow for plastic flow $\mathring{T}_{ij} = E^{ep}_{ijkl}D_{kl} = 0$ if $D_{kl} \neq 0$. The diagnostics of the elastoplastic operator can be conveniently performed examining the value of K. The vanishing second-order work corresponds [141] to $K = \frac{1}{2}\left[\sqrt{(\vec{\mathbf{n}}_g : \mathsf{E} : \vec{\mathbf{n}}_g)(\vec{\mathbf{n}}_f : \mathsf{E} : \vec{\mathbf{n}}_f)} - \vec{\mathbf{n}}_f : \mathsf{E} : \vec{\mathbf{n}}_g\right] \geq 0$ and the unconfined flow to $K = 0$.

[4]It has been shown by Runesson and Mróz that the specific form of E^{ep} assures the real-valued spectrum

3.4 Homogeneity and proportional paths

In this section we are considering the response of the hypoplastic model to proportional compression started near the stress-free state. It is convenient to use the tensorial notation. The proportional paths are generated by radial compression and correspond to deformation paths with a given fixed direction $\vec{\mathbf{D}} = \text{const}$ such that $\operatorname{tr}\mathbf{D} < 0$. The principal axes of $\mathbf{D}$ are assumed fixed so that the strain increments are proportional and coaxial. We calculate a sequence of small time increments Δt with $\vec{\mathbf{D}} = \text{const}$ updating (Euler forward integration) stress

$$\mathbf{T}^{t+\Delta t} = \mathbf{T}^t + (\mathsf{L}^t : \mathbf{D} + \mathbf{N}^t\|\mathbf{D}\|)\Delta t \tag{3.110}$$

wherein t is a time-like parameter. The initial stress state $\mathbf{T}_0 \neq \mathbf{0}$ is assumed to lie inside the hypoplastic yield surface $y(\mathbf{T}) = 0$, i.e. $\|\mathbf{B}\| < 1$ holds and invertibility of (2.61) is ensured. For early hypoplastic models we recall that:

- $\mathring{\mathbf{T}}$ is a positive homogeneous function of the first order of $\mathbf{D}$ and $\mathbf{T}$
- L can be represented as a symmetric positive-definite matrix with $\mathbf{D} : \mathsf{L} : \mathbf{D} > 0$ for any $\mathbf{D}$,
- $\mathbf{N}$ is an isotropic function of stress and it is always coaxial with $\mathbf{T}$.
- L and $\mathbf{N}$ are smooth functions of stress.

The reference model (2.61) by Wolffersdorff satisfies these requirements except for being positively homogeneous in stress. As discussed further, we need not the homogeneity of $\mathring{\mathbf{T}}(\mathbf{T}, \mathbf{D})$ in stress, i.e. $(\lambda^2)^n\mathring{\mathbf{T}}(\mathbf{T}, \mathbf{D}) = \mathring{\mathbf{T}}(\lambda^2\mathbf{T}, \mathbf{D})$ is not necessary. For the present purpose a *directional homogeneity*

$$\vec{\mathring{\mathbf{T}}}(\mathbf{T}, \mathbf{D}) = \vec{\mathring{\mathbf{T}}}(\lambda^2\mathbf{T}, \mathbf{D}) \tag{3.111}$$

suffices and therefore stress inhomogeneities due to scalar functions f_e and f_b in (2.63) and (2.64) are of no importance. Condition (3.111) requires merely that the pressure and the void ratio evolve in agreement with (2.69) keeping f_d constant.

In the next two subsections we assume $f_d \approx \text{const}$, that is, changes in relative void ratio $r_e \approx \text{const.}$ (cf. (2.41)) remain negligible. We investigate how the reference hypoplastic model can generate proportional stress paths for $\vec{\mathbf{D}} = \text{const}$, what $\vec{\mathbf{D}}$ corresponds to a given initial stress $\mathbf{T}_0$, and why stress paths commenced at inadequate stresses ($\neq \mathbf{T}_0$) converge to the proportional path. It is argued that the rigorous requirement of stress

homogeneity of (3.7) is not necessary for proportional paths and may be replaced by the directional homogeneity condition (3.111). Moreover we show that convergent asymptotic behaviour is *not* a consequence of the homogeneity in $\mathbf{T}$ as sometimes suggested in the literature but follows from the negative definiteness of $(\partial\mathring{\mathbf{T}}/\partial\mathbf{T})$ during proportional compression $\vec{\mathbf{D}} = \text{const}$.

3.4.1 Response to proportional paths

In a true triaxial apparatus, any proportional (radial) *stress* path $\mathring{\mathbf{T}} \sim \mathbf{T}$ within the limits of the Coulomb cone can be followed. It has been observed, e.g. by Goldscheider [63], that the corresponding directions $\vec{\mathbf{D}}$ of strain rate remain constant upon such paths. This observation gave rise to the so-called SOM-hypothesis (swept out of memory) posed by Gudehus [67]. More recent triaxial and true triaxial tests by Chu and Lo [36] confirmed the existence of a unique proportional (or asymptotic) stress ratio line for a prescribed constant strain increment ratio, viz.

$$\left.\frac{q}{p}\right|_{asy} = M_0(1 + \frac{1}{3}\frac{D_v}{D_1}) \quad \text{with} \quad M_0 \approx 1.38 \quad \text{found empirically} \tag{3.112}$$

approximately for the range $-0.54 < -D_v/D_1 < 1$, i.e., unless the yield surface is encountered [5].

Hypoplastic models can reproduce proportional stress paths generated by strain path with $\vec{\mathbf{D}} = \text{const}$ and $\operatorname{tr}\mathbf{D} < 0$. This can be shown applying a suitable deformation rate $\mathbf{D} = \bar{\mathbf{D}}$ at an initial stress $\mathbf{T}_0$ inside the limit surface (to assure invertibility of (2.61)). Strain rate $\bar{\mathbf{D}}$ is found from the condition $\mathring{\mathbf{T}} = \lambda^2\mathbf{T}_0$ with a positive proportionality factor λ^2. For this purpose we solve

$$\lambda^2\mathbf{T}_0 = \mathsf{L}(\mathbf{T}_0) : \mathbf{D} + f_d\mathbf{N}(\mathbf{T}_0)\|\mathbf{D}\|, \tag{3.113}$$

for $\mathbf{D}$ and denote the solution as $\mathbf{D} = \bar{\mathbf{D}}$. Next, we repeat this calculation with the same $\mathbf{D} = \bar{\mathbf{D}}$ replacing $\mathbf{T}_0$ by the updated stress i.e. by $(1 + \lambda^2\Delta t)\mathbf{T}_0$ as the argument in $\mathsf{L}()$ and $\mathbf{N}()$ in (3.113). Due to the directional homogeneity property of L and $\mathbf{N}$ with respect to $\mathbf{T}$ also in this updated state satisfies the condition $\mathring{\mathbf{T}} \sim \mathbf{T}_0$ for the same $\bar{\mathbf{D}}$. Sequence of such increments is a process in which both directions $\bar{\mathbf{D}}$ and $\mathring{\vec{\mathbf{T}}}$ are fixed and the radial compression line[6] is obtained.

[5] Deviation from this rule is reported in post-yield region, for certain strain rates commenced at the yield surface.

[6] Under an additional assumption of strict homogeneity (not only directional) of order one we may introduce a scalar stress parameter T with $\mathbf{T}_0 = T\vec{\mathbf{T}}_0$ with $\vec{\mathbf{T}}_0 = \text{const}$ and integrate the equation $\mathrm{d}T = -\frac{1}{\lambda}T\mathrm{d}\epsilon$ obtaining $\epsilon - \epsilon_0 = -\lambda\ln(T/T_0)$ in accordance with the proposal of Butterfield [28] wherein λ denotes the compression coefficient (a material constant which is often used in Section 4.2).

We conclude that the *directional homogeneity* (3.111) suffices to describe radial paths at a constant direction of stretching inside the yield surface.

3.4.2 Asymptotic behaviour

For a constant strain rate $\bar{\mathbf{D}}$ (with fixed principal axes) the directional homogeneity causes that the material model generates a series of stress increments all proportional to the initial stress $\mathbf{T}_0$, wherein $\bar{\mathbf{D}}$ and $\mathbf{T}_0$ are interrelated by (3.113). Suppose now that a disturbance $\mathbf{s}$ shifts the initial stress $\mathbf{T}_0$ to $\mathbf{T} = \mathbf{T}_0 + \mathbf{s}$ off the line $\mathbf{0T}_0$. The former rate of deformation $\bar{\mathbf{D}}$ does not generate a proportional stress path for the process originated at the disturbed stress $\mathbf{T}$. In such case, according to experimental evidence, e.g. [9, 63, 64, 240], the model should predict a stress path converging slowly towards the asymptote $\mathbf{0T}_0$. For some materials the stress paths commenced at a disturbed stress $\mathbf{T}$ converge to the asymptote very quickly and finally reach it. From this moment the influence of the disturbance $\mathbf{s}$ is completely 'swept out of memory' (SOM-state, [67]). In most soils the observed convergence is rather slow [9,240]. If this convergence is guaranteed for any disturbance the material is said to have a convergent asymptotic behaviour. In this section we investigate, what causes that a hypoplastic constitutive equation reproduces such behaviour.

Let us treat the calculation of the stress increment with a constitutive model and the subsequent update of stress as a mapping $\mathbf{H}$ of the stress space into itself $\mathbf{T}^t \to \mathbf{T}^{t+\Delta t}$. In the present context we examine this mapping under an application of a constant strain rate $\bar{\mathbf{D}}$ with the time increment Δt. The stress path can be calculated as a sequence of mappings $\mathbf{T}$, $\mathbf{H}(\mathbf{T})$, $\mathbf{H}(\mathbf{H}(\mathbf{T}))$ etc. The mapping is convergent if images of two different points are closer to each other than the originals. In general this condition is not satisfied by most constitutive equations used in soil mechanics because of the well-known property that the soil stiffness increases with the stress level. This renders all radial disturbances growing.

However, the asymptotic convergence of stress paths means something different than the conventional convergence of mapping. We require merely that the distance between the *radial path* (asymptote) and the subsequent images of $\mathbf{T}$ decreases. It is essential that this distance is measured perpendicularly to the asymptote. Having decomposed the disturbance $\mathbf{s} = \mathbf{T} - \mathbf{T}_0$ into radial $\vec{\mathbf{T}}_0\vec{\mathbf{T}}_0 : \mathbf{s}$ and perpendicular $\mathbf{s}_\perp = \mathbf{s} - \vec{\mathbf{T}}_0\vec{\mathbf{T}}_0 : \mathbf{s}$ portion it suffices that the norm of the latter one becomes smaller. For brevity we introduce the tensor P such that $\mathbf{s}_\perp = \mathsf{P} : \mathbf{s}$. It has the form

$$P_{ijkl} = \delta_{ik}\delta_{jl} - \vec{T}_{0ij}\vec{T}_{0kl} \tag{3.114}$$

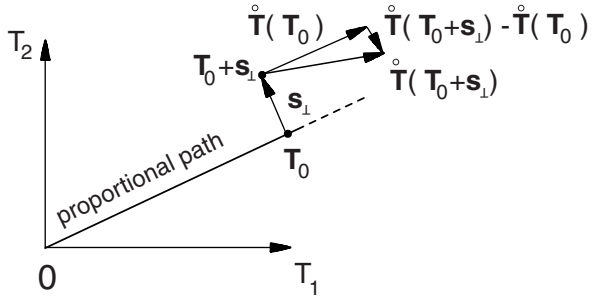

Figure 3.9: During the asymptotic nearing of the stress path to the proportional path the distance between the latter and the subsequent stresses $\mathbf{T}$ decreases. This is the case if $\mathbf{s}_\perp : \left[\mathring{\mathbf{T}}(\mathbf{T}_0+\mathbf{s}_\perp) - \mathring{\mathbf{T}}(\mathbf{T}_0)\right] < 0$ holds. However $\mathring{\mathbf{T}}(\mathbf{T}_0+\mathbf{s}_\perp) - \mathring{\mathbf{T}}(\mathbf{T}_0) \approx \dfrac{\partial \mathring{\mathbf{T}}}{\partial \mathbf{T}} : \mathbf{s}_\perp$ so the convergence condition is $\mathbf{s}_\perp : \dfrac{\partial \mathring{\mathbf{T}}}{\partial \mathbf{T}} : \mathbf{s}_\perp < 0$

Tensor P has the following properties:

$$\mathsf{P} : \mathbf{T}_0 = \mathbf{0}, \qquad \text{so} \qquad \mathsf{P} : (\mathbf{x} - \lambda \mathbf{T}_0) = \mathsf{P} : \mathbf{x};$$

$$\mathsf{P} : \mathsf{P} = \mathsf{P} \qquad \text{and} \qquad \mathbf{x}_\perp = \mathbf{x} : \mathsf{P} = \mathsf{P} : \mathbf{x}$$

so that

$$\mathbf{x}_\perp : \mathbf{y}_\perp = \mathbf{x} : \mathsf{P} : \mathsf{P} : \mathbf{y} = \mathbf{x} : \mathbf{y}_\perp = \mathbf{x}_\perp : \mathbf{y}$$

where $\mathbf{x}$ and $\mathbf{y}$ are second-order tensors.

For asymptotic behaviour we require that the perpendicular distance $\|\mathsf{P} : \mathbf{H}(\mathbf{T})\|$ between the image $\mathbf{H}(\mathbf{T})$ and the asymptote is smaller than the distance $\|\mathsf{P} : \mathbf{T}\|$ between the original $\mathbf{T}$ and the asymptote. Without restrictions to generality we choose the initial disturbance $\mathbf{s}$ perpendicular to $\mathbf{T}_0$ so that $\mathbf{s} = \mathbf{s}_\perp$. Admitting linearization of the operator $\mathbf{H}$ in the neighbourhood of $\mathbf{T}_0$ (if $\mathbf{s}$ is small) and using the first term of the Taylor's expansion we obtain

$$\mathbf{H}(\mathbf{T}) \approx \overbrace{\mathbf{T}_0 + \mathbf{s}}^{=\mathbf{T}} + \Delta\mathbf{T}|_{\mathbf{T}=\mathbf{T}_0} + \left.\frac{\partial \Delta \mathbf{T}}{\partial \mathbf{T}}\right|_{\mathbf{T}=\mathbf{T}_0} : \mathbf{s} + \dots \tag{3.115}$$

wherein $\Delta\mathbf{T} = \left.\mathring{\mathbf{T}}\right|_{\mathbf{T}=\mathbf{T}_0} \Delta t$ and $\left.\frac{\partial \Delta \mathbf{T}}{\partial \mathbf{T}}\right|_{\mathbf{T}=\mathbf{T}_0}$ are the stress increment and its stress derivative calculated at the strain increment $\bar{\mathbf{D}}\Delta t$. For convergent asymptotic behaviour we require that the (squared) distance $\mathbf{s}_\perp : \mathbf{s}_\perp$ becomes smaller. Such distance (from the asymptote to the disturbed stress after being updated) can be calculated using

$$\mathsf{P} : \mathbf{H}(\mathbf{T}) = \mathbf{s}_\perp + \mathsf{P} : \frac{\partial \mathring{\mathbf{T}}}{\partial \mathbf{T}} : \mathbf{s}\Delta t \tag{3.116}$$

and neglecting the small terms with $(\Delta t)^2$ we obtain

$$\|\mathsf{P} : \mathbf{H}(\mathbf{T})\|^2 - \mathbf{s} : \mathbf{s} = 2\mathbf{s} : \frac{\partial \mathring{\mathbf{T}}}{\partial \mathbf{T}} : \mathbf{s}\Delta t + \dots \tag{3.117}$$

Evidently, for convergent asymptotic behaviour the change in the distance (3.117) should be negative. Therefore the condition

$$\boxed{\mathbf{s} : \frac{\partial \mathring{\mathbf{T}}}{\partial \mathbf{T}} : \mathbf{s} < 0 \quad \text{for} \quad \mathbf{T} = \mathbf{T}_0, \quad \mathbf{D} = \bar{\mathbf{D}} \quad \text{and} \quad \mathbf{s} : \mathbf{T} = 0} \tag{3.118}$$

should be satisfied for any $\mathbf{s}$ perpendicular to $\mathbf{T}_0$ (necessary condition). This condition assures the convergence of stress paths generated with $\bar{\mathbf{D}}$ given in (3.113) and commenced in a close vicinity of $\mathbf{T}_0$ only.

Illustrative example

Consider a simplified 2-dimensional version of the hypoplastic model

$$\begin{Bmatrix} \dot{T}_1 \\ \dot{T}_2 \end{Bmatrix} = \begin{bmatrix} L_{11} & L_{12} \\ L_{21} & L_{22} \end{bmatrix} \cdot \begin{Bmatrix} D_1 \\ D_2 \end{Bmatrix} + c \cdot \begin{Bmatrix} N_1 \\ N_2 \end{Bmatrix} \sqrt{D_1^2 + D_2^2}. \tag{3.119}$$

Let (3.119) be invertible and of zeroth order homogeneous in stress. We choose $L_{ij} = \text{const}$ and $N_i = T_i/\sqrt{T_1^2 + T_2^2}$. In the following it will be demonstrated that the asymptotic behaviour of model (3.119) depends on the sign of the material parameter c. Condition (3.118) takes the form

$$\frac{c}{(T_1^2 + T_2^2)^{3/2}} \begin{Bmatrix} s_1, & s_2 \end{Bmatrix} \cdot \begin{bmatrix} T_2^2 & -T_1 T_2 \\ -T_1 T_2 & T_1^2 \end{bmatrix} \cdot \begin{Bmatrix} s_1 \\ s_2 \end{Bmatrix} = c \frac{(s_1 T_2 - s_2 T_1)^2}{(T_1^2 + T_2^2)^{3/2}} < 0 \tag{3.120}$$

from which follows that $c < 0$ must hold. For the special case $s_1 T_2 - s_2 T_1 = 0$ the trajectories started from $\mathbf{T}_0$ and $\mathbf{T}$ are parallel so they do not converge. However, this case corresponds to disturbance *along* the proportional path so the trajectories coincide. The convergence observed in numerical tests (Fig. 3.10) confirms the validity of the condition $c < 0$. We may conclude that for the convergent asymptotic behaviour of the hypoplastic model the negative value of $\mathbf{N}$ is of primary importance!

For comparison, we discuss shortly the consequences of (3.118) for elastoplasticity. Let us consider an elastoplastic constitutive equation in the form

$$\mathring{\mathbf{T}} = \mathsf{E} : (\mathbf{D} - \mathbf{D}^p) \quad \text{and} \quad \mathbf{D}^p = \dot{\lambda} \vec{\mathbf{n}}_g = \frac{\vec{\mathbf{n}}_f : \mathsf{E} : \mathbf{D}}{K + \vec{\mathbf{n}}_f : \mathsf{E} : \vec{\mathbf{n}}_g} \vec{\mathbf{n}}_g \tag{3.121}$$

where $\mathbf{D}^p$ denotes the plastic strain rate, $\vec{\mathbf{n}}_f$ is the tensor normal to the yield surface, $\vec{\mathbf{n}}_g$ is the direction of plastic flow and K is the plastic modulus. For simplicity let us assume that $\mathsf{E} = \text{const}$. For this case the condition (3.118) can be rewritten in the form

$$-\mathbf{s} : \mathsf{E} : \frac{\partial \mathbf{D}^p}{\partial \mathbf{T}} : \mathbf{s} < 0 \quad \text{or} \quad \mathbf{s} : \mathsf{E} : \frac{\partial \vec{\mathbf{n}}_g^p}{\partial \mathbf{T}} : \mathbf{s} > 0 \quad \text{or} \quad \mathbf{s} : \mathsf{E} : \frac{\partial^2 g(\mathbf{T})}{\partial \mathbf{T} \partial \mathbf{T}} : \mathbf{s} > 0 \tag{3.122}$$

where $\vec{\mathbf{n}}_g = (\partial g(\mathbf{T})/\partial \mathbf{T})\vec{}$ is obtained from the plastic potential. Thus, increasing the

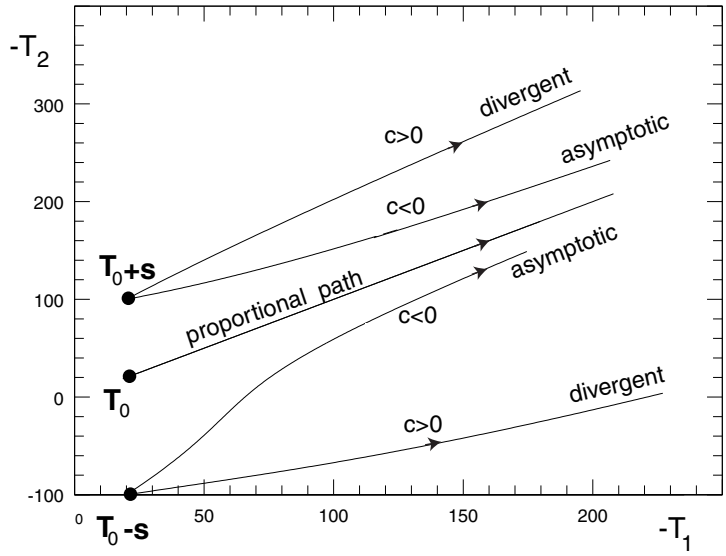

Figure 3.10: Stress paths that converge ($c < 0$) and diverge ($c > 0$) from the proportional path

convexity of the plastic potential $g(\mathbf{T}) = 0$ we may strengthen, roughly speaking, the convergence of the disturbed paths and foster convergent asymptotic behaviour.

Let us finally remark that convergent asymptotic behaviour is by no means a matter of course in contemporary constitutive models for soils. For example, Simpson [221] had to introduce a special modification into his 'brick' model to assure this convergence.

3.5 Localized bifurcation

As already remarked at the beginning of this chapter, a macroscopically 'uniform' deformation field is a simplification used for mathematical convenience. Strong spatial fluctuations of strain field are present in granular materials and can hardly be smoothed by monotonic or cyclic loading, see Section 3.5.2. In calculations we usually deal with average strain fields and the fluctuations are replaced by some artificial state variables or just neglected. At certain stress ratios, however, spatial fluctuations of strain cannot be ignored. They grow spontaneously obtaining the well known form of shear bands and patterns thereof. In mean-field models an onset of a shear band is described by *conditions of*

localized bifurcation. If these conditions are satisfied at a sufficiently low stress level, then (for simple boundary conditions) quite realistic deformation fields with shear localization can be obtained from FE calculation. Here, necessary conditions for such localization of deformation are discussed in the framework of the hypoplastic model.

The analysis of post-localization deformation requires sophisticated modeling techniques. This subject was analyzed in the hypoplastic framework by Tejchman [235], Huang [97], Bauer [11] using Cosserat polar-continuum, by Maier [142] using a non-local modeling and by Niemunis and Maier [175] using the gradient-continuum theory. Here, we restrict attention to the onset of localization and to a somewhat artificial situation with perfectly homogeneous stress and homogeneous strain rate fields just before hypothetical localization. It is demonstrated that even the simplest versions of the hypoplastic model can satisfactorily predict the possibility of strain localization, far below the peak of the stress - strain curve. The phenomenon of strain localization is termed localized *bifurcation* because appearance of a localized strain zone is not deterministic: it may occur or it may not. It is merely a possibility, an optional solution of the BVP, that can be triggered out by some initial imperfections. Of course, soil is fraught with inhomogeneities and in one way or another shear bands appear (see Section 3.5.2).

Hypoplasticity predicts fairly well the onset of localization treating the deformation field 'as if it were homogeneous'. This advantage was discovered by Kolymbas and Rombach [121] who presented a shear band analysis under simplifying assumption of 2-D deformation field and with $\mathbf{D} = \mathbf{0}$ outside the shear band. The same topic was further studied by Sikora [219] and Wu and Sikora [275] in 2-D case. With respect to those works the following new topics are raised here:

- full 3-D analysis without additional assumptions about $\mathbf{D}$ inside or outside the localized zone,
- consideration of finite rotations
- closed expression for the lower bound of stress for which localization is possible
- distinction between the lower bound of localization and the onset localization in the course of a deformation process.

3.5.1 Compatibility and equilibrium conditions

We seek for a *continuous* velocity field $\mathbf{v}(\mathbf{x})$ with possible discontinuities of the gradient,

$$\partial \mathbf{v}/\partial \mathbf{x} \neq 0 \tag{3.123}$$

across π-planes, see Fig. 3.11.

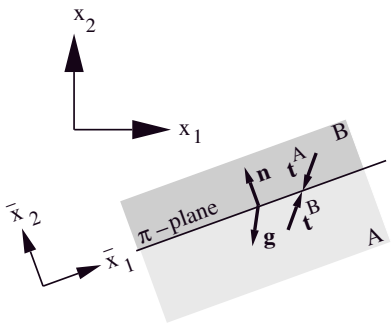

Figure 3.11: Coexistence of two stress and strain fields along the common border π

The stress field associated with the gradient $\partial\mathbf{v}/\partial\mathbf{x}$ must be in equilibrium, in particular, tractions (stress *vectors*) on both sides of the inhomogeneity plane are identical. In other words, we formulate coexistence conditions for two *different* stress rate fields: $\dot{\mathbf{T}}^A, \dot{\mathbf{T}}^B$ and for two velocity gradient fields $(\partial\mathbf{v}/\partial\mathbf{x})^A$ and $(\partial\mathbf{v}/\partial\mathbf{x})^B$ that meet at the boundary π. The superscripts A and B refer to the values of a field quantity at π in the respective zones. The same initial state $\mathbf{T}^A = \mathbf{T}^B$ and the same constitutive equation are assumed for the calculation of $\dot{\mathbf{T}}^A$ and $\dot{\mathbf{T}}^B$. With reference to Fig. 3.11, the jump of the velocity gradient across the π-plane can be written as follows

$$[\![\partial\mathbf{v}/\partial\mathbf{x}]\!] = (\partial\mathbf{v}/\partial\mathbf{x})^B - (\partial\mathbf{v}/\partial\mathbf{x})^A, \tag{3.124}$$

Making use of Maxwell's theorem [244] on the compatibility conditions for a discontinuity of order one it can be shown that the jump of the velocity gradient has the dyadic structure

$$[\![\partial\mathbf{v}/\partial\mathbf{x}]\!] = \mathbf{g}\ \mathbf{n}, \tag{3.125}$$

in which $\mathbf{n}$ is the unit vector normal to the inhomogeneity plane and $\mathbf{g}$ is an arbitrary vector. If $\mathbf{g} = \mathbf{0}$ then $\mathbf{D}^A = \mathbf{D}^B$ and no jump is observed. The vector $\mathbf{g}$ cannot be determined from the geometric considerations only. It is discussed further in this section. In order to derive Equation (3.125) consider first two smooth *scalar* fields $v^A(\mathbf{x})$ and $v^B(\mathbf{x})$ continuous and smooth in subdomains A and B, respectively. The interface plane is expressed by the equation $\pi(\mathbf{x}) = 0$ and the continuity $v^A(\mathbf{x}) = v^B(\mathbf{x})$ is satisfied everywhere on this π-plane. The continuity requires that the gradients of $v^A(\mathbf{x})$ and $v^B(\mathbf{x})$ with respect to any direction lying along the π-plane are identical. Let us introduce a local coordinate system $\bar{\mathbf{x}}$ such that $\bar{x}_2$ is perpendicular to π, Fig. 3.11. Then the following gradients are equal

$$\frac{\partial\bar{v}^A}{\partial\bar{x}_1} = \frac{\partial\bar{v}^B}{\partial\bar{x}_1}, \tag{3.126}$$

$$\frac{\partial\bar{v}^A}{\partial\bar{x}_3} = \frac{\partial\bar{v}^B}{\partial\bar{x}_3} \tag{3.127}$$

and the only non-vanishing difference in gradients is in the direction of $\bar{x}_2$. This can be written as

$$\left[\!\!\left[\frac{\partial\bar{v}}{\partial\bar{\mathbf{x}}}\right]\!\!\right] = \bar{g}\ \bar{\mathbf{n}} \tag{3.128}$$

where $\bar{\mathbf{n}} = [0,1,0]^T$ is a unit vector normal to the π-plane and $\bar{g}$ is a scalar value of the jump. This scalar may change with the position on the π-plane so generally $\bar{g} = \bar{g}(\bar{x}_1, \bar{x}_3)$.

Let us apply this results to three components of velocity: $\bar{v}_1$, $\bar{v}_2$, $\bar{v}_3$, treating them as independent scalar fields. The restrictions on jumps of their gradients are

$$\left[\!\left[\frac{\partial \bar{v}_1}{\partial \bar{\mathbf{x}}}\right]\!\right] = \bar{g}_1\ \bar{\mathbf{n}}, \qquad \left[\!\left[\frac{\partial \bar{v}_2}{\partial \bar{\mathbf{x}}}\right]\!\right] = \bar{g}_2\ \bar{\mathbf{n}}, \quad \text{and} \quad \left[\!\left[\frac{\partial \bar{v}_3}{\partial \bar{\mathbf{x}}}\right]\!\right] = \bar{g}_3\ \bar{\mathbf{n}}, \tag{3.129}$$

wherein $\bar{g}_1$, $\bar{g}_2$, $\bar{g}_3$ can be seen as components of a vector $\bar{\mathbf{g}}$. It is convenient to rewrite the above results in a tensorial form using the dyadic product

$$\left[\!\left[\frac{\partial \bar{\mathbf{v}}}{\partial \bar{\mathbf{x}}}\right]\!\right] = \bar{\mathbf{g}}\ \bar{\mathbf{n}}. \tag{3.130}$$

A tensorial equation must hold in any coordinate system and therefore Equation (3.125) applies. The matrix form reads as

$$\left[\!\left[\frac{\partial \bar{\mathbf{v}}}{\partial \bar{\mathbf{x}}}\right]\!\right] = \begin{bmatrix} 0 & \bar{g}_1 & 0 \\ 0 & \bar{g}_2 & 0 \\ 0 & \bar{g}_3 & 0 \end{bmatrix}. \tag{3.131}$$

which can be decomposed into the symmetric jump of stretching and the antisymmetric jump of spin, viz.

$$[\![\mathbf{D}]\!] = \frac{1}{2}(\bar{\mathbf{g}}\ \bar{\mathbf{n}} + \bar{\mathbf{n}}\ \bar{\mathbf{g}}) = \frac{1}{2}\begin{bmatrix} 0 & \bar{g}_1 & 0 \\ \bar{g}_1 & 2\bar{g}_2 & \bar{g}_3 \\ 0 & \bar{g}_3 & 0 \end{bmatrix}, \tag{3.132}$$

$$[\![\mathbf{W}]\!] = \frac{1}{2}(\bar{\mathbf{g}}\ \bar{\mathbf{n}} - \bar{\mathbf{n}}\ \bar{\mathbf{g}}) = \frac{1}{2}\begin{bmatrix} 0 & \bar{g}_1 & 0 \\ -\bar{g}_1 & 0 & -\bar{g}_3 \\ 0 & \bar{g}_3 & 0 \end{bmatrix}. \tag{3.133}$$

The eigenvalues of $[\![\mathbf{D}]\!]$ are $0, \frac{1}{2}(\bar{g}_2 + \sqrt{\bar{g}_1{}^2 + \bar{g}_2^2 + \bar{g}_3^2})$ and $\frac{1}{2}(\bar{g}_2 - \sqrt{\bar{g}_1^2 + \bar{g}_2^2 + \bar{g}_3^2})$ or, more generally, the jump of strain has a diagonal form

$$[\![\mathbf{D}]\!] = \ \mathrm{diag}[0, \frac{1}{2}(\mathbf{n}\cdot\mathbf{g} + \|\mathbf{g}\|), \frac{1}{2}(\mathbf{n}\cdot\mathbf{g} - \|\mathbf{g}\|)] \tag{3.134}$$

with a dilatancy angle

$$\mathrm{tr}\ [\![\mathbf{D}]\!]\ /\|\ [\![\mathbf{D}]\!]\ \| = 2\mathbf{n}\cdot\mathbf{g}/\sqrt{\mathbf{n}\cdot\mathbf{g} + \mathbf{g}\cdot\mathbf{g}}\,. \tag{3.135}$$

The static equilibrium condition across the discontinuity plane has the form

$$[\![\mathbf{t}]\!] = [\![\mathbf{T}]\!]\cdot\mathbf{n} = \mathbf{0}. \tag{3.136}$$

Let the initial stress field on the both sides of the discontinuity plane π be in equilibrium. In the subsequent state it is therefore necessary that the condition

$$[\![\dot{\mathbf{t}}]\!] = \left[\!\left[\dot{\mathbf{T}}\right]\!\right]\cdot\mathbf{n} + [\![\mathbf{T}]\!]\cdot\dot{\mathbf{n}} = \mathbf{0}. \tag{3.137}$$

is satisfied. This equation can be simplified to

$$[\![\dot{\mathbf{t}}]\!] = \left[\!\left[\dot{\mathbf{T}}\right]\!\right] \cdot \mathbf{n} \tag{3.138}$$

because we have assumed that the current state is still homogeneous (localized bifurcation is just beginning) and therefore the jump in the stress field is absent[7], $[\![\mathbf{T}]\!] = \mathbf{0}$. In the local coordinate system (3.138) can be expressed as

$$\left[\!\left[\dot{\hat{T}}_{12}\right]\!\right] = \left[\!\left[\dot{\hat{T}}_{22}\right]\!\right] = \left[\!\left[\dot{\hat{T}}_{23}\right]\!\right] = 0. \tag{3.139}$$

and the remaining stress rate components $\dot{\hat{T}}_{11}$, $\dot{\hat{T}}_{13}$ and $\dot{\hat{T}}_{33}$ may be discontinue across the π-plane.

Now, let us substitute the jump of the stress rate calculated with the hypoplastic constitutive model into (3.138). Due to the incremental nonlinearity the jump in the stress rate $\left[\!\left[\dot{\mathbf{T}}\right]\!\right]$ cannot be directly expressed by $[\![\mathbf{D}]\!]$ and $[\![\mathbf{W}]\!]$.

The equilibrium condition states that the stress rate *vectors*, on the both sides of the discontinuity surface, inside and outside of the shear band, are in equilibrium $\dot{\mathbf{T}}^A \cdot \mathbf{n} + \dot{\mathbf{T}}^B \cdot (-\mathbf{n}) = \mathbf{0}$, hence $\left[\!\left[\dot{\mathbf{T}}\right]\!\right] \cdot \mathbf{n} = 0$. The jump of the Cauchy stress rate $\dot{\mathbf{T}}$ will be calculated as

$$\left[\!\left[\dot{T}_{ij}\right]\!\right] = \left[\!\left[\mathring{T}_{ij}\right]\!\right] - T_{ik}\,[\![W_{kj}]\!] + [\![W_{ik}]\!]\,T_{kj} \tag{3.140}$$

with $[\![W_{ij}]\!] = \frac{1}{2}(g_i n_j - n_i g_j)$ and $[\![D_{ij}]\!] = \frac{1}{2}(g_i n_j + n_i g_j)$. Hence

$$[\![\dot{t}_j]\!] = n_i \left[\!\left[\dot{T}_{ij}\right]\!\right] = n_i \left[\!\left[\mathring{T}_{ij}\right]\!\right] + A_{jk} g_k = 0 \tag{3.141}$$

with

$$2A_{jk} = n_i T_{ij} n_k - T_{kj} - n_j n_i T_{ik} + n_i T_{ir} n_r \delta_{jk} \tag{3.142}$$

The symmetry of tensor L_{ijkl} with respect to the indices kl has been used. The tensor $\mathbf{A}$ can be written in the following matrix form:

$$[\mathbf{A}] = \frac{1}{2} \begin{bmatrix} \omega_i n_i - T_{11} & \omega_1 n_2 - \omega_2 n_1 & \omega_1 n_3 - \omega_3 n_1 \\ \omega_2 n_1 - \omega_1 n_2 & \omega_i n_i - T_{22} & \omega_2 n_3 - \omega_3 n_2 \\ \omega_3 n_1 - \omega_1 n_3 & \omega_3 n_2 - \omega_2 n_3 & \omega_i n_i - T_{33} \end{bmatrix} \tag{3.143}$$

[7]The simplification of (3.137) to the form (3.138) is not justifiable in the deformation analysis of composite materials and may lead to considerable errors, as it has been shown numerically by Niemunis, Karcher und Theile in [173] www.AN . At the interface of two materials A and B the stresses $\mathbf{T}^A$ and $\mathbf{T}^B$ may evolve quite differently from the very beginning and $[\![\mathbf{T}]\!] \neq \mathbf{0}$ holds. In the bifurcation analysis we have assumed homogeneity prior to the occurrence of strain localization so the stresses $\mathbf{T}^A$ and $\mathbf{T}^B$ are not only compatible but identical, i.e. $\mathbf{T}^A = \mathbf{T}^B$, and the term $[\![\mathbf{T}]\!] \cdot \dot{\mathbf{n}}$ in (3.137) can indeed be neglected.

wherein $\omega_i = T_{ij} n_j$ denotes the component of the traction vector. The equilibrium condition for stress vectors reads now:

$$\boxed{(n_i L_{ijkl} n_l + A_{jk}) g_k + n_i N_{ij} (\|\mathbf{D}^+\| - \|\mathbf{D}^-\|) = 0} \tag{3.144}$$

and $n_i L_{ijkl} n_l$ resembles the acoustic tensor known from elasticity, see e.g. [167] www.AN . Let us introduce the abbreviations

$$\bar{L}_{jk} = n_i L_{ijkl} n_l + A_{jk} \quad \text{and} \quad \bar{N}_i = N_{ij} n_j \,. \tag{3.145}$$

Note that A_{jk} is of the magnitude of stress so usually it is much smaller than $n_i L_{ijkl} n_l$ which is of the magnitude of stiffness and and therefore $\bar{L}_{jk}$ is always positive definite. The localized bifurcation is possible if equation

$$\bar{\mathbf{L}} \cdot \mathbf{g} + \bar{\mathbf{N}} (\|\mathbf{D}^A\| - \|\mathbf{D}^B\|) = \mathbf{0} \tag{3.146}$$

has a real solution $\mathbf{g} \neq \mathbf{0}$. However, $\mathbf{D}^A$, $\mathbf{D}^B$ and $\mathbf{g}$ are not independent! Sikora and Wu [276] investigated localized bifurcation of hypoplastic model in plane strain conditions. They concluded that additional restriction on the length of the jump $[\![\mathbf{D}]\!] = \frac{1}{2}(\mathbf{n}\,\mathbf{g} + \mathbf{g}\,\mathbf{n})$ must be imposed if the lengths $\|\mathbf{D}^A\|$ and $\|\mathbf{D}^B\|$ are given, namely, the elementary triangle inequalities

$$|\|\mathbf{D}^A\| - \|\mathbf{D}^B\|| < \| [\![\mathbf{D}]\!] \| < \|\mathbf{D}^A\| + \|\mathbf{D}^B\| \tag{3.147}$$

must be satisfied.

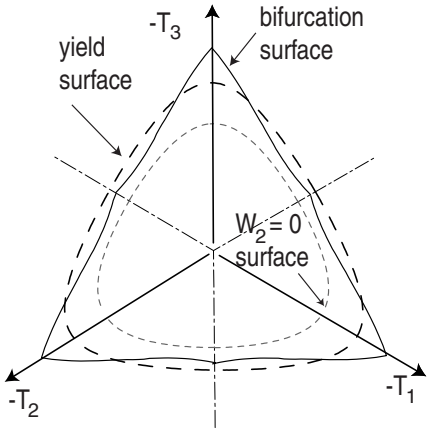

Figure 3.12: Bifurcation surface of the reference model ($e = e_c$) cut by the deviatoric plane. Theoretically, localized bifurcation should not occur for triaxial compression for which the bifurcation surface lies beyond the yield surface, see also [267]

Let us introduce the following definition

$$d_b = \| [\![\mathbf{D}]\!] \| / |\|\mathbf{D}^A\| - \|\mathbf{D}^B\|| \tag{3.148}$$

and let us call d_b the *degree of bifurcation*. Localization is possible if $d_b = 1$ because the other triangle inequality turns out to be less important. In order to find stresses for which bifurcation is just possible (we may call it *bifurcation surface* in stress space, see Fig. 3.12) we resort to a numerical procedure. Starting from the hydrostatic axis (where $d_b < 1$) we increase radially the stress deviator and examine the values d_b. The subsequent stress states are tested until the bounding surface $b(\mathbf{T}) = 0$ or $d_b = 1$ is encountered. At each stress level, we must calculate d_b for all inclinations $\mathbf{n}$ of discontinuity plane assuming say $(\|\mathbf{D}^A\| - \|\mathbf{D}^B\|) = 1$ and finding $\mathbf{g}$ from (3.146). The triangle inequality is first satisfied

(lower bound, $d_b = 1$) when $\mathbf{D}^A$, $\mathbf{D}^B$ and $\mathbf{D}^A - \mathbf{D}^B$ are parallel i.e. all three tensors are proportional. In this case $\|\mathbf{D}^A\| - \|\mathbf{D}^B\| = \pm\| [\![\mathbf{D}]\!] \| = \pm\frac{1}{\sqrt{2}}\sqrt{\mathbf{g}\cdot\mathbf{g} + (\mathbf{g}\cdot\mathbf{n})^2}$ holds, cf. (3.134), and our localization condition can be simplified to

$$\bar{\mathbf{L}}\cdot\mathbf{g} = \pm\frac{1}{\sqrt{2}}\bar{\mathbf{N}}\sqrt{\mathbf{g}\cdot\mathbf{g} + (\mathbf{g}\cdot\mathbf{n})^2} \tag{3.149}$$

in which $\mathbf{g}$ must be proportional to $\bar{\mathbf{L}}^{-1}\cdot\bar{\mathbf{N}}$ and as such may be eliminated. The criterion to be numerically checked is thus

$$\boxed{2 = \|\bar{\mathbf{L}}^{-1}\cdot\bar{\mathbf{N}}\|^2 + (\mathbf{n}\cdot\bar{\mathbf{L}}^{-1}\cdot\bar{\mathbf{N}})^2} \tag{3.150}$$

In order to find the inclination $\mathbf{n}$ of the localization plane we could search for the maximum of the right-hand side of (3.150) but this has not been solved as yet. Equation (3.150) with the right-hand side maximized over all $\mathbf{n}$-s is the lower bounding solution for $\mathbf{T}$ at which localization can theoretically be triggered out. This can only occur during a deformation process with $\mathbf{D} \sim \frac{1}{2}(\mathbf{n}\ \mathbf{g} + \mathbf{g}\ \mathbf{n})$ with $\mathbf{g} \sim \pm\bar{\mathbf{L}}^{-1}\cdot\bar{\mathbf{N}}$. If we increase the stress obliquity the fan of directions of stretching that allow for localization becomes wider. We conclude that for localization of strain not only the achieved stress level but also the current direction of stretching is of importance. Localization should be therefore considered also as a property of the *process* characterized (at least) by $\mathbf{T}$ and $\mathbf{D}$. An extensive studies on localized bifurcation for CLoE-hypoplasticity were presented by Chambon and Crochepeyre [31, 38, 39] inclusive the post-critical analysis with the extended model 'Daphnis'.

In the classical associative elastoplasticity with smooth yield surface, the localized bifurcation may occur first with vanishing hardening modulus. The elastoplastic models are known to respond overly stiff if 'loaded to the side', i.e. for the stress path tangential to the yield surface. The resistance against localization is sometimes attributed to this fact and Vermeer [256] proposed gradual modification of elastic stiffness as the stress approaches the yield surface. However, this modification alone does not facilitate the onset of localization if the associative flow rule is preserved. A decisive improvement can be achieved choosing a non-associative flow rule and/or vertex plasticity, [151, 161, 203, 209, 252, 254]. Bardet reviewed this aspect for various elastoplastic vertex models using response envelopes [7]. The discussion of localized bifurcation in the elastoplastic framework is outside the scope of this text.

3.5.2 Observation of deformation by PIV

We finish this section by a short contribution to the discussion whether the continuum approach with the classical concepts of stress and strain is appropriate for soils.

In hypoplasticity we deal with averaged stress and strain rate fields and the condition (3.150) of localized bifurcation has been derived starting from a perfectly homogeneous state assuming that spatial fluctuations of stress or void ratio are represented somehow within the constitutive model. Here an attempt is made to measure the actual fluctuations of strain in a triaxial sample. An explicit correspondence between a back stress (or a similar state variable) and the fluctuation of stress or strain could be of interest in formulation of new constitutive models.

In a simple 1-D model, Fig. 3.13, with two parallel coupled elastic-ideal-plastic materials a and b ($\epsilon_a = \epsilon_b$, $T = T_a + T_b$) which have different partial strengths ($y_a \neq y_b$) the back stress α (middle point of the elastic region) can be interpreted as the difference of partial stresses $T_a - T_b$. An analogous coupling of hypoplastic materials is discussed in Section 4.3.7. This simple 1-D illustration shows that constitutive models may benefit from a careful analysis of spatial fluctuation of stress because some state variables could be clearly interpreted. During a deformation process an evolution of spatial fluctuation of strain can be continuously monitored.

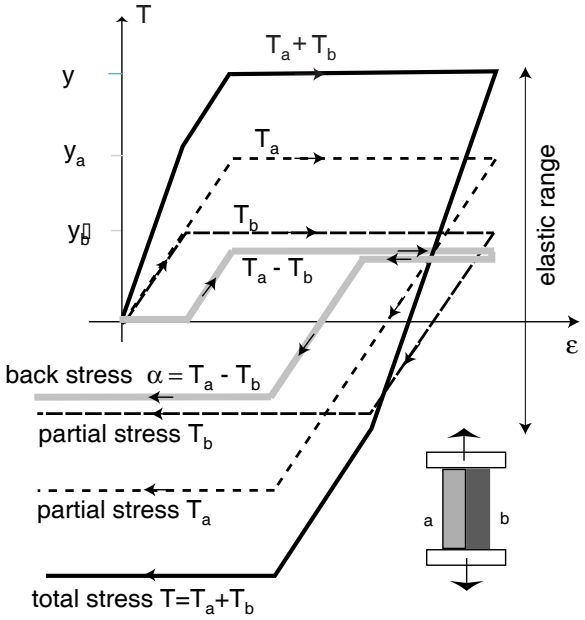

Figure 3.13: Parallel coupled (common strain) materials a and b with different partial stresses $T_a \neq T_b$ due to different yield limits $y_a \neq y_b$. Back stress $\alpha = T_a - T_b$ can be interpreted as a measure of stress fluctuation

In Fig. 3.14 different axial strain fields $\epsilon_1(\mathbf{x})$ are compared. They have been measured by particle image velocimetry technique (PIV) on the surface of a triaxial sample. For example, comparing the first one and the last one of 7200 cycles of the axial force we observe that the spatial fluctuation has been smoothed proportionally to the decrease of average amplitude. Fig. 3.14 shows that the assumption of homogeneous state is evidently artificial.

The particle image velocimetry technique, cf. [200], is a valuable tool to evaluate a superficial displacement field of a soil sample. This can be done by comparison of two digital photographs taken from the same position of the camera before and after deformation of the sample. A computer program[8] compares locations of small fragments (so-called interrogation windows, say 128 by 128 pixels) of two pictures (original

[8] `MatPIV v1.4`, freeware, needs MATLAB) by Sveen `jks@math.uio.no`

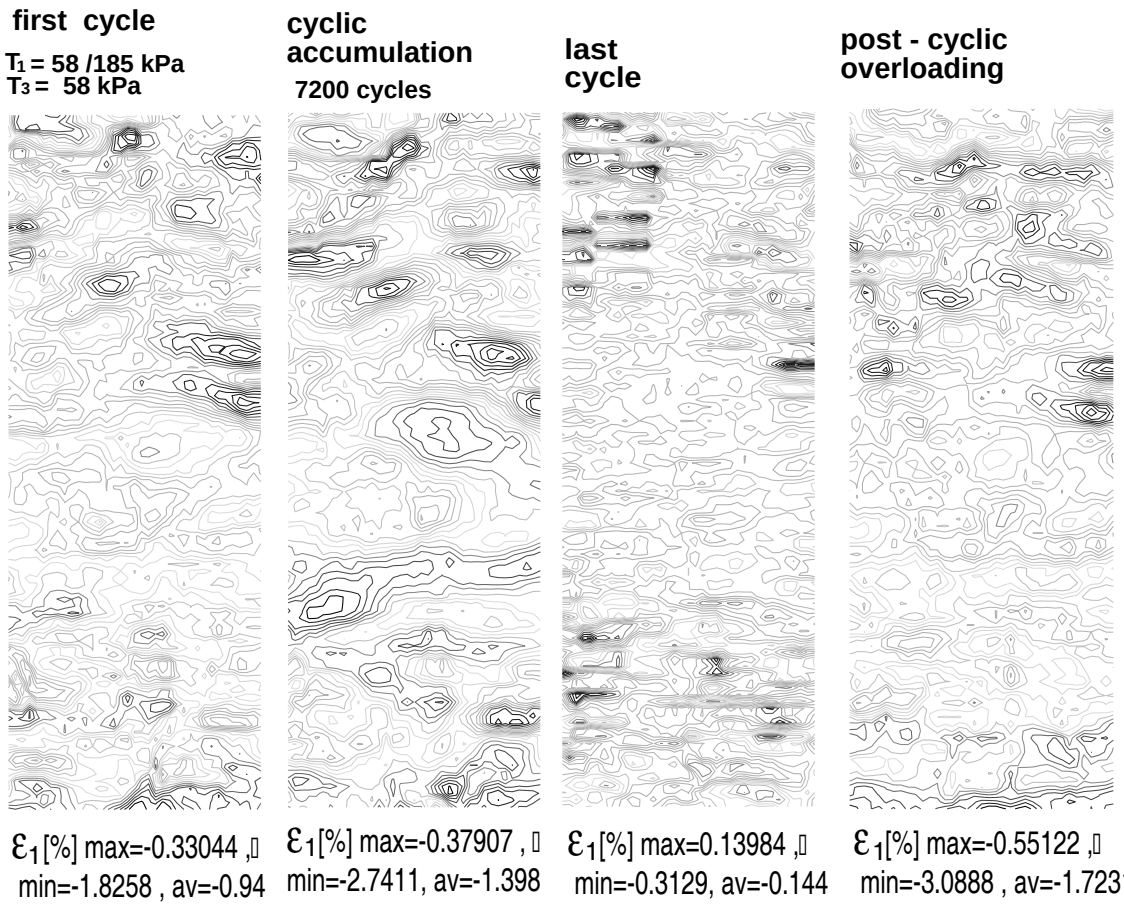

Figure 3.14: Fluctuation of strain indicates that intrinsic inhomogeneities may be of importance in geomechanics. Smoothing due to cyclic axial loading is surprisingly small so cyclic loadings do not necessarily make the strain field homogeneous. Here fluctuations of axial strain ϵ_1 in a sample of sand, $d_{50} = 0.2$mm, at medium density

and after deformation) of an appropriate quality, say 3 10^6 pixels. The program recognizes a fragment of the original picture in the second one looking for maximal correlation of mean brightness, its range within the window etc. Such correlations are efficiently computed using FFT. After the maximum correlation is found the relative shift (in pixels) of the original window can be calculated. For technical reasons this shift must be smaller than one half of the width of the original window and ascribed to the centre of the interrogation window. Subsequently the window is shifted, say by 16 pixels to evaluate the next shift vector. A discrete displacement field is finally obtained which can be used to evaluate the strain field. The PIV programs are widely used in fluid mechanics, and many sophisticated noise filtering and optimization techniques have been developed.

Fields of individual strain components are calculated from the displacement field by means of numerical differentiation. The MATLAB procedures for differentiation of displacement fields and for batch-processing of a sequence of pictures can be obtained from the author

www.AN .

A triaxial sand sample $d = 100$mm $h = 200$mm of medium density was carefully prepared by uniform pluviation. The fall height and the intensity of sand rain were continuously controlled. The membrane of the specimen was spotted to ease the comparison of interrogation windows (this operation is known as 'seeding' in PIV applications in fluid mechanics). The sample was supported by vacuum applied to the drainage system and the tests could be performed without a triaxial cell to obtain high quality pictures. Under lateral pressure of 60 kPa the sample was subjected to monotonic and cyclic vertical loading. The differences between subsequent pictures were evaluated with PIV. The diagrams referring to single cycles, Fig. 3.14, are to be interpreted as strain amplitudes and the one corresponding to the cyclic load shows the accumulated displacements only (both pictures at isotropic stress). Two other samples were similarly tested, confirming qualitatively the results.

It is evident that the inhomogeneity of deformation does not disappear so that the spatial fluctuation of strain and stress field is a remaining and presumably important factor in the description of soil behaviour. The influence of fluctuation of the void ratio was studied within the hypoplastic framework in Cosserat continuum by Nübel [181] using extremely fine FE meshes. The distributions of vertical strain components presented in Fig. 3.14 suggest introduction of at least some statistical description of spatial strain fluctuation in geotechnical models. The importance of such consideration is discussed within the hypoplastic framework by Nübel and Karcher [182].

Chapter 4

Extensions and modifications

4.1 Intergranular strain

4.1.1 Motivation

In order to improve the performance of the hypoplastic model in the range of small load cycles a new state variable called *intergranular strain*, **h**, has been introduced. The new state variable is thought to represent the deformation of an interface layer between soil particles[1]. The new state variable is dictated by the recent history of deformation, see Fig. 4.1, and the stiffness tensor is increased with the angle between **h** and **D**. This section presents this concept and its implementation to the referential hypoplastic model. The intergranular strain was originally proposed by Niemunis and Herle [172] www.AN .

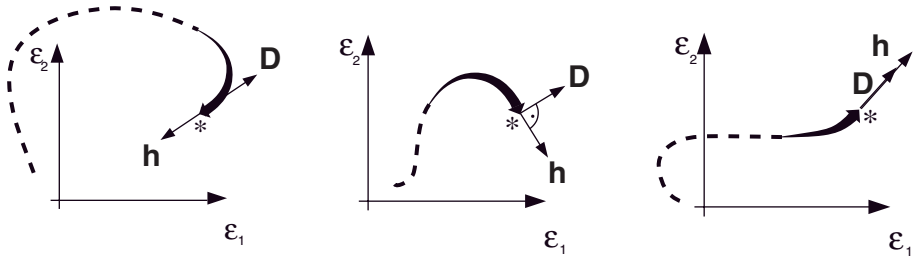

Figure 4.1: Different intergranular strains **h** related with different deformation histories. Only the recent part of the previous strain path (bold arrow) has an influence on **h**. Current stress, void ratio and strain rate at the point * may be the same in all three cases

One of the most striking shortcomings of hypoplasticity is an excessive accumulation of deformation predicted for small stress cycles, and the inability of modeling small hysteretic loops in in the strain-stress diagram. The hypoplastic model predicts saw-tooth-like diagrams instead of loops, such performance is often called ratcheting. For undrained cyclic shearing the hypoplastic approach predicts a far too high build-up of pore pressure

[1]Recently Gudehus (private communication 2002) suggested an alternative interpretation related to spatial fluctuation of stress and void ratio.

[162] www.AN . Neither the small-strain stiffness nor effects of the recent history have been adequately modeled in the referential hypoplastic model. Our present purpose is to extend hypoplasticity in order to improve the small strain performance after changes of direction of stress or strain path. In Section 4.2 we implement the same idea to visco-hypoplasticity.

According to measurements, e.g. [4,108,109,199], the soil stiffness at a given state (defined by stress and void ratio) and for a certain direction of strain rate depends strongly on the deformation history. In particular, after a rapid change in the direction of the strain path an increase of stiffness is observed, and the maximum value appears with a complete (i.e. 180°) strain rate reversal [4]. If straining is continued in a fixed direction the stiffness decreases gradually, and after a certain strain path, of length ϵ_{SOM} (measured from the reversal *), the stiffness regains the low value typical for monotonic paths (SOM is an abbreviation for *swept-out memory* [77]).

Micromechanical considerations [72, 99] indicate that intergranular forces are transferred through thin amorphous zones in intergranular interface. The present elastic range is qualitatively related with properties of such zones, see Fig. 4.4. The elastic range is defined in strain space because the required evolution equations are simpler (pressure independent).

The proposed extension requires five additional constants. Three of them, the size of the elastic range and two ratios of characteristic stiffnesses, have a clear physical meaning and can be obtained in direct measurements. The remaining two constants describe transitions between strain path reversal and SOM state and can be correlated to the rate of strain accumulation. A detailed procedure for the determination of the constants will be given.

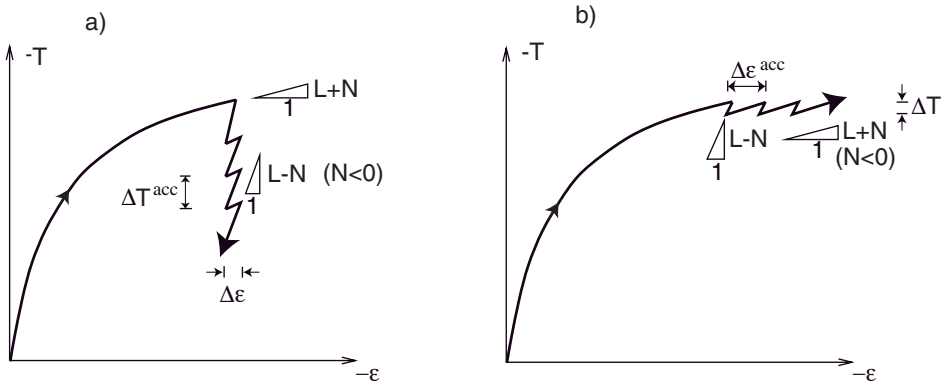

Figure 4.2: Excessive accumulation of a) stress and b) strain (ratcheting) during stress and strain cycles, respectively

We start with a one-dimensional demonstration of excessive ratcheting produced by hypoplasticity. For sufficiently small strain cycles (2.61) can be simplified to the scalar form

(2.32)

$$\dot{T} = LD + N|D| \; ; \qquad 0 < -N < L \; . \tag{4.1}$$

wherein values of L and N can be considered as approximately constant during a cycle, provided that the changes in stress are small compared to its average value. The accumulated stress in one strain cycle, $\pm\Delta\epsilon = \pm D\Delta t$ (Fig. 4.2a), is then

$$\Delta T^{acc} = L\Delta\epsilon + N|\Delta\epsilon| + L(-\Delta\epsilon) + N|-\Delta\epsilon| = 2N|\Delta\epsilon| \quad . \tag{4.2}$$

The accumulation of strain, viz.

$$\Delta\epsilon^{acc} = \frac{\Delta T}{L+N} + \frac{-\Delta T}{L-N} = \frac{-2N}{L^2-N^2}\Delta T \quad , \tag{4.3}$$

is obtained for a small stress cycle (Fig. 4.2b). In both cases the accumulation is generally too large. Note that the accumulation is linearly proportional to the amplitude, i.e. it is present also during the smallest cycles. Analogous calculation with the reference model in three-dimensional case reveals that such accumulation is independent of the polarization of the strain or stress amplitude and is only slightly reduced if the stress obliquity becomes smaller. It continues even for relatively dense soils and does not vanish until the limit $e = e_d$ is reached, i.e., for the smallest possible void ratio.

Such excessive ratcheting is typical for several constitutive models and has been discussed in the literature [15, 156, 204, 211] in different contexts. Here, let us examine shortly whether (4.1) is stable in the sense of Liapunov, i.e. if small changes $|\Delta\mathbf{q}(0)| < \xi$ in the initial conditions lead to small changes in the solution $|\Delta\mathbf{q}(t)| < \zeta$ for all $t > 0$, wherein $\mathbf{q}$ is a vector containing generalized displacements and their rates. Investigation of stability may be reduced to the investigation of stability of a zero solution $\mathbf{q} = \mathbf{0}$ so we may omit Δ-s, cf. [14],p.175. Components of $\mathbf{q}$ constitute a so-called phase space. In a 1-D case of a single mass vibrating freely on a hypoplastic spring the phase space consists of the deformation of the spring and its rate, $\mathbf{q} = \{\epsilon, D\}$. From parametric plots $\epsilon(t) - D(t)$ (so-called phase diagrams) we could easily infer if a system is stable, i.e. whether a sufficiently small ξ may restrict the solution $\mathbf{q}(t)$ to lie within an arbitrary sphere of radius ζ. Numerical experiments can be facilitated by the following MATHEMATICA script

```
mass = 10; length=1; area=1; LL=8; NN=-5
eqn1= de[t] == e'[t];
eqn2= mass*de''[t]*length + (LL*de[t]+NN*Abs[de[t]])*area==0; (*if N=const or...*)
eqn2 = mass*de''[t]*length + (LL*de[t] -  s[t]*Abs[de[t]]) area == 0;  (*if N=-T*)
eqn3 = s'[t] == LL*de[t] - s[t]*Abs[de[t]];
inie = {e[0] == 0, de[0] == 1, de'[0] == 0};          inis = s[0] == 5;
solution = NDSolve[{eqn1, eqn2, eqn3, inie, inis}, {e, de, s}, {t, 0, 550},
                                Method -> RungeKutta, MaxSteps -> 100000];
ParametricPlot[Evaluate[{e[t],de[t]} /. solution],{t,0,550}
                        PlotPoints -> 100,  PlotRange -> {{0, 8}, {-7, 10}}]
```

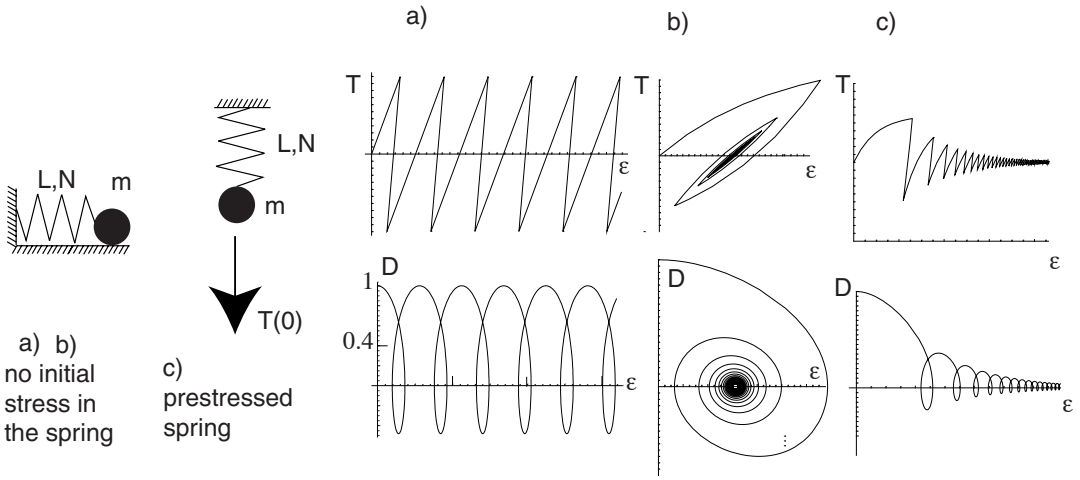

Figure 4.3: Phase diagrams and strain-stress plots of a freely vibrating mass m attached to a spring with a 'hypoplastic' response (4.1). In case a: ($N = \text{const}$ and $T(0) = 0$) an unrestricted accumulation of deformation is obtained, which means instability; in case b: ($N = -T$ and $T(0) = 0$) the phase plot converges as desired but in case c: ($N = -T$ and $T(0) \neq 0$) excessive accumulation is evident

In this script strain is denoted by `e[t]`, its rate by `de[t]` and stress by `s[t]`. Equation `eqn2` is the time derivative of the equilibrium condition $TA + m\ddot{u} = 0$. As it can be seen in Fig. 4.3-a, the solution for $N = \text{const}$ is unstable because every disturbance ξ result in an infinite accumulation of ϵ. Also for $N = -T$ an excessive dissipation of energy is obtained, especially if free vibrations are overlaid by a dead load, see Fig. 4.3-c. A rigorous proof that such material violates the Liapunov stability condition was presented by Niemunis and Triantafyllidis [177]. The objective in this section is to remove the excessive ratcheting from hypoplasticity.

4.1.2 Extended hypoplastic model

Consider a representative volume element (say an assemblage of several thousand grains) used in the macroscopic description of granular materials. The macroscopically homogeneous deformation can be decomposed into two portions

- deformations in intergranular interface layers,
- irreversible rearrangement of grains with slips, loss and generation of grain contacts

The deformation of grain interfaces is expressed by the *intergranular strain* $\mathbf{h}$. It is a new state variable beside stress and void ratio. We can imagine that straining of a representative element corresponds, on a micromechanical level, to much greater deformations within interface zones in particular in case of sliding along contact planes. This situation is depicted for a 1-D case in Fig. 4.4.

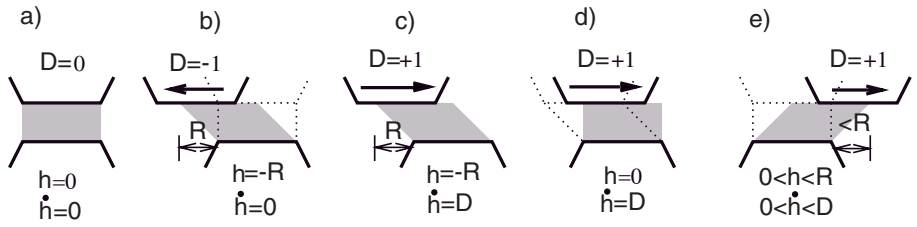

Figure 4.4: 1-D interpretation of the intergranular strain as the shear deformation of a 'hockey puck' between two grains

The interface zone is represented by the shaded area. At the beginning we set $h = 0$, Fig. 4.4 (a), the interface zone is undeformed, and we start with the deformation rate $D = -1$. While the deformation is being continued the intergranular strain is evolving towards $h = -R$ (b) and simultaneously sliding of grains is occurring. On continuing this deformation the interface zone reaches its maximum value, $h = -R$ and $\dot{h} = 0$. Further deformation of the representative volume is due the sliding and due to rearrangements of grains only. After a reversal of stretching, $D = 1$ (c), a micro-rebound is observed. At first, the deformation concentrates at the interface zone only. According to the model such pure interfacial rebound is lasting as long as $h \cdot D \leq 0$ (d). Finally, h approaches the limit $h = R$ on the opposite side (e).

The maximum $|h| = R$ of the intergranular strain is assumed to be a material constant that is not affected by pressure. Only the contact *areas* become larger with pressure, cf. dry friction as a contact adhesion [72, 130, 236, 281]. The evolution equation of h in the above 1-D model can be written as

$$\dot{h} = \begin{cases} \left(1 - \dfrac{|h|}{R}\right) D & \text{for } h \cdot D > 0 \\ D & \text{for } h \cdot D \leq 0 \end{cases} \quad . \tag{4.4}$$

A geometrical interpretation of (4.4) is shown in Fig. 4.4 and in Fig. 4.5. At the beginning of the deformation, the rate of intergranular strain jumps from $\dot{h} = 0$ to $\dot{h} = D = -1$ (point a), which means that no rearrangement of grains takes place. As the deformation continues (with $h \cdot D > 0$), the rate $|\dot{h}|$ gradually decreases until $\dot{h} = 0$ for $h = -R$ is reached, (point b). Upon further deformation in the same direction h cannot grow any more. This corresponds to a pure rearrangement of grains. The change of sign of D results in an 'elastic' micro-rebound. We have $h \cdot D \leq 0$, and $\dot{h} = D = +1$ (point c) as long as $h \cdot D \leq 0$ holds (point d). Subsequently the condition

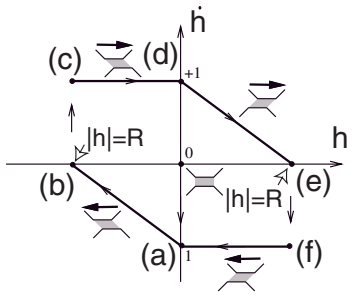

Figure 4.5: Evolution of the intergranular strain.

$h \cdot D > 0$ is fulfilled, and $\dot{h}$ decreases towards zero (point e). A cycle is closed after the deformation rate $D = -1$ is applied (f) and $h = 0$ (point a) is reached.

The general tensorial formulation for 3-D works similarly. The intergranular strain $\mathbf{h}$ must be treated as a second-order tensor because it can be obtained by accumulation of $\mathbf{D}\Delta t$. It is convenient to introduce the normalized magnitude of $\mathbf{h}$ as

$$\rho = \|\mathbf{h}\|/R \tag{4.5}$$

and its direction $\vec{\mathbf{h}}$. The general stress-strain relation is written as

$$\mathring{\mathbf{T}} = \mathsf{M} : \mathbf{D} \quad , \tag{4.6}$$

wherein the fourth order tensor M represents the tangential stiffness. It is calculated from the hypoplastic tensors $\mathsf{L}(\mathbf{T}, e)$ and $\mathbf{N}(\mathbf{T}, e)$, which are suitably increased, depending on ρ and on $(\vec{\mathbf{h}} : \mathbf{D})$ as presented in Fig. 4.6. For this purpose two scalar multipliers m_T and m_R (material constants) are proposed.

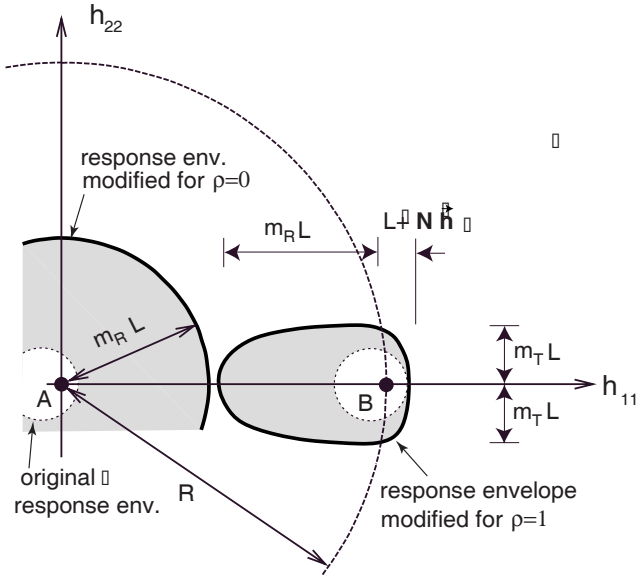

Figure 4.6: Modification of the stiffness with m_R and m_T for $\rho = 0$ and for $\rho = 1$. For simplicity in this figure we assume $\mathring{\mathbf{T}}(\mathbf{D}) \sim \mathbf{D}$

First, we consider the special case of $\rho = 1$ (point B in Fig. 4.6) corresponding to the maximal intergranular strain.

1. For monotonic deformation with $\mathbf{D} \sim \vec{\mathbf{h}} \approx$ const. over a considerable length of the strain path, we take

   $$\mathsf{M} = \mathsf{L} + \mathbf{N}\vec{\mathbf{h}} \tag{4.7}$$

   In this case $\mathbf{D} = \vec{\mathbf{h}}\|\mathbf{D}\|$ holds, so we have $\mathbf{N}\vec{\mathbf{h}} : \mathbf{D} = \mathbf{N}\|\mathbf{D}\|$ and we recover the hypoplastic equation (2.61).

2. For reversed deformation (elastic micro-rebound), i.e. for $\mathbf{D} \sim -\vec{\mathbf{h}}$, we postulate an increased stiffness with

$$\mathsf{M} = m_R \mathsf{L} \ . \tag{4.8}$$

wherein $m_R > 2$. Note that the second hypoplastic term unlike in (4.7) is switched off.

3. For a 'neutral' strain rate, i.e. for $\mathbf{D} \perp \vec{\mathbf{h}}$, or $\mathbf{D} : \vec{\mathbf{h}} = 0$, we postulate a slightly increased stiffness

$$\mathsf{M} = m_T \mathsf{L} \quad , \tag{4.9}$$

with a constant m_T in the range $m_R > m_T > 1$.

Next, we consider another special case $\rho = 0$ (point A in Fig. 4.6) for which

$$\mathsf{M} = m_R \mathsf{L} \tag{4.10}$$

is assumed to hold independently of the direction of $\mathbf{D}$.

Having postulated the above three special cases we combine them now into a general expression for M with $0 < \rho < 1$ and with arbitrary $\mathbf{D}$. For this purpose the following interpolation is chosen

$$\boxed{\mathsf{M} = [\rho^\chi m_T + (1-\rho^\chi) m_R]\mathsf{L} + \begin{cases} \rho^\chi (1-m_T)\mathsf{L} : \vec{\mathbf{h}}\vec{\mathbf{h}} + \rho^\chi \mathbf{N}\vec{\mathbf{h}} & \text{for } \vec{\mathbf{h}} : \mathbf{D} > 0 \\ \rho^\chi (m_R - m_T)\mathsf{L} : \vec{\mathbf{h}}\vec{\mathbf{h}} & \text{for } \vec{\mathbf{h}} : \mathbf{D} \le 0 \end{cases}} \tag{4.11}$$

In order to recover the special cases mentioned above, we may substitute $\vec{\mathbf{h}}\vec{\mathbf{h}} : \mathbf{D} = \mathbf{D}$ and $\vec{\mathbf{h}} : \mathbf{D} = \|\mathbf{D}\|$ for $\mathbf{D} \sim \vec{\mathbf{h}}$ and, of course, $\vec{\mathbf{h}} : \mathbf{D} = 0$ for $\mathbf{D} \perp \vec{\mathbf{h}}$. The transition from $m_R\mathsf{L}$ to $\mathsf{L} + \mathbf{N}\vec{\mathbf{h}}$ for $0 < \rho < 1$ is smoothed by a weighting factor ρ^χ, wherein χ is yet another constant. Immediately after a full (180°) strain reversal the stiffness $m_R\mathsf{L}$ is the largest possible one for a given stress and void ratio. The increased stiffness applies as long as $\vec{\mathbf{h}} : \mathbf{D} \le 0$ holds. The intergranular strain $\mathbf{h}$ evolves in this case according to $\mathring{\mathbf{h}} = \mathbf{D}$, see Fig. 4.7. The skeleton is assumed fixed i.e. no sliding occurs and the dissipative term $\mathbf{N}\vec{\mathbf{h}}$ does not appear in (4.11) - case $\vec{\mathbf{h}} : \mathbf{D} \le 0$. If $\vec{\mathbf{h}} : \mathbf{D}$ is positive the intergranular strain is evolving slower than $\mathbf{D}$ and is accompanied by sliding. Therefore the dissipative term $\mathbf{N}\vec{\mathbf{h}}$ becomes active. Finally, as the intergranular strain is approaching its limit value $\|\mathbf{h}\| = R$ the stiffness M is reduced back to the value $\mathsf{L} + \mathbf{N}\vec{\mathbf{h}}$ of the reference model.

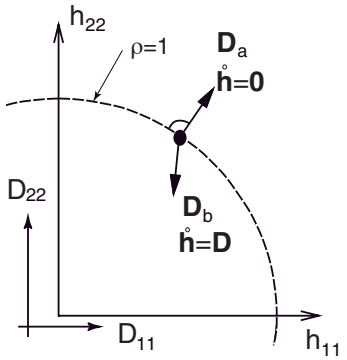

Figure 4.7: Rate of the intergranular strain for the special case $\rho = 1$. According to (4.12) the rate $\mathring{\mathbf{h}}$ vanishes in the case of $\mathbf{D}_a = \hat{\mathbf{h}}\|\mathbf{D}_a\|$ ($\hat{\mathbf{h}} : \mathbf{D}_a > 0$), and $\mathring{\mathbf{h}} = \mathbf{D}$ in the case of $\mathbf{D}_b$ ($\hat{\mathbf{h}} : \mathbf{D}_b < 0$)

The following generalized evolution equation for the intergranular strain tensor $\mathbf{h}$ is proposed,

$$\boxed{\mathring{\mathbf{h}} = \begin{cases} (\mathsf{I} - \vec{\mathbf{h}}\vec{\mathbf{h}}\rho^{\beta_r}) : \mathbf{D} & \text{for } \vec{\mathbf{h}} : \mathbf{D} > 0 \\ \mathbf{D} & \text{for } \vec{\mathbf{h}} : \mathbf{D} \leq 0 \end{cases}} \tag{4.12}$$

where $\mathring{\mathbf{h}}$ is the objective co-rotational rate of intergranular strain, see Fig. 4.7. The exponent β_r is a material constant which controls the rate $\mathring{\mathbf{h}}$. In the 1-D example (4.4) we have assumed $\beta_r = 1$ for simplicity.

According to (4.12), during a sufficiently long monotonic deformation with $\mathbf{D}$ =const, $\vec{\mathbf{h}} : \mathbf{D} > 0$ and $\rho \to 1$ the asymptotic value of the intergranular strain is $\mathbf{h} = \vec{\mathbf{D}}R$ and Equations (4.6) and (4.11) become equivalent to (2.61). In case of a sudden change in the direction of straining (by less than 90°) $\mathbf{h}$ rotates towards the new $\mathbf{D}$, while $\rho = 1$ remains.

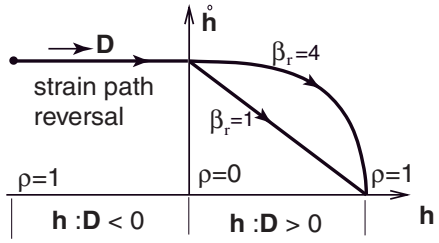

Figure 4.8: Evolution of the intergranular strain $\mathbf{h}$. After a 180° strain reversal $\mathbf{D}$ is assumed to remain constant. At first $\mathbf{D} \sim -\vec{\mathbf{h}}$ so $\mathring{\mathbf{h}} = \mathbf{D}$, then $\mathbf{D} \sim \vec{\mathbf{h}}$ so $\|\mathring{\mathbf{h}}\|$ decreases according to (4.12)

In (4.12) at $\rho = 1$ and $\vec{\mathbf{h}} : \mathbf{D} > 0$ only the 'neutral' part $\mathbf{D} - \vec{\mathbf{h}}\vec{\mathbf{h}} : \mathbf{D}$ contributes to the evolution of $\mathbf{h}$ and therefore $\dot{\rho} = 0$. For $\rho = 0$, (4.12) gives $\mathring{\mathbf{h}} = \mathbf{D}$ independently of the direction of $\mathbf{D}$, and for $0 < \rho < 1$ and $\vec{\mathbf{h}} : \mathbf{D} > 0$ Equation (4.12) can be seen as a power law interpolation (with weighting factor ρ^{β_r}) between the special cases $\rho = 0$ and $\rho = 1$ (Fig. 4.8). Alternatively to (4.12) one may consider an evolution equation of $\mathbf{h}$ in form

$$\mathring{\mathbf{h}} = c_h(\mathbf{D} - \mathbf{h}/R\|\mathbf{D}\|)\,. \tag{4.13}$$

The limit value for proportional straining is $\mathbf{h} = R\vec{\mathbf{D}}$ and follows directly from the condition $\mathring{\mathbf{h}} = 0$. The constant c_h controls how fast $\mathbf{h}$ evolves. For example, in 1-D case after a 180° reversal at $t = 0$ and with the initial conditions $\epsilon(0) = 0$ and $h(0) = -R$ we can easily obtain $h(\epsilon) = R(1 - 2e^{-c_h\,\epsilon/R})$ solving `DSolve[h'[e] == c (1 - h[e]/R), h[0] == -R, h, e]`. Having $h(\epsilon)$ we may correlate c_h with the length ϵ_{SOM} of the proportional strain path after which the reversal is swept out of memory, see Section 4.1.4.

Now, we may compare the 1-D phase plots generated by the reference model, see also Subsection 4.1.1, with the ones of extended model with intergranular strain. For the extended model we use the following MATHEMATICA script

```
mass = 10; length = 1; area = 1; LL = 8; mR = 2; R = 0.05;
eqn1 = de[t] == e'[t];  eqn2 = mass*de''[t]*length + s'[t]* area == 0;
eqn3 = s'[t] == If[ h[t]*de[t] >=  0,
      (1-Abs[h[t]]/R)mR*LL* de[t]+(Abs[h[t]]/R) (LL*de[t]-s[t] Sign[h[t]]*de[t]),
       mR*LL*de[t]];
eqn4 = h'[t] == If[h[t]*de[t] >= 0 , (1 - Abs[h[t]]/R) *de[t], de[t] ] ;
```

```
inie = {e[0] == 0, de[0] == 1, de'[0] == 0};     inis = {s[0] == 5, h[0] == 0};
solution = NDSolve[{eqn1, eqn2, eqn3, eqn4, inie, inis}, {e, de, s, h}, {t, 0, 100},
                   Method -> RungeKutta, MaxSteps -> 100000];
ParametricPlot[Evaluate[{e[t], de[t]} /. solution], {t, 0, 100}] (* or other plots *)
```

Free vibrations of a mass on various hypoplastic springs overloaded with $T(0) \neq 0$ are presented in Fig. 4.9. The influence of intergranular strain and of parameter R is evident.

In the closure of this presentation let us remark that the stress response $\mathring{\mathbf{T}}(\mathbf{D})$ of the extended model is a continuous function of $\mathbf{D}$ but the stiffness $\partial\mathring{\mathbf{T}}/\partial\mathbf{D}$ is not (see Eq. (4.11)). Therefore, the extended constitutive model presented above is not strictly hypoplastic in the sense of Wu and Kolymbas [271]. On the contrary, there is a striking similarity between the above hypoplastic version and the elastoplastic model by Armstrong and Frederic [3] with a 'hypoplastic' kinematic hardening rule. As we see, similar ideas have been developed from the elastoplastic and the hypoplastic side!

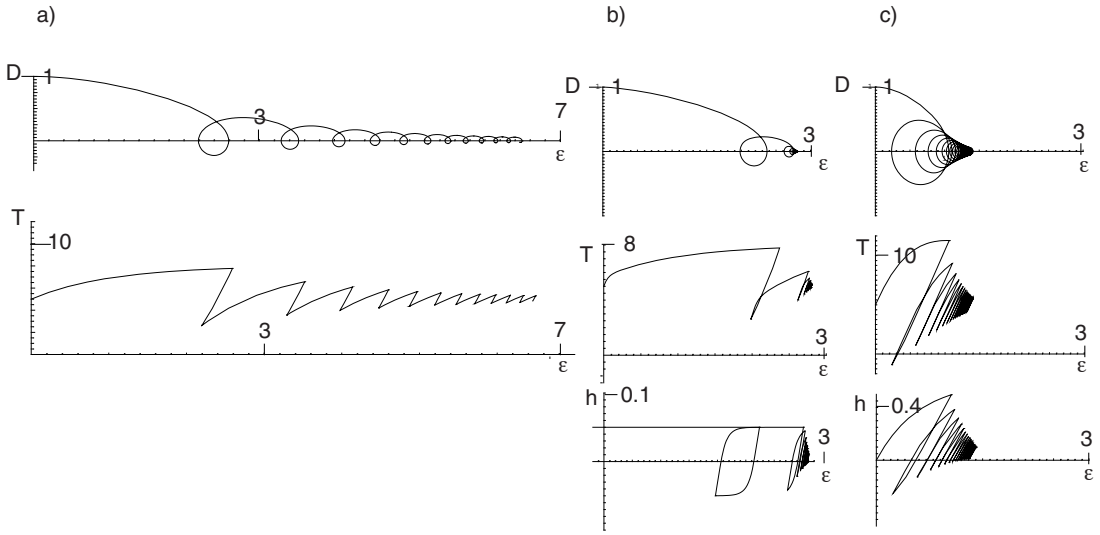

Figure 4.9: Phase diagrams and stress-strain plots of a freely vibrating mass on a hypoplastic spring and under a constant load $T(0)$: a) reference model b) extended model with small intergranular strain $\mathbf{h}$ (within $R = 0.05$) c)extended model large intergranular strain (within $R = 0.6$). Remaining parameters can be found in the MATHEMATICA script

Using the extended model in BVPs with cyclic *multiaxial* loading, cf. Section 4.4.3, we should be aware of the fact that the linear part of the model is hypoelastic. It refers to both the reference model and the extended one[2]. In Section 4.3 a general strategy has been presented, how L could be replaced by a *hyper*elastic stiffness without spoiling the performance of the model in other aspects. An appropriate formulation for L can be found, e.g., in [162, 169, 255] www.AN .

[2]We should expect that also the linear part L of stiffness may contribute to accumulation.

4.1.3 Numerical aspects

Tangential stiffness for FE

For an efficient FE equilibrium iteration in the framework of the standard Newton procedure[3] [89] a constitutive model should provide not only the exact stress response to a given increment of deformation but also an accurate Jacobian matrix ($\partial\Delta\mathbf{T}/\partial\Delta\boldsymbol{\epsilon}$) that says how the stress increment changes due to a change of strain increment. An inexact Jacobian matrix deteriorates the convergence of the iteration. For numerical reasons the values of Jacobian matrix should be rather too high than too low. It must not be singular or negative definite. For the hypoplastic model without intergranular strain a sufficient approximation of the Jacobian matrix can be obtained from

$$(\partial\Delta\mathbf{T}/\partial\Delta\boldsymbol{\epsilon}) = \mathsf{E}^{hp} = \mathsf{L} + f_d\mathbf{N}\vec{\mathbf{D}} \tag{4.14}$$

in which we use the most recent approximation of $\mathbf{D}$. It is not a good idea to check the positive definiteness of E^{hp} using the non-singularity criterion

$$\det(\mathsf{E}^{hp}) > 0 \tag{4.15}$$

because double negative eigenvalues may not be detected. A sure method is to check all eigenvalues but such calculation for an nonsymmetric matrix E^{hp} is tedious. A faster (but less accurate) alternative is to check whether the smallest eigenvalue of the symmetrized matrix $\frac{1}{2}\left[\mathsf{E}^{hp} + (\mathsf{E}^{hp})^T\right]$ is positive. According to Bromwich bounds, this guarantees that E^{hp} is also positive definite. Determination of the minimum eigenvalue for a symmetric matrix is easier, and due to the particular form [141] of E^{hp} we may equivalently check

$$2/f_d > \sqrt{(\mathbf{N}:\mathbf{B})(\vec{\mathbf{D}}:\mathsf{L}^{-1}:\vec{\mathbf{D}})} - \mathbf{B}:\vec{\mathbf{D}} \tag{4.16}$$

wherein $\mathbf{B}$ and L^{-1} can be found analytically. If E^{hp} is collected (weighted average) from several subincrements (a strategy described further in this section) we may benefit from the fact that $\vec{\mathbf{D}}$ is identical in all subincrements. If the calculation is performed with the intergranular strain we may use M given in (4.11) as the Jacobian matrix but the 'smart' method given in (4.16) cannot be applied because of subincrements. The test of the eigenspectrum of the symmetrized matrix $\frac{1}{2}(\mathsf{M} + \mathsf{M}^T)$ may still appear faster.

If a negative definite Jacobian matrix occurs it must be artificially made positive (at the cost of the efficiency of the equilibrium iteration).

In earlier FE-implementations of hypoplasticity (without intergranular strain) in place of E^{hp} given by () the doubled linear stiffness 2 L was used for the purpose of equilibrium iteration. This stiffness was always-positive, it did not change during iteration and

[3]Equations are reformed in every increment and in every iteration

provided stable solutions. However, some subtile FE-tests demonstrated that such stiffness artificially constrained some deformation modes. Similar constraining effect may be caused by too large time increments independently of the stiffness used. Both sources of constraints should be avoided.

Inverse and mixed problem

Consider a numerical element test with stress control or mixed control. The solution of (4.11) turns out to be more complicated than the one of purely hypoplastic relation, because the new relation is bilinear, and the sign of $\vec{\mathbf{h}} : \mathbf{D}$ has to be tested. Unless $\mathbf{D}$ is given directly, we have to solve the auxiliary equation (a linear substitute of (4.6))

$$\mathring{\mathbf{T}} = \mathsf{L} : \mathbf{D}^{\diamond} \tag{4.17}$$

for $\mathbf{D}^{\diamond}$, wherein $\mathbf{D}^{\diamond}$ is an estimate of the strain rate. In stress-controlled problems all components of $\mathring{\mathbf{T}}$ are given and $\mathbf{D}^{\diamond}$ can be obtained from (4.17). The rate $\mathbf{D}$ can then be found from (4.6) and (4.11) using the sign of $\vec{\mathbf{h}} : \mathbf{D}^{\diamond}$ which is identical with the one of $\vec{\mathbf{h}} : \mathbf{D}$. The proof of this fact and the discussion of the uniqueness of the solution of mixed problems is given is Section 4.1.6. Moreover it can be shown that a *unique* strain rate $\mathbf{D}$ is obtained provided the invertibility of the reference model for the same state $(\mathbf{T}, e)$ is granted. In mixed problems some components of $\mathbf{D}$ and some components of $\mathring{\mathbf{T}}$ are given. In this case, first, the prescribed parts of rate tensors must be substituted for the respective components of $\mathring{\mathbf{T}}$ and $\mathbf{D}^{\diamond}$, and (4.17) must be solved for the remaining unknown components of $\mathbf{D}^{\diamond}$. The estimation $\mathbf{h} : \mathbf{D}^{\diamond}$ (with $\mathbf{D}^{\diamond}$ in place of $\mathbf{D}$) suffices to determine the sign of $\vec{\mathbf{h}} : \mathbf{D}$. Having this sign we may proceed with solving a mixed problem using (4.6) with an appropriate M given by (4.11).

Substepping

A special sub-incrementation algorithm (on the material level) is used in the numerical implementation. In particular, directly after a sharp reversal of the strain path the stiffness changes rapidly and local sub-increments may improve the efficiency of the calculation. The strain increments used in the following numerical calculations are chosen as $\Delta\epsilon \approx 0.001$ for $\vec{\mathbf{h}} : \mathbf{D} > 0$ and smaller than $0.2R$ for $\vec{\mathbf{h}} : \mathbf{D} < 0$ in order to assure numerical stability. The recommended maximum of strain increment $\Delta\epsilon$ for micro-loading $\vec{\mathbf{h}} : \mathbf{D} > 0$ can be estimated from (4.12) to be

$$\Delta\epsilon_{max} = \frac{\mu\, R}{1 - \rho^{\beta_r}} \quad . \tag{4.18}$$

where $0 < \mu < 1$ is a parameter that controls the magnitude of the increment $\Delta\epsilon_{max}$ (in numerical experiments $\mu \approx 0.2$ worked fine). However, even these small increments may cause second-order inaccuracies. In classical stress-space elasto-plastic models the necessary correction is usually made by return mapping algorithms. In case of our strain-space formulation for the case of $\rho > 1$ it is preferable to correct $\mathbf{h}$ rather than to modify the actual strain. Although some correction of $\mathbf{h}$ may follow automatically in the next time-steps due to the ρ^{β_r} term in (4.12), it is not recommended to rely on this 'self-healing' property of the evolution equation in predictions of cyclic response.

The Euler forward time integration scheme

$$\begin{cases} \mathbf{T}^{t+\Delta t} = \mathbf{T}^t + \overset{\circ}{\mathbf{T}}{}^t \Delta t \\ \mathbf{h}^{t+\Delta t} = \mathbf{h}^t + \overset{\circ}{\mathbf{h}}{}^t \Delta t \quad , \end{cases} \tag{4.19}$$

applied for $\mathbf{T}^t, \mathbf{h}^t$ and e^t at the beginning of an increment needs rather small steps, and an implicit scheme described further in this section improves numerical stability. The Jaumann term $(-\mathbf{W} \cdot \mathbf{h} + \mathbf{h} \cdot \mathbf{W})\Delta t$ has to be added to the intergranular strain. As usual, we must avoid updating of state variables during equilibrium iteration because of impending non-physical (numerical) reversals of the strain/stress path. In other words: as long as the equilibrium is not reached the FE program repeatedly passes to the constitutive subroutine with the *same* state ($\mathbf{T}^t, \mathbf{h}^t$ and e^t) but *different* strain increments $\Delta\boldsymbol{\epsilon}$.

Implicit integration of h

The Euler forward integration scheme may become numerically unstable for evolution equation (4.12), especially if too large time steps are chosen. In such case, in order to improve the numerical performance an implicit integration scheme has been developed for the upper equation in (4.12), i.e. for the one with $\vec{\mathbf{h}} : \mathbf{D} > 0$. For finite increments $\mathbf{h}$ the Taylor's expansion may be used

$$\Delta\mathbf{h}(\mathbf{h}, \boldsymbol{\epsilon}) \approx \frac{\partial \overset{\circ}{\mathbf{h}}}{\partial \boldsymbol{\epsilon}} : \Delta\boldsymbol{\epsilon} + \Delta\mathbf{h} : \left[\frac{\partial^2 \overset{\circ}{\mathbf{h}}}{\partial \boldsymbol{\epsilon} \partial \mathbf{h}}\right] : \Delta\boldsymbol{\epsilon} \tag{4.20}$$

or

$$\overset{\circ}{\mathbf{h}}\Delta t = \left[\mathsf{I} - \vec{\mathbf{h}}\vec{\mathbf{h}}\ \rho^{\beta_r}\right] : \mathbf{D}\Delta t + \Delta t\ \ \overset{\circ}{\mathbf{h}} : \left\{\frac{\partial \left[\mathsf{I} - \vec{\mathbf{h}}\vec{\mathbf{h}}\ \rho^{\beta_r}\right]}{\partial \mathbf{h}}\right\} : \mathbf{D}\Delta t \tag{4.21}$$

wherein

$$\frac{\partial \left[I_{ijkl} - \vec{h}_{ij}\vec{h}_{kl}\ \rho^{\beta_r}\right]}{\partial h_{mn}} = -\frac{\rho^{\beta_r}}{\|\mathbf{h}\|}\left((\beta_r - 2)\vec{h}_{ij}\vec{h}_{kl}\vec{h}_{mn} + \vec{h}_{kl}J_{imjn} + \vec{h}_{ij}J_{kmln}\right) \tag{4.22}$$

with $J_{ijkl} = \delta_{ik}\delta_{jl}$. The unknown increment $\overset{\circ}{\mathbf{h}}\Delta t$ can be calculated from (4.21), noting that $\overset{\circ}{\mathbf{h}}\Delta t$ appears on both sides so it must be algebraically extracted.

4.1.4 Determination of the new material constants

The maximum value R of intergranular strain can relatively easy be found from stress-strain curves obtained either from dynamic tests or from static tests with strain path reversals, Fig. 4.10. In order to determine the constants m_T and m_R, let us consider a deformation process with $\vec{\mathbf{D}} = \text{const}$ over a sufficiently short strain path, so that the stiffness $\mathsf{E}^{hp} = \mathsf{L} + f_d \mathbf{N}\vec{\mathbf{D}}$ remains approximately constant. In Fig. 4.10 this referential stiffness is denoted as E_0. Three tests with identical deformation rate $\mathbf{D}$ (here shearing) and started from the same state $*$ (identical $\mathbf{T}$ and e) must be compared. The respective initial values $\mathbf{h}$ should be different, i.e. our three samples should have the same starting point $*$ but different deformation histories. After a sufficiently long monotonous stretching $\mathbf{D}$ the value $\mathbf{h} = R\vec{\mathbf{D}}$ is induced, as shown already in Fig. 4.1. The asterisk in Fig. 4.1 corresponds to the starting point of the stiffness-strain plots in Fig. 4.10. Consider the bottom curve in Fig. 4.10. It shows that the 'monotonic' stiffness E_0 changes slowly, $E_0(\mathbf{T}(\boldsymbol{\epsilon}))$. This dependence of stiffness on stress is of secondary importance here. The analogous stiffness E_T, after a 90° reversal of the strain path, is initially much higher. As the shearing is continued the additional stiffness gradually decreases. The highest stiffness E_R (for a given $\mathbf{T}$ and e) corresponds to a 180° strain reversal. Also this additional stiffness declines upon shearing path to E_0. The constants $m_T = E_T/E_0$ and $m_R = E_R/E_0$ can be directly evaluated [225, 241]. An alternative way to estimate m_R is to use the ratios of the so-called 'dynamic stiffness' to the 'static stiffness', see [113].

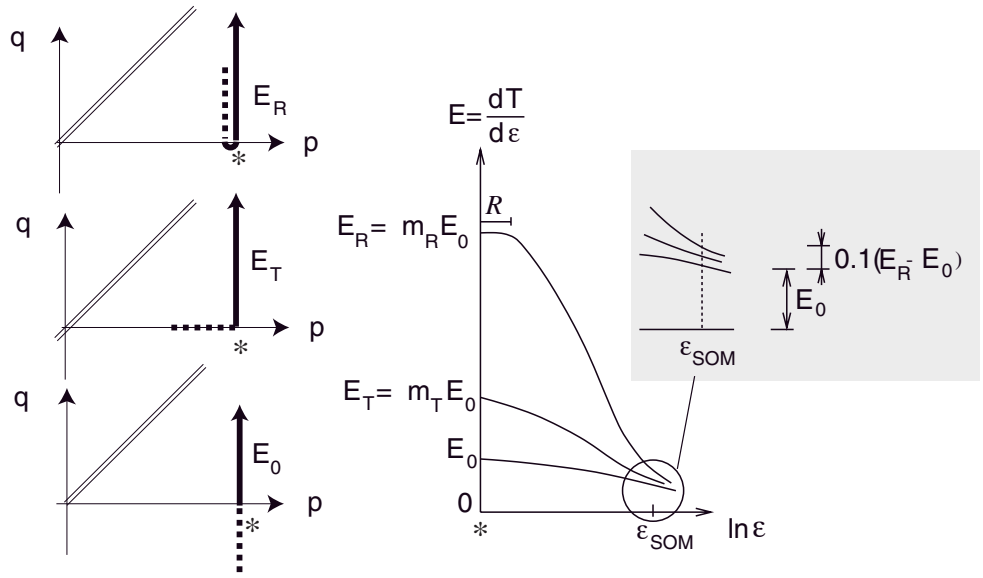

Figure 4.10: Characteristic stiffness values for the model calibration

All three stiffnesses almost coincide at $\epsilon = \epsilon_{SOM}$ which means that the sharp turn in the strain path is already forgotten there. Small discrepancies in the final stiffness at

$\epsilon = \epsilon_{SOM}$ are caused by different *stresses* reached after the same length of deformation path. In tests in Fig. 4.10 the initial stresses (for $\epsilon = 0$) are identical but the final ones (for $\epsilon = \epsilon_{SOM}$) are not.

The parameter β_r influences the evolution of intergranular strain and can be correlated with ϵ_{SOM}. We define ϵ_{SOM} as the length of a strain path, (straight and measured from the reversal point) needed for the additional stiffness to decline in 90%, see Fig. 4.10. Let the upper curve in Fig. 4.10 be approximated as

$$E = \begin{cases} m_R E_0 \quad (= E_R) & \text{for } \epsilon < R \\ E_0 + E_0(m_R - 1)[1 - \rho^\chi] & \text{for } \epsilon > R. \end{cases} \tag{4.23}$$

This follows directly from Equation (4.11) for $\mathbf{D} \sim \mathbf{h}$ and with $\mathbf{N} = \mathbf{0}$.

The dependence of ρ on $\mathbf{h}$ can be found for $\epsilon > R$ from (4.5) and (4.12) under assumption of a 1-D monotonic path with $\dot{\epsilon} \sim \vec{h}$ and $\dot{\epsilon}\vec{h} > 0$. The resulting ordinary differential equation

$$\frac{\mathrm{d}\rho}{\mathrm{d}\epsilon} = (1 - \rho^{\beta_r})/R \tag{4.24}$$

can be solved for the known boundary conditions $\rho^\chi\big|_{\epsilon=R} = 0$ and $\rho^\chi\big|_{\epsilon=\epsilon_{SOM}} = 0.9$, Fig. 4.11. In this diagram the dependence $E_0(\mathbf{T})$ over the strain path $0 < \epsilon < \epsilon_{SOM}$ has been disregarded.

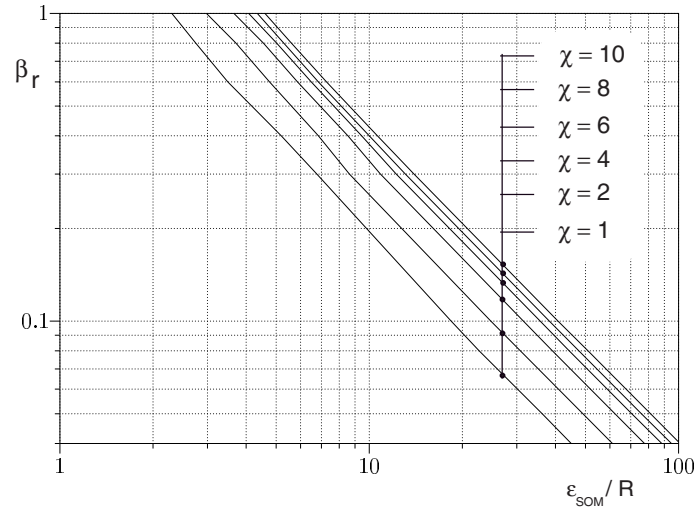

Figure 4.11: Correlation of β_r vs. ϵ_{SOM}/R for different χ

The solution of (4.24) has been presented in Fig. 4.11 for different values χ. For example, for $\chi = 6$, $R = 0.0001$ and $\epsilon_{\mathrm{SOM}}/R \approx 8$ we obtain $\beta_r \approx 0.50$ from this diagram.

The parameter χ ($\chi > 1$) describes the degradation of the stiffness from E_R to E_0 during monotonic deformation. Equation (4.11) provides a smooth transition from E_R ($= m_R L$) to the fundamental stiffness $E_0 = L \pm N$ as ρ evolves from 0 to 1. The parameter χ can be calibrated from a cyclic test with a small strain amplitude denoted ϵ_A in our 1-D example. The stress accumulated during a single strain cycle of the amplitude ϵ_A depends on both χ and β_r.

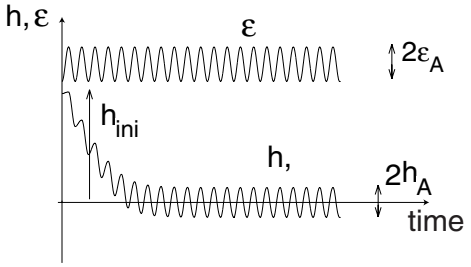

Figure 4.12: Evolution of **h** for strain cycles with a small amplitude ϵ_A. **h** tends towards symmetric oscillation with the number of cycles

Consider a series of small strain cycles such that **T** and e and thus the referential stiffness remain nearly constant. According to (4.12), after a number of cycles a stable situation establish itself (micro-shakedown) in which h oscillates periodically around $h = 0$ with the amplitude $\pm h_A$ (Fig. 4.12). The accumulation of stress after one cycle, cf. (4.2), is then

$$\Delta T^{acc} = 2NR \int_0^{\rho_A} \frac{\rho^\chi}{1-\rho^{\beta_r}} \mathrm{d}\rho \quad . \tag{4.25}$$

The maximum intergranular strain during such a cyclic deformation is $h_A = R \cdot \rho_A$. The relation between ρ_A and the straining amplitude ϵ_A can be found from (4.5) and (4.12)

$$2\frac{\epsilon_A}{R} \; - \; \rho_A \; - \int_0^{\rho_A} \frac{\mathrm{d}\rho}{1-\rho^{\beta_r}} = 0 \; . \tag{4.26}$$

Equations (4.25) and (4.26) must be solved numerically for different β_r. The results are plotted in diagrams (Fig. 4.13).

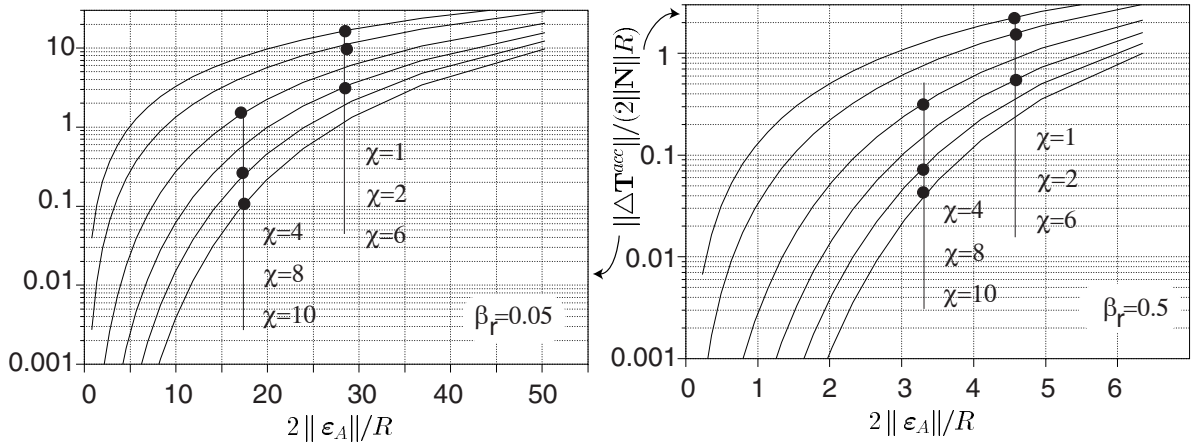

Figure 4.13: Relation between the normalized double strain amplitude $2|\epsilon|/R$ and the accumulated stress in one-half of the strain cycle for different χ; $\beta_r = 0.05$ (left) and $\beta_r = 0.5$ (right)

In order to find χ, one can perform a cyclic strain test and measure the cumulative stress response. For example, undrained cycles with a small amplitude of axial strain $\boldsymbol{\epsilon}_A = \text{const}$

produce a pore pressure build-up i.e. a decrease of the mean effective stress. Having $\Delta\mathbf{T}^{acc}$ for a given $\boldsymbol{\epsilon}_A$, the corresponding value of χ can be found from Fig. 4.13 (only the cases $\beta_r = 0.05$ (left) and $\beta_r = 0.5$ (right) are shown).

4.1.5 Numerical simulation of element tests

In this section the extended hypoplastic model is compared with the reference version presented in Section 2.5. The material constants in Tab. 4.1 have been found for Hochstetten sand [263, 265].

Table 4.1: Hypoplastic parameters of Hochstetten sand.

φ_c [°]	h_s [MPa]	n	e_{c0}	e_{d0}	e_{i0}	α	R	m_R	m_T	β_r	χ
33	1000	0.25	0.95	0.55	1.05	0.25	$1 \cdot 10^{-4}$	5.0	2.0	0.50	6.0

In all tests the initial value $\mathbf{h} = \mathbf{0}$ is used. According to Jardine [109], an increased stiffness, similar to the one after a sharp strain reversals is observed at the beginning of a deformation after a long resting period, which partly justifies our assumption. We may also argue that a perfectly motionless equilibrium is a mathematical simplification and there are always some small vibrations in soil. According to Equation (4.12) such small cyclic straining causes $\mathbf{h}$ to drift towards zero. Alternatively, one could introduce a gradual degradation $\overset{\circ}{\mathbf{h}} = -k\mathbf{h}$, with k being a positive scalar but as yet this aging phenomenon is not well understood [16] and therefore we use $\mathbf{h} = \mathbf{0}$ after each resting period.

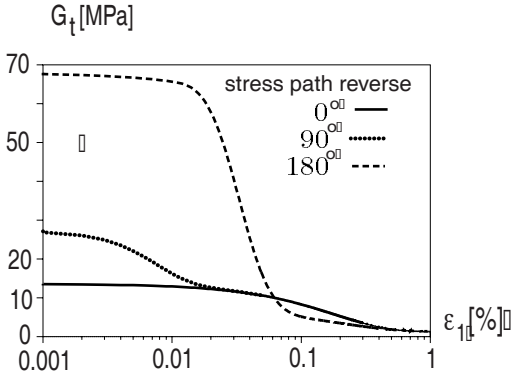

Figure 4.14: Calculated stiffness G_t for a biaxial compression with constant volume after a change of strain path direction

Using the constants in Tab. 4.1, an influence of the recent deformation history on the stiffness has been numerically calculated and depicted in Fig. 4.14. The tangential shear modulus $G = \frac{1}{2}\mathrm{d}(T_1 - T_2)/\mathrm{d}(\epsilon_1 - \epsilon_2)$ has been computed under plane strain conditions at identical isotropic stress $\mathbf{T} = -\,\mathrm{diag}[100, 100, 100]$ kPa, $e_0 = 0.695$ and for the same shear deformation rate but preceded by different deformation histories, according to Fig. 4.1. A distinct elastic range (a plateau with increased G) can be observed directly after the sharp reversal of the strain path. All three curves coincide at a strain of about 10^{-3} which

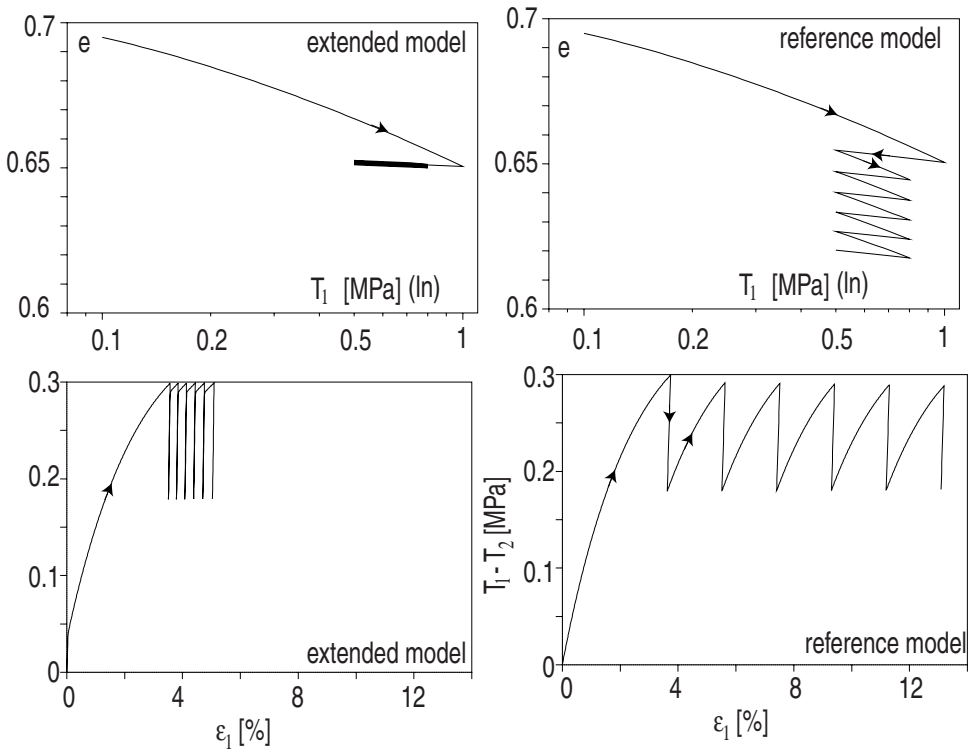

Figure 4.15: Oedometric compression stress cycles (top) and triaxial drained stress cycles (bottom). Left: extended model, right: reference model

may be taken as the ϵ_{SOM} value. At this point the information about the previous non-proportional deformation is indeed swept out from the material memory. The curves $G(\epsilon)$ do not exactly coincide at ϵ_{SOM} for the reason discussed already with reference to Fig. 4.10.

As a next example let us consider stress cycles during a one-dimensional (oedometric) compression test and during a drained triaxial test. It is evident from Fig. 4.15 that the extended hypoplastic model accumulates much less strain, if compared to the pronounced ratcheting of the reference model.

An undrained cyclic triaxial test causes a build-up of a pore water pressure or, equivalently, a decrease the mean effective stress p, see Fig. 4.17. This leads eventually to a characteristic "butterfly"-like stress path in pq-space accompanied by a growing strain amplitude γ_A. Although this butterfly attractor can be fairly well modeled by the reference version of hypoplasticity the preceding zigzag stress path is moving to the left much too fast. The increase of the amplitude γ_A, not shown in the Figure, is too slow in both versions of hypoplasticity. Presumably patterns of localized strain zones amplify γ_A in experiments. Numerical simulations of non-symmetric and symmetric deviatoric stress cycles are presented in Figs. 4.16 and 4.17, respectively. All calculations were started

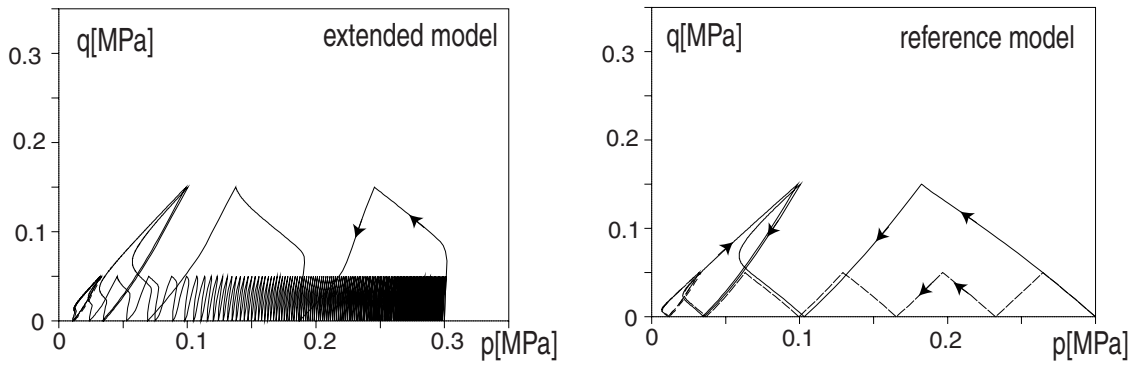

Figure 4.16: Undrained triaxial compression with non-symmetric deviatoric stress cycles of different amplitudes (left: extended model, right: reference model)

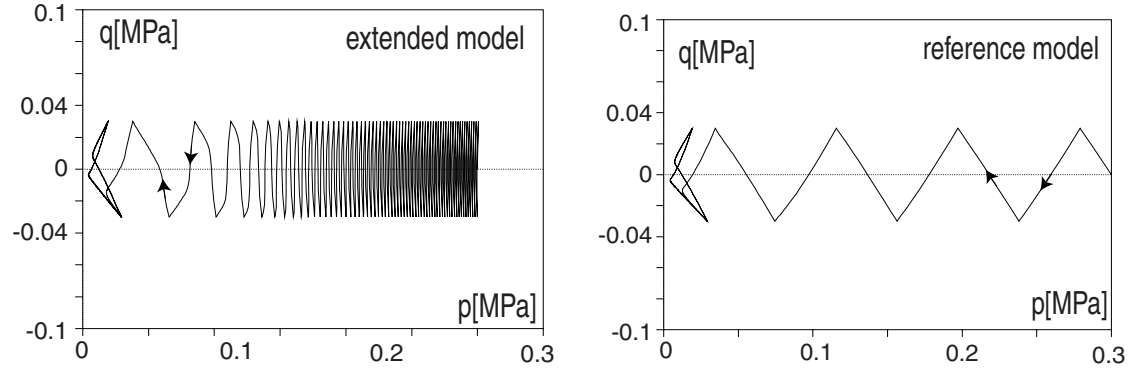

Figure 4.17: Undrained triaxial compression with symmetric deviatoric stress cycles (left: extended model, right: reference model)

from the initial void ratio $e_0 = 0.695$ and $p = 0.3$ MPa.

The number of undrained stress cycles sustained by the sample prior to cyclic mobility may be practically important. The results for symmetric deviatoric stress cycles are shown in Fig. 4.18. The relation obtained in the numerical calculations coincides qualitatively with the experimental results in [239]. From Fig. 4.18 it is also apparent that the reference hypoplastic model predicts a far too low number of cycles necessary to reach the yield surface under undrained conditions. For low stress amplitudes the predictions are extremely conservative.

4.1.6 Solvability

Suppose now that we have to solve (4.6) for $\mathbf{D}$, i.e., the stress rate $\mathring{\mathbf{T}}$ is prescribed and the stiffness M has to be inverted. In the expression (4.11) for stiffness, however, two M cases $\vec{\mathbf{h}} : \mathbf{D} > 0$ and $\vec{\mathbf{h}} : \mathbf{D} \leq 0$ are separately considered. It is *not* obvious which of the two cases in equation (4.11) should be used for the inversion. One may even ask if there is always a unique solution of such a problem.

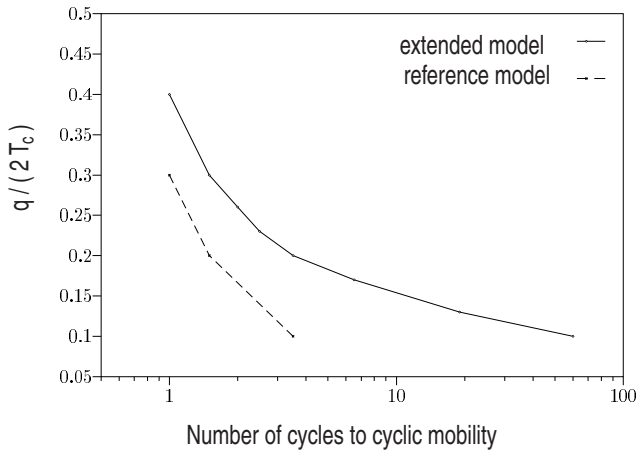

Figure 4.18: The number of cycles needed for cyclic mobility in undrained triaxial compression with symmetric deviatoric stress cycles of different amplitudes $q/(2T_c)$ where T_c is the cell pressure

In this subsection the approximation $\mathbf{D}^{\diamond}$ obtained from (4.17) is demonstrated to be sufficient to distinguish uniquely between $\vec{\mathbf{h}} : \mathbf{D} > 0$ and $\vec{\mathbf{h}} : \mathbf{D} < 0$. Let us decompose $\mathbf{D} = \mathbf{D}^{(n)} + \mathbf{D}^{(t)}$, wherein

$$\mathbf{D}^{(n)} = \vec{\mathbf{h}}\vec{\mathbf{h}} : \mathbf{D} \; ; \qquad \mathbf{D}^{(t)} = (\mathsf{I} - \vec{\mathbf{h}}\vec{\mathbf{h}}) : \mathbf{D} \tag{4.27}$$

We call them the normal and the tangential part of $\mathbf{D}$ with reference to the surface $\|\mathbf{h}\| = R$ shown in Fig. 4.7. Evidently, $\mathbf{D}^{(n)} \| \vec{\mathbf{h}}$ and $\mathbf{D}^{(t)} \perp \vec{\mathbf{h}}$. The stress response can be expressed as a sum of the responses to $\mathbf{D}^{(t)}$ and to $\mathbf{D}^{(n)}$

$$\mathring{\mathbf{T}} = \mathring{\mathbf{T}}(\mathbf{D}^{(n)}) + \mathring{\mathbf{T}}(\mathbf{D}^{(t)}) = a\mathsf{L} : \mathbf{D}^{(n)} + b\mathsf{L} : \mathbf{D}^{(t)} + c\mathbf{N}\vec{\mathbf{h}} : \mathbf{D}^{(n)} \,, \tag{4.28}$$

wherein

$$a = (1 - \rho^{\chi})m_R + \begin{cases} \rho^{\chi} & \text{for } \vec{\mathbf{h}} : \mathbf{D} > 0 \\ \rho^{\chi} m_R & \text{for } \vec{\mathbf{h}} : \mathbf{D} \leq 0 \end{cases} \tag{4.29}$$

$$b = \rho^{\chi} m_T + (1 - \rho^{\chi}) m_R \tag{4.30}$$

$$c = \begin{cases} \rho^{\chi} & \text{for } \vec{\mathbf{h}} : \mathbf{D} > 0 \\ 0 & \text{for } \vec{\mathbf{h}} : \mathbf{D} \leq 0 \end{cases} \tag{4.31}$$

It is tentatively assumed that the solution of (4.28) is unique for all $\mathring{\mathbf{T}}$ (this assumption will be proven further below).

The essential observation is that the sign of $\vec{\mathbf{h}} : \mathbf{D}$ can be tested taking

$$\mathbf{D}^{\diamond} = a^* \mathbf{D}^{(n)} + b^* \mathbf{D}^{(t)} \quad \text{with any } a^* > 0 \quad \text{and any } b^* \tag{4.32}$$

instead of $\mathbf{D}$. In the following, only the case of $\vec{\mathbf{h}} : \mathbf{D} \leq 0$ is discussed, since the opposite results automatically. The constitutive equation takes the form

$$\mathring{\mathbf{T}} = \mathsf{M} : \mathbf{D} = a\mathsf{L} : \mathbf{D}^{(n)} + b\mathsf{L} : \mathbf{D}^{(t)} \tag{4.33}$$

We choose $a^* = a$ and $b^* = b$ so that Equation (4.28) takes the simple form

$$\mathring{\mathbf{T}} = a\mathsf{L} : \mathbf{D}^{(n)} + b\mathsf{L} : \mathbf{D}^{(t)} = \mathsf{L} : \mathbf{D}^{\diamond} \tag{4.34}$$

With the limitation $m_R > 0$ and $0 < \rho < 1$ the value of a is positive, so the product $\vec{\mathbf{h}} : \mathbf{D}^{\diamond}$ gives the true sign of $\vec{\mathbf{h}} : \mathbf{D}$. The solution of stress controlled or mixed controlled problems (element tests) is now straightforward. First, we solve the auxiliary problem $\mathring{\mathbf{T}} = \mathsf{L} : \mathbf{D}^{\diamond}$ for $\mathbf{D}^{\diamond}$ or its unknown components. Next, depending on the sign of $\vec{\mathbf{h}} : \mathbf{D}^{\diamond}$, we build the stiffness M using (4.11) and solve the linear relation $\mathring{\mathbf{T}} = \mathsf{M} : \mathbf{D}$ for $\mathbf{D}$ or for missing components of $\mathring{\mathbf{T}}$ and $\mathbf{D}$.

Let us now prove the uniqueness of the solution of (4.28) for $\mathbf{D}$. The uniqueness is lost if two strain rates $\mathbf{D}^1 \neq \mathbf{D}^2$ exist such that $\mathring{\mathbf{T}}^1 = \mathring{\mathbf{T}}^2$. If both $\mathbf{D}^1$ and $\mathbf{D}^2$ belong to the same regime, that is, if $\text{sign}(\vec{\mathbf{h}} : \mathbf{D}^1) = \text{sign}(\vec{\mathbf{h}} : \mathbf{D}^2)$, the stiffness M in both cases is identical and (as long as M is a positive definite matrix) the inversion of such a linear system must be unique. Due to continuity of the stress response $\mathring{\mathbf{T}}(\mathbf{D})$, the stress rates corresponding to the tangential strain rate $\mathbf{D}^{(t)}$ are for both regimes ($\vec{\mathbf{h}} : \mathbf{D} \geq 0$ and $\vec{\mathbf{h}} : \mathbf{D} \leq 0$) equal. According to the superposition (4.28), it is therefore sufficient to consider $\mathbf{D}^{(n)}$ only. Without loss of generality we may investigate $\mathbf{D}^1 = \vec{\mathbf{h}}$ and $\mathbf{D}^2 = -\xi^2\vec{\mathbf{h}}$ with ξ^2 being a positive number. If a non-unique solution exists, the difference of the respective stress rates must vanish

$$a\mathsf{L} : \mathbf{D}^1 + c\mathbf{N}\vec{\mathbf{h}} : \mathbf{D}^1 - a'\mathsf{L} : \mathbf{D}^2 = \mathsf{L} : \vec{\mathbf{h}}(a + a'\xi^2) + c\mathbf{N} = \mathbf{0} \tag{4.35}$$

wherein $a = (1-\rho^\chi)m_R + \rho^\chi$ and $a' = (1-\rho^\chi)m_R + \rho^\chi m_R$. Solving (4.35) for $\vec{\mathbf{h}}$ and using $\|\vec{\mathbf{h}}\| = 1$ we arrive at the following condition for loss of uniqueness

$$\left|\frac{a + \xi^2 a'}{c}\right| = \| - \mathsf{L}^{-1} : \mathbf{N}\| \tag{4.36}$$

Since a and $\xi^2 a'$ are positive the condition (4.36) takes the form

$$\| - \mathsf{L}^{-1} : \mathbf{N}\| \geq \left|\frac{a}{c}\right| = \left|\frac{m_R - \rho^\chi m_R + \rho^\chi}{\rho^\chi}\right| \tag{4.37}$$

With the limitation $m_R > 0$ and $0 < \rho < 1$ Eq. (4.37) may be fulfilled only if $\|\mathsf{L}^{-1} : \mathbf{N}\| > 1$ that is in the stress range where the hypoplastic model itself yields non-unique solutions, see [162] www.AN or Equation (3.14) in Section 3.1.1. Thus, the uniqueness of (4.28) is insured for stresses at which reference Eq. (2.61) of the reference model is unique.

4.2 Visco-hypoplastic model

4.2.1 Introduction

The stress-strain-*time* behaviour of clay-like soils is important for the evaluation of long-term performance in geotechnical engineering. Here, an implementation of simple rheological effects into the hypoplastic framework is discussed. The visco-hypoplastic model can be shown to describe the phenomena as creep, relaxation and rate dependence. These effects may be of primary concern in relatively soft soils, i.e., at low overconsolidation ratios (OCR). The intergranular strain described in Section 4.1 is implemented[4]. Earlier attempts to introduce the viscous flow into the hypoplastic framework have been critically reviewed in [165] www.AN . Recently, Gudehus [76] proposed a visco-hypoplastic formulation similar to the one discussed here. It is less phenomenological and adheres closely to the physics of friction and to the laws of physical chemistry.

The presented three-dimensional model is relatively simple and more sophisticated concepts like strain acceleration[5] [117], history dependence of viscous creep [110] or hesitation effect due to relaxation of the back stress [125] or 'delayed contractancy' [218] are not implemented.

Preliminary assumptions

We consider fully saturated clayey soils at slow rates of deformation and at OCRs smaller than two. For large values of OCR the formula for the intensity of creep is less precise. Changes of temperature, discussed by Mitchell [155] or recently by Krieg [123], and of ion concentration in the pore water, discussed e.g. by Hueckel [98–100] or by Zou [284], are disregarded.

The primary consolidation phenomenon is left out: not because the presented extension is unable to describe creep coming along with the primary consolidation but because the consolidation as such does not belong to the subject of constitutive modeling. Principally, it should be dealt with on the finite element level and not on the material level because of the scale effect related to the transport of water, see e.g. the textbook by Lewis and Schrefler [134]. Only in some simplified models (a sample of a given height under oedometric conditions), the consolidation equation is combined with the expression for the creep rate. For example, Klobe [114] implemented in this way an early visco-hypoplastic

[4]Actually, the intergranular strain concept was primarily dedicated to visco-hypoplasticity [80] and later it was ported to the hypoplastic model for non-viscous soils

[5]Recently, the importance of the temporal strain fluctuation for unstable response and liquefaction of loose sand was pointed out (see also [18]). di Prisco and Imposimato [196] proposed a fabric evolution dependent on the strain acceleration.

formulation of Kolymbas [116, 117]. A different joint consideration of consolidation and creep was attempted in [163] www.AN to investigate differences between a stepped loading and a constant-strain-rate (CRSN) loading.

In this section the decomposition of the strain rate into elastic and viscous portion is assumed. With this simplification all irreversible deformations are treated collectively as a time-dependent variable $\mathbf{D}^{vis}$, and the following formula

$$\boxed{\mathbf{D} = \mathbf{D}^e + \mathbf{D}^{vis}} \tag{4.38}$$

is used. The viscous rate $\mathbf{D}^{vis} = \mathbf{D}^{vis}(\mathbf{T}, e)$ is a function of stress and void ratio, in particular it does not depend on the intergranular strain. Similarly as in the visco-plastic approach proposed by Olszak and Perzyna [185] we adapt an elastoplastic yield function. It may be surpassed by the stress (numerical errors are not meant here) and the 'distance' between the stress and the yield surface, termed 'overstress', is used to evaluate the intensity of viscous flow. Here Norton's rule [179] and the hypoplastic flow rule ($\vec{\mathbf{D}}^{vis} = -\vec{\mathbf{B}}$) are adopted. Of course, the strain rate homogeneity of function $\mathring{\mathbf{T}}(\mathbf{D})$, introduced in (2.15), is dropped.

The decomposition (4.38) is sufficient [123, 163, 174] in most geomechanical applications of the model, except for combined calculation of creep and cyclic loading. For monotonic processes an additional decomposition of the irreversible strain portion, e.g. [278, 279], cf. (2.13), has proven dispensable. The absence of the explicit plastic strain rate is in accordance with the hypoplastic line of thought, and hypoplasticity has turned out to be a convenient framework to implement viscous deformations in the sense of Equation (4.38).

It is well known that the duration of primary vertical consolidation is proportional to the square of the height of the sample. Contrary to this, creep or secondary compression strains are assumed here independent of the height of the sample. This fact has been carefully verified in experiments [105, 107, 233]. In the literature, the approaches which are in agreement with these observations are traditionally said to obey the *hypothesis B*. It originates from the concept of isotachs by Suklje [229]. The so-called *hypothesis A* by Mesri [152] postulates a unique (for samples of different heights) end-of-primary line in the $e - \ln p$ diagram, assuming the viscous creep to be a phenomenon similar to consolidation, i.e. dependent on the square of the height of the sample. Readers interested in this subject are referred to the experimental evidence and discussion by Imai and Tang [105].

4.2.2 One-dimensional version

In the following, the one-dimensional model given in [174] www.AN is briefly revisited with necessary modifications to render it consistent with the compression law by Butterfield [28] and with the logarithmic strain measure used throughout this text. Note that the compression law by Butterfield given in (4.60) and (4.61) needs *different* values of material parameters λ and κ than the compression model by Terzaghi $e - e_0 = -\lambda^* \ln(p/p_0)$. Moreover, for a 20% compression the logarithmic strain measure $\epsilon^v = \ln \dfrac{1+e}{1+e_0}$, is considerably greater (about 2.3%) than the small deformation strain[6] $\epsilon^{v\ Biot} = \dfrac{e-e_0}{1+e_0}$ used in [174].

We start from the standard equations commonly used in evaluation of oedometric tests. For (A) CRSN first loading, i.e. with $D = \text{const}$, for (B) unloading or reloading and for (C) creep at $T = \text{const}$ we have, respectively,

$$\epsilon - \epsilon_0 = -\lambda \ln(T/T_0) \quad \text{or} \quad D = -\lambda\, \dot{T}/T, \tag{4.39}$$

$$\epsilon - \epsilon_0 = -\kappa \ln(T/T_0) \quad \text{or} \quad D = -\kappa\, \dot{T}/T, \tag{4.40}$$

$$\epsilon - \epsilon_0 = -\psi \ln \frac{t+t_0}{t_0} \quad \text{or} \quad D = -\psi\, \frac{1}{t+t_0}, \tag{4.41}$$

where $T < 0$ is the vertical stress and D is the vertical (= volumetric) strain rate. These well known relations need the following material constants: the compression index λ, the swelling index κ, and the coefficient of secondary compression ψ. The quantities ϵ_0, T_0, t_0 are reference values of strain, void ratio, stress and time, respectively. In (4.39), both points (ϵ_0, T_0) and (ϵ, T) must lie on the virgin compression line and in (4.40) the states (ϵ_0, T_0) and (ϵ, T) must lie on the same unloading branch. For the case when the creep process is commenced from the first compression line the reference time t_0 in (4.41) is sometimes interpreted as the duration of the primary consolidation $t_0 = t_p$. Even if (4.41) should hold for this special case only, the assumption $t_0 = t_p$ is not appropriate, and actually the meaning of t_0 in (4.41) is not clear. Another deficit of the system (4.39) to (4.41) is its inability to describe relaxation or (practically more important) to predict creep after small unloading. These shortcomings are removed introducing a simple one-dimensional model consisting of the following three equations

$$\dot{T} = \frac{-T}{\kappa}(D - D^{vis}) \tag{4.42}$$

$$D^{vis} = -D_r \left(\frac{-T}{T_e}\right)^{1/I_v} \tag{4.43}$$

$$T_e = T_{e0} \left(\frac{1+e}{1+e_{e0}}\right)^{-1/\lambda} \quad \text{or} \quad \dot{T}_e = -\frac{T_e D}{\lambda} \tag{4.44}$$

[6] Biot strain

where $T_e(>0)$ is an equivalent stress and $D = \dot{e}/(1+e)$. The material constants are the viscosity index I_v and the already known coefficients λ and κ. Let the reference creep rate (fluidity parameter) be chosen as $D_r = 1\%/\text{h}$ then the reference state T_e and e_{e0} must be chosen on the primary compression line or reference isotach[7] corresponding to the creep rate D_r.

The standard equations (4.39),(4.40) and (4.41) will be shown to result from the model defined by (4.42),(4.43) and (4.44) as special cases, see also [163, 174] www.AN . Let us start with isotachs, i.e. compression lines corresponding to $D(t) = \text{const}$. For this purpose we consider the condition

$$\frac{\partial D^{vis}}{\partial t} = 0 \tag{4.45}$$

which can be impose on (4.43). It results in $\dot{T}/T = \dot{T}_e/T_e$ which may be combined with (4.42) and (4.44) to obtain

$$-\frac{D - D^{vis}}{\kappa} = -\frac{D}{\lambda} \quad \text{or} \quad D = D^{vis}\frac{\lambda}{\lambda - \kappa} = \text{const} \tag{4.46}$$

so the condition (4.45) corresponds to a CRSN compression ($D(t) = \text{const}$). Moreover, the above equation can be used to eliminate D^{vis} from (4.42) and we conclude that:

$$D^{vis}/D = (\lambda - \kappa)/\lambda \quad \text{and} \tag{4.47}$$

$$\dot{T} = -(T/\lambda)D \tag{4.48}$$

hold. Notice that we have just rediscovered (4.39) as a special case for the CRSN compression. In order to recover (4.40) we simply consider a situation when viscous effects are negligible and drop D^{vis} in (4.42).

Equation (4.40) results from the condition $T = \text{const}$. This condition and (4.42) imply $D = D^{vis}$. Substituting T_e from (4.44) into (4.43) and substituting $D^{vis} = D = \dot{e}/(1+e)$ we obtain

$$\frac{\dot{e}}{1+e} = -D_r \left[\frac{-T}{T_{e0}\left(\dfrac{1+e}{1+e_{e0}}\right)^{-1/\lambda}} \right]^{1/I_v} \tag{4.49}$$

which is an ordinary differential equation of $e(t)$. With abbreviations $\vartheta(t) = 1 + e(t)$ and $k = D_r \left[\dfrac{-T}{T_{e0}\,(1+e_{e0})^{1/\lambda}} \right]^{1/I_v} = \text{const}$ we obtain a simpler form of differential equation

[7] A λ-line obtained from a CRSN test with $D = D_r\lambda/(\lambda - \kappa)$, i.e., from a CRSN test slightly faster than D_r. The above formula is derived further in text.

(4.49), namely

$$\dot{\vartheta} = -k\vartheta^{1+1/(\lambda I_v)} \quad \text{with a solution} \quad \vartheta = \left(\frac{\lambda I_v}{kt - C_1}\right)^{\lambda I_v}, \tag{4.50}$$

wherein C_1 is an undetermined as yet integration constant. Substituting this solution into $D = \dot{\vartheta}/\vartheta$ we obtain

$$D = \frac{\dot{\vartheta}}{\vartheta} = -\frac{\lambda I_v}{t - C_1/k} \tag{4.51}$$

which can be compared it with the rate form of (4.41) and the parameters

$$\psi = \lambda I_v \tag{4.52}$$

$$t_0 = -C_1/k \tag{4.53}$$

can be identified. With $D^{vis} = D$ we may find C_1 from the initial creep rate (at $t = 0$) comparing (4.43) and (4.51):

$$C_1 = I_v \lambda k / D^{vis} \tag{4.54}$$

and hence

$$t_0 = -\frac{I_v \lambda}{D^{vis}} = \frac{\lambda I_v}{D_r} \mathrm{OCR}^{1/I_v} \quad \text{with} \quad OCR = -T_e/T\,. \tag{4.55}$$

We have shown that t_0 is not a material constant but a function of state. Substituting the last expression to (4.41)-left we can evaluate OCR at the beginning of the creep process, i.e. at $t = 0$. Note that the present equations are generally much simpler than those for Biot strain and Terzaghi's compression given in [174]. It should be emphasized that the simplicity of the model results from the assumption that the creep rate depends solely on OCR. This fact was verified experimentally in [174], see Fig. 4.21. Moreover, contrary to the original concept of overstress [185], there is no need of a switch function in (4.43), which simplifies the model.

Let us remark that in the present model index of viscosity I_v is very similar but not identical with the one proposed by Leinenkugel [131]. For one-dimensional case Leinenkugel described a stress jump $T_b - T_a$ due to a rapid change of the deformation velocity from D_a to D_b by equation

$$T_b - T_a = I_v T_a \ln(D_b/D_a) \tag{4.56}$$

According to our model

$$D_b/D_a = D_b^{vis}/D_a^{vis} = (T_b/T_a)^{1/I_v} \tag{4.57}$$

and hence $I_v \ln(D_b/D_a) = \ln(T_b/T_a)$. If we agree on approximation $\ln(1+x) \approx x$ for small $x = (T_b - T_a)/T_a$ Leinenkugel's expression is recovered.

Comparing a 3-D model presented in the following subsection with the above 1-D oedometric analysis one should be aware of the fact that we could not consider the variability of stress obliquity here. The definitions of OCR in (4.55) and in (4.78) are *different* and small quantitative discrepancies are therefore inevitable. In the general 3-D version, OCR is *not* just the ratio of the vertical stress component to T_e but a complex function depending on the pressure, the void ratio and the stress obliquity, see Section 4.2.5. Moreover, differently to 1-D definition of T_e by Hvorslev, we prefer to use equivalent pressure p_e measured along the hydrostatic axis in 3-D version.

4.2.3 From hypoplasticity to visco-hypoplasticity

Adapting hypoplasticity to describe viscous effects, our first concern is an adequate modeling under simple triaxial and oedometric conditions. We consider clayey soils in normally consolidated or moderately overconsolidated state. In order to incorporate viscous phenomena within the hypoplastic framework several modifications seem to be necessary:

- Replacement of the nonlinear term $\mathbf{N}\|\mathbf{D}\|$ by an expression that depends on true time increment (see Section 4.2.5)
- Removal of the pycnotropy factor f_e (void-ratio dependence) and the factor f_d that accounts for the critical density of sand. A generalized notion of overconsolidation ratio OCR (defined in Section 4.2.5) will be used instead[8] The void ratio enters the constitutive equation via equivalent pressure p_e.
- Modification of the barotropy factor f_b (see Section 4.2.4)
- Modification of the intergranular strain formulation (see Section 4.2.11)

Let us rewrite the reference hypoplastic equation (2.61) with $f_e \equiv 1$ and $f_d \equiv 1$:

$$\mathring{\mathbf{T}} = f_b \hat{\mathsf{L}} : \Big[\mathbf{D} - (-\hat{\mathsf{L}}^{-1} : \hat{\mathbf{N}}\,\|\mathbf{D}\|)\Big] \tag{4.58}$$

and replace $-\mathsf{L}^{-1} : \mathbf{N}\|\mathbf{D}\|$ in (4.58) by the creep rate $\mathbf{D}^{vis}$. The resulting formula

$$\boxed{\mathring{\mathbf{T}} = f_b \hat{\mathsf{L}} : (\mathbf{D} - \mathbf{D}^{vis})}, \tag{4.59}$$

is the basic constitutive equation of the visco-hypoplastic model. It is discussed in detail in the next subsections. In order to describe the intensity of creep, $\|\mathbf{D}^{vis}\|$, the concept

[8] In a recent visco-hypoplastic model by Gudehus [76] these factors are preserved.

of overstress [185] originally applied outside the yield surface ($f(\mathbf{T}, e) > 0$) only is generalized, following the outline of Section 4.2.2. Here, this concept is said to apply also for stresses *inside* the yield surface. We allow for viscous deformation at any stress, thus the switch function with the concept of a *perfectly* non-viscous locus is rejected. The intensity of flow is assumed to be proportional to OCR^{-1/I_v} (typically to OCR^{-20}) and in the definition of OCR proposed in Subsection 4.2.5 both $OCR \geq 1$ and $OCR < 1$ (!) are admitted. Note that due to the high value of the exponent $1/I_v$ the creep rate rapidly decreases inside the yield surface (that is assumed to correspond to $OCR = 1$), and for $OCR = 2$ the creep rate is practically negligible (10^6 times smaller than the creep rate for OCR=1).

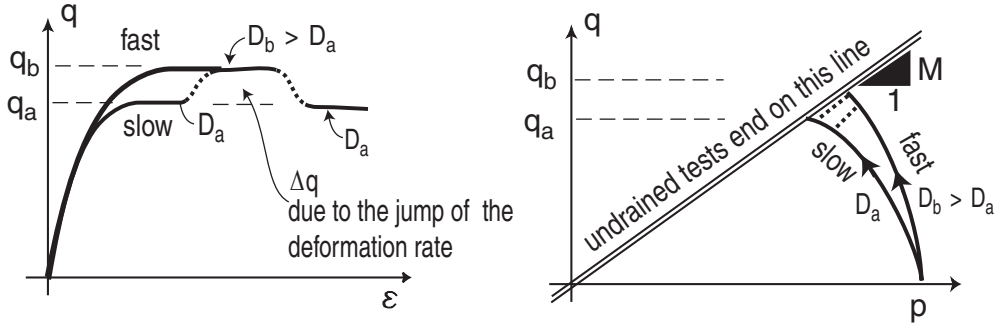

Figure 4.19: Rate dependence for triaxial undrained compression test

4.2.4 Barotropy

In the hypoplastic model the stress obliquity $\hat{\mathbf{T}} = \mathbf{T}/\mathrm{tr}\,\mathbf{T}$ appears in the expressions for $\hat{\mathsf{L}}$ and $\hat{\mathbf{N}}$ whereas the mean stress $\mathrm{tr}\,\mathbf{T}$ is separated and appears in the barotropy function f_b only. The barotropy function given in Section 2.5 is based on the oedometric first compression curve of sand. In the following we need a function f_b precisely describing the stiffness upon oedometric/isotropic unloading and reloading rather than the stiffness for the first loading. For this reason an alternative barotropy function is introduced consistently with the well established formulation by Butterfield [28]. Consider an isotropic deformation along the hydrostatic axis p. According to Butterfield we have

$$\ln\left[\frac{1+e_0}{1+e}\right] = \lambda \ln\left[\frac{p}{p_0}\right] \tag{4.60}$$

for the first isotropic loading and

$$\ln\left[\frac{1+e_0}{1+e}\right] = \kappa \ln\left[\frac{p}{p_0}\right] \tag{4.61}$$

for a perfectly reversible isotropic unloading or reloading. Note that the void ratio e_0, the pressure p_0 and the current values e and p must belong to the same process (first

loading / unloading /reloading). It is more convenient, therefore, to use the rate form of the above equations. After time differentiation of (4.60) and (4.61) we obtain two simple equations

$$\dot{p} = -\frac{p}{\lambda}\frac{\dot{e}}{1+e} = -\frac{p}{\lambda}D^v \tag{4.62}$$

for the first loading and

$$\dot{p} = -\frac{p}{\kappa}D^v \tag{4.63}$$

for unloading/reloading wherein the volumetric strain rate is $D^v = \dfrac{\dot{e}}{1+e}$.

The next modification of barotropy consists in removing the factor $1/\hat{\mathbf{T}} : \hat{\mathbf{T}}$ from the expressions (2.63) and (2.64) for L and $\mathbf{N}$. For sand, this factor emphasized the fact that the overall compressibility at large stress ratios is evidently larger than at the isotropic stress. For clays this difference is small and, for simplicity, it is disregarded here. It is known that the first compression lines for clay are approximately parallel for different radial stress paths, see Fig. 4.23. The same is often assumed for swelling (unloading /reloading) lines and therefore the linear part of stiffness takes the form

$$\mathsf{L} = f_b\hat{\mathsf{L}} = f_b(F^2\mathsf{I} + a^2\hat{\mathbf{T}}\hat{\mathbf{T}})\,, \tag{4.64}$$

wherein new barotropy function $f_b(\mathrm{tr}\,\mathbf{T})$ is supposed to describe the volume changes at the absence of creep, i.e. for $\mathbf{D}^{vis} = \mathbf{0}$. From the comparison of (4.59) and (4.63) for the case of isotropic compression along the hydrostatic axis with $D_{kl} = \delta_{kl}\frac{1}{3}D^v$ and $\hat{T}_{ij} = \frac{1}{3}\delta_{ij}$ and $F = 1$ so $\dot{p} = -\frac{1}{3}\delta_{ij}\mathring{T}_{ij}$ and without $1/(\mathbf{T} : \mathbf{T})$ we have

$$\dot{p} = -\frac{p}{\kappa}D^v = -\frac{1}{3}f_b\delta_{ij}\overbrace{(\delta_{ik}\delta_{jl} + a^2\,\frac{1}{3}\delta_{ij}\frac{1}{3}\delta_{kl})}^{=\hat{L}_{ijkl}}\,\delta_{kl}\frac{1}{3}D^v \tag{4.65}$$

resulting (after substitution $p = -\frac{1}{3}\mathrm{tr}\,\mathbf{T}$) in the new barotropy function

$$\boxed{f_b(\mathrm{tr}\,\mathbf{T}) = -\frac{\mathrm{tr}\,\mathbf{T}}{(1+a^2/3)\kappa} = -\beta_b\mathrm{tr}\,\mathbf{T}} \tag{4.66}$$

with the abbreviation $\beta_b = [(1+a^2/3)\kappa]^{-1}$. This function is in accordance with an isotropic unloading along the slope κ. Unfortunately, isotropic compression tests are less convenient than the oedometric ones to determine the material constant β_b in laboratory.

Calibration of f_b from oedometric test

Usually we prefer to determine the factor β_b from an oedometric test, namely from the slope κ^o which is the coefficient of compression by Butterfield measured (or calculated with the model) for oedometric unloading (starting at the K_0 stress state). According to the reference model, the value κ^o is slightly smaller than analogous coefficient κ from isotropic unloading (even without $1/\hat{\mathbf{T}} : \hat{\mathbf{T}}$ term). Here, an expression for β_b in relation to κ^o is derived. We start with

$$\dot{p} = -\frac{p}{\kappa^o} D^v \quad \text{for} \quad D_{kl} = \delta_{k1}\delta_{l1} D^v \quad \text{and} \quad \hat{T}_{ij} = \frac{1}{1+2K_0}\,\mathrm{diag}(1, K_0, K_0) \tag{4.67}$$

for which $F = 1$. The coefficient of earth pressure at rest K_0 is discussed in Section 4.2.7 and for the present purpose it can be calculated from Eq. (4.94). As previously, the viscous strain is not considered ($\mathbf{D}^{vis} = \mathbf{0}$). From the linear part of the constitutive model we extract three equations for the principal components $\mathring{T}_{pp}$, viz.

$$\mathring{T}_{pp} = f_b \hat{\mathsf{L}}_{pp11} D_{11} \qquad \text{no sum over } p \tag{4.68}$$

or in the full form

$$\begin{Bmatrix} \mathring{T}_{11} \\ \mathring{T}_{22} \\ \mathring{T}_{33} \end{Bmatrix} = \frac{f_b^o}{(1+2K_0)^2} \begin{Bmatrix} (1+2K_0)^2 + a^2 \\ a^2 K_0 \\ a^2 K_0 \end{Bmatrix} D^v \tag{4.69}$$

and combine them with (4.67) to obtain

$$\mathrm{tr}\,\mathring{\mathbf{T}} = -\frac{\mathrm{tr}\,\mathbf{T}}{\kappa^o} D^v = f_b \frac{1}{(1+2K_0)^2}\left[(1+2K_0)^2 + (1+2K_0)a^2\right] D^v \tag{4.70}$$

Finally

$$f_b = -\frac{\mathrm{tr}\,\mathbf{T}}{[1 + a^2/(1+2K_0)]\,\kappa^o} = -\beta_b \mathrm{tr}\,\mathbf{T} \tag{4.71}$$

which means

$$\beta_b = \frac{1}{(1+a^2/3)\kappa} = \frac{1}{[1 + a^2/(1+2K_0)]\,\kappa^o}\,. \tag{4.72}$$

We may treat Equation (4.66) as the (theoretical) definition of β_b and (4.71) as a practical calibration formula. For $\varphi_c = 30^\circ$ we obtain $a = 3.062$, $K_0 = 0.631$ and $\kappa/\kappa^o = 1.24$. The requirement $\kappa^o = \kappa$ cannot be satisfied by the reference model and if their difference seems too large compared with the laboratory tests, a correction function must be be introduced, for example taking $f_b^x = -\left(\frac{1}{3}\hat{\mathbf{T}} : \hat{\mathbf{T}}\right)^4 \frac{\mathrm{tr}\,\mathbf{T}}{(1+\frac{a^2}{3})\kappa}$. Notice, that the original factor $1/\hat{\mathbf{T}} : \hat{\mathbf{T}}$ in (2.63) and (2.64) increases the ratio κ/κ^o.

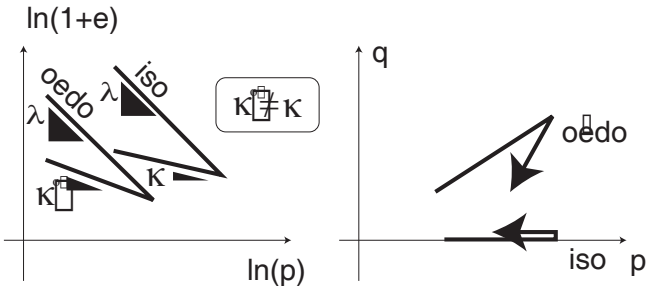

Figure 4.20: Different slopes κ and κ^o of swelling lines

4.2.5 Creep rate

The creep rate is proposed to be a function of the void ratio e and of the effective stress $\mathbf{T}$ only, i.e. $\mathbf{D}^{vis}(\mathbf{T}, e)$. This simple assumption has been supported experimentally [174]

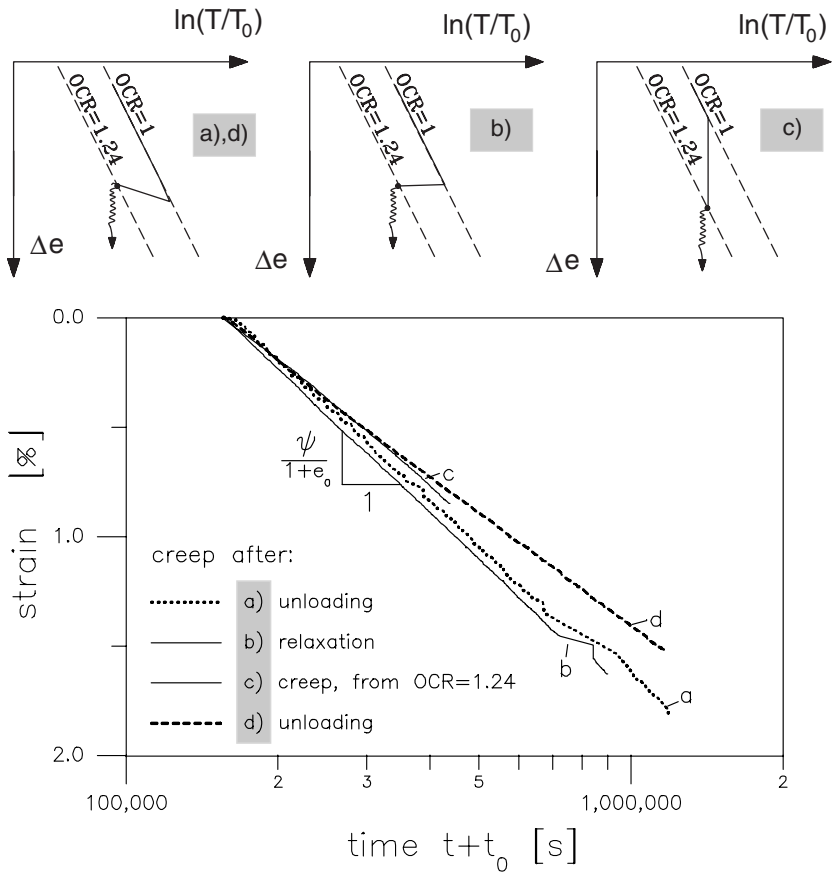

Figure 4.21: Oedometric creep tests started at the same OCR=1.24 but preceded by different deformation/stress histories. The creep rate turns out to be almost constant irrespectively of the recent history. This observation supports the assumption that $\mathbf{D}^{vis}(\mathbf{T}, e)$ is a function of stress and void ratio only

www.AN by a comparison of three different oedometric creep tests commenced at the same OCR=1.24 and preceded (directly) by unloading, relaxation or another creep process. The

recent history turned out to have practically no influence on the observed creep rate, see Fig. 4.21. Let us consider separately the intensity of the creep rate and its direction. For the direction of creep we use the hypoplastic flow rule. Comparing (4.58) and (4.59) we obtain

$$\mathbf{D}^{vis} \sim -\vec{\mathbf{B}} = -\frac{\hat{\mathsf{L}}^{-1} : \hat{\mathbf{N}}}{\|\hat{\mathsf{L}}^{-1} : \hat{\mathbf{N}}\|} = -\frac{\left(\frac{F}{a}\right)^2 (\hat{\mathbf{T}} + \hat{\mathbf{T}}^*) + \hat{\mathbf{T}} : \hat{\mathbf{T}}\hat{\mathbf{T}}^* - \hat{\mathbf{T}}\hat{\mathbf{T}} : \hat{\mathbf{T}}^*}{\| \left(\frac{F}{a}\right)^2 (\hat{\mathbf{T}} + \hat{\mathbf{T}}^*) + \hat{\mathbf{T}} : \hat{\mathbf{T}}\hat{\mathbf{T}}^* - \hat{\mathbf{T}}\hat{\mathbf{T}} : \hat{\mathbf{T}}^* \|} \tag{4.73}$$

The intensity of creep is described analogously to Norton's power law [179] using OCR, viz.

$$\boxed{\mathbf{D}^{vis} = -D_r \vec{\mathbf{B}} \left(\frac{1}{\mathrm{OCR}}\right)^{(1/I_v)}} \tag{4.74}$$

cf. (4.43) in the 1-D version. The exponent $15 < (1/I_v) < 30$ is a material constant and D_r is a reference creep rate, e.g. $D_r = 1\%/\mathrm{h}$[9]. The usage of Leinenkugel's [131] index of viscosity I_v in the exponent follows from a comparison of (4.56) and (4.57), as presented in 1-D version of the model. Instead of $1/I_v$ one can also use λ/ψ, see Equation (4.52). The parameter I_v is discussed in Subsection 4.2.8.

In order to use (4.74) we need a precise (based on stress invariants and e) definition of OCR. Following Hvorslev [103] we introduce the equivalent isotropic pressure $p_e(e)$. This is the pressure necessary to reach a given void ratio e during a CRSN isotropic first compression test carried out with the referential rate of deformation[10] $D^v = D_r\lambda/(\lambda-\kappa)$, cf. (4.47). From the Butterfield's approximation (4.60) of the CRSN first compression curve we have

$$\boxed{\ln\left[\frac{1+e_{e0}}{1+e}\right] = \lambda \ln\left[\frac{p_e}{p_{e0}}\right]}, \tag{4.75}$$

see Fig. 4.24, wherein the reference state $p_{e0}(e_{e0})$ describes a fixed point on this *reference isotach*. Equation (4.75) is a one-to-one correspondence between the void ratio e and the equivalent pressure p_e. The parameters e_{e0} and p_{e0} are truly referential, i.e. (4.75) holds for any sequence of processes, unlike p_0 and e_0 in (4.60) and (4.61) which had to be redefined for loading, unloading, reloading, creep etc. Moreover, all creep tests commenced from the reference isotach start with the same rate $\|\mathbf{D}\| = \|\mathbf{D}^{vis}\| = D_r$, termed the fluidity parameter. As demonstrated in (4.47) for 1-D model, the reference creep rate is slightly smaller than the reference rate of deformation needed to generate

[9] In the presented model D_r need not be a material constant. As discussed in Section 4.2.6 many triples of reference values: D_r, e_{e0} and p_{e0} can be mathematically shown equivalent. Gudehus [76] provides physical arguments for a material-specific D_r.

[10] This rate for 3-D case is derived in the next subsection.

the reference isotach. It can be shown, however, that (4.47) holds in 3-D model only for the special case of isotropic compression . The rate form of (4.75) is

$$\frac{\dot{e}}{1+e} = -\lambda \frac{\dot{p}_e}{p_e} \qquad (= \operatorname{tr} \mathbf{D}). \tag{4.76}$$

For stress states on the hydrostatic axis the calculation of the overconsolidation ratio is straightforward: $\mathrm{OCR} = p_e/(-\frac{1}{3}\operatorname{tr}\mathbf{T})$. For the general case, however, we need a better definition in the form $\mathrm{OCR}(\mathbf{T}, p_e)$ that would account also for the deviatoric components of stress. For this purpose we use the equation

$$p(p - p_e) + q^2/M^2 = 0, \tag{4.77}$$

of the yield surface from the modified Cam-clay (MCC) model [206]. All states (p, q) that satisfy (4.77) for a given p_e, i.e. for a given e, lie on the half-ellipse that passes through p_e in Fig. 4.22 and are said to be normally consolidated ($\mathrm{OCR} = 1$). The inclination $q/p = M$ corresponds to the critical state (our $y(\mathbf{T}) \equiv \|\mathbf{B}\| - 1 = 0$). The critical stress ratio M is not a material constant in hypoplasticity. It depends on the Lode angle, namely $M(\mathbf{T}) = 6F(\mathbf{T})\sin\varphi_c/(3 - \sin\varphi_c)$ with F given in (2.66) and (2.67). For general states (p, q, e) the overconsolidation ratio OCR is defined by

$$\boxed{\mathrm{OCR} = p_e/p_e^+} \quad , \tag{4.78}$$

wherein p_e is given by (4.75), and the value $p_e^+(\mathbf{T})$ has to be found from

$$p(p - p_e^+) + q^2/M^2 = 0 \tag{4.79}$$

analogous[11] to (4.77). For a given p_e (or e) and p_e^+ all stresses (p, q) satisfying (4.79), i.e. lying on the smaller half-ellipse in Fig. 4.22 have by definition the same $\mathrm{OCR} = p_e/p_e^+$. Being given $\mathbf{T}$ and e we first calculate p_e from (4.75) and p_e^+ from[12]

$$\boxed{p_e^+ = p\left[1 + \bar{\eta}^2\right] = p\left[1 + \left(\frac{q}{M\,p}\right)^2\right]} \tag{4.80}$$

wherein p, q, M and $\bar{\eta} = q/(Mp)$ are functions of stress, and then OCR from (4.78). In Section 4.2.10 a more elaborated form of function $\mathrm{OCR} = \mathrm{const}$ is proposed in order to improve the prediction of undrained shearing.

Note that the stress $\mathbf{T}$ and the void ratio e alone determine our OCR. This implies that neither the shape nor the orientation of the surface $OCR = 1$ can change[13]. Only the size p_e of the ellipse may evolve depending on the void ratio e via (4.75).

[11] Equation (4.79) describes the smaller half-ellipse in Fig. 4.22.

[12] Graphically we find p_e^+ drawing an ellipse homologous to (4.77) that passes through $\mathbf{T}$. Its diameter along p-axis is p_e^+.

[13] Induced anisotropy is planned to be introduded in future to account for the anisotropy of the undrained strength. It is known that the undrained cohesion of naturally consolidated sample can be much higher for triaxial compression than for triaxial extension, $c_{uC} > c_{uE}$. The idea of anisotropic cap-surface has been introduced into elastoplastic constitutive models already in the eighties, see [5, 6, 157]

Equation (4.74) applies to stresses $\mathbf{T}$ inside (OCR > 1) and outside (OCR < 1) of the yield surface, so OCR=1 corresponds to states with the referential creep intensity D_r (say 1%/h) and is not a limit of an elastic locus, as it is the case in many viscoplastic models, e.g. [1, 41, 184]. No stress is excluded from the applicability of (4.74) because no elastic locus is needed in visco-hypoplasticity. The term 'overstress' is therefore slightly misleading here. A similar approach was presented by Kutter [126].

Rate dependence in undrained tests

As an illustrative example we may shortly discuss an asymptotic state reached after an isochoric CRSN shearing. The concept of OCR-dependent creep rate may be used to explain the rate dependence of strength c_u, presented qualitatively in Fig. 4.19. In undrained case strength $c_u = \frac{1}{2}q_{\max}$ depends on the applied deformation rate although the void ratio and the initial stress may be identical. With reference to Fig. 4.22, the critical state line, CSL, corresponds to the yield surface $y(\mathbf{T}) \equiv \|\mathbf{B}\| - 1 = 0$ for which the flow direction is purely deviatoric i.e. $-\mathrm{tr}\,\mathbf{B} = 0$. Isochoric shearing tests (with $\mathrm{tr}\,\breve{\mathbf{D}} \equiv 0$ and $\dot{e} = 0$) cannot change the equivalent pressure $p_e(e)$ because the void ratio e remains constant. However, OCR may change because p_e^+ depends on stress. All stress paths generated by CRSN undrained deformation paths reach eventually some asymptotic states $(\mathbf{T}, e)$ on CSL because they require $\mathring{\mathbf{T}} = \mathbf{0}$ and $\mathrm{tr}\,\mathbf{B} = 0$. The critical states A,B,C shown in Fig. 4.22 correspond to different prescribed deformation rates $\breve{\mathbf{D}}$ but to the same e. We need, therefore, three different creep rates $\breve{\mathbf{D}} = \mathbf{D}^{vis}$, cf. (4.59), and thus three different OCR values. If the prescribed rate $\breve{\mathbf{D}}$ is faster/slower than the referential D_r then the asymptotic stress lies on CSL higher=C/lower=A than the intersection point B of CSL and OCR=1. This is so because the balance $\breve{\mathbf{D}} = \mathbf{D}^{vis}$ needs OCR < 1 or OCR > 1, respectively.

Viscous response to proportional paths

Now let us inspect how the creep rate influences the response to the proportional stress path[14] $\mathring{\mathbf{T}} \sim \hat{\mathbf{T}} = \text{const}$. We are investigating a CRSN test with $\mathbf{D} = \text{const}$ which generates such path, see Fig. 4.23-left. The direction of flow $-\vec{\mathbf{B}}$ is a function of $\hat{\mathbf{T}} = \text{const}$ so is does not change. Moreover, from (4.59) we may conclude that proportional paths requires that $\mathbf{D}$ and $\mathbf{D}^{vis}$ are in a certain constant proportion, which means that

[14] We expect that after a sufficiently large deformation with $\mathbf{D} = \text{const}$ stress ratio $\hat{\mathbf{T}}$ will establish itself for which $\mathring{\mathbf{T}} \sim \mathbf{T}$. This property can be examined checking if $(\partial\mathring{\mathbf{T}}/\partial\mathbf{T})$ is negative definite, see Eq. 3.118. Moreover, approximately the same asymptotic stress ratio $\hat{\mathbf{T}}$ corresponds to different rates but the same directions $\vec{\mathbf{D}}$.

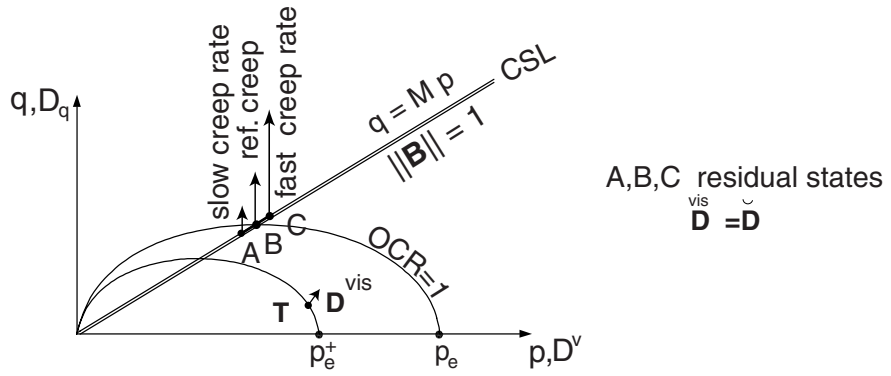

Figure 4.22: Depending on the deformation rate three undrained shearing paths reach different ultimate stresses A,B,C although the void ratios in all experiments are identical. On one hand we need three different OCRs and on the other we need a purely deviatoric viscous flow, so all ultimate stresses lie on CSL but at different heights. Each of the presented half-ellipses corresponds to OCR $= p_e/p_e^+ =$ const.

$\|\mathbf{D}^{vis}\| =$ const. According to (4.74) this implies OCR = const and therefore from differentiation $\dfrac{\mathrm{d}(p_e/p_e^+)}{\mathrm{d}t} = 0$ we obtain

$$\frac{\dot{p_e^+}}{p_e^+} = \frac{\dot{p_e}}{p_e} \tag{4.81}$$

Note that in the present model the condition OCR = const can be maintained *only* during an active loading. If the deformation is fixed, $\mathbf{D} = \mathbf{0}$, then OCR increases due to the stress relaxation $\overset{\circ}{\mathbf{T}} = \mathsf{L} : (\mathbf{0} - \mathbf{D}^{vis})$. If the stress is fixed, $\overset{\circ}{\mathbf{T}} = \mathbf{0}$, then OCR increases due to creep $\mathbf{D} = \mathbf{D}^{vis}$ which follows from $\mathbf{0} = \mathsf{L} : (\mathbf{D} - \mathbf{D}^{vis})$.

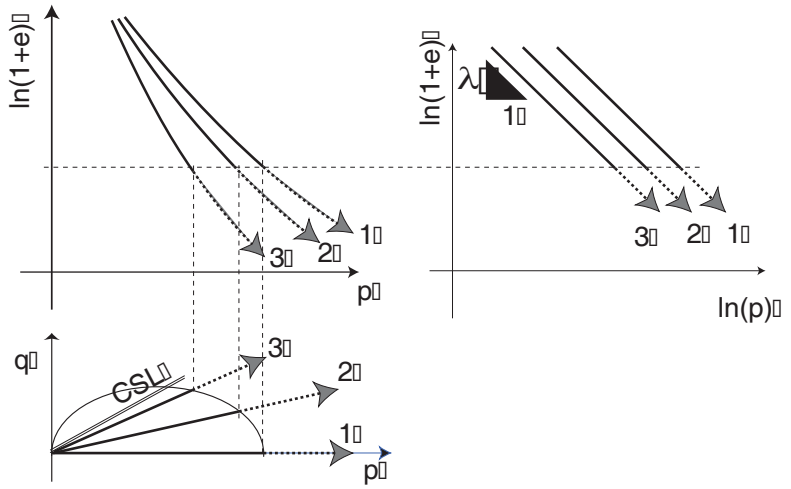

Figure 4.23: Parallel compression lines for three proportional stress paths with different deformation rates $\vec{\mathbf{D}}^{(1)} \neq \vec{\mathbf{D}}^{(2)} \neq \vec{\mathbf{D}}^{(3)}$ but with the same value $\|\mathbf{D}^{(1)}\| = \|\mathbf{D}^{(2)}\| = \|\mathbf{D}^{(3)}\| =$ const

Applying $\overset{\circ}{\mathbf{T}} \sim \hat{\mathbf{T}} =$ const to the left-hand side of (4.81) and (4.76) to the right-hand side

we obtain

$$\frac{\operatorname{tr}\mathring{\mathbf{T}}}{\operatorname{tr}\mathbf{T}} = \frac{\dot{p_e^+}}{p_e^+} = \frac{\dot{p_e}}{p_e} = -\frac{\dot{e}}{\lambda(1+e)} \quad (= -\frac{\operatorname{tr}\mathbf{D}}{\lambda}). \tag{4.82}$$

The resulting relation $\mathbf{D} = -\lambda \operatorname{tr}\mathring{\mathbf{T}}/\operatorname{tr}\mathbf{T}$ describes the well known first compression λ-lines. Let us emphasize that this equation holds *independently* of the stress obliquity $\hat{\mathbf{T}}$, i.e., the compression lines for various $\hat{\mathbf{T}} = \text{const}$ are parallel, as shown in Fig. 4.23-right. This is in agreement with MCC and with many other cap-type soil models that use the volumetric hardening rule. Note that similar assumption would be unacceptable for sands.

4.2.6 Reference creep rate D_r

In the previous subsection we noticed that CRSN compression tests with $\mathring{\mathbf{T}} \sim \hat{\mathbf{T}} = \text{const}$ and with $\mathring{\mathbf{T}}$ given by (4.59) require that $\mathbf{D}$ and $\mathbf{D}^{vis}$ are in a certain constant proportion. In the special case of isotropic compression $\mathbf{D}$ and $\mathbf{D}^{vis}$ are both parallel to $-\mathbf{1}$ so we may easily find a constant factor $x = \|\mathbf{D}\|/\|\mathbf{D}^{vis}\|$. For additional simplicity let us first consider the case $p_e^+ = p_e$, i.e. OCR $= 1$. According to (4.74) we may denote the intensity of creep as $\|\mathbf{D}^{vis}\| = D_r$. Knowing from (4.73) that $\mathbf{D}^{vis} \sim -\vec{\mathbf{B}}$ is isotropic for stresses on the p-axis we search for a constant isotropic deformation rate

$$\mathbf{D} = -D_r x \frac{1}{\sqrt{3}}\,\mathbf{1} = x\mathbf{D}^{vis} \tag{4.83}$$

that is required to sustain the condition OCR $= 1$. Using Equation (4.82) together with (4.59,4.66,4.83), as well as $\vec{B}_{kl} = -\frac{1}{\sqrt{3}}\delta_{kl}$ and $\hat{L}_{ijkl} = \delta_{ik}\delta_{jl} + a^2\frac{1}{3}\delta_{ij}\frac{1}{3}\delta_{kl}$ one obtains

$$\begin{aligned} -\frac{\operatorname{tr}\mathbf{D}}{\lambda} &= \frac{\sqrt{3}D_r x}{\lambda} = -\beta_b \delta_{ij}\hat{L}_{ijkl}\delta_{kl} D_r \frac{1}{\sqrt{3}}(1-x) = \\ &= -\beta_b(3+a^2)D_r\frac{1}{\sqrt{3}}(1-x) \end{aligned} \tag{4.84}$$

and finally

$$x = \frac{\lambda}{\lambda-\kappa} \quad \text{or} \quad D_r = \frac{\lambda-\kappa}{\lambda}\|\mathbf{D}\|\,. \tag{4.85}$$

The same ratio D/D_r was obtained in the 1-D version [174] of the model, cf. Eq. (4.47). We may use (4.85) to determine experimentally the fluidity parameter D_r that corresponds to a reference isotach of our choice.

Next, we derive an analogous factor x for a more general case of isotropic compression with $\mathbf{D} = \text{const}$ but OCR $= \text{const} \neq 1$. In such case

$$x = \frac{\|\mathbf{D}\|}{\|\mathbf{D}^{vis}\|} = \text{const} \tag{4.86}$$

holds and x is also given by (4.85). Let us examine isotropic compression along the hydrostatic axis. $\mathbf{D} \sim \mathbf{D}^{vis} \sim \mathbf{1} = \text{const}$ holds independently of OCR. The direction of creep is therefore constant. The intensity of creep rate is constant too, since OCR is. Thus (4.86) is proven and $x = \text{const}$ holds. Again, we write out (4.82)

$$-\frac{\operatorname{tr}\mathbf{D}}{\lambda} = \frac{\operatorname{tr}\overset{\circ}{\mathbf{T}}}{\operatorname{tr}\mathbf{T}} = -\beta_b\ \mathbf{1} : \hat{\mathsf{L}} : \left[\mathbf{D} - \frac{(-\mathbf{1})}{\sqrt{3}}\|\mathbf{D}^{vis}\|\right] \quad \text{or}$$

$$\frac{x\sqrt{3}\|\mathbf{D}^{vis}\|}{\lambda} = -\beta_b\ \mathbf{1} : \hat{\mathsf{L}} :\ \mathbf{1}\frac{1-x}{\sqrt{3}}\|\mathbf{D}^{vis}\|, \tag{4.87}$$

which leads to (4.85) analogously as in the case of OCR=1. Choosing a particular value of $\mathbf{D}$ we distinguish the *reference isotach*.

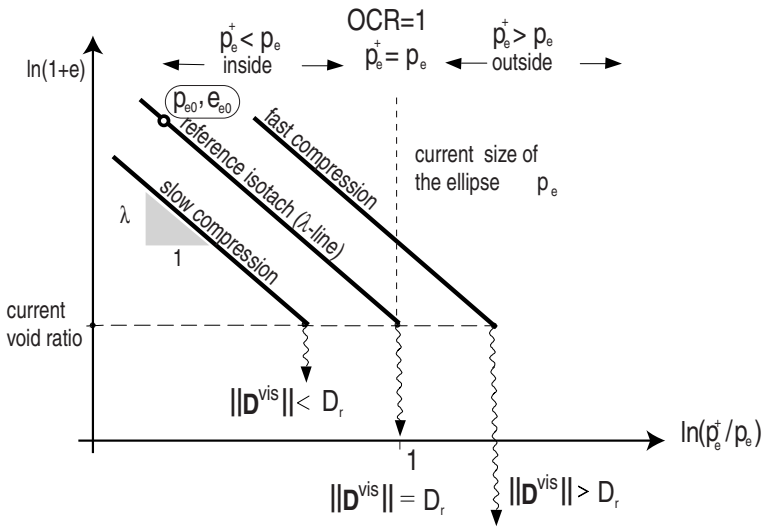

Figure 4.24: The reference isotach and parallel isotachs for proportional compression at different prescribed rates $\overset{\circ}{\mathbf{D}} = \text{const}$

The referential values e_{e0}, p_{e0} can be set to any point on this isotach. Of course, we may also easily determine its slope λ, see Fig. 4.24. Choosing the compression rate of the reference isotach we determine the reference creep rate D_r at OCR = 1. The determination of the fluidity parameter D_r from an oedometric compression test is more complicated, see Section 4.2.7.

Reference isotach described by λ and Γ^i

The reference isotach corresponding to the fluidity parameter D_r is specified by its slope λ and by its position, i.e. the reference state p_{e0} and e_{e0} through which it should pass. Of course, λ is a material constant but the reference parameters D_r, p_{e0} and e_{e0} are not.

Goldscheider (1994, private communication) posed an interesting question of replacing the triple D_r, p_{e0} and e_{e0} by a single (and more elegant) material constant. Indeed, we have some freedom in choosing these reference values and actually *any two* of them may be set quite arbitrarily and then the third one can be regarded as a material property. Within the proposed model there is no reason for choosing $D_r = 1\%/\mathrm{h}$ to be the reference rate, and there is no need or objective criterion of taking any particular value either. Consistently, the notions like reference isotach or OCR are subjective.

A simple solution of the problem posed by Goldscheider follows from the observation that whatever our choice of D_r, p_{e0} and e_{e0} will be, the creep rate $\mathbf{D}^{vis}$ at a given state $\mathbf{T}, e$ must not be affected. From the requirement $\mathbf{D}^{vis} = \text{const}$ we obtain with reference to (4.74) that $D_r \cdot (p_e)^{-1/I_v} = \text{const}$. The direction of creep $\vec{\mathbf{B}}$ and the parameter $p_e^+ = \text{const}$ are constant for a given stress. Substituting p_e from (4.75) at $e = \text{const}$ we conclude that for a unique value $\mathbf{D}^{vis}(\mathbf{T}, e)$ the following condition

$$D_r^{I_v}(p_{e0})^{-1}(1 + e_{e0})^{-1/\lambda} = \text{const}. \tag{4.88}$$

must be fulfilled (one of many equivalent expressions). An alternative form denoted as Γ is proposed in [174]. Unfortunately, the above expression and its alternatives have undefined dimension and therefore they are not convenient. In order to tackle this problem Krieg [123] employed a modified expression with $(D_r/1\%/\mathrm{h})^{I_v}$ in place of $(D_r)^{I_v}$ and determined the respective value Γ for several soils. In our case an analogous expression would be

$$\Gamma^i = (D_r/1\%/\mathrm{h})^{-I_v}(p_{e0})(1 + e_{e0})^{1/\lambda} \tag{4.89}$$

which has a dimension of stress. However, in (4.89) Krieg (re)introduced de facto the reference fluidity parameter $1\%/\mathrm{h}$, against the intention of Goldscheider. Therefore advantages of using Γ^i are not convincing.

Nevertheless, the attempt of replacing three reference values by one material constant is worth mentioning because it provides some lucidity to the subject of reference variables. Evidently, the notions of 'normally consolidated state' or OCR are subjective in the present model unless D_r is treated as a material constant or a material-specific function.

4.2.7 Earth pressure coefficient K_0

The geostatic K_0-stress ratio is the starting point for calculation of most geotechnical problems. The value of K_0 is also important for estimation of other material parameters. In this text the parameter K_0 refers to the normally consolidated (OCR=1) material describing the ratio of horizontal and vertical stress under oedometric compression, i.e.

$K_0 = T_{22}/T_{11} = T_{33}/T_{11}$. The value K_0 is not a basic material constant in hypoplasticity. Neither the reference model nor the present visco-hypoplastic model allow for independent choice of K_0. It depends on the residual friction angle φ_c via parameter a, see (2.65). In the following we demonstrate that in the visco-hypoplastic version K_0 is also influenced by the ratio λ/κ. A subtle difference between the value of K_0 from an oedometric CRSN compression test ($\mathbf{D} \sim$ diag$[-1, 0, 0] =$ const) and an analogous value from an oedometric creep test ($\mathring{T}_1 = 0$ and $D_2 = D_3 = 0$) is presented.

Approximated K_0 from CRSN oedometric test with OCR=1 and $\mathbf{D} \sim \mathbf{D}^{vis}$

In order to find the value of K_0 at OCR $= 1 =$ const we consider an oedometric CRSN compression with

$$\mathbf{D} = D_r x \vec{\mathbf{D}} = D_r x \text{ diag}[-1, 0, 0] = \text{const}, \tag{4.90}$$

wherein the vertical strain rate $D_1 = -xD_r$ is a product of the reference creep rate a dimensionless factor[15] x. In Section 4.2.5 we found that *any* proportional CRSN loading ($\mathbf{D} =$ const) leads eventually to a situation in which OCR and $\hat{\mathbf{T}}$ become constant, and (4.82) holds. Then the direction $\vec{\mathbf{B}}$ of viscous strain rate $\mathbf{D}^{vis}$ (function of $\hat{\mathbf{T}}$) and its intensity $\|\mathbf{D}^{vis}\|$ (function of OCR) become constant. We can conclude that $\mathbf{D} =$ const implies $\mathbf{D}^{vis} =$ const in the asymptotic state (first loading). In this subsection we assume additionally $\mathbf{D} \sim \mathbf{D}^{vis}$, i.e. the total and viscous deformation rates are proportional. With this simplifying assumption the value K_0 follows directly from the definition of uniaxial deformation

$$\mathbf{D} \sim \mathbf{D}^{vis} = D_r \left(\frac{1}{\text{OCR}}\right)^{1/I_v} \text{ diag}[-1, 0, 0] \tag{4.91}$$

which according to (4.74) implies that the lateral components of the deformation rate must vanish, i.e. $\vec{B}_{22} = \vec{B}_{33} = 0$. Substituting

$$\hat{\mathbf{T}} = \frac{1}{1 + 2K_0} \text{ diag}[1, K_0, K_0], \tag{4.92}$$

with the still unknown value K_0, into (4.73) we obtain:

$$\vec{\mathbf{B}} = \frac{-1}{\sqrt{g}} \begin{bmatrix} 5 + 2(4 + a^2)K_0 - 2(2 + a^2)K_0^2 & & \\ & -1 + a^2(-1 + K_0) + 2K_0 + 8K_0^2 & \\ & & -1 + a^2(-1 + K_0) + 2K_0 + 8K_0^2 \end{bmatrix} \tag{4.93}$$

with

$$g = 4a^2 \left(1 + K_0 - 2K_0^2\right)^2 + 2a^4(-1 + K_0)^2 \left(1 + 2K_0^2\right) + 9 \left(3 + 8K_0 + 16K_0^4\right)$$

[15] A similar factor x has been derived in Section 4.2.6, Eq. (4.85) for *isotropic* compression and OCR=1.

Imposing the condition $\vec{B}_{22} = \vec{B}_{33} = 0$ on (4.93) one obtains

$$K_0^{up} = K_0 = \frac{-2 - a^2 + \sqrt{36 + 36\,a^2 + a^4}}{16} \tag{4.94}$$

The solution (4.94) is shown also in Fig. 4.25. The superscript ^{up} indicates that K_0^{up} is the upper limit of the K_0 values derived in the next subsection without assumption of proportionality $\mathbf{D} \sim \mathbf{D}^{vis}$

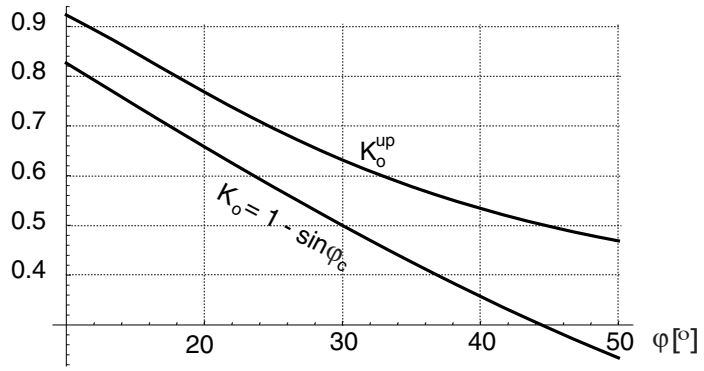

Figure 4.25: The values of K_0^{up} obtained from the condition of uniaxial creep, i.e. from $\vec{B}_{22} = \vec{B}_{33} = 0$, see (4.94), overestimate Jaky's value of $K_0 = 1 - \sin\varphi_c$

Coefficient K_0 for a CRSN oedometric test with OCR $= 1$ and $\mathbf{D} \not\sim \mathbf{D}^{vis}$

We reconsider the oedometric CRSN loading given in (4.90), however without the simplifying assumption $\mathbf{D} \sim \mathbf{D}^{vis}$. Under the uniaxial deformation conditions we expect to obtain a proportional stress path with

$$\hat{\mathbf{T}} = \frac{1}{1 + 2K_0}\ \mathrm{diag}(1, K_0, K_0)$$

(for such $\hat{\mathbf{T}}$ we have $F = 1$) and OCR $= 1 =$ const and thus $\mathbf{D}^{vis}$ must be constant too. We recall that according to (4.78) the condition OCR $=$ const implies $\dot{p}_e/p_e = \dot{p}_e^+/p_e^+$ and Eq. (4.82) holds for any proportional first loading with $\mathbf{D} =$ const see Fig. 4.23. In the special case of oedometric loading we have

$$-\frac{\mathrm{tr}\,\mathbf{D}}{\lambda} = \frac{xD_r}{\lambda} = \frac{\mathrm{tr}\,\mathring{\mathbf{T}}}{\mathrm{tr}\,\mathbf{T}} = \beta_b \mathbf{1} : \hat{\mathsf{L}} : (\vec{\mathbf{D}} xD_r - \vec{\mathbf{B}} D_r), \tag{4.95}$$

wherein β_b and $\vec{\mathbf{B}}$ are given by (4.72) and (4.73). We seek now for the deformation rate $D_{11} = -xD_r$ that corresponds to OCR $= 1$ and yields the compression line with the slope $-\lambda$. As one might recall from Section 4.2.2 that $D_{11} = \frac{\lambda}{\lambda-\kappa} D_r$ has been obtained for the

one-dimensional version. In the following we derive an analogous relation for 3-D case. From (4.95) follows

$$\frac{xD_r}{\lambda\beta_b} = \delta_{ij}\hat{L}_{ijkl}\left(-\delta_{1k}\delta_{1l}xD_r - D_r\vec{B}_{kl}\right) \tag{4.96}$$

or equivalently

$$\frac{x}{\lambda\beta_b} = -\hat{L}_{ii11}x - (\hat{L}_{ii11}\vec{B}_{11} + \hat{L}_{ii22}\vec{B}_{22} + \hat{L}_{ii33}\vec{B}_{33}) \tag{4.97}$$

Let us supplement it with the requirement of proportional loading i.e.

$$\mathring{\mathbf{T}} \sim \hat{\mathbf{T}} \sim \hat{\mathsf{L}} : (\vec{\mathbf{D}}xD_r - \vec{\mathbf{B}}D_r) \tag{4.98}$$

or

$$K_0 = \frac{-\hat{L}_{2211}x - (\hat{L}_{2211}\vec{B}_{11} + \hat{L}_{2222}\vec{B}_{22} + \hat{L}_{2233}\vec{B}_{33})}{-\hat{L}_{1111}x - (\hat{L}_{1111}\vec{B}_{11} + \hat{L}_{1122}\vec{B}_{22} + \hat{L}_{1133}\vec{B}_{33})} \tag{4.99}$$

with $\mathring{\mathbf{T}} = \frac{1}{1+2K_0}\,\mathrm{diag}(1, K_0, K_0)$. Finally we substitute $F = 1$ and $\hat{L}_{1111} = 1 + a^2\frac{1}{(1+2K_0)^2}$, $\hat{L}_{2222} = \hat{L}_{3333} = 1 + a^2\frac{K_0^2}{(1+2K_0)^2}$, $\hat{L}_{1122} = \hat{L}_{1133} = a^2\frac{K_0}{(1+2K_0)^2}$, $\hat{L}_{2233} = a^2\frac{K_0^2}{(1+2K_0)^2}$, and $\vec{\mathbf{B}}$ given by (4.93) into (4.99) and (4.97).

Equations (4.97) and (4.99) must be solved simultaneously for x and K_0. Analytical solution is cumbersome so we solve the problem numerically (MATHEMATICA script available from the author). The results are shown in Fig 4.26.

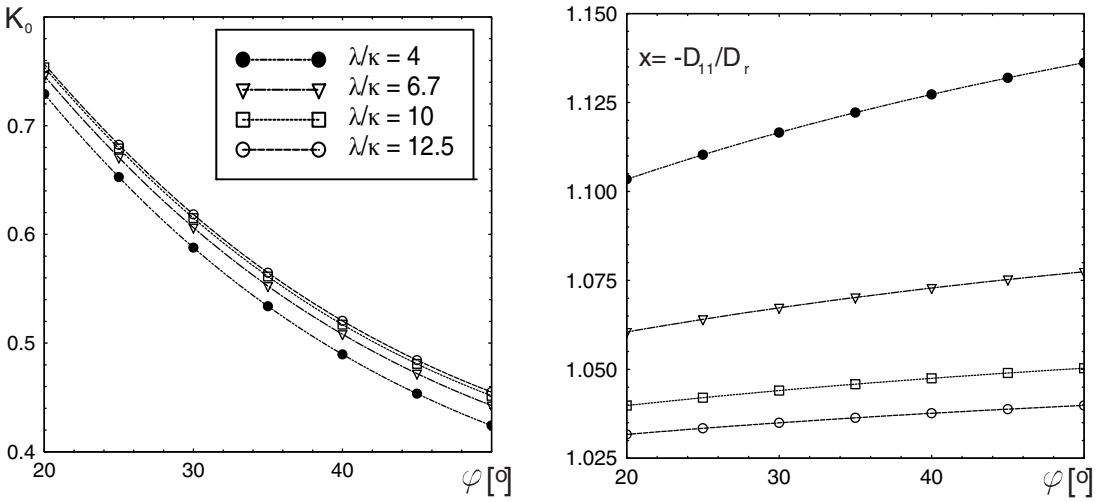

Figure 4.26: Values of K_0 and $x = \|\mathbf{D}\|/D_r$ referred to the isotropic swell index κ

We conclude that the approximate value of K_0^{up} obtained in the previous section is slightly overestimated and corresponds to the special case $\lambda/\kappa \to \infty$. For the convenience of the practical calibration of the model the values K_0 and $x = -D_{11}/D_r$ are recalculated with reference to oedometric parameter κ^o, i.e. for various λ/κ^o values as shown in Fig. 4.27.

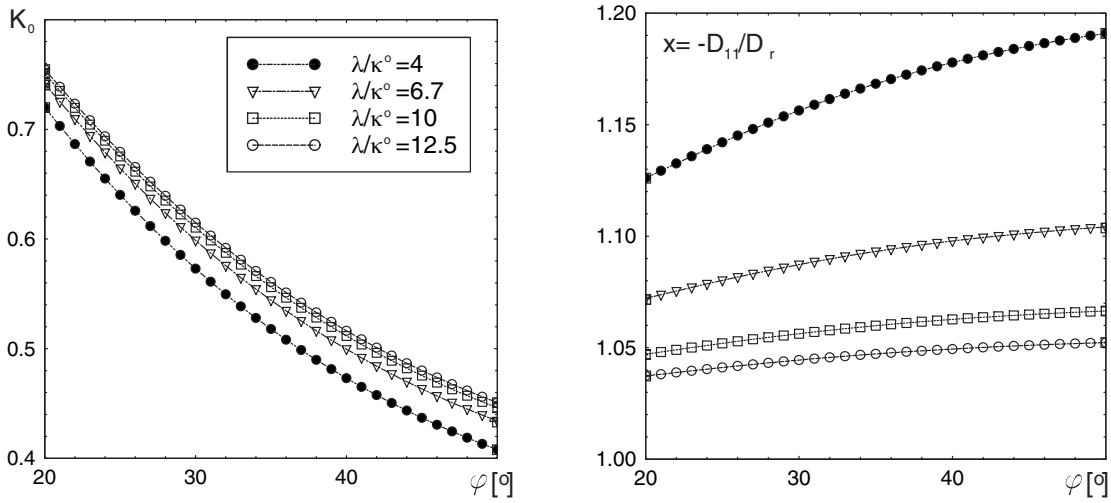

Figure 4.27: Values of K_0 and $x = \|\mathbf{D}\|/D_r$ referred to the oedometric swell index κ^o

Evaluation of K_0 from uniaxial creep tests

Consider now an oedometric creep test with $\mathring{T}_{11} = 0$ and $D_{ij} = \delta_{1i}\delta_{1j}$. Independently of the initial stress, we expect that a specific 'K_0-stress state' establishes itself eventually (as an asymptotic state) for which

$$T_{22}/T_{11} = T_{33}/T_{11} = \text{const} \tag{4.100}$$

The condition $\mathring{T}_{11} = 0$ with (4.100) implies $\mathring{\mathbf{T}} = \mathbf{0}$ and consistently $\mathbf{D} = \mathbf{D}^{vis}$ which leads to the value

$$T_{22}/T_{11} = T_{33}/T_{11} = K_0^{up} \tag{4.101}$$

which was derived in (4.94). The OCR is increasing during the test and the stress ratio tends to K_0^{up}. The asymptotic value K_0^{up} reached after a long uniaxial creep seems to be appropriate for most geotechnical problems. at least for normally consolidated or slightly overconsolidated states.

Closing the discussion on K_0 let us repeat that our model does not offer a possibility of choosing an arbitrary value for $K_0 = K_{0NC}$ for normally consolidated soils. K_0^{up} is one-to-one related with φ_c. In particular the value $K_0 = 1 - \sin\varphi$ cannot be set, as shown in Fig. 4.25. If the application of self weight is calculated with the hypoplastic model initial stress ratio K_0 given in Fig. 4.26 or Fig. 4.26 establishes itself for $OCR = 1$. In Section 4.3 this problem will be alleviated because the basic constitutive equation will obtain some additional flexibility. Using ABAQUS the problem may also be apparently circumvented with a simple trick. At the beginning of a FE-calculation we may prescribe

any K_0 state using the special user's procedure[16] After the self weight of soil is applied we may change the material model to the hypoplastic one [80]. A disadvantage of such artificial stress initialization makes itself remarkable in a subsequent calculations. For example, in a creep phase the stress ratio T_2/T_1 would leave the set value tending towards K_0^{up} given by (4.94).

4.2.8 Exponent $1/I_v$

As already mentioned in Section 4.2.5 the exponent $1/I_v$ in the Norton's rule is conventionally written using the viscosity index I_v proposed by Leinenkugel [131]. Several experiments can be used to determine the exponent $1/I_v$.

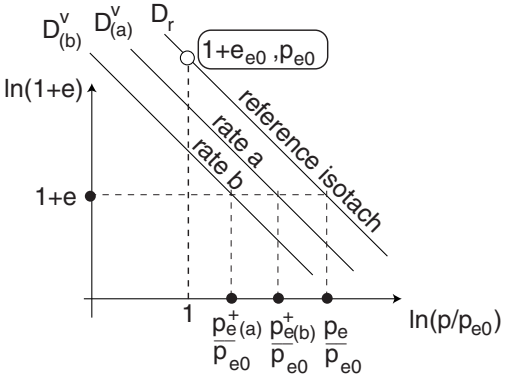

Figure 4.28: Determination of I_v from isotropic compression tests

We discuss here the following methods (hypothetically, without technical details):

1) isotropic compression test with variation of deformation rate,

2) oedometric compression test with variation of deformation rate,

3) isochoric shear test with variation of deformation rate,

4) isotropic creep test,

5) oedometric creep test,

6) relaxation test.

Consider two **isotropic compression tests** with different deformation rates $\mathbf{D}_{(a)}$ and $\mathbf{D}_{(b)}$ for which we have determined (experimentally) the pressures $p_{(a)}$ and $p_{(b)}$ at exactly the same void ratio e. The values $p_a = p^+_{e(a)}$ and $p_b = p^+_{e(b)}$ are different but the equivalent pressures are identical $p_{e(a)} = p_{e(b)} = p_e$ because measurements are taken at the same void ratio e, see Fig 4.28. Using (4.86) with (4.74) and (4.78) we obtain

$$\|\mathbf{D}_{(a)}\| = xD_r \left(\frac{p^+_{e(a)}}{p_e}\right)^{1/I_v} \quad \text{and} \quad \|\mathbf{D}_{(b)}\| = xD_r \left(\frac{p^+_{e(b)}}{p_e}\right)^{1/I_v} \tag{4.102}$$

[16]The initial stress field can be prescribed independently of the material model within the procedure `sigini`, however, this field must be in equilibrium. If the soil surface is not perfectly horizontal it might be a problem so a pragmatic to deal with the problem is to use temporarily an orthotropic elastic material models with suitably chosen material constants.

Dividing these equations by sides we find

$$1/I_v = \ln \frac{\|\mathbf{D}_{(a)}\|}{\|\mathbf{D}_{(b)}\|} \,/\, \ln \frac{p_{(a)}}{p_{(b)}}\,. \tag{4.103}$$

An analogous derivation may be carried out for **oedometric compression** using x given by (4.85). For the same deformation path (although different deformation rates) the stresses are proportional $\mathbf{T}_{(a)} \sim \mathbf{T}_{(b)}$ so the the result (4.103) remains valid. We may write (4.103) in equivalent forms

$$I_v = \ln \frac{q_{(a)}}{q_{(b)}} \,/\, \ln \frac{\|\mathbf{D}_{(a)}\|}{\|\mathbf{D}_{(b)}\|} \;=\; \ln \frac{T_{11(a)}}{T_{11(b)}} \,/\, \ln \frac{\|\mathbf{D}_{(a)}\|}{\|\mathbf{D}_{(b)}\|} \tag{4.104}$$

Consider now two **isochoric triaxial compression** tests carried out at different strain rates $\mathbf{D}_{(a)}$ and $\mathbf{D}_{(b)}$, Fig. 4.19. Let the samples have the same void ratio e. The equivalent pressures are therefore identical $p_{e(a)} = p_{e(b)}$ and they remain constant because e does not change. Let both stress paths start from the same point on the p-axis. At the end of the test both stresses $\mathbf{T}_{(a)}$ and $\mathbf{T}_{(b)}$ reach the critical state line $q = Mp$, i.e., they satisfy the condition $\|\mathbf{B}\| = 1$. Therefore, considering the triaxial critical state condition the final stresses are proportional. We have $p^+_{e(a)}/p^+_{e(b)} = p_{(a)}/p_{(b)} = q_{(a)}/q_{(b)} = T_{11(a)}/T_{11(b)}$ etc. and Equations (4.103) and (4.104) hold again. Let us put down yet another useful formula

$$I_v = \ln \frac{c_{u(a)}}{c_{u(b)}} \,/\, \ln \frac{\|\mathbf{D}_{(a)}\|}{\|\mathbf{D}_{(b)}\|}. \tag{4.105}$$

This (and not the exponent $(1/I_v)$) was the original proposition of I_v given by Leinenkugel. Next, we examine an **isotropic creep** ($\mathbf{T} = -p\ \mathbf{1} = \text{const}$, $\mathring{\mathbf{T}} = \mathbf{0}$). The experimental curve for void ratio $e(t)$ or for volumetric strain $\epsilon^v(t)$ must be known. The creep tests begins at time $t = 0$ for which $p = p^+_e = p_{e0}/\mathrm{OCR}_B$, wherein OCR_B denotes the initial value $\mathrm{OCR}(t = 0)$. The earlier deformation history is irrelevant [174]. Since $\mathring{\mathbf{T}} = \mathbf{0}$ we have $p(t) \equiv p^+_e(t) = \text{const}$ and

$$\operatorname{tr} \mathbf{D} = \operatorname{tr} \mathbf{D}^{vis} = -\operatorname{tr} \vec{\mathbf{B}} D_r \left(\frac{p^+_e}{p_e(t)} \right)^{1/I_v} \tag{4.106}$$

We combine Equation (4.106) with (4.75) taking the reference void ratio equal to the initial one, i.e. $e_{e0} = e|_{t=0}$ and $p_{e0} = \mathrm{OCR}_B\ p^+_e$. Moreover, we replace $\ln \left[\dfrac{1 + e_{e0}}{1 + e} \right]$ with $-\epsilon^v$. Equation (4.75) takes the form

$$\exp(-\epsilon^v/\lambda) = p_e/p_{e0} \tag{4.107}$$

with an unknown function $\epsilon^v(t)$. Substituting (4.107) into (4.106) with $\mathrm{d}\epsilon^v/\mathrm{d}t = \operatorname{tr} \mathbf{D}^{vis}$ and $p_{e0} = p^+_e\ \mathrm{OCR}_B$ we obtain

$$\frac{\mathrm{d}\epsilon^v}{\mathrm{d}t} = -\frac{\operatorname{tr} \vec{\mathbf{B}} D_r}{\mathrm{OCR}_B^{1/I_v}} \exp\left(\frac{\epsilon^v}{I_v \lambda} \right) \tag{4.108}$$

which is an ordinary differential equation with the initial condition $\epsilon^v|_{t=0} = 0$. The solution for ϵ^v is

$$\epsilon^v(t) = -\lambda I_v \ln\left(1 + \frac{\operatorname{tr}\vec{\mathbf{B}} D_r t}{\mathrm{OCR}_B^{1/I_v} I_v \lambda}\right) \tag{4.109}$$

Knowing D_r and $\operatorname{tr}\vec{\mathbf{B}} = \sqrt{3}$ we may now easily find I_v that would fit to the experimental creep curve $\epsilon^v(t)$. At this point, the one-dimensional description of creep

$$\epsilon^{vis} = -\psi \ln \frac{t + t_0}{t_0} \tag{4.110}$$

can be revisited. We recognize that

$$t_0 = \frac{\mathrm{OCR}_B^{1/I_v} I_v \lambda}{\operatorname{tr}\vec{\mathbf{B}} D_r} \quad \text{and} \tag{4.111}$$

$$\psi = \lambda I_v \tag{4.112}$$

from comparison of (4.110) and (4.109), see also Leinenkugel [131].

An analogous derivation can be performed for **oedometric creep** with the initial condition $p_e^+ = p_e$. Of course $p \neq p_e^+$ but this fact does not affect the final result. The only change to be made consists in substituting $\operatorname{tr}\vec{\mathbf{B}} = \vec{B}_{11}$ into (4.111), (use (4.93)), Parameters D_r and K_0 must be known before calibration of exponent $1/I_v$. Having a time-deformation plot from a creep test, like one in Fig. 4.21, we may try to determine ψ and t_0 directly using curve fitting for (4.110). In other words, we may try out different t_0 values until the points $(\epsilon^{vis}, \frac{t+t_0}{t_0})$ lie on a straight line in a half-logarithmic diagram.

Finally we consider **isotropic relaxation** test with $\mathbf{D} = \mathbf{0}$ and $\mathbf{T} = -p\,\mathbf{1}$, taking for simplicity the initial condition $p = p_e = p_e^+$. The stress rate is

$$\mathring{\mathbf{T}} = \overbrace{\beta_b 3p\,(\mathsf{I} + \frac{a^2}{9}\,\mathbf{1}\,\mathbf{1})}^{=\hat{\mathsf{L}}} : \left[\mathbf{0} - \overbrace{D_r(-\frac{1}{\sqrt{3}}\,\mathbf{1})\left(\frac{p}{p_e}\right)^{1/I_v}}^{=\mathbf{D}^{vis}}\right] \tag{4.113}$$

wherein $\vec{\mathbf{B}} = -\frac{1}{\sqrt{3}}\,\mathbf{1}$. Taking trace of both sides we obtain an ordinary differential equation with unknown function $p(t)$

$$-3\dot{p} = \beta_b 3p\;\mathbf{1} : (\mathsf{I} + \frac{a^2}{9}\,\mathbf{1}\,\mathbf{1}) :\; \mathbf{1}\frac{D_r}{\sqrt{3}}\left(\frac{p}{p_e}\right)^{1/I_v} \tag{4.114}$$

It is convenient to define an alternative unknown function $\pi(t) = \dfrac{p(t)}{p_e} = \dfrac{1}{\mathrm{OCR}}$. Using this function our equation takes a simple form

$$-\dot{\pi} = K\pi^{1+1/I_v} \quad \text{with} \quad K = \beta_b(3 + a^2)\frac{D_r}{\sqrt{3}} = \text{const} \tag{4.115}$$

The solution with initial condition $\pi(0) = 1$ is

$$\pi(t) = \left(1 + \frac{Kt}{I_v}\right)^{-I_v} \tag{4.116}$$

so knowing e.g. relaxation time t required for OCR $= 1/\pi(t)$ to change from, say, 1 to 1.1 we may easily find I_v. The parameters a and β_b are given in (2.65) and (4.72).

4.2.9 Comparison with experimental results

In order to verify the model, several numerical predictions for different triaxial and oedometric tests have been compared with results of tests carried out on organic clayey silt [123]. The following parameters were used in all calculations: $D_r = 2.8 \cdot 10^{-6}$[-/sec], $\lambda = 0.76$, $\kappa = 0.05$ except for $\kappa = 0.08$ in oedometric test, $\varphi_c = 48^o$ except for $\varphi_c = 52^o$ in test 68, $I_v = 0.05$ and $\beta_R = 0.95$. Other parameters of the organic clayey silt are:

water content, w	$\approx$ 184%	plastic limit, w_P	= 106%
sand fraction	= 15%	unit weight, γ	= 12.2 kN/m^3
silt fraction	= 75%	organic content	= 33%
liquid limit, w_L	= 220%	$CaCO_3$ content	= 35%
clay fraction	= 10%	specific weight, γ_s	= 20.4 kN/m^3

A CU triaxial test carried out with different rates of strain is presented in Fig 4.29. Each letter corresponds to shearing at a constant rate D_q: $a = 3.4\%$/h, $g = 2.45\%$/h, $b = f = h = 0.245\%$/h, $c = e = i = 0.0245\%$/h, $d = j = 0.00245\%$/h. The prescribed evolutions of strain in the experiment and in the numerical prediction are practically identical.

An oedometric compression test and its numerical prediction are presented in Fig. 4.30. The experiment consists of several constant-rate-of-strain stages with different rates D_v: $a = 0.936\%$/h, $b = g = j = n = 0.156\%$/h, $c = k = -0.0156\%$/h, $m = -0.156\%$/h. One relaxation phase h and three creep stages (d, i, l) were accomplished. In the experiment all processes were strain-controlled and therefore relaxation could easily be performed by keeping the piston at a fixed position. Creep stages with constant vertical stress were technically more complex and required a special correction algorithm (described in [174]).

In the numerical calculations usually strain control was applied, i.e. increments of strain were prescribed in all directions except for creep stages d, f, i, l and for the large unloading reloading loop m, n in which mixed control was used (vertical stress component and horizontal strain component equal zero). Further details are given in [174] www.AN . This and other experiments with the Schwerin gyttja with details about the soil properties and testing device are also described by Krieg [123] (in German).

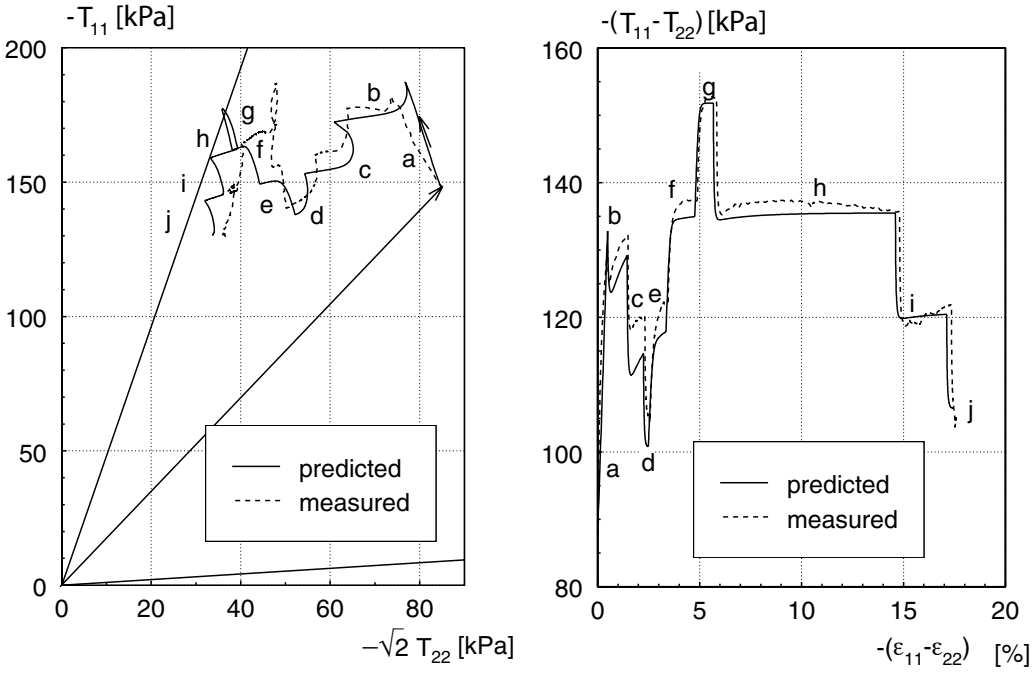

Figure 4.29: CU traxial test (Nr 1) with altering the rate of deformation

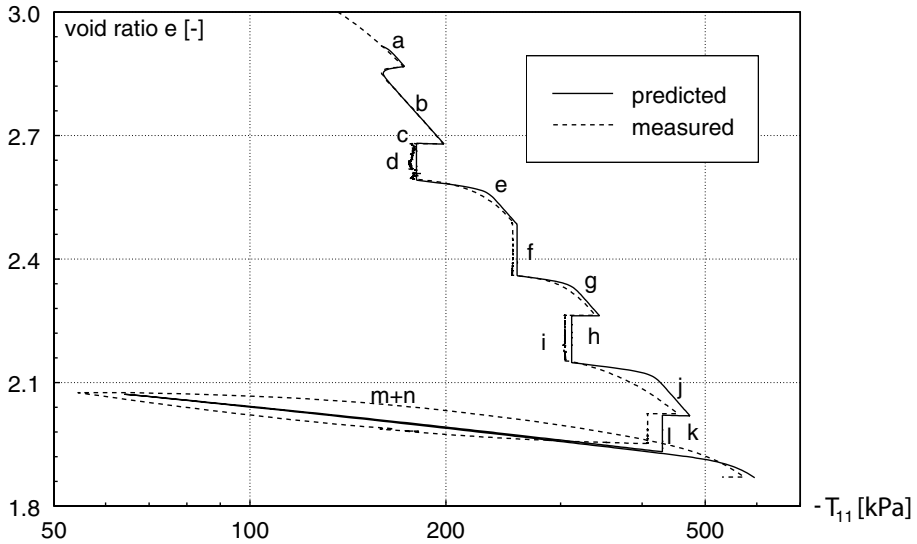

Figure 4.30: Oedometric compression test (Nr 2) with creep and relaxation

Two relaxation tests performed by Krieg and presented in Fig. 4.31 consist of three phases a, b, c and a', b', c'. After an undrained axisymmetric shearing (a, a') up to the CSL (straight line) the piston of the triaxial apparatus was stopped and relaxation $(b,\ b')$ took place. After about 7 h the samples were sheared under constant volume $(c,\ c')$ again and the stress paths reached the CSL.

In Fig. 4.32 the results of three drained triaxial creep tests (by Krieg, unpublished) at different T_{11}/T_{22} are performed and the intensity and direction of creep has been shown.

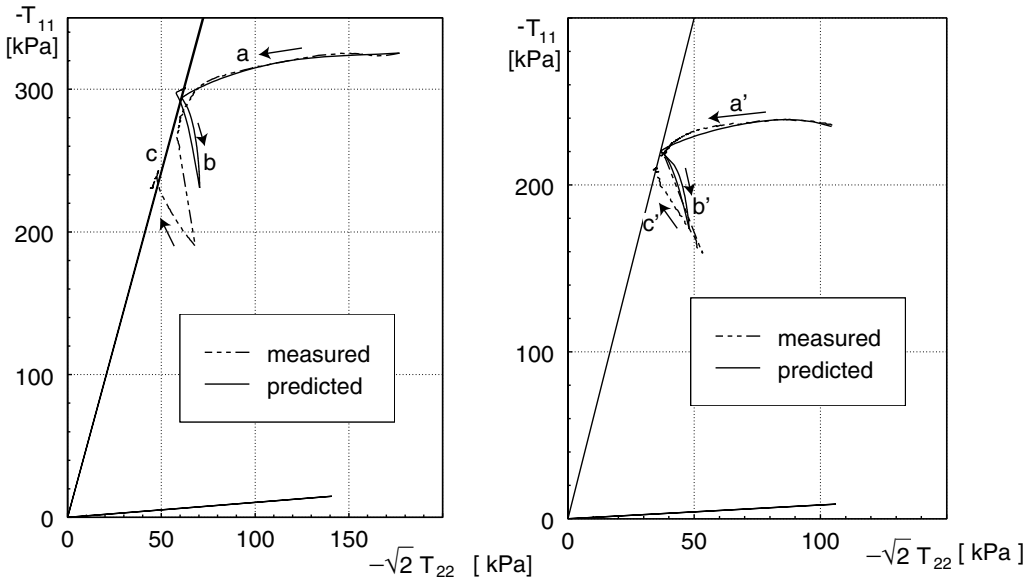

Figure 4.31: Relaxation tests (Nr 68, 69) started from the CS-Line

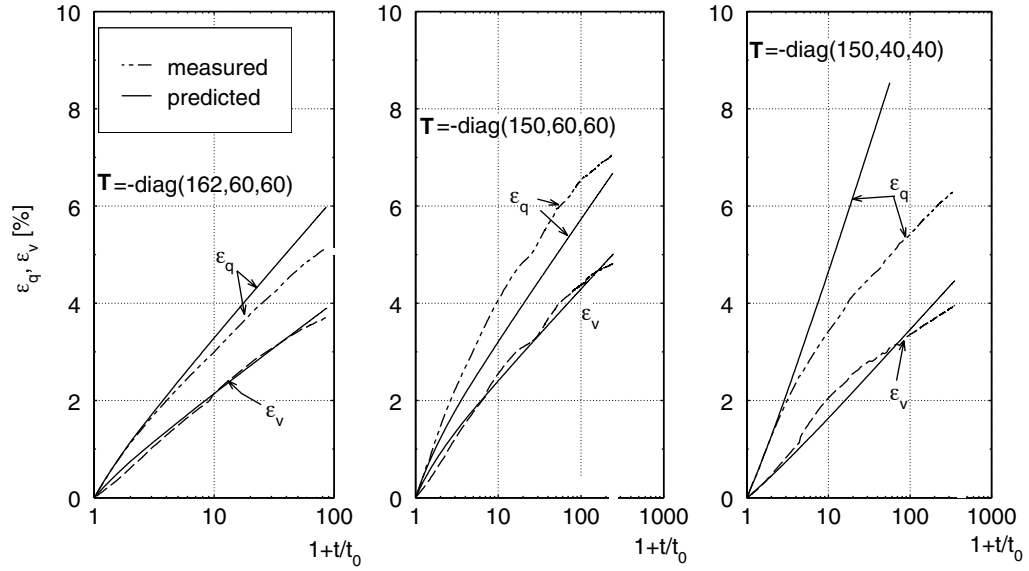

Figure 4.32: Creep deformation vs. time at different stresses (test 65, 66, 67). The reference time t_0 is a parameter used in the conventional description of oedometric creep, see (4.110) and (4.111)

The effective stress was kept constant and volumetric and deviatoric strain components were monitored. The reference time of $t_0 = 8000$ s corresponds to OCR=1.04. The reference time originates from the commonly used description of creep (4.110) derived in previous subsection, Equation (4.111). All results of the numerical calculations are satisfactory. The CU tests are well predicted and the rate dependence is properly modeled. The predicted direction and intensity of creep and relaxation are also acceptable. From Fig. 4.32 it can be observed that the ratio D_q/D_v slightly changes . This delayed

contractancy appear at high stress ratios only and cannot be described by the model. Recently Krieg (private communication) has attributed this effect (at least a part of it) to the experimental technique.

4.2.10 Modified shape of the yield surface

Some numerical tests indicate that a modification [89] of (4.77) might be useful. In place of (4.77) one may introduce two different equations: one for the stress states below and one for the states above the critical state surface $\|\mathbf{B}\| = 1$. We explicitly distinguish between so-called 'wet' and 'dry' states [206] and propose separate equations for these regions.

The modification shown in Fig. 4.33 needs one additional parameter $0 < \beta_R < 1$. The equivalent pressure $p_e^+ = p(1 + \bar{\eta}^2)$, cf. (4.80), can be now expressed as the following function of the actual stress

$$p_e^{+\text{new}} = \frac{p}{\beta_R - 1}\left[\beta_R\sqrt{1 + \bar{\eta}^2(\beta_R^2 - 1)} - 1\right] \qquad \text{for} \quad \bar{\eta} < 1, \tag{4.117}$$

$$p_e^{+\text{new}} = p(1 + \bar{\eta}^2)\frac{1 + \beta_R}{2} \qquad \text{for} \quad \bar{\eta} > 1, \tag{4.118}$$

where $\bar{\eta} = q/(Mp)$. This allows for some freedom in constitutive modeling.

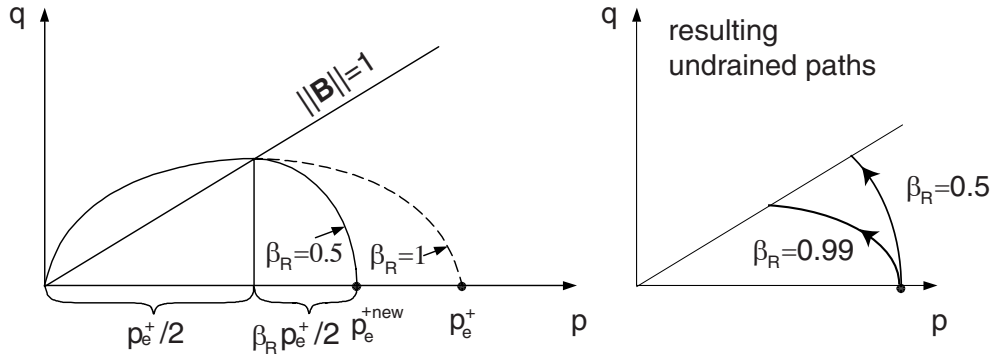

Figure 4.33: Modification of the cap surface proposed in [89]. Such modified shape is used in the Cam-clay model to improve its prediction of K_0. It should be noted, that the overestimated K_0 values from (4.94) as shown in Fig. 4.25 cannot be improved by the parameter β_R. It can be used, however, to capture the ratio between the preconsolidation pressure and the undrained cohesion and to influence the stress response (shape of the stress path) for undrained shearing in saturated, normally consolidated soil

The above modification requires some changes in the numerical algorithm. For the dry side ($\bar{\eta} > 1$) the right-hand-side expression in (4.80) and (4.133) must be multiplied by $(1 + \beta_R)/2$. For the wet side ($\bar{\eta} < 1$) we use (4.117). in place of $p_e^+(p, q) = p(1 + \bar{\eta}^2)$ given

by (4.80). Consistently the derivatives $\partial p_e^+(p,q)/\partial p$ and $\partial p_e^+(p,q)/\partial q$ in the differential chain in (4.133) must be replaced by

$$\frac{\partial p_e^{+\text{new}}}{\partial p} = \frac{p_e^{+\text{new}}(p,q)}{p} - \frac{\beta_R \bar{\eta}^2(\beta_R+1)}{\sqrt{1+\bar{\eta}^2(\beta_R^2-1)}} \tag{4.119}$$

and

$$\frac{\partial p_e^{+\text{new}}}{\partial q} = \frac{\beta_R \bar{\eta}(\beta_R+1)}{M\sqrt{1+\bar{\eta}^2(\beta_R^2-1)}} \tag{4.120}$$

In order to determine the parameter β_R (≈ 0.5) it is recommended to conduct an undrained test for a normally consolidated sample, if possible also altering the rate of straining, and to do several element calculations trying out different values of β_R. In the MCC model the analogous modification is used to improve the K_0 prediction. In our case K_0 is not influenced by β_R. This parameter controls the pore pressure generation during undrained shearing, similarly to the Schofield's parameter A.

4.2.11 Intergranular strain

In order to improve the small strain behaviour of the model the intergranular strain $\mathbf{h}$, is introduced. As already discussed in Section 4.1 the intergranular strain tensor increases stiffness after abrupt changes in the direction of deformation. Although excessive ratcheting (like in non-viscous hypoplasticity, e.g. Fig. 4.15) is absent in the presented visco-hypoplastic model also this version is incapable (without $\mathbf{h}$) of reproducing hysteretic loops known from the experimental stress-strain diagrams. One can discover this defect in the large loop at the bottom of Fig. 4.30.

The general stress-strain relation is proposed to be

$$\boxed{\mathring{\mathbf{T}} = \mathsf{M} : \mathbf{D} - \mathsf{L} : \mathbf{D}^{vis}} \quad , \tag{4.121}$$

wherein the fourth order tensor M represents the increased stiffness which is calculated from the hypoplastic tensor $\mathsf{L}(\mathbf{T}, e)$ as

$$\mathsf{M} = m\mathsf{L} \tag{4.122}$$

The factor m is interpolated between the following material constants: $m_M = 1$ for monotonic loading, $m_T(\approx 2)$ for transversal loading or $m_R(\approx 5)$ for strain path reversal. More precisely, the value of m depends on the angle $\alpha = \arccos(\vec{\mathbf{h}} : \vec{\mathbf{D}})$. The special cases m_M, m_T and m_R correspond to $\alpha = 0°$, $\alpha = 90°$ and $\alpha = 180°$, respectively. The factor $m = m(\rho, \alpha)$ depends not only on α but also on the value of the intergranular strain $\rho = \|\mathbf{h}\|/R$, see (4.5), wherein R is the radius of the elastic locus, see Section 4.1. In

general, stiffness M is calculated with the following formula that considers an arbitrary $\rho \leq 1$ viz.,

$$\boxed{\mathsf{M} = [\rho^{\chi} m_T + (1-\rho^{\chi}) m_R]\mathsf{L} + \begin{cases} \rho^{\chi}(1-m_T)\mathsf{L} : \vec{\mathbf{h}}\vec{\mathbf{h}} & \text{for } \vec{\mathbf{h}} : \mathbf{D} > 0 \\ \rho^{\chi}(m_R - m_T)\mathsf{L} : \vec{\mathbf{h}}\vec{\mathbf{h}} & \text{for } \vec{\mathbf{h}} : \mathbf{D} \leq 0 \end{cases}}, \tag{4.123}$$

wherein χ is a material constant used for interpolation. Equation (4.123)interpolates the stiffness matrix varying $m(\rho, \alpha)$ between the special cases m_M, m_T and m_R mentioned above. The interpolation depending on the angle α is overlaid with the interpolation between $m = m_R$ for $\rho = 0$ and $m = m(\alpha)$ for $\rho = 1$. The evolution of the intergranular strain tensor $\mathbf{h}$ is given by (4.12).

According to (4.121) the rate of relaxation ($\mathring{\mathbf{T}} = \mathsf{M} : \mathbf{0} - \mathsf{L} : \mathbf{D}^{vis}$) is *not* influenced by multiplier m. This is essential for the stability of numerical calculations. If a constitutive relation $\mathring{\mathbf{T}} = \mathsf{M} : (\mathbf{D} - \mathbf{D}^{vis})$ were used, then infinitesimal disturbances from the state $\mathbf{D} = \mathbf{0}$ could evoke finite changes in the rate of relaxation, namely $-\Delta\mathsf{M} : \mathbf{D}^{vis}$, wherein $\Delta\mathsf{M}$ is the difference in M calculated for different signs of $\mathbf{h} : \mathbf{D}$.

Calibration of material parameters for small-strain stiffness has been discussed in Section 4.1. In Fig. 4.34 a simple oedometric element test demonstrates the capability of the model to perform the hysteretic unloading-reloading loop.

4.2.12 Numerical aspects

The visco-hypoplastic model requires a special numerical treatment because the viscous strain rate $\mathbf{D}^{vis}$ is very sensitive to changes in the void ratio and in the stress even within a single strain increment of 0.1%. Using Euler forward integration scheme this would inevitably result in numerical problems. Moreover, sudden changes in the direction of stretching evoke rapid evolution of the intergranular strain which may still aggravate the overall numerical instability. The substepping as well as the implicit updating of stress (described in the following) and implicit integration of $\mathbf{h}$ as described in Section 4.1.3 are therefore recommended.

The visco-hypoplastic model has been successfully implemented into the FE code and used for predictions of deformations [78, 80, 102]. Recently the same computer code was extensively applied to large scale deformation predictions in three dimensional BVPs by Karcher [111].

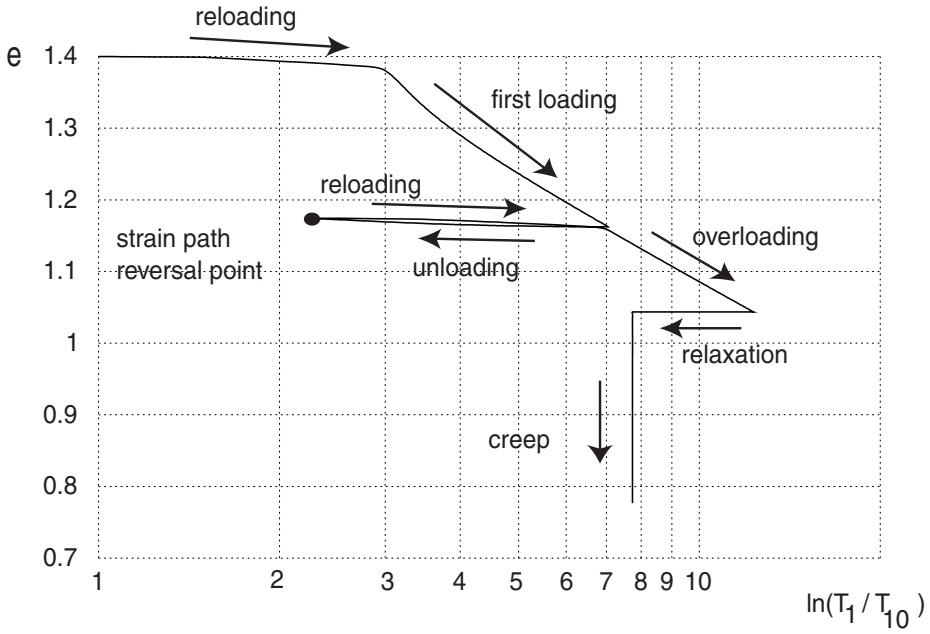

Figure 4.34: Oedometric test calculated with visco-hypoplastic model with intergranular strain. The test was performed with the following parameters: $\lambda = 0.2$; $\beta_R = 0.95$; $\kappa = 0.03$; $m_T = 2.0$; $\varphi_c = 30°$; $m_R = 5.0$; $I_v = 0.05$; $R = 1.0 \cdot 10^{-4}$ and $\beta_r = 0.12$

Solvability

The solution strategy for the constitutive equation (4.121) is more complicated than the solution of the visco-hypoplastic formulation (4.59). Equation (4.121) is bilinear and needs a loading/unloading test. Suppose we simulate an element test under a mixed control. At the beginning of each step we calculate the rate of viscous strain $\mathbf{D}^{vis} = D_r(1/\mathrm{OCR})^{1/I_v}$ and, unless $\mathbf{D}$ is given directly, we solve the auxiliary equation

$$\mathring{\mathbf{T}} = \mathsf{L}(\mathbf{D}^{\diamond} - \mathbf{D}^{vis}) \tag{4.124}$$

for $\mathbf{D}^{\diamond}$. This approximation of the strain rate suffices (in place of $\mathbf{D}$) to determine the sign of the product $\mathrm{sign}(\vec{\mathbf{h}} : \mathbf{D}^{\diamond}) = \mathrm{sign}(\vec{\mathbf{h}} : \mathbf{D}^{\diamond})$ needed in (4.123). It has been already demonstrated in Section 4.1.6. Other remarks to the implementation of intergranular strain discussed in Section 4.1.3 are also relevant.

Implicit integration of stress

The substepping strategy with implicit integration of the intergranular strain $\mathbf{h}$ as described in Section 4.1.3 works sufficiently well also in visco-hypoplastic model and therefore we consider here a monotonic deformation with insignificant rates $\mathring{\mathbf{h}}$ only. Even in this case, however, direct forward integration of (4.121) needs irrationally small time increments. It is commonly known that in all viscoplastic models the time integration should

be performed with an improved material Jacobian matrix $\partial\Delta\mathbf{T}/\partial\Delta\boldsymbol{\epsilon}$. For this purpose, recommendations given in [282] should be considered. The Euler explicit (forward) time integration scheme

$$\mathbf{T}^{t+\Delta t} = \mathbf{T}^t + \mathring{\mathbf{T}}^t\Delta t - (\mathbf{T}^t\cdot\mathbf{W} - \mathbf{W}\cdot\mathbf{T}^t)\Delta t \quad , \tag{4.125}$$

with $\mathring{\mathbf{T}}^t$ being calculated using the stress state $\mathbf{T}^t$ and the void ratio e^t from the beginning of the increment is insufficient. In this section a quantity evaluated using state variables at the beginning of the increment is denoted by $\bullet^t$ and the one corresponding to the end of the increment by $\bullet^{t+\Delta t}$. In the constitutive equation (incremental form)

$$\Delta\mathbf{T} = \mathring{\mathbf{T}}^t\Delta t = \mathsf{M}^t : \Delta\boldsymbol{\epsilon} - \mathsf{L}^t : \mathbf{D}^{vis}\Delta t \tag{4.126}$$

stiffnesses $\mathsf{M}(\mathbf{T}, e)$, $\mathsf{L}(\mathbf{T}, e)$ are 'slow' functions (the dependence $\mathsf{M}(\mathbf{T}, e, \mathbf{h})$ on $\mathbf{h}$ is handled separately) but viscous rate $\mathbf{D}^{vis}(\mathbf{T}, e)$ is a 'quick' functions of stress and void ratio (because of high exponent $1/I_v$), i.e. it may significantly change within a single increment. The viscous rate is very sensitive even to seemingly small changes Δe and $\Delta\mathbf{T}$. Therefore, the Jacobian matrix $\partial\Delta\mathbf{T}/\partial\Delta\boldsymbol{\epsilon}$ must be precisely evaluated (not just M^t). The desirable improvement of the Jacobian matrix is obtained by writing

$$\Delta\mathbf{T} = \mathsf{M}^t : \Delta\boldsymbol{\epsilon} - \mathsf{L}^t : \left(\mathbf{D}^{vis\ t} + \underbrace{\frac{1}{2}\frac{\partial\mathbf{D}^{vis\ t}}{\partial\mathbf{T}}}_{=\mathsf{A}} : \Delta\mathbf{T} + \underbrace{\frac{1}{2}\frac{\partial\mathbf{D}^{vis\ t}}{\partial e}(1+e^t)\mathbf{1}}_{=\mathsf{B}} : \Delta\boldsymbol{\epsilon} \right)\Delta t \quad , \tag{4.127}$$

where Δe has been substituted by $(1+e^t)\mathbf{1} : \Delta\boldsymbol{\epsilon}$. We notice that the stress increment $\Delta\mathbf{T}$ appears on both sides of (4.127) and must be extracted for the calculation as follows

$$\Delta\mathbf{T} = [\mathsf{I} + \mathsf{L}^t : \mathsf{A}\Delta t]^{-1} : \left[(\mathsf{M}^t - \mathsf{L}^t : \mathsf{B}\Delta t) : \Delta\boldsymbol{\epsilon} - \mathsf{L}^t : \mathbf{D}^{vis\ t}\Delta t\right] \quad . \tag{4.128}$$

Denoting

$$\mathsf{K} = [\mathsf{I} + \mathsf{L}^t : \mathsf{A}\Delta t]^{-1} : [\mathsf{M}^t - \mathsf{L}^t : \mathsf{B}\Delta t] \tag{4.129}$$

$$\mathsf{C} = [\mathsf{M}^t - \mathsf{L}^t : \mathsf{B}\Delta t]^{-1} : \mathsf{L}^t \tag{4.130}$$

the constitutive equation reads

$$\Delta\mathbf{T} = \mathsf{K} : (\Delta\boldsymbol{\epsilon} - \mathsf{C} : \mathbf{D}^{vis\ t}\Delta t) \quad , \tag{4.131}$$

where K can be interpreted as a modified stiffness and C as a linear transformation of the viscous strain rate $\mathbf{D}^{vis}$.

In the numerical procedure the fourth order tensors A and B are *approximated* since their accurate determination is troublesome. We disregard the dependence of the *direction* of

viscous strain rate $\vec{\mathbf{B}}$ on stress, i.e. $\partial\vec{\mathbf{B}}/\partial\mathbf{T} = \mathbf{0}$. Moreover we assume $M \approx$const, i.e. $\partial F_m/\partial\mathbf{T} = \mathbf{0}$. Thereby

$$2\mathsf{A} \approx \mathbf{D}^{vis}\mathrm{OCR}\frac{1}{I_v p_{et}}\frac{\partial p_{et}^{+}(\mathbf{T})}{\partial\mathbf{T}} \quad . \tag{4.132}$$

Using the definitions of $\bar{\eta}, p$ and q we obtain

$$\frac{\partial p_e^{+}(\mathbf{T})}{\partial\mathbf{T}} = \left(1 - \frac{q^2}{M^2p^2}\right)\frac{\partial p}{\partial\mathbf{T}} + \left(\frac{2q}{M^2p}\right)\frac{\partial q}{\partial\mathbf{T}} \tag{4.133}$$

with

$$\frac{\partial p}{\partial\mathbf{T}} = -\frac{1}{3}\mathbf{1} \qquad \frac{\partial q}{\partial\mathbf{T}} = \frac{3\mathbf{T}^*}{2q} \quad .$$

The fourth order tensor B can be calculated from

$$2\mathsf{B} = \frac{\partial\mathbf{D}^{vis\ t}}{\partial e}(1+e^t)\mathbf{1} = \frac{1+e^t}{I_v\lambda}\mathbf{D}_t^{vis}\mathbf{1} \quad . \tag{4.134}$$

Alternatively, using index notation B has the form

$$2B_{ijkl} = \frac{1+e^t}{I_v\lambda}D_{ij}^{vis\ t}\delta_{kl} \quad .$$

In spite of the above simplification the presented Jacobian matrix allows for a significant increase of time steps which considerably speeds up the calculation if compared with (4.126). Based on the above derivation a 'user's material' subroutine umat for the FE-program ABAQUS has been written. This subroutine has been successfully applied in FE solutions of numerous BVPs [78, 80, 102, 111].

4.3 Generalized hypoplasticity

In this section several modifications of hypoplasticity are proposed. Most of them still need to be worked out in full detail.

4.3.1 Motivation

From various aspects the hypoplastic model still need to be improved. The concept of intergranular strain is not flawless and should be molded to become a robust model. There are some inaccuracies in simultaneous prediction of large cycles and small cycles with the same set of material constants. In the extended model the incremental 'perfect' nonlinearity is absent. The version presented in Section 4.1 is analogous to elastoplastic models by Armstrong or Chaboche [3, 30] with 'hypoplastic' hardening rule. More recent

attempts, shown in Section 4.3.7, are aimed to re-introduce the incremental nonlinearity into the model.

As already mentioned in Section 3.1 some improvements in the linear part are desirable. In the present version, accumulation of stress and extraction of work (perpetuum mobile of the second kind) are possible in infinitesimally small *multiaxial* cycles (cf. Section 4.4.5), even if the nonlinear term and the intergranular strain vanish ($\mathbf{N} \equiv \mathbf{0}$ and $\mathbf{h} \equiv \mathbf{0}$). A suitable *hyperelastic* expression for stiffness L was proposed, e.g., by Niemunis and Cudny [169, 170] www.AN . From (3.5) is evident that the ratio of shear to bulk stiffness in L depends via a in (2.65) on the friction angle. For small friction angles $\varphi_c \approx 20^\circ$ this dependence may lead to inadequate predictions [82] and requires some modification.

A further shortcoming of the reference version is related to the attractors e_i and e_d which have been postulated a priori, inconsistently with the response of the basic equation (2.61), see [176] www.AN . Although states $e < e_d$ may be physically acceptable, according to the author's knowledge, neither a suitable constitutive model nor a transition phase from hypoplasticity to another model (as the void ratio passes through e_d) has been proposed.

The modifications and extensions of the original hypoplastic equation are handicapped by the form of the basic equation (2.29) as it is still fraught with unwanted interrelations. For example, if we change the analytical expression for L (say, to make it hyperelastic) we will spoil the flow rule $-\mathsf{L}^{-1} : \mathbf{N}$, the yield surface $\|\mathsf{L}^{-1} : \mathbf{N}\| - 1 = 0$, the K_0 value etc. Because of these interrelations modifications of particular features of the model are difficult and the achieved improvement is often not worth damaging the performance in several others aspects. Moreover, the meaning of the second term in the constitutive equation in (2.29) is intuitively rather unclear, especially, if one is not familiar with the one-dimensional version presented in Section 2.2. In order to provide the necessary flexibility to (2.29), it has been rewritten in a more intuitive form and furnished with components that are responsible for distinct features of soil behaviour (next subsection). Rewriting (2.29) using the flow rule and *degree of nonlinearity* proves to be convenient in future modifications of the model.

4.3.2 Rearrangements of the basic equation

We reconsider the reference hypoplastic model using the following abbreviations $\mathbf{B} = \mathsf{L}^{-1} : \mathbf{N}$, $\mathbf{m} = -\vec{\mathbf{B}}$ and $f(\mathbf{T}) = \|\mathbf{B}\| - 1$. The alternative form of the hypoplastic model (2.29) is

$$\mathring{\mathbf{T}} = \mathsf{L} : [\ \mathbf{D} - (f(\mathbf{T}) + 1)\ \mathbf{m}\ \|\mathbf{D}\|\ ]\ . \tag{4.135}$$

The unit tensor $\mathbf{m}$ denotes the direction of flow for $\overset{\circ}{\mathbf{T}} = \mathbf{0}$ (denoted as $\vec{\mathbf{n}}_g$ in elastoplasticity, see Section 2.2) and the scalar function $f(\mathbf{T})$ is similar to the yield surface. If $f(\mathbf{T}) = 0$ holds, unconfined plastic flow in the direction $\mathbf{D} \sim \mathbf{m}$ is possible. Inside the yield surface the following inequality

$$-1 < f(\mathbf{T}) < 0 \tag{4.136}$$

must hold. The function $f(\mathbf{T})$ *interpolates* the material response between hypoelasticity for $f(\mathbf{T}) = -1$ and perfect plasticity for $f(\mathbf{T}) = 0$. Therefore, the values of $f(\mathbf{T})$ are of importance not only as this function passes through zero (unlike the situation in elastoplasticity with a 'switch'-type yield function). Function $f(\mathbf{T})$ must be carefully chosen for all stresses to yield an appropriate value from the range (4.136). This value controls the degree of nonlinear behaviour.

In comparison to (2.29) the advantage of the form (4.135) follows from the fact that instead of *one* term $\mathbf{N}\|\mathbf{D}\|$ we have *two* functions $\mathbf{m}(\mathbf{T})$ and $f(\mathbf{T})$ which enable an independent constitutive description of the direction of flow and the intensity of flow, respectively. Thus the form (2.29) can be seen as a special case of (4.135) which can be called 'generalized'. It is convenient to introduce yet another abbreviation

$$Y(\mathbf{T}) = f(\mathbf{T}) + 1 \tag{4.137}$$

termed here the *degree of nonlinearity*. The hypoplastic constitutive model takes the form

$$\boxed{\overset{\circ}{\mathbf{T}} = \mathsf{L} : (\mathbf{D} - Y\,\mathbf{m}\,\|\mathbf{D}\|)} \tag{4.138}$$

and $Y(\mathbf{T})$ may vary from $Y = 0$ for incremental linear elasticity to $Y = 1$ for the unconfined plastic flow. The reference model is obtained as a special case with $Y = \|\mathbf{B}\|$ and $\mathbf{m} = -\vec{\mathbf{B}}$. We recall that early hypoplastic models were formulated by trying out different analytical expressions for $\mathbf{N}(\mathbf{T})$ until the resulting yield surface $\|\mathbf{B}\| = 1$ got a desirable form in the stress space. It seems more convenient, however, to define a yield condition $Y(\mathbf{T}) = 1$ explicitly. Some suitable functions can be found in the literature.

Let us start with the criterion (2.62) by Matsuoka and Nakai [148, 149] presented in Section 2.5. The values of the required function $f(\mathbf{T})$ should coincide with $y_{M-N}(\mathbf{T})$ in (2.62) at its zero passage. Moreover, (unlike the yield surface in classical elastoplasticity) $f(\mathbf{T})$ should smoothly interpolate the material response between elasticity and perfect plasticity. Therefore, it is important to have several contours of $f(\mathbf{T}) = \text{const}$ also inside the yield surface, as shown on the deviatoric plane in Fig. 4.35. For example, $I_1 I_2 / I_3$ varies from -9 (and not from -1) on the hydrostatic axis to $-11\frac{2}{3}$ on the yield surface obtained with $\varphi_c = 30°$.

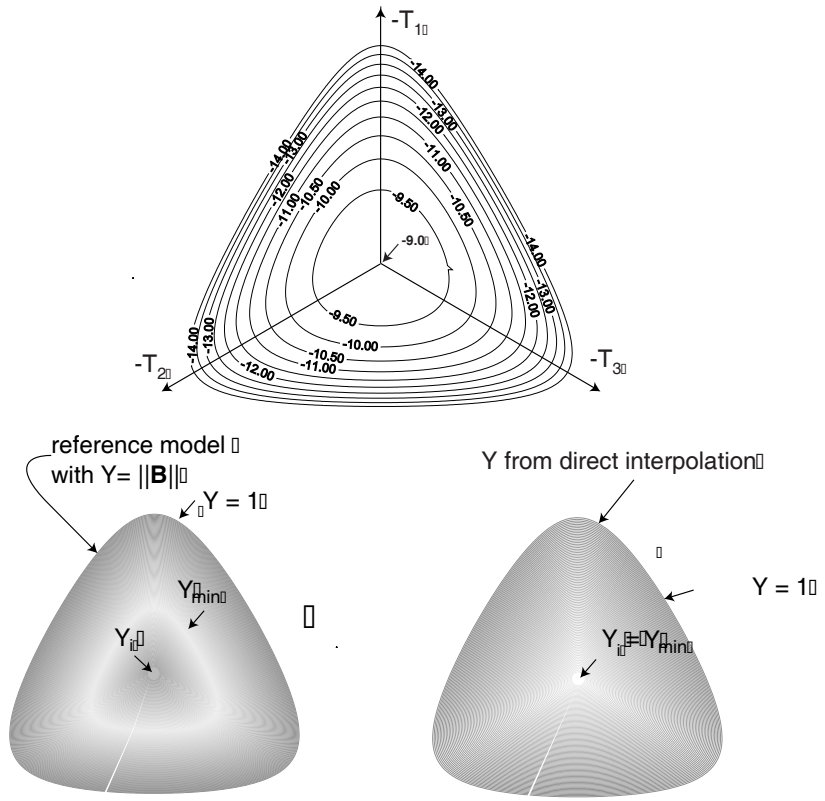

Figure 4.35: The function $I_1 I_2 / I_3$ proposed by Matsuoka and Nakai plotted on the deviatoric plane (left). The critical friction angle $\varphi_c = 30°$ corresponds to $I_1 I_2 / I_3 = -11\frac{2}{3}$ and the hydrostatic axis to -9. This values can be used for direct interpolation (middle shadowed area) of the degree of nonlinearity Y as done in (4.144) Function $Y = \|\mathbf{B}\|$ or the one in (4.139) leads to minimum nonlinearity off the hydrostatic axis (as it is shown on the right shadowed area). Moreover, this formulation is less flexible than (4.144)

4.3.3 Interpolation of degree of nonlinearity

Suppose we want to make the material response less nonlinear inside the yield surface. This can be easily done introducing

$$\overset{\circ}{\mathbf{T}} = \mathsf{L} : \left[\mathbf{D} - \|\mathbf{B}\|^n (-\vec{\mathbf{B}}) \|\mathbf{D}\| \right] \tag{4.139}$$

with an exponent $n > 1$. The new material constant n may be chosen to fit the experimental data. The exponent n controls the interpolation between $Y = Y_i$ on the p-axis and $Y = 1$ on the yield surface. Note that higher values of n shift the second-order work surface and the bifurcation surface outwards and the bounding surface inwards.

Continuing this line, we slightly modify the reference hypoplastic model choosing $Y(\mathbf{T})$ and $\mathbf{m}$ quite independently. For the sake of simplicity, in the present discussion we assume the void ratio to be critical $e = e_c$, i.e. $f_d = 1$. The stiffness L can be inverted analytically

using

$$\hat{\mathsf{L}}^{-1} = \frac{1}{F^2}\left[\mathsf{I} - \frac{\hat{\mathbf{T}}\hat{\mathbf{T}}}{(F/a)^2 + \hat{\mathbf{T}} : \hat{\mathbf{T}}}\right] \tag{4.140}$$

and hence

$$\mathbf{B} = \hat{\mathsf{L}}^{-1} : \hat{\mathbf{N}} = \frac{a}{F}\left[\mathsf{I} - \frac{\hat{\mathbf{T}}\hat{\mathbf{T}}}{(F/a)^2 + \hat{\mathbf{T}} : \hat{\mathbf{T}}}\right] : (\hat{\mathbf{T}} + \hat{\mathbf{T}}^*) \tag{4.141}$$

In agreement with the intentions of Wolffersdorff [265] the reference model provides the following properties of $\mathbf{B}$:

- $\|\mathbf{B}\| \leq 1$ holds for stresses inside the Matsuoka-Nakai surface, i.e. for

$$y_{M-N}(\mathbf{T}) \equiv -\frac{I_1 I_2}{I_3} - \frac{9 - \sin^2\varphi_c}{1 - \sin^2\varphi_c} \leq 0 \quad \text{with} \tag{4.142}$$

$$I_1 = \operatorname{tr}\mathbf{T} \quad \text{and} \quad I_2 = \frac{1}{2}[\mathbf{T} : \mathbf{T} - (I_1)^2] \quad \text{and} \quad I_3 = \det\mathbf{T} \tag{4.143}$$

- $-\mathbf{B}$ dictates a purely deviatoric direction of the hypoplastic flow for $y(\mathbf{T}) = 0$ (for the critical density with $f_d = 1$).

These properties are important assets of the model. Plotting $\|\mathbf{B}\|$ over a deviatoric stress path we may discover, however, that the minimum of $\|\mathbf{B}\|$ lies off the p-axis, i.e. is lower than the isotropic value $Y_i = a/(3 + a^2)$, e.g. for $\varphi_c = 30°$ $Y_i = 0.2474$, see Fig. 4.35. In other words, certain stresses may have a degree of nonlinearity significantly smaller than the isotropic ones, which seems unrealistic. Using (4.138) with independent $\mathbf{m}$ and $Y(\mathbf{T})$ we can easily remove this shortcoming and enforce $\|\mathbf{B}\| = Y_i$ i.e. the minimum should lie on the p-axis. For this purpose we choose

$$Y(\mathbf{T}) \equiv (1 - Y_i)\left[\frac{-I_1 I_2/I_3 - 9}{c_2 - 9}\right]^n + Y_i \quad \text{with} \quad c_2 = \frac{9 - \sin^2\varphi_c}{1 - \sin^2\varphi_c} \tag{4.144}$$

In the above equation we keep the original expression for the yield surface $Y = 1$ and the flow direction $\mathbf{m} = -\vec{\mathbf{B}}$ unchanged. Taking the hypoplastic model by Wolffersdorff this $\mathbf{m}$ insures isochoric flow at the critical state. Actually we could take a different flow rule $\mathbf{m}$, however, the condition $\operatorname{tr}\mathbf{m} = 0$ at the critical state $Y(\mathbf{T}) = 1$ should be obeyed. A simple alternative could be an interpolation between

$$\begin{cases} \mathbf{m} = \hat{\mathbf{T}}^*/\|\hat{\mathbf{T}}^*\| & \text{for} \quad y(\mathbf{T}) = 0 \quad \text{and} \\ \mathbf{m} = \frac{1}{\sqrt{3}}\,\mathbf{1} & \text{for} \quad \mathbf{T} \sim -\mathbf{1} \end{cases} \tag{4.145}$$

i.e. at $Y(\mathbf{T}) = 1$ and on the hydrostatic axis, respectively. Although the original hypoplastic flow rule (Eqs (2.37), (2.39) and (2.74)) better fits the experiments by Pradhan's et. al. [195] and the dilatancy theory by Rowe [207] than the flow rule (4.145) written above, it should be emphasized that the formulation (4.138) is more general and more flexible. For example, having enough reliable data one could fit any deviatoric flow rule as shown in diagram $\cos 3\theta - \cos 3\theta_D$ in Fig. 2.6. A tensorial function $\mathbf{m}(\mathbf{T}, e)$ may implement any dilatancy rule and it does not affect the yield surface. As we recall from (2.74) of the reference model, the dilatancy $d(\mathbf{T})$ was a function of stress only[17]. Treating $\mathbf{m}(\mathbf{T})$ as an independent function one may also impose a consistency of K_0 with the desired value, say $1 - \sin\varphi_c$. This means that for $\mathbf{T} \sim \mathrm{diag}(-1, -K_0, -K_0)$ the new flow rule should be $\mathbf{m} = \mathrm{diag}(-1, 0, 0)$. We recall from Fig. 4.25 that the reference model gives higher values than the Jaky's formula. Note that all this can be done independently of the shape of the yield function and independently of the stiffness L.

4.3.4 Enforced coincidence of bounding and yield surfaces

Having obtained some more flexibility in the constitutive modeling provided by the generalized formulation (4.138) we revisit the problem of limit surface consistency, i.e. the coincidence of bounding and yield surfaces discussed at the end of Section 2.3.2.

We recall that the response of the hypoplastic model to a stress rate $\mathring{\mathbf{T}}$ applied at a stress state $\mathbf{T}$ beyond the yield surface ($Y(\mathbf{T}) > 1$) is either non-unique (two solutions) or nonexistent (zero solutions)[18], see Section 3.1.1 and Fig. 2.10. For numerical convenience we try to prevent such situations. For this purpose a small modification of the reference hypoplastic model is proposed that renders the yield surface $y(\mathbf{T}) = 1$ identical with the bounding surface $b(\mathbf{T}) = 0$. Using the language of response envelopes, Fig. 4.36, we intend to rotate the original ellipse (dotted) so that it becomes tangent to the yield surface. If the reference model satisfied the condition (2.53) in Section 2.3.2 the coincidence between the yield bounding surfaces would be assured and no modifications would be necessary. However, it does not.

An alternative hypoplastic model proposed independently by Chambon and his co-workers in Grenoble performs differently in this aspect. In a recent detailed comparison of 'Karlsruhe' and 'Grenoble' versions [232] by Tamagnini, Viggiani and Chambon, the statement is given that the major difference between these versions is that only the 'Grenoble' model CLoE ensures invertibility for all attainable stresses [31, 33, 39]. This advantage follows

[17] The multiplier f_d influences the intensity but not the direction of irreversible deformations at a given stress. This is in agreement with Rowe [207] dilatancy law which is also a function of stress only.

[18] Strictly speaking, for a few specially chosen rates $\mathring{\mathbf{T}}$ the unique solution may be found.

from the explicit definition of the yield surface. Since the yield surface has been also explicitly defined in the reference hypoplastic model, we may attempt to make the Wolffersdorff's version fully invertible too. Our strategy, however, will be different than the one used in CLoE.

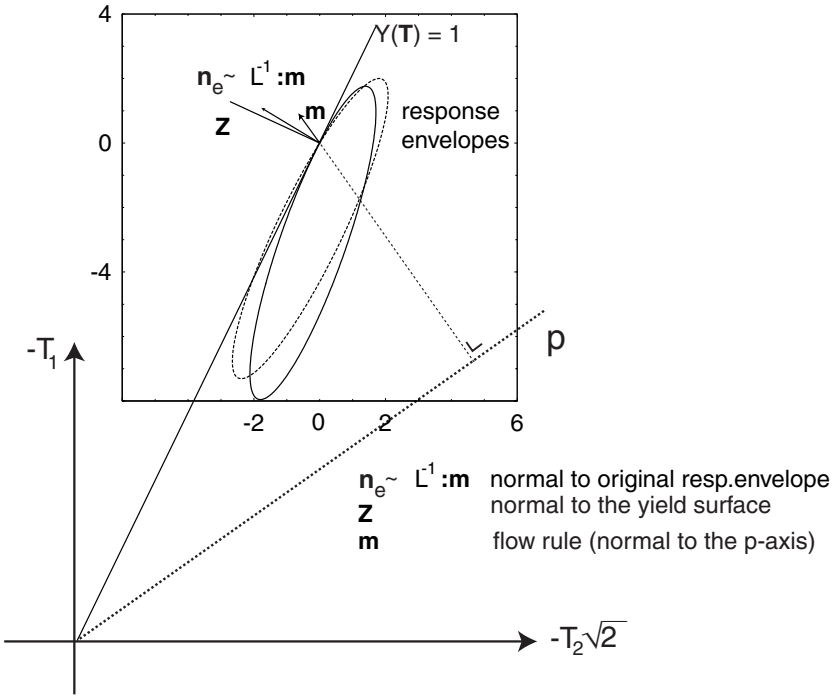

Figure 4.36: The original (dashed) response envelope is rotated to prohibit the stress path to surpass the yield surface $Y(\mathbf{T}) = 1$

Our intention is to change slightly L preserving the Matsuoka-Nakai [148,149] limit surface and the isochoric flow rule on this surface. The response envelopes before and after modification are shown in Fig. 4.36. Discussing invertibility of the hypoplastic equation we keep in mind that the linear part of stiffness L is always positive definite and thus L^{-1} can always be found.

Consider a bounding surface $b(\mathbf{T}) = 0$ with the outer normal direction $\mathbf{Z} = (\partial b/\partial \mathbf{T})$ defined already in (2.42). For any stress $\mathbf{T}$ lying on this surface all stress rates $\mathring{\mathbf{T}}$ are directed inwards this surface, which is expressed by inequality (2.43). Exactly one exception is possible for the stress rate satisfying $\mathbf{Z} : \mathring{\mathbf{T}} = 0$, i.e. lying *on* the bounding surface. The corresponding stretching $\mathbf{D}_{\max}$ can be obtained from (2.45). The analogous condition for the generalized hypoplastic formulation takes the form

$$\mathbf{Z} : \mathring{\mathbf{T}} = \mathbf{Z} : \mathsf{L} : (\mathbf{D}_{\max} - Y\mathbf{m}\|\mathbf{D}_{max}\|) = \mathbf{Z} : \mathsf{L} : (\mathbf{Z} : \mathsf{L} - Y\mathbf{m}\|\mathbf{Z} : \mathsf{L}\|) = 0\,. \quad (4.146)$$

If the bounding surface should coincide with the yield surface then (4.146) must hold for $Y(\mathbf{T}) = 1$. In this case the stress $\mathbf{T}$ lies both on the bound/yield surface and on the

response envelope. Using Y and $\mathbf{m}$ (instead of $\mathbf{N}$) the response envelope equation can be expressed as

$$o(\mathbf{T}) \equiv \|\mathsf{L}^{-1} : (\mathbf{T} - \mathbf{T}_0) + \mathbf{m} Y r_D\|^2 - r_D^2 = 0 \tag{4.147}$$

analogously to (2.21). Alternatively, the rate form (2.22) with $\|\mathbf{D}\| = 1$ is now

$$o(\mathring{\mathbf{T}}) \equiv \|\mathsf{L}^{-1} : \mathring{\mathbf{T}} + \mathbf{m} Y\|^2 - 1 = 0\,. \tag{4.148}$$

The yield surface and the bounding surface are convex, and due to inequality (2.43) the whole response envelope lies inside $b(\mathbf{T}) = 0$ except for $\mathbf{T} = \mathbf{T}_0$ or for $\mathring{\mathbf{T}} = \mathbf{0}$ at which they touch each other. If smooth bounding surface and the response envelope (ellipsoid) are connected at exactly one point $\mathbf{T}_0$, they must have a common tangent plane there. The normal to the response envelope can be calculated from (4.148) by differentiation with respect to $\mathring{\mathbf{T}}$ and evaluated for $\mathring{\mathbf{T}} = \mathbf{0}$ and for the stress on the yield surface $Y = 1$, i.e.

$$\left.\frac{\partial o(\mathring{\mathbf{T}})}{\partial \mathring{T}_{rs}}\right|_{\mathring{\mathbf{T}}=\mathbf{0},\ Y=1} \sim m_{ij} L^{-1}_{ijrs} \quad \text{and} \quad \vec{\mathbf{n}}_e = \frac{\mathbf{m} : \mathsf{L}^{-1}}{\|\mathbf{m} : \mathsf{L}^{-1}\|} \tag{4.149}$$

which we want to force to be parallel to $\mathbf{Z}$ (the major symmetry $L_{ijkl} = L_{klij}$ is assumed). Since the yield/bounding surface is explicitly given in (4.142), its outer normal direction $\mathbf{Z}$ can be directly obtained (e.g. with MATHEMATICA rules available from www.AN), viz.

$$\begin{aligned}\mathbf{Z} \sim \frac{\partial y_{M-N}}{\partial T_{ij}} \ \sim\ & T_{ik}T_{kj}[-3\|\mathbf{T}\|^2 \mathrm{tr}\,\mathbf{T} + 3\mathrm{tr}\,{}^3\mathbf{T}] + 2\mathrm{tr}\,{}^3\mathbf{T}(-T_{ij}\mathrm{tr}\,\mathbf{T} + \|\mathbf{T}\|^2\delta_{ij}) \\ & + T_{kl}T_{lm}T_{mk}(2T_{ij}\mathrm{tr}\,\mathbf{T} + \|\mathbf{T}\|^2\delta_{ij} - 3\mathrm{tr}\,{}^2\mathbf{T}\delta_{ij})\end{aligned} \tag{4.150}$$

For the coincidence of bound/yield surface we require

$$\mathbf{Z} \sim \vec{\mathbf{n}}_e \qquad (\sim \mathbf{m} : \mathsf{L}^{-1}) \tag{4.151}$$

For a given stress $\mathbf{T}$ the direction $\mathbf{Z}$ is fixed because the yield/bounding surface is given a priori. The direction $\mathbf{m}$ should not be changed because we want to preserve the flow direction (e.g. isochoric) at the critical state. The only possibility left is thus to modify the stiffness L given in (2.63). The tensors $\mathbf{Z}$ and $\mathbf{n}_e$ are coaxial (both are isotropic stress functions) are they are almost parallel (proportional) to each other, as shown in Fig. 4.36. We seek for a small fourth order rotation tensor R_{ijkl} which:

- should not be very different from the unit tensor, i.e. $\mathsf{R} \approx \mathsf{I}$
- should satisfy the relation $\vec{\mathbf{Z}} = \mathsf{R} : \vec{\mathbf{n}}_e$

The well-known Euler-Rodrigues formula for the 2nd order rotation matrix R_{ij} is applicable to vectors only, i.e., its validity is restricted to the eigenvalues of $\vec{\mathbf{Z}}$ and $\vec{\mathbf{n}}_e$ treated as "vectors" $[Z_1, Z_2, Z_3]^T$ and $[n_1, n_2, n_3]^T$. In such case we could use the vector product $\mathbf{w} = \vec{\mathbf{n}}_e \times \vec{\mathbf{Z}}$ and the scalar product $c = \vec{\mathbf{Z}} \; . \; \vec{\mathbf{n}}_e$ of two *vectors* to formulate the rotation matrix

$$\mathbf{R} = c \;\; \mathbf{1} + (1-c)\vec{\mathbf{w}} \; \vec{\mathbf{w}} + \sqrt{1-c^2} \begin{bmatrix} 0 & -\vec{w}_3 & \vec{w}_2 \\ \vec{w}_3 & 0 & -\vec{w}_1 \\ -\vec{w}_2 & \vec{w}_1 & 0 \end{bmatrix} \tag{4.152}$$

This matrix satisfies the vectorial equation $\vec{\mathbf{Z}} = \mathbf{R} \; . \; \vec{\mathbf{n}}_e$

The analogous fourth order rotation tensor R_{ijkl} that satisfies $\vec{\mathbf{Z}} = \mathsf{R} : \vec{\mathbf{n}}_e$ in any coordinate system has been formulated by Brannon [24] and by Xiao [277] using two orthonormal tensors

$$\mathbf{w}_1 = \vec{\mathbf{Z}} + \vec{\mathbf{n}}_e \quad \text{and} \quad \mathbf{w}_2 = \vec{\mathbf{Z}} - \vec{\mathbf{n}}_e \tag{4.153}$$

and has the form

$$\mathsf{R} = \mathsf{I} + (c-1)(\vec{\mathbf{w}}_1\vec{\mathbf{w}}_1 + \vec{\mathbf{w}}_2\vec{\mathbf{w}}_2) - \sqrt{1-c^2}(\vec{\mathbf{w}}_1\vec{\mathbf{w}}_2 - \vec{\mathbf{w}}_2\vec{\mathbf{w}}_1) \tag{4.154}$$

where $c = \vec{\mathbf{Z}} : \vec{\mathbf{n}}_e$. Since

$$\vec{\mathbf{w}}_1 = \frac{\vec{\mathbf{Z}} + \vec{\mathbf{n}}_e}{\sqrt{2(1+c)}} \quad \text{and} \quad \vec{\mathbf{w}}_2 = \frac{\vec{\mathbf{Z}} - \vec{\mathbf{n}}_e}{\sqrt{2(1-c)}} \tag{4.155}$$

the explicit expression for R in terms of $\vec{\mathbf{Z}}$ and $\vec{\mathbf{n}}_e$ is

$$\mathsf{R} = \mathsf{I} + \frac{1+2c}{1+c}\vec{\mathbf{Z}}\vec{\mathbf{n}}_e - \frac{1}{1+c}(\vec{\mathbf{Z}}\vec{\mathbf{Z}} + \vec{\mathbf{n}}_e\vec{\mathbf{Z}} + \vec{\mathbf{n}}_e\vec{\mathbf{n}}_e) \tag{4.156}$$

Now the equation $\vec{\mathbf{Z}} = \mathsf{R} : \vec{\mathbf{n}}_e$ can be easily proven (substituting $\vec{\mathbf{n}}_e : \vec{\mathbf{n}}_e = 1$ and $\vec{\mathbf{Z}} : \vec{\mathbf{n}}_e = c$). Using the tensorial package `nova.m` www.AN and writing

```
orthonormality={u[i_,j_]*u[i_,j_]->1,w[i_,j_]*w[i_,j_]->1,
                u[i_,j_]*w[i_,j_]->0, w[i_,j_]*u[i_,j_]->0};
R[i_,j_,k_,l_] := One[i,j,k,l] + (c-1)*( u[i,j]*u[k,l] + w[i,j]*w[k,l] ) -
                  Sqrt[1-c^2]*(u[i,j]*w[k,l] - w[i,j]*u[k,l]);
Expand[R[i, j, k, l]*R[r, s, k, l]];
Simplify[%]  //.orthonormality
```

one may also show that

$$\mathsf{R} : \mathsf{R}^T = \mathsf{I} \tag{4.157}$$

holds (as could be expected for a rotation operator), wherein transposition refers to the pairs of indices, i.e., $R^T_{ijkl} = R_{klij}$. The modified hypoplastic model is

$$\mathring{\mathbf{T}} = \bar{\mathsf{L}} : (\mathbf{D} - Y\mathbf{m}\|\mathbf{D}\|) \tag{4.158}$$

with nonsymmetric stiffness

$$\bar{\mathsf{L}} = \mathsf{R} : \mathsf{L}. \tag{4.159}$$

The new tensor outer normal to the response ellipse is

$$\vec{\mathbf{n}}_{e\ \mathrm{new}} \sim \mathbf{m} : \bar{\mathsf{L}}^{-1} \tag{4.160}$$

which follows from stress-rate derivative of (4.148) with L replaced by $\bar{\mathsf{L}}$. Comparing $\vec{\mathbf{n}}_{e\ \mathrm{new}}$ to the original direction $\vec{\mathbf{n}}_e \sim \mathbf{m} : \mathsf{L}^{-1}$ we obtain $\mathbf{m} \sim \vec{\mathbf{n}}_{e\ \mathrm{new}} : \bar{\mathsf{L}} \sim \vec{\mathbf{n}}_e : \mathsf{L}$ so substituting (4.159) we obtain $\vec{\mathbf{n}}_{e\ \mathrm{new}} : \mathsf{R} = \vec{\mathbf{n}}_e$ or equivalently $\vec{\mathbf{n}}_{e\ \mathrm{new}} = \mathsf{R} : \vec{\mathbf{n}}_e$ as initially intended. A MATHEMATICA package `small_tensor_algebra.m` www.AN might be helpful for experiments with R.

As shown in Fig. 4.36 the above modification assures that the bounding surface and the yield surface coincide preserving the previous shape of the yield surface given by (4.142) and the property of purely deviatoric plastic flow (i.e. $\operatorname{tr}\mathbf{m} = 0$) for any stress on this surface. The modification is relatively subtle and, in a sense, bridges the 'Grenoble' and 'Karlsruhe' hypoplastic models.

4.3.5 Improved prediction of undrained shearing

The version of hypoplastic model proposed by Wolffersdorff has been already used for the calculation of undrained shear behaviour of loose or dense sand [86]. For loose sand the model is able to predict softening after peak strength at

$$q/p = F\frac{3\sqrt{6}}{2a}(f_d - \sqrt{f_d^2 - 1}) \tag{4.161}$$

as shown in Fig 4.37 (path $e/e_c = 1.1$). This expression follows immediately from the second line of (3.48) applying $D_v = 0, D_q = 1$ and requiring $\dot{q} = 0$, of course for the loose sand with $f_d > 1$ only.

Also for dense sand the pore pressure build-up is correctly predicted. It is followed by a reduction of pore pressure (suction) which allows for a considerable increase of strength with the stress path moving along the critical state line CSL as shown in Fig. 4.37 (path with $e_c/e = 1.1$). This relatively complex behaviour is surprisingly well reproduced by the reference model, although no phase transition PTL mechanism has been implemented. However, several aspects of the undrained material response still need some improvement:

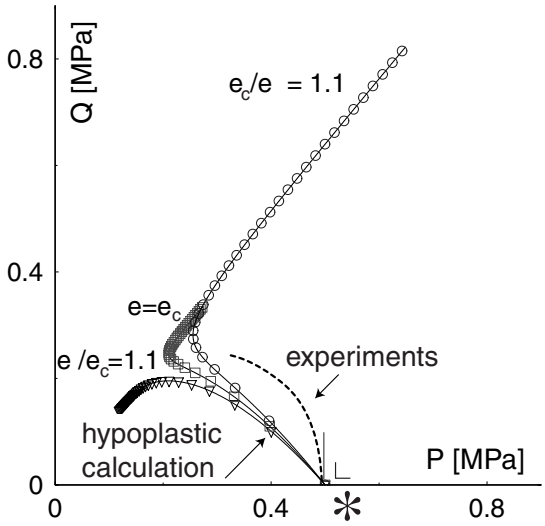

Figure 4.37: Undrained paths for different initial e/e_c values predicted by hypoplastic model by Wolffersdorff. At the beginning (point $*$) of isochoric shearing pore pressure generation is too high so the stress path is not perpendicular to the p-axis (as observed in experiments). For loose sand (the curve marked with triangles) the peak strength has been surpassed. All markers are placed after every 1% deformation $D_q \mathrm{d}t$

- Lack of the anisotropic effects after K_0-consolidation. The dilatancy cf.(2.74) is isotropic whereas $d_E < d_C$ and therefore the anisotropic undrained strength $c_{uC} > c_{uE}$ is observed in experiments [104] (C, E = triaxial compression, extension). This means that liquefaction during triaxial extension is not not predicted by the isotropic model.

- The pore pressure build-up in the deviatoric deformation (especially in the vicinity of the p-axis) is overestimated, see Fig. 4.37, in comparison to experimental data, e.g. in Fig. 4.41. The predicted number of load cycles that causes liquefaction is too low. This overly conservative prognosis was demonstrated in Section 4.1.5 and discussed in [162, 172] www.AN , see also Fig. 4.39.

- Lack of quasi steady state (QSS) in the reference model. It could enable the stress path to climb along the Coulomb surface after partial softening as it is observed in experiments, e.g. [280] (elbow-like path). Moreover it could amplify softening during undrained paths, which is desirable to compensate the lack of strain localization in element tests.

Moderate changes

Let us start with the rate of cyclic accumulation. A single closed strain cycle with the amplitude $\|\mathbf{D}\Delta t\| = A$, see Fig. 4.38, causes according to (2.29) and for $\mathbf{T} \approx$ const an

accumulation of stress $\int_0^{4\Delta t} \mathring{\mathbf{T}} \mathrm{d}t = 4\mathbf{N}A$. This was already discussed for 1-D case, Eq. (4.2), using the double amplitude $\Delta\epsilon$.

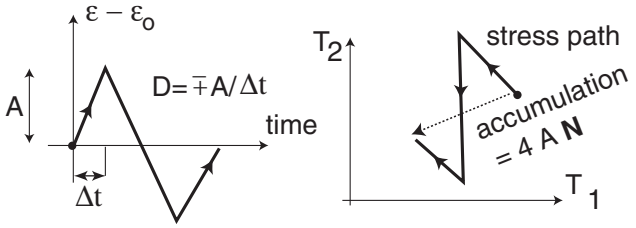

Figure 4.38: Accumulation of stress during a strain cycle

In 3-D case we easily notice that the accumulation is independent of the direction (polarization) of the strain cycle. Also during monotonic undrained shear the amount of stress relaxation is too large. Considering purely isotropic initial stress states we should significantly reduce $\mathbf{N}$ to be in agreement with undrained experiments, on one hand, but on the other hand, we should preserve a relatively large value of $\mathbf{N}$ as a difference in stiffness between isotropic compression and isotropic extension (the difference between first compression swelling coefficients λ and κ). This problem has been mitigated by the implementation of the intergranular strain, see Section 4.1, but some resulting stress paths are still awkward for large amplitudes, see Fig. 4.16 left. Now, we develop a simple solution which is especially suitable for monotonic paths. We propose the following constitutive equation

$$\mathring{\mathbf{T}} = f_e f_b \hat{\mathsf{L}} : \{\mathbf{D} - f_d Y[w_Y \ \mathbf{m}\|\mathbf{D}\| + (1 - w_Y) \ \mathbf{r}|\mathbf{r} : \mathbf{D}|] \ \} \tag{4.162}$$

wherein

$$\begin{cases} w_Y = \left(\dfrac{Y - Y_i}{h(1 - Y_i)}\right)^{\xi} & \text{for} \quad Y - Y_i < \ (1 - Y_i)h \\ w_Y = 1 & \text{for} \quad Y - Y_i \geq \ (1 - Y_i)h \end{cases} \tag{4.163}$$

is an interpolation function with $w_Y = 0$ on the p-axis and $w_Y = 1$ on the surface $Y(\mathbf{T}) = h$ and beyond it. Using the language of response envelopes, (4.162) introduces the nonlinearity in two ways: elastoplastic 'squeezing' and hypoplastic 'shifting' of the response envelopes, see Fig. 4.39. In the vicinity of the hydrostatic axis, i.e. for small values $Y - Y_i$, dominates squeezing. Farther from the p-axis we have a combination of both operations: increasing the stress obliquity shifting becomes stronger and squeezing weakens. Beyond $(Y(\mathbf{T}) - Y_i)/(1 - Y_i) = h$ ($h \approx 0.3$) we have $w_Y = 1$ and the reduction term ($\mathbf{r}$-term) vanishes, so the original hypoplastic model is recovered. The $\mathbf{r}$ is a unit tensor in stress space that points in the direction of squeezing. As we recall from Fig.

2.3, the direction of $\mathbf{r}$ may be specially chosen to keep the response envelope smooth, i.e., in our case:

$$\mathbf{r} \sim \hat{\mathsf{L}}^{-1} : \hat{\mathbf{T}} \sim \hat{\mathbf{T}} \tag{4.164}$$

As a result we obtain the response envelopes with the 'rear' part ($\mathbf{r} : \mathbf{D} < 0$) stretched and the 'front' part ($\mathbf{r} : \mathbf{D} > 0$) squeezed along the direction of $\mathbf{T}$. The response envelopes are not elliptic but the convexity is preserved, see Fig. 4.39. The important difference between the reference model and the present one lies in the isochoric response. In the present formulation, the corresponding points (marked with filled squares) are not shifted as the ones of the reference model (marked with stars).

The influence of the $|\mathbf{r} : \mathbf{D}|$ term depends on w_Y and on the angle between $\mathbf{D}$ and $\mathbf{r}$:

- for $\mathbf{D} \sim \pm\, \mathbf{r}$ we have $\|\mathbf{D}\| = |\mathbf{r} : \mathbf{D}|$ and since $\mathbf{r} \approx \mathbf{m}$ in the vicinity of the hydrostatic axis, the original hypoplastic response for such $\mathbf{D}$-s is recovered.
- for $\mathbf{D} \perp \mathbf{r}$ we have $|\mathbf{m} : \mathbf{D}| = 0$ so that the reduction term vanishes and the degree of nonlinearity is reduced by factor $w_Y(\mathbf{T})$.

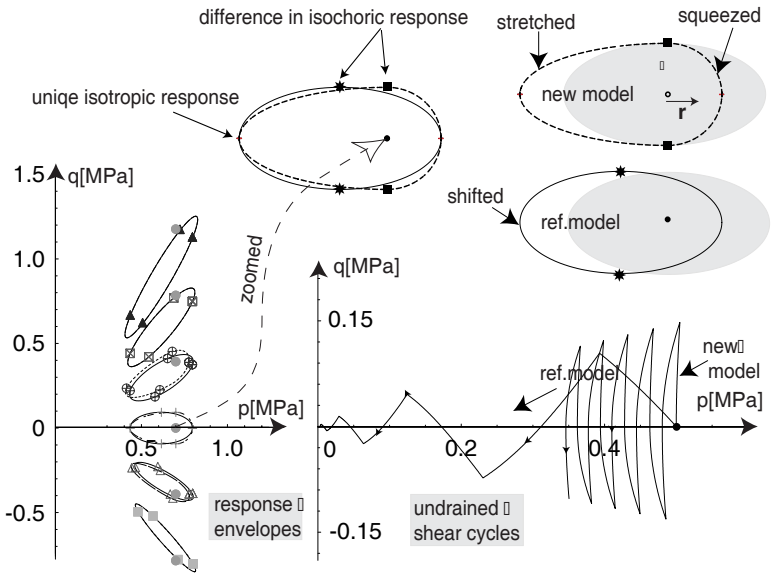

Figure 4.39: Modification of response envelopes and its effect on the rate of reduction during cyclic loading. The modified envelopes are plotted in $p - q$ diagram with the dashed lines. The difference between modified and original envelopes vanishes in the vicinity of the critical state. On the p-axis the response to isochoric deformation has been changed and the response to purely volumetric deformation is preserved. The improvement of the undrained cyclic response is achieved without the intergranular strain, cf. Fig. 4.16 and 4.17

With other words, for stresses in the vicinity of the hydrostatic axis the proposed modification considerably reduces volumetric-deviatoric coupling preserving the original hypoplastic response to isotropic (purely volumetric) compression and extension. For stresses in

the vicinity of the yield surface (beyond the line $Y = Y_i + (1 - Y_i)h$) no modification at all is made. Equation (4.162) expresses the interpolation between these cases. The formulation (4.162) can be inverted (resolved for $\mathbf{D}$), provided the response envelope is convex and the initial stress $\mathbf{T}_0$ lies inside of it. Solutions for mixed control loading programs have not been investigated as yet.

Using the matrix notation in the $p - q$ space with $\dot{\mathbf{t}} = [\dot{p}, \dot{q}]^T = \mathbf{M}\mathring{\mathbf{T}}$ and $\mathbf{d} = [D_v, D_q]^T = \mathbf{M}^{-T}\mathbf{D}$ as given in Section 3.2, with the usual symmetries $\dot{z} \equiv 0$ and $D_z = 0$ we obtain:

$$\dot{\mathbf{t}} \;=\; f_e f_b \bar{\mathsf{L}} : \left\{ \mathbf{d} - f_d Y \left[w_Y \bar{\mathbf{m}} \sqrt{\mathbf{d} : \mathbf{C} : \mathbf{d}} + (1 - w_Y)\bar{\mathbf{r}} \quad |\bar{\mathbf{r}} : \mathbf{C} : \mathbf{d}| \right] \right\} \tag{4.165}$$

with $\bar{\mathsf{L}}, \bar{\mathbf{N}}, \mathbf{C}$ given by (3.46), and

$$\bar{\mathbf{r}} = \mathbf{M}^{-T}\mathbf{r} = \frac{1}{\sqrt{3p^2 + \frac{2}{3}q^2}} \begin{Bmatrix} 3p \\ \frac{2}{3}q \end{Bmatrix} \tag{4.166}$$

The expressions for Y and Y_i can be derived from the reference version using $Y = \|\hat{\mathsf{L}}^{-1} : \hat{\mathbf{N}}\|$. This results in the stress obliquity $\eta = q/p$ are

$$\begin{aligned} Y \;&=\; a \, \frac{\sqrt{(729\,F^4 + 18\;(a^4 + 6\,a^2\,F^2 + 36\,F^4)\;\eta^2 + 4\,a^4\,\eta^4)}}{\sqrt{3}\,(9\,F\;(a^2 + 3\,F^2) + 2\,a^2\,F\,\eta^2)} \quad \text{and} \\ Y_i \;&=\; \sqrt{3}\frac{a\,F}{a^2 + 3\,F^2} \end{aligned} \tag{4.167}$$

The above modification allows for a decrease of the rate of stress accumulation during shear deformation under undrained conditions as shown in Fig 4.39-bottom,right.

It should be reminded that the above draft proposition still need much testing to become a mature constitutive model. The purpose of this presentation was to show an example of how the new formalism may ease the formulation of new hypoplastic models. Another way to weaken $\mathbf{N}$ upon deviatoric path could be to replace $\mathbf{r}|\mathbf{r} : \mathbf{D}|$ in (4.162) by the following nonlinear term $\mathbf{m}\sqrt{\mathbf{D} : \vec{\mathcal{H}} : \mathbf{D}}$ in which the fourth order dyadic tensor is $\vec{\mathcal{H}} = \mathbf{1}\;\mathbf{1}/3$. Applying purely deviatoric deformation $\mathbf{D}^*$ the nonlinear term vanishes because $\mathbf{D}^* : \mathbf{1}\;\mathbf{1} : \mathbf{D}^* = 0$.

Radical changes

Introducing modifications to the hypoplastic model we usually changed as little as possible in the reference model to preserve its main properties. In this subsection, in order to improve the performance of the model in undrained shearing we do not execute this strategy.

Although, the modifications presented in the previous section significantly improved the response of the model for shearing after isotropic consolidation, they do not work well for some other cases. For example, numerical tests of undrained shearing preceded by an *anisotropic* consolidation are not satisfactorily modeled. For such cases an implementation of an anisotropic dilatancy rule seems inevitable.

It has been experimentally observed that the inclination of the critical state surface is approximately isotropic [194] but dilation or contraction induced by shearing (or reduction/ build-up of pressure p in undrained test) may be strongly anisotropic, depending on the recent deformation history. In order to account for this effect and to improve the general performance of the hypoplastic model we use Equation (4.162) with the following innovations:

1. The referential expression for $\hat{\mathsf{L}}$ is replaced by a simple isotropic stiffness. The isochoric unloading paths were correctly inclined to the p-axis in its closest vicinity only. One can infer it from the position of the deviatoric markers of the response envelopes in Fig. 4.39. Since the future response envelopes will lie along the p-axis we must consistently choose $\mathbf{r} = -\frac{1}{\sqrt{3}}\,\mathbf{1}$ to preserve their convexity.

2. The degree of nonlinearity Y is formulated as a direct function of $\hat{\mathbf{T}}$ (and not via the value of $\|\mathbf{B}\|$) because function $Y = \|\mathbf{B}\|$ used up till now in (4.139) is not monotonously growing with the stress obliquity q/p. Isochoric stress paths become more realistic, without waves obtained from (4.162).

3. An additional structural tensor $\hat{\mathbf{A}}$ is introduced. It describes the stress obliquity $\hat{\mathbf{T}}$ for which the degree of nonlinearity $Y(\hat{\mathbf{A}}) = Y_{\min}$ has the minimum. The structural tensor $\hat{\mathbf{A}}$ may evolve only during compression with $\operatorname{tr}\mathbf{D} < 0$ and only up to a certain limit value. This is correlated with the K_0 value during oedometric compression.

4. The direction $\mathbf{m}$ is interpolated between the purely isotropic one, ($\mathbf{m} \sim \mathbf{1}$), for $\hat{\mathbf{T}} = \hat{\mathbf{A}}$ to the purely deviatoric one $\mathbf{m} \sim \hat{\mathbf{T}}^*$ at the critical state ($Y = 1$). Using the interpolation for $\hat{\mathbf{T}}$ between $\hat{\mathbf{A}}$ and the critical state surface (CSS) we must find the so-called *conjugate stress* by projection of $\hat{\mathbf{T}}$ on CSS perpendicularly to the line $\mathbf{0} - \hat{\mathbf{A}}$

5. The quasi steady state void ratio e_{QSS} has been introduced into the function f_d

In the $p - q$ space we use (4.165) wherein the isotropic stiffness for normalized stress is

$$\bar{\mathsf{L}} = \begin{bmatrix} K/E & 0 \\ 0 & 3G/E \end{bmatrix} = \begin{bmatrix} \dfrac{1}{3-6\nu} & 0 \\ 0 & \dfrac{3}{2+2\nu} \end{bmatrix} \tag{4.168}$$

We introduce the normalized vectors

$$\bar{\mathbf{r}} = \bar{\mathbf{m}}_A = \left\{ \begin{array}{c} \sqrt{3} \\ 0 \end{array} \right\}, \quad \bar{\mathbf{m}}_{yC} = \left\{ \begin{array}{c} 0 \\ \sqrt{\frac{2}{3}} \end{array} \right\} \text{ and } \bar{\mathbf{m}}_{yE} = \left\{ \begin{array}{c} 0 \\ -\sqrt{\frac{2}{3}} \end{array} \right\} \tag{4.169}$$

wherein $\bar{\mathbf{m}}_{yC}$ and $\bar{\mathbf{m}}_{yE}$ denote the flow directions at critical states for triaxial compression $q/p = \eta_{yC} = M_{csl\ C} = \dfrac{6\sin\varphi_c}{3+\sin\varphi_c}$ and for triaxial extension $q/p = \eta_{yE} = -M_{csl\ E} = -\dfrac{6\sin\varphi_c}{3-\sin\varphi_c}$, respectively. The anisotropy is described by the stress obliquity η_A, and the conjugate stress can be found comparing $\eta = q/p$ and η_A:

- for $\eta > \eta_A$ we take the conjugate stress $\eta_y = \eta_{yC}$ with the flow direction $\bar{\mathbf{m}}_{yC}$
- for $\eta < \eta_A$ we take the conjugate stress $\eta_y = \eta_{yE}$ with the flow direction $\bar{\mathbf{m}}_{yE}$

The interpolation of the 'degree of nonlinearity' Y between Y_i at $\hat{\mathbf{T}} = \hat{\mathbf{A}}$ and $Y = 1$ for plastic flow at the critical state is based on the stress position between $\hat{\mathbf{A}}$ and the yield surface. In the $p - q$ space we calculate the ratio

$$\rho_A = \frac{\eta - \eta_A}{\eta_y - \eta_A}, \tag{4.170}$$

wherein η_y corresponds to the conjugate stress $\mathbf{T}_y$ on the yield surface i.e. $y(\mathbf{T}_y) = 0$. The same ratio ρ_A is used to interpolate the current value of $\bar{\mathbf{m}}$ between $\bar{\mathbf{m}}_A$ and $\bar{\mathbf{m}}_y$.

In the general case, the conjugate stress $\hat{\mathbf{T}}_y$ can be easily determined by radial projection of $\hat{\mathbf{T}}$ from $\hat{\mathbf{A}}$ onto the critical surface $Y(\mathbf{T}) = 1$, i.e. from

$$\hat{\mathbf{T}}_y = \hat{\mathbf{A}} + \alpha(\hat{\mathbf{T}} - \hat{\mathbf{A}})^* \text{ and } Y(\hat{\mathbf{T}}_y) = 1 \text{ with } \alpha > 0 \tag{4.171}$$

(we take the smallest positive root α). Then the flow direction $\mathbf{m}$ is proportional to $\hat{\mathbf{T}}_y^*$. The interpolation is carried out using the normalized distance

$$\rho_A = \frac{\|\hat{\mathbf{T}}^* - \hat{\mathbf{A}}^*\|}{\|\hat{\mathbf{T}}_y^* - \hat{\mathbf{A}}^*\|}, \tag{4.172}$$

and the flow rule is interpolated between

- $\mathbf{m} = \mathbf{m}_A = \frac{1}{\sqrt{3}}\,\mathbf{1}$ for $\rho_A = 0$ and
- $\mathbf{m} = \hat{\mathbf{T}}_y^*/\|\hat{\mathbf{T}}_y^*\|$ for $\rho_A = 1$

Replacement of the earlier elastic stiffness by the isotropic one can also be considered for the visco-hypoplastic model of clay. Especially for low critical friction angles (say below 20°) it could correct the too narrow response envelopes reported in [82]. Alternatively one could implement a *hyperelastic* stiffness tensor [169, 170] www.AN .

Finally, a very simple concept of quasi steady state is proposed. This concept can be helpful to increase softening after the stress path reached the maximum strength (4.161). The general idea is to increase f_d for loose soils, independently of the void ratio but only for stresses below the PTL:

$$f_d = \left(\frac{e - e_d}{k_{\text{qss}} e_c - e_d} \right), \tag{4.173}$$

wherein the coefficient $k_{\text{qss}} < 1$ for stresses below the PTL and $k_{\text{qss}} = 1$ on this line. For simplicity we may admit PTL identical with CSL. The response of the hypoplastic model after these radical changes is shown in Fig. 4.40.

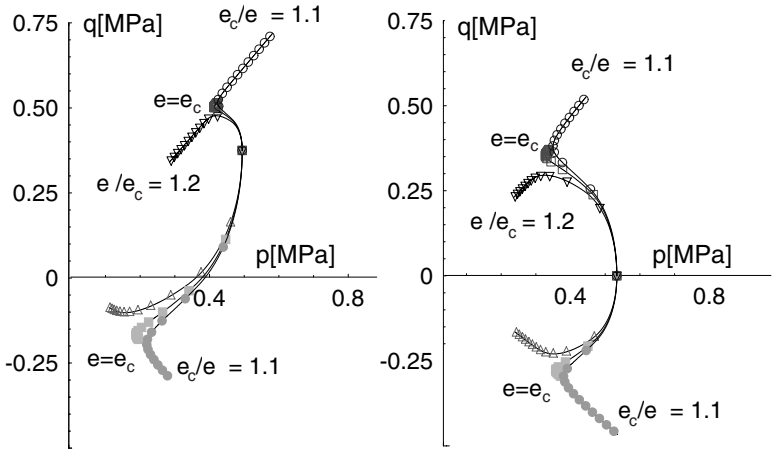

Figure 4.40: The performance of the radically modified hypoplastic model plotted for different densities in the $p-q$ diagram. The quasi steady state option has been switched off, i.e. $k_{\text{qss}} = 1$

An adequate anisotropic response might be especially important for the simulation of static liquefaction problems. The tests on loose Hostun RF sand [54] are at least qualitatively well modeled, see Fig. 4.41. The comparison of the original hypoplastic model by Wolffersdorff with these tests is discussed in detail in [84]. Dynamic liquefaction was successfully modeled in the hypoplastic framework by Osinov and Loukatschev [187].

4.3.6 Modification of shear stiffness

As already discussed in the previous subsection the stress response to isochoric shearing given by the reference hypoplastic model is inaccurate, especially in the vicinity of

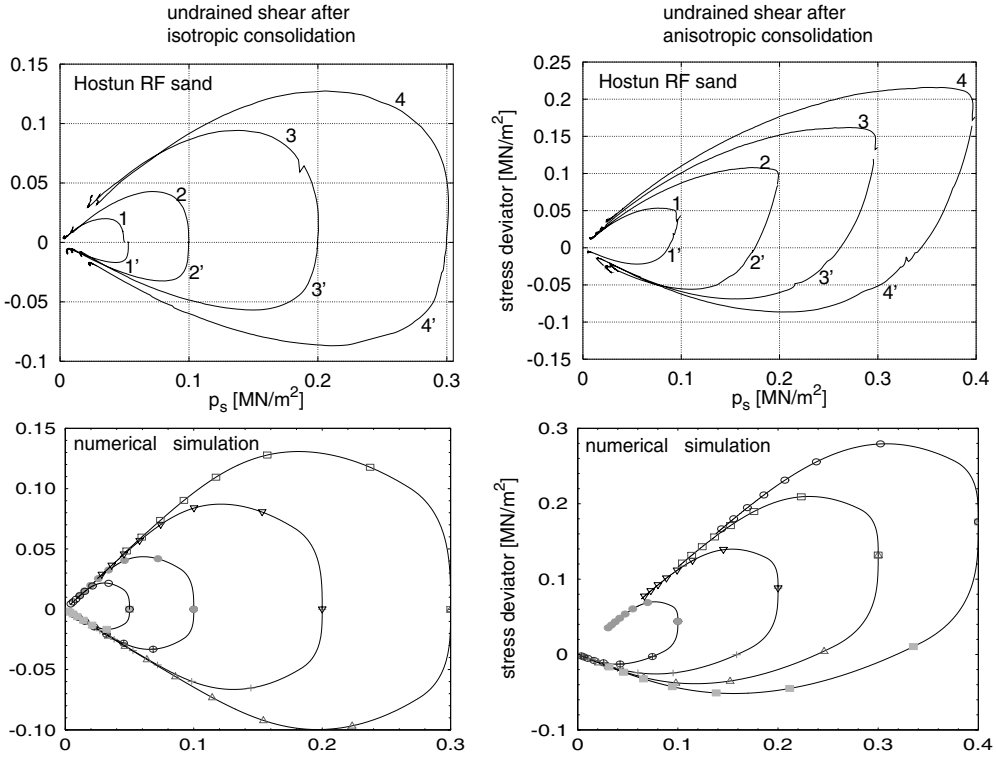

Figure 4.41: Above, the undrained tests [54] with loose sand after isotropic and anisotropic consolidation. Below the simulation with material parameters taken from [84]. New parameters are $\xi = 2$ and $h = 0.3$ in (4.163) and $k_{\text{qss}} = 0.75$ in (4.173). The same axial deformation of 15% was applied in the experiment and in the calculation

hydrostatic axis because of excessive reduction of p. We have tried to ameliorate the hypoplastic response reducing the coupling between shear and volumetric response. On one hand, judging by the Fig. 4.37, we could expect that this coupling is too strong leading to overly contractive behaviour during shearing. In isochoric shearing it is observed as a strong reduction of pressure p (build up of pore pressure). On the other hand, however, we remember that the dilatancy itself is relatively well predicted by the hypoplastic model as it can be seen from Fig. 2.18. Therefore the shear-volumetric coupling or the flow rule $\mathbf{m} = -\vec{\mathbf{B}}$ (with $\mathbf{B}$ given in (4.141)) should not be modified. Closer inspection of this contradiction reveals that an inaccuracy in stiffness matrix L is responsible for the poor isochoric response. Here we demonstrate that the shape of the response envelope is too strongly stretched along the p-axis, i.e. the shear stiffness is too small in the reference model.

Let us calculate the ratio of stiffness upon isotropic unloading to stiffness upon isochoric shearing and compare values obtained from the hypoplastic and the isotropic elastic model. It is convenient to express this ratio by the Poisson number ν. In this comparison we assume $q/p = 0$, $f_d = 1$ and $\varphi = 30°$.

The formulation of the constitutive model in terms of isomorphic variables p^+ and q^+ introduced in Section 3.2 is sufficient for our task. The isotropic elastic relation is

$$\begin{Bmatrix} \dot{p^+} \\ \dot{q^+} \end{Bmatrix} = \begin{bmatrix} E/(1-2\nu) & 0 \\ 0 & E/(1+\nu) \end{bmatrix} \cdot \begin{Bmatrix} D_v^+ \\ D_q^+ \end{Bmatrix} \tag{4.174}$$

with Young modulus E and the Poisson number ν. The reference hypoplastic model in terms of p^+ and q^+ is given in (3.48). From their comparison follows that

$$\frac{-\dot{p}^+|_{D_v^+=-1, D_q^+=0}}{\dot{q}^+|_{D_v^+=0, D_q^+=1}} = 1 + \frac{1}{3}a^2 + \frac{a}{\sqrt{3}} = \frac{(1+\nu)}{(1-2\nu)} \tag{4.175}$$

and the hypoplastic response corresponds to the Poisson ratio $\nu \approx 0.38$ which is larger than the experimentally obtained values. For example, a much lower value of $\nu = 0.15$ is reported [122] for Toyoura sand. For Hostun sand a value of $\nu = 0.1$ is used [61]. This means that the shear stiffness component $L_{qq} = F^2 + \frac{1}{3}a^2(\eta^+)^2$ should be increased in hypoplasticity . The modified hypoplastic equation (3.48) rewritten in terms of L and $\mathbf{m}$ takes the form

$$\begin{Bmatrix} \dot{p^+} \\ \dot{q^+} \end{Bmatrix} = f_s \begin{bmatrix} F^2 + \frac{1}{3}a^2 & \frac{1}{3}a^2\eta^+ \\ \frac{1}{3}a^2\eta^+ & F^2 + \frac{1}{3}a^2 \left[(\eta^+)^2 + \boxed{1-(\eta^+)^2} \right] \end{bmatrix} \cdot \left(\begin{Bmatrix} D_v^+ \\ D_q^+ \end{Bmatrix} - f_d Y \begin{Bmatrix} m_p \\ m_q \end{Bmatrix} \sqrt{(D_v^+)^2 + (D_q^+)^2} \right) \tag{4.176}$$

wherein $f_s = \dfrac{f_b\, f_e}{\frac{1}{3}\left[1 + (\eta^+)^2\right]}$ and

$$Y = \frac{a\sqrt{\left[3F^2 - a^2(\eta^+)^2\right]^2 + (a^2 + 6F^2)^2(\eta^+)^2}}{\sqrt{3}(a^2 + 3F^2 + a^2(\eta^+)^2)F} \tag{4.177}$$

$$m_p = \frac{3F^2 - a^2(\eta^+)^2}{\sqrt{\left[3F^2 - a^2(\eta^+)^2\right]^2 + (a^2 + 6F^2)^2(\eta^+)^2}} \tag{4.178}$$

$$m_q = \frac{(a^2 + 6F^2)\eta^+}{\sqrt{\left[3F^2 - a^2(\eta^+)^2\right]^2 + (a^2 + 6F^2)^2(\eta^+)^2}} \tag{4.179}$$

The new term is boxed i.e. the shear stiffness (originally $L_{qq} = F^2 + \frac{1}{3}a^2(\eta^+)^2$) is increased by $\frac{1}{3}a^2\left[1 - (\eta^+)^2\right]$. Of course this is just an example of how the shear stiffness can be increased.

It turns out that keeping $\mathbf{m}$ constant and changing L_{qq} only the dilatancy $d = \operatorname{tr}\mathbf{D}/\|\mathbf{D}\|$ is not affected so that the dilatancy diagram shown in Fig. 2.18 remain valid. This somewhat

surprising independence can be explained inverting relation (4.138). We obtain

$$\mathbf{D} = \mathbf{A} + \mathbf{m}Y \left[\frac{\mathbf{A} : \mathbf{m}Y}{Y^2 - 1} + \sqrt{\left(\frac{\mathbf{A} : \mathbf{m}Y}{Y^2 - 1} \right)^2 - \frac{\mathbf{A} : \mathbf{A}}{Y^2 - 1}} \right] \tag{4.180}$$

applying the procedure presented in Subsection 3.1.1. Using isomorphic variables p^+ and q^+ tensor $\mathbf{A} = \mathsf{L}^{-1} : \mathring{\mathbf{T}}$ takes the form $[(L^{-1})_{pq}\dot{q}^+, (L^{-1})_{qq}\dot{q}^+]^T$ because our dilatancy is defined over deviatoric stress paths only and $\dot{p}^+ = 0$. The expression for dilatancy is then

$$d = \frac{\sqrt{3}D_v^+}{|D_q^+|} = \frac{\sqrt{3}\left[(L^{-1})_{pq}\dot{q}^+ + m_p Y x\right]}{(L^{-1})_{qq}\dot{q}^+ + m_q Y x} \tag{4.181}$$

wherein x is an abbreviation for the expression in rectangular brackets in (4.180). Expression (4.181) is not influenced by the term L_{qq} because it may enter $\mathbf{A}$ via the determinant of L only. In order to demonstrate this fact we simply write out

$$\begin{bmatrix} L_{pp} & L_{pq} \\ L_{qp} & L_{qq} \end{bmatrix}^{-1} = \frac{1}{\det \mathsf{L}} \begin{bmatrix} L_{qq} & -L_{pq} \\ -L_{qp} & L_{pp} \end{bmatrix}$$

Due to the specific form of (4.181) the term $\det \mathsf{L} > 0$ in $\mathbf{A}$ can be eliminated from this fraction. Therefore L_{qq} is indeed absent in the expression (4.181) for d.

The increased value of L_{qq} improves the undrained stress path reducing the accumulation of pore pressure in the calculation as shown in Fig. 4.42.

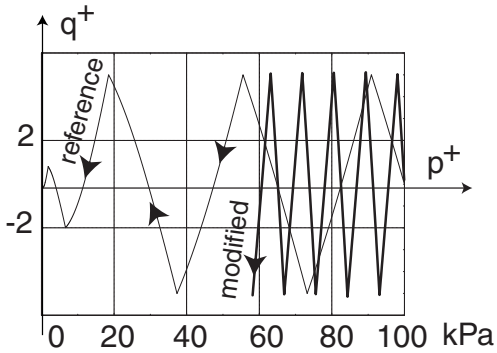

Figure 4.42: The excessive accumulation of pore pressure in undrained shear tests can be reduced by the increased shear stiffness

In general 3-D case the correction of L_{qq} should be written out in a form of an isotropic stress function. Perusal of the original form for $\hat{\mathsf{L}}$ given in (2.63) with $\hat{\mathbf{T}} = \hat{\mathbf{T}}^* + \frac{1}{3}\,\mathbf{1}$, viz.

$$\begin{aligned} \hat{\mathsf{L}} &= F^2 \mathsf{I} + a^2 (\frac{1}{3}\,\mathbf{1} + \hat{\mathbf{T}}^*)(\frac{1}{3}\,\mathbf{1} + \hat{\mathbf{T}}^*) \\ &= F^2 \mathsf{I} + a^2 \frac{1}{9}\,\mathbf{1}\,\mathbf{1} + a^2 \frac{1}{3}\,\mathbf{1}\hat{\mathbf{T}}^* + a^2 \frac{1}{3}\hat{\mathbf{T}}^*\,\mathbf{1} + a^2 \hat{\mathbf{T}}^* \hat{\mathbf{T}}^* \end{aligned} \tag{4.182}$$

may suggest increasing the last term $a^2\hat{\mathbf{T}}^*\hat{\mathbf{T}}^*$ in the above equation. However, this would have no effect if stress lies at the hydrostatic axis for which $\hat{\mathbf{T}}^* = \mathbf{0}$. Therefore adding $b^2(\mathsf{I} - \frac{1}{3}\,\mathbf{1}\,\mathbf{1})$ to the original $\hat{\mathsf{L}}$ is a more reliable method. In this modification b^2 is a new material constant that can be related to the desired Poisson number at the hydrostatic stress as follows

$$\frac{-\dot{p}^+|_{D_v^+=-1,D_q^+=0}}{\dot{q}^+|_{D_v^+=0,D_q^+=1}} = \frac{1+\frac{1}{3}a^2+\frac{a}{\sqrt{3}}}{1+b^2} = \frac{1+\nu}{1-2\nu}, \tag{4.183}$$

for example for $\varphi = 30^\circ$ and $\nu = 0.2$ we obtain $a = 3.06186$ and hence $b^2 = 1.94638$.

It should be emphasized that the above modification refers to L in (4.138) and should be carried out keeping the original $\mathbf{m}$ unchanged. The modification *should not* be applied to L in the original form (2.61) because it would cause undesired side effects.

4.3.7 Coupling of hypoplastic materials

Our intention here is to improve the performance of the reference model for cyclic loading preserving the incremental 'perfect' nonlinearity. As it has been already mentioned, the generalized hypoplasticity with the intergranular strain is bilinear and therefore 'perfect' nonlinearity is lost. Another possibility of generalization of the hypoplastic model consists in parallel coupling of several equations similar to (2.29). The common strain rate is applied and the partial stresses are added. Of course, such parallel coupling makes sense only if the partial yield surfaces are different. A similar coupling was performed already by Valanis, e.g. [251] in his *endochronic theory* with the kernel function in form of Dirichlet series. The endochronic model [13, 15, 96, 246–250] is similar to the hypoplastic one. For example, from the early endochronic theory the hypoplastic equation follows (2.29) as a special case. Of course, it is only a formal similarity, the soil-specific features like a conical yield surface the pycnotropy and barotropy factors etc. were not considered in endochronic formulations. Later, Valanis [247] introduced an elastic locus to his model because the early version was criticized [204, 211] for predicting too large accumulation during infinitesimally(!) small nonsymmetric cycles. The introduction of the elastic locus, however, makes the model elasto-plastic (at least formally, due to bilinearity). The endochronic evolution equation can be interpreted as hardening function. Actually, the same refers to the extended version of hypoplasticity with the intergranular strain. Both hypoplastic and late endochronic models resemble the well known approach of Armstrong and Frederick [3] with 'hypoplastic' hardening, see the review of similar approaches by Chaboche [30]. In the following subsection, in order to keep the 'perfect' nonlinearity, we examine only the early endochronic formulation without decomposition of the strain rate into plastic and elastic portion.

Prototypal endochronic model

Let us start with a simplified endochronic model with a single kernel function. Consider the following stress function

$$\mathbf{T}(z) = \int_0^z \mathsf{K}(z, z^+) : \frac{\mathrm{d}\boldsymbol{\epsilon}(z^+)}{\mathrm{d}z^+}\mathrm{d}z^+, \tag{4.184}$$

wherein

$$\mathsf{K}(z, z^+) = \hat{\mathsf{K}} e^{-b(z-z^+)} \tag{4.185}$$

is the hereditary function (kernel function) with the elastic stiffness tensor $\hat{K}_{ijkl}$. The internal time is defined by

$$\mathrm{d}z = \mathrm{d}z^+ = \sqrt{\mathrm{d}\boldsymbol{\epsilon} : \mathsf{P} : \mathrm{d}\boldsymbol{\epsilon}} \tag{4.186}$$

We assume $\mathsf{P} = \mathsf{I}$ so that $\mathrm{d}z = \|\mathrm{d}\boldsymbol{\epsilon}\|$. The derivative of (4.184) with respect to z has the form[19]

$$\frac{\mathrm{d}\mathbf{T}}{\mathrm{d}z} = \mathsf{K}(z, z) : \frac{\mathrm{d}\boldsymbol{\epsilon}(z^+)}{\mathrm{d}z^+}\bigg|_{z^+=z} + \overbrace{\int_0^z \frac{\partial \mathsf{K}(z, z^+)}{\partial z} : \frac{\mathrm{d}\boldsymbol{\epsilon}(z^+)}{\mathrm{d}z^+}\mathrm{d}z^+}^{=\mathbf{N}} = \hat{\mathsf{K}} : \frac{\mathrm{d}\boldsymbol{\epsilon}}{\mathrm{d}z} + \mathbf{N} \tag{4.187}$$

in which $\mathbf{N}$ can be simplified using (4.184)

$$\mathbf{N} = -b \int_0^z e^{-b(z-z^+)} \hat{\mathsf{K}} : \frac{\mathrm{d}\boldsymbol{\epsilon}(z^+)}{\mathrm{d}z^+}\mathrm{d}z^+ = -b\ \mathbf{T} \tag{4.188}$$

The incremental form of the constitutive equation is

$$\mathrm{d}\mathbf{T} = \hat{\mathsf{K}} : \mathrm{d}\boldsymbol{\epsilon} + \mathbf{N}\mathrm{d}z = \hat{\mathsf{K}} : \mathrm{d}\boldsymbol{\epsilon} - b\ \mathbf{T}\ \mathrm{d}z \tag{4.189}$$

which for one-dimensional case can easily be verified with MATHEMATICA:

```
t = Integrate[k  Exp[-b (z - zp)] e'[zp] , {zp, 0, z}] ;
Expand[D[t, z]] /. Integrate[ k  Exp[-b (z - zp)] e'[zp] , {zp, 0, z}] -> tc
```

[19] Differentiating (4.184) with respect to z we should note that the upper limit of the integral on the right-hand side is dependent on z. In such case the following rule applies

$$\frac{\mathrm{d}}{\mathrm{d}z}\int_{L(z)}^{U(z)} y(z,t)\mathrm{d}t = \int_{L(z)}^{U(z)} \frac{\partial y(z,t)}{\partial z}\mathrm{d}t - y(z, L(z))L'(z) + y(z, U(z))U'(z)$$

for any function $y(z,t)$ *continuous* with respect to z and integrable with respect to t. We may admit discontinuities in function $y(z,t)$ due to jumps of $\dfrac{\mathrm{d}\boldsymbol{\epsilon}(z^+)}{\mathrm{d}z^+}$ at sharp reversals of strain path.

Substituting $\dfrac{\mathrm{d}\mathbf{T}}{\mathrm{d}t} = \mathring{\mathbf{T}}$ and $\dfrac{\mathrm{d}\boldsymbol{\epsilon}}{\mathrm{d}t} = \mathbf{D}$ we arrive at

$$\mathring{\mathbf{T}} = \hat{\mathsf{K}} : \mathbf{D} + \mathbf{N}\|\mathbf{D}\| = \hat{\mathsf{K}} : \mathbf{D} - b\mathbf{T}\|\mathbf{D}\| \tag{4.190}$$

The material constant b is positive and therefore the term $-b\ \mathbf{T}\ \|\mathbf{D}\|$ in (4.190) reduces the stress rate $\mathring{\mathbf{T}}$ as $\mathbf{T}$ increases. Eventually, keeping $\vec{\mathbf{D}} = \text{const}$, the stress rate vanishes for $\mathbf{T} = \hat{\mathsf{K}} : \vec{\mathbf{D}}/b$. The one-dimensional version of the endochronic theory is identical with (2.32) with $L = \hat{K}$ and $N = -b\,T$, as presented in Section 2.2. We consider a proportional straining in the one-dimensional case with $D = \text{const}$. For $\mathrm{d}\epsilon(z^+)/\mathrm{d}z^+ \equiv 1$ we have

$$T(z) = \int_0^z \hat{K} e^{-b(z-z^+)} \mathrm{d}z^+ = \frac{\hat{K}}{b}(1 - e^{-bz}) \tag{4.191}$$

and for $\mathrm{d}\epsilon(z^+)/\mathrm{d}z^+ \equiv -1$:

$$T(z) = -\int_0^z \hat{K} e^{-b(z-z^+)} \mathrm{d}z^+ = -\frac{\hat{K}}{b}(1 - e^{-bz}) \tag{4.192}$$

so the possible stress states lie in the range

$$-\frac{\hat{K}}{b} < T < \frac{\hat{K}}{b}. \tag{4.193}$$

In general the requirement $\mathring{\mathbf{T}}\Big|_{\mathbf{D}\neq\mathbf{0}} = \mathbf{0}$ imposed on (4.190) results in a function of stress which we interpret as an *endochronic yield surface*. We derive this function directly from (4.190) as

$$y(\mathbf{T}) = \|b\ \hat{\mathsf{K}}^{-1} : \mathbf{T}\| - 1 = 0 \tag{4.194}$$

which is analogous to the hypoplastic yield surface in Section 2.3.1. Similarly we may conclude from (4.190 the endochronic flow rule

$$\vec{\mathbf{D}} = b\hat{\mathsf{K}}^{-1} : \mathbf{T} \tag{4.195}$$

The incremental stiffness $\mathsf{E} = \dfrac{\partial \mathring{\mathbf{T}}}{\partial \mathbf{D}}$ is also a smooth function of $\vec{\mathbf{D}}$, viz.

$$\mathring{T}_{ij} = \left[\hat{K}_{ijkl} + N_{ij}\vec{D}_{kl}\right] D_{kl} \tag{4.196}$$

Endochronic overlay models

Parallel coupled endochronic/hypoplastic models can be generated automatically. A suitable procedure is presented in this subsection. Unfortunately, it turns out that a simple

parallel superposition of partial stresses insufficiently restrain ratcheting. As it has been demonstrated here, still an excessive accumulation (not only for infinitesimal cycles) is predicted. Therefore, at the end of this subsection an additional constraint for parallel coupling is proposed.

Already in his early papers Valanis proposed the kernel function in the form of a Dirichlet series

$$\mathsf{K}(z, z^+) = \sum_{r=1}^{n} \mathsf{K}_r(z, z^+) = \sum_{r=1}^{n} \hat{\mathsf{K}}_r e^{-b_r(z-z^+)} \tag{4.197}$$

This offers more flexibility in modeling and may reduce ratcheting effects understood as an inability of the constitutive model to reproduce the hysteretic loop in a stress-strain diagram. We have discussed it already in Section 4.1. Ratcheting may lead to prediction of excessive accumulation for cyclic loading. It is convenient to rewrite Equation (4.184) in the form

$$\mathbf{T}(z) = \sum_{r=1}^{n} \mathbf{T}_r(z) \qquad \text{with} \tag{4.198}$$

$$\mathbf{T}_r(z) = \int_0^z \mathsf{K}_r(z, z^+) : \frac{\mathrm{d}\boldsymbol{\epsilon}(z^+)}{\mathrm{d}z^+} \mathrm{d}z^+, \tag{4.199}$$

in which $\mathbf{T}_r$ denotes the r-th partial stress. In the differential form we obtain

$$\mathrm{d}\mathbf{T}(z) = \sum_{r=1}^{n} \mathrm{d}\mathbf{T}_r(z) \qquad \text{with} \tag{4.200}$$

$$\mathrm{d}\mathbf{T}_r = \hat{\mathsf{K}}_r : \mathrm{d}\boldsymbol{\epsilon} - b_r \, \mathbf{T}_r \mathrm{d}z \qquad \text{(no sum over r)} \tag{4.201}$$

All partial stresses $\mathbf{T}_r$ with $r = 1, 2, \ldots$ must be updated and stored individually. In the following example we use just two kernel functions, see Fig. 4.43.

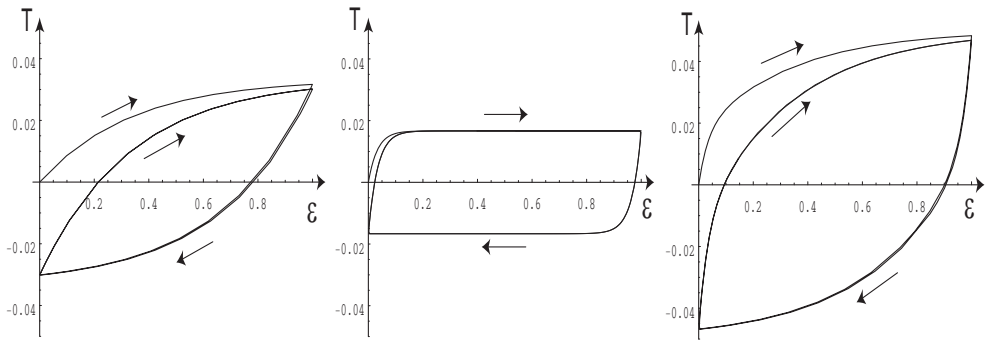

Figure 4.43: The shape of a stress strain loop in a symmetric strain cycle can be modeled by superposition of several (here two) hypoplastic models

```
ed[z_] := Sign[Sin[Pi*z]]                                    (* epsilon dot *)
e[z_] := If[EvenQ[Floor[z]] , z-Floor[z] ,  Ceiling[z]-z   ]     (* epsilon *)
s1=NDSolve[{stress1'[z] ==  0.1*ed[z] - 3*stress1[z]  , stress1[0] == 0} ,
                          {stress1},{z,0,5}, MaxStepSize -> 0.01]    (*T_1*)
s2=NDSolve[{stress2'[z] ==  0.5*ed[z] - 30*stress2[z]  , stress2[0] == 0} ,
                           {stress2},{z,0,5}, MaxStepSize -> 0.01]   (*T_2*)
}
```

The smallest possible strain cycle amplitude should be known a priori. It is required to implement a partial stress with sufficiently small range (4.194) into (4.198). If smaller cycles occur, ratcheting will be inevitable.

The following simulation of *nonsymmetric* strain cycles reveals that excessive accumulation effects occur even for larger cycles, see Fig. 4.44. Therefore, parallel coupling is not sufficient to generate closed stress-strain loops at strongly anisotropic average stresses. Note that the accumulation occurs in spite of the hysteretic loop generated by the second material.

```
ed[z_] := If[z < 3, 1, Sign[Sin[Pi*z]] ]
e[z_] :=
If[z < 3, z, 2+(If[EvenQ[Floor[z]] , z-Floor[z] ,  Ceiling[z]-z   ])]
s1= NDSolve[{stress1'[z] ==   2*ed[z] - 0.5*stress1[z]  , stress1[0] == 0} ,
                            {stress1},{z,0,7}, MaxStepSize -> 0.01]    (*T_1*)
s2= NDSolve[{stress2'[z] ==  6.0*ed[z] - 10*stress2[z]  , stress2[0] == 0} ,
                            {stress2},{z,0,7}, MaxStepSize -> 0.01]   (*T_2*)
```

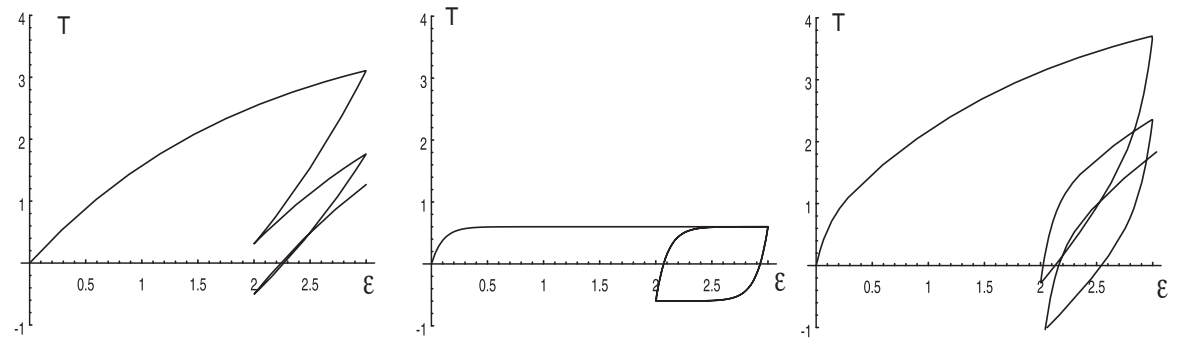

Figure 4.44: Superposition of two hypoplastic models reduces ratcheting for nonsymmetric strain cycles but the rate of stress relaxation per cycle is still too large

A similar observation was also made by Chaboche [30] with respect to kinematic hardening rules for elasto-plastic materials. To avoid excessive ratcheting he proposed a threshold value of partial stress above which kinematic hardening is active. Here, an alternative approach is proposed, namely a modified coupling. Consider again a 1-D model with m parallel coupled materials. Let the r-th material have the stress rate

$$\dot{T}_r = E_r \left[D - \left(\frac{|T_r|}{y_r} \right)^{n_r} \overbrace{\operatorname{sign}(T_r)}^{=m} |D| \right] \tag{4.202}$$

where $y_r = E_r/b_r$ is the limit for the partial stress and b_r is the exponent of the kernel function used by Valanis. The direction m denotes the flow direction, which for one dimensional case means $m = \pm 1$. The expression $(|T_r|/y_r) \leq 1$ is the relative partial stress obtained as a fraction of the yield stress y_r. The expression $\text{sign}(T_r)$ is the flow rule.

It is useful to generate the individual material properties automatically, viz.

$$E_{r+1} = E_r \lambda_E \tag{4.203}$$

$$y_{r+1} = y_r \lambda_y \tag{4.204}$$

$$n_{r+1} = n_r \lambda_n \tag{4.205}$$

with $\lambda_E < 1$ $\lambda_n < 1$ and $\lambda_y > 1$. Having calculated $\dot{T}_{r+1}$ from (4.202) the following modification to the conventional parallel coupling is proposed

$$\boxed{\dot{T}_{r+1} = \text{sgn}(\dot{T}_{r+1}) \max(|\dot{T}_{r+1}|, |\dot{T}_r|)} \quad \text{with} \quad \dot{T}_0 = 0 \tag{4.206}$$

This means that the material with relatively large stiffness dictates also the partial stress response of materials which have larger yield surfaces thereof. The above draft model yields an acceptable response for strain loops of various amplitudes including anisotropic average stresses, as shown in Fig. 4.45

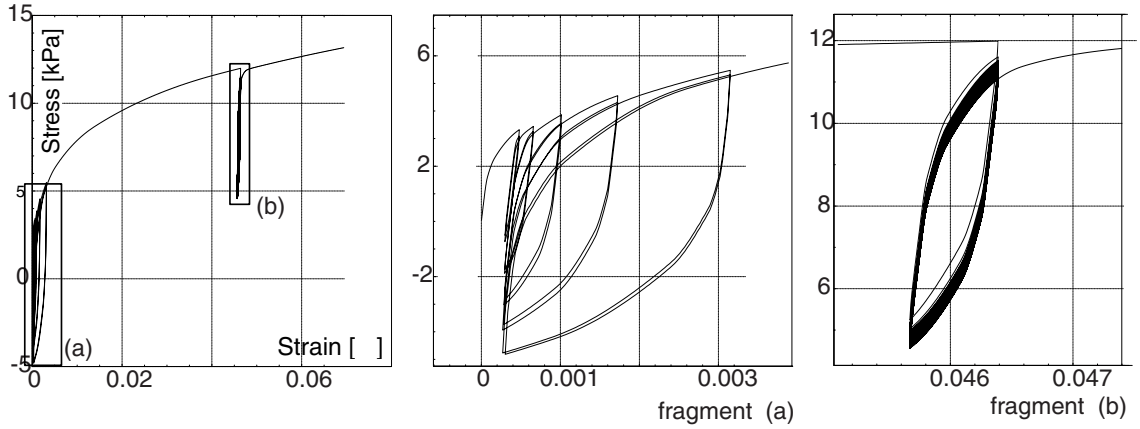

Figure 4.45: Improved hypoplastic response of an overlay model by the constraint (4.206). The calculation was performed with 12 materials generated with $E_0 = 4000, y_0 = 0.1, n_0 = 5, \lambda_E = 0.5, \lambda_n = 0.9$ and $\lambda_y = 1.5$

4.3.8 Consistency at $e = e_d$

The so-called granular phase diagram (Fig. 2.17) illustrates the range of void ratios between the pressure dependent bounds $e_i(\text{tr}\,\mathbf{T})$ and $e_d(\text{tr}\,\mathbf{T})$ for which the reference hypoplastic model may be used. This *a priori* imposed range lies between the respective

two lines in the $e - \operatorname{tr}\mathbf{T}$ space. It can be shown [176] www.AN that in the framework of the actual hypoplastic model these bounds can be surpassed by particular deformation paths. Using a reasonable set of material constants the lower bound cannot be surpassed during a proportional compression with $\operatorname{tr}\mathring{\mathbf{T}} < 0$, cf. [83]. However, isotropic extension may lead to a violation of the condition $e \geq e_d$ (Fig. 4.47 left), even if one disregards the intergranular strain. The surpassing of the upper bound $e_i(\operatorname{tr}\mathbf{T})$, although possible, causes no numerical problems. The surpassing of the lower bound $e_d(\operatorname{tr}\mathbf{T})$, however, is troublesome, especially in FE-calculations with density fluctuations [182]. The trouble is evident from the definition (2.71) of f_d which is undetermined for $r_e < 0$. Although for some deformation paths such surpassing of the bounds may be physically correct [73], the respective phase transition requires a fundamental change of the material model. To the author's knowledge, a suitable 'working' solution has not been proposed as yet.

For this reason, let us discuss a minor modification of f_d in order to keep the state $(\mathbf{T}, e)$ above the $e_d(\mathbf{T})$-line [176] www.AN . The nonlinear part $\mathbf{N}$ of the reference hypoplastic model is multiplied by the factor $f_d = \left(\frac{e-e_d}{e_c-e_d}\right)^{\alpha}$, so this part must vanish in the vicinity of $e = e_d$ (because of $f_d \approx 0$) and (2.61) takes the form

$$\mathring{\mathbf{T}} \approx \mathsf{L} : \mathbf{D}\,. \tag{4.207}$$

In order to keep the void ratio above the lower bound line, i.e. for a given $\operatorname{tr}\mathbf{T}$

$$e > e_d(\operatorname{tr}\mathbf{T}) = e_{d0}\exp\left[-\left(\frac{-\operatorname{tr}\mathbf{T}}{h_s}\right)^n\right] \tag{4.208}$$

we require that for any rate of deformation $\mathbf{D}$ the increment of the void ratio must be sufficiently large. Let us rewrite the lower bound line in the following form

$$F_d(e, \operatorname{tr}\mathbf{T}) \equiv e - e_{d0}\exp\left[-\left(\frac{-\operatorname{tr}\mathbf{T}}{h_s}\right)^n\right] = 0\,. \tag{4.209}$$

The vector

$$\mathbf{M}(\operatorname{tr}\mathbf{T}, e)^{(d)} = \left[M_e^{(d)}, M_T^{(d)}\right] = \left[\frac{\partial F_d}{\partial e}, \frac{\partial F_d}{\partial \operatorname{tr}\mathbf{T}}\right]\,, \tag{4.210}$$

normal to the surface F_d, see Fig. 4.46, has two components

$$M_e^{(d)} = \frac{\partial F_d}{\partial e} = 1 \quad \text{and} \quad M_T^{(d)} = \frac{\partial F_d}{\partial \operatorname{tr}\mathbf{T}} = -\frac{e_d}{h_s} n \left(\frac{-\operatorname{tr}\mathbf{T}}{h_s}\right)^{n-1}\,. \tag{4.211}$$

Any admissible process of deformation described in terms of $\dot{e}$ and $\operatorname{tr}\dot{\mathbf{T}}$ must satisfy the following condition

$$A^{(d)} = \frac{\partial f}{\partial e}\dot{e} + \frac{\partial f}{\partial \operatorname{tr}\mathbf{T}}\operatorname{tr}(\dot{\mathbf{T}}) \geq 0\,, \tag{4.212}$$

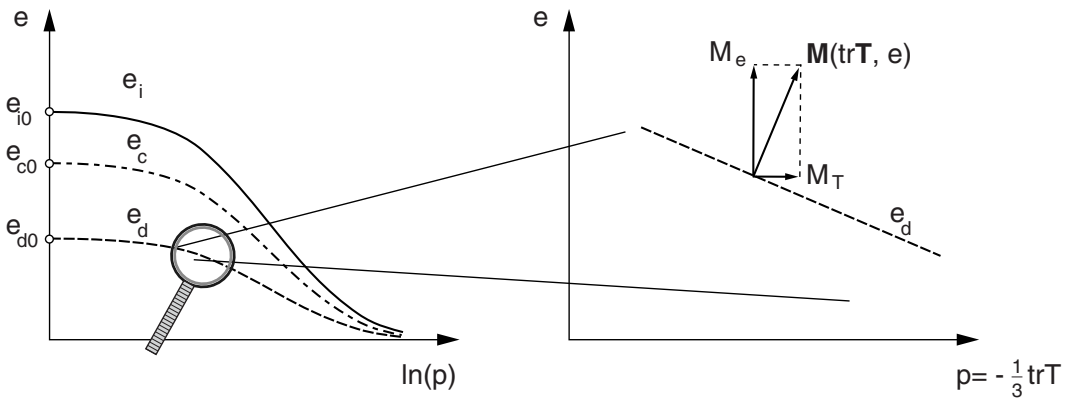

Figure 4.46: Definition of vector M in the $e - \mathrm{tr}\mathbf{T}$ space on e_d

for all strain rates $\mathbf{D}$, i.e. the evolved state must remain above the $e_d(\mathrm{tr}\,\mathbf{T})$ line. Briefly, for $e = e_d$, $A^{(d)} \geq 0$ must hold and this condition is not fulfilled by the reference hypoplastic model. Equation (4.207) is thus *inconsistent* with the requirement $e > e_d$. Attempts of evaluation of f_d from (2.71) with $e < e_d$ must lead, of course, to complex numbers.

In order to establish the consistency condition at the maximum density limit we modify the expression (2.71) for f_d so that

$$A^{(d)} = M_e^{(d)} \mathrm{tr}\,\mathbf{D}\ (1+e) + M_T^{(d)} \mathrm{tr}\,(\mathsf{L} : \mathbf{D} + f_d \mathbf{N} \|\mathbf{D}\|) \geq 0 \tag{4.213}$$

holds for all $\mathbf{D}$ at $e = e_d$. Note that the tensors L and $\mathbf{N}$ contain already the barotropy and pycnotropy multipliers f_e and f_b. We calculate the strain rate $\mathbf{D} = \bar{\mathbf{D}}$ for which $A^{(d)}$ reaches minimum under the condition $\|\mathbf{D}\| = 1$:

$$\left\{ \begin{array}{ll} \dfrac{\partial [A^{(d)} + \lambda(\|\mathbf{D}\| - 1)]}{\partial D_{rs}} & = 0 \\ \|\mathbf{D}\| & = 1 \end{array} \right. \tag{4.214}$$

and we find the direction of maximum contraction which for the reference model corresponds to

$$\bar{D}_{rs} \sim M_e^{(d)}(1+e)\delta_{rs} + M_T^{(d)} \delta_{ij} L_{ijrs} \tag{4.215}$$

from which

$$\bar{D}_{rs} = \frac{M_e^{(d)}(1+e)\delta_{rs} + M_T^{(d)} \dfrac{f_b f_e}{\hat{\mathbf{T}} : \hat{\mathbf{T}}} \left[3F^2 \delta_{rs} + a^2 \hat{T}_{rs} \right]}{\| M_e^{(d)}(1+e)\ \mathbf{1} + M_T^{(d)} \dfrac{f_b f_e}{\hat{\mathbf{T}} : \hat{\mathbf{T}}} \left[3F^2\ \mathbf{1} + a^2 \hat{\mathbf{T}} \right] \|} \tag{4.216}$$

can be derived. Note that in [176] www.AN only the special case of an *isotropic stress* $\mathbf{T} = p\ \mathbf{1}$ is considered for which

$$\delta_{ij} L_{ijrs} = L_{iirs} = \frac{f_b f_e}{1/3} \delta_{ij} \left(\delta_{ir}\delta_{js} + a^2 \frac{1}{3}\frac{1}{3} \delta_{ij}\delta_{rs} \right) = 3 f_b f_e \left(\delta_{rs} + a^2 \frac{1}{3} \delta_{rs} \right) \tag{4.217}$$

and therefore $\bar{D}_{rs}$ corresponds to the *isotropic* extension

$$\bar{D}_{rs} = \frac{1}{\sqrt{3}}\delta_{rs}\,. \tag{4.218}$$

in this case.

Modification of f_d to establish consistency

We may now modify the stiffness of the hypoplastic constitutive model in order to make it consistent with the lower bound (4.209) by changing the expression for the density factor f_d.

The required value of $\bar{f}_d = f_d(e_d)$ follows directly from the condition $A^{(d)}(\bar{\mathbf{D}}) = 0$, i.e.

$$M_e^{(d)}\mathrm{tr}\,\bar{\mathbf{D}}\;(1+e) + M_T^{(d)}\mathrm{tr}\,(\mathsf{L}:\bar{\mathbf{D}} + \bar{f}_d\mathbf{N}\|\bar{\mathbf{D}}\|) = 0\,. \tag{4.219}$$

The value of f_d is therefore given by

$$\bar{f}_d \;=\; -\frac{M_e^{(d)}\mathrm{tr}\,\bar{\mathbf{D}}\;(1+e) + M_T^{(d)}\mathrm{tr}\,(\mathsf{L}:\bar{\mathbf{D}})}{M_T^{(d)}\mathrm{tr}\,\mathbf{N}} \tag{4.220}$$

and for the special case $\bar{\mathbf{D}} = \frac{1}{\sqrt{3}}\;\mathbf{1}$, i.e. for the isotropic stress $\mathbf{T} \sim -\;\mathbf{1}$ (as assumed in [176])

$$\bar{f}_d \;=\; -\frac{M_e^{(d)}\sqrt{3}\;(1+e) + M_T^{(d)} f_b f_e \dfrac{3}{\sqrt{3}}(3+a^2)}{M_T^{(d)} f_b f_e 3a} \tag{4.221}$$

This value of the f_d-factor (usually less than zero) applies at $e = e_d$ only. In order to keep the rest of the hypoplastic model intact we replace the expression (2.71) for f_d with the following interpolation rule

$$f_d = \left(\frac{e-e_d}{e_c-e_d}\right)^{\alpha} + \left[1 - \left(\frac{e-e_d}{e_c-e_d}\right)^{\alpha}\right]^{z} \bar{f}_d\,. \tag{4.222}$$

The smoothing factor with exponent $z = 2n+1$ (odd number) turned out to be useful. Despite this precaution the void ratio may *numerically* become smaller than e_d due to large strain increments. Therefore, for a better numerical stability the following interpolation

$$f_d = \mathrm{sign}(e-e_d)\left(\frac{|e-e_d|}{e_c-e_d}\right)^{\alpha} + \left[1 - \mathrm{sign}(e-e_d)\left(\frac{|e-e_d|}{e_c-e_d}\right)^{\alpha}\right]^{z} \bar{f}_d \tag{4.223}$$

can be recommended. The modified expression for f_d applies to $e < e_c$ only.

Fig. 4.47 illustrates the effect of the modification for the extension path that originally goes below the lower bound (left, calculated with the reference model). After the proposed

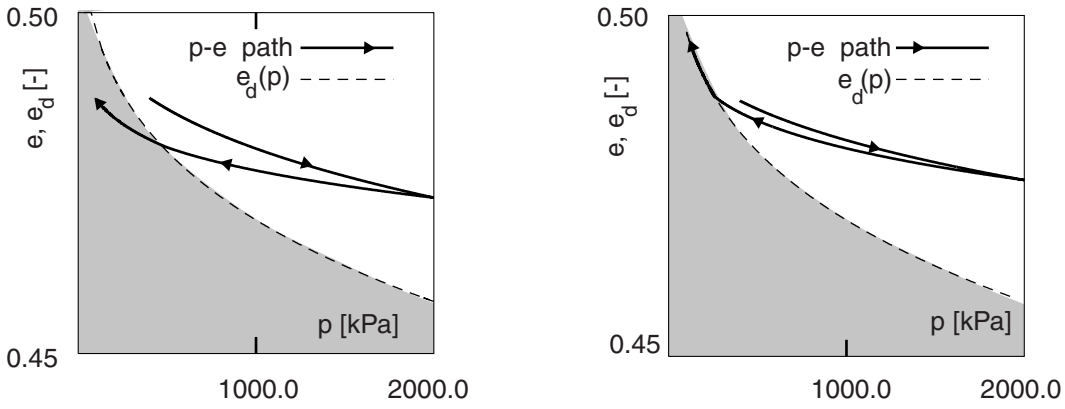

Figure 4.47: (left) Violation of the condition $e \geq e_d$ while decreasing p_s in reference version, (right) the lower bound cannot be surpassed with modified formulation of f_d

modification of scalar f_d the lower bound cannot be surpassed anymore, as it is shown in Fig. 4.47 (right).

Summing up, the response of the reference model has been made consistent with $e_d(\mathrm{tr}\,\mathbf{T})$. It has been achieved preserving the pycnotropy and barotropy functions. The values of the pycnotropy factor f_d are slightly modified in the closest vicinity of $e_d(\mathrm{tr}\,\mathbf{T})$ bound only. The price of this patch, however, may be an unpleasant cyclic accumulation effect at $e = e_d$. For example, since the new f_d for $e = e_d$ does not disappear, a strain cycle with the double amplitude $\Delta\mathbf{D}$ generates a stress accumulation $2f_d\mathbf{N}\|\Delta\mathbf{D}\|$ per cycle. Be warned that after the proposed modification the model responds for $e = e_d$ inelastically ($f_d(e = e_d) \neq 0$), which may cause some unexpected side effects even in one-dimensional strain cycles. For multiaxial loading neither the referential nor the modified model are conservative. For possible improvement see [169] www.AN .

4.4 Explicit model for cyclic accumulation

4.4.1 Introduction

A considerable displacement of structures may be caused by accumulation of the irreversible deformation of soil with load cycles. Even relatively small amplitudes may significantly contribute. This can endanger the long-term serviceability of structures which have large cyclic load contribution and small displacement tolerance (e.g. for a magnetic levitation train). Under undrained conditions similar phenomena may lead to an accumulation of pore water pressure, to soil liquefaction and eventually to a loss of overall stability. From the practical point of view this is therefore an important problem. However, the reference hypoplastic model performs poorly in such accumulations and needs

modification or extension. Although the introduction of intergranular strain removes the severe problem of ratcheting, this version is not precise enough for a big number of cycles. We propose an extension to hypoplasticity for cyclic loading based on a so-called *explicit* formulation.

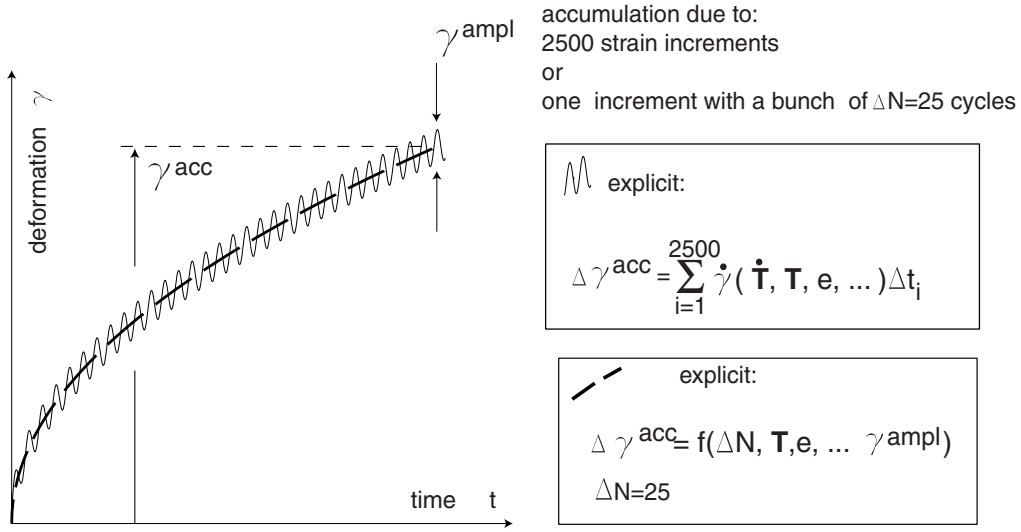

Figure 4.48: Cumulative models (explicit models or N-type models) describe only the main tendency of strain accumulation without following each cycle in detail

From a physical point of view, displacements due to cyclic loading are rather difficult to describe. They depend strongly on several subtle properties of state (distribution of grain contact normals, arrangement of grains) which cannot be expressed by the customary state variables (stress and void ratio) only. Such hidden structural variables are difficult to assess. From a numerical point of view, two computational strategies can be considered: an implicit and an explicit one (time integration is not meant here).

Explicit [5] or *N-type* [210] models are similar to creep laws in which in place of time the number N of cycles is used. Therefore in this Section 4.4 rates are understood in terms of the number of cycles, i.e., $\dot{\sqcup} = \mathrm{d}\sqcup/\mathrm{d}N$. Generally, explicit models can be seen as special-purpose constitutive relations that are thought to predict the accumulation due to a bunch of cycles at a time. For example, for $\Delta N = 25$ cycles of amplitude $\gamma^{\mathrm{ampl}} = 0.0001$ we have a direct formula to find the resulting irreversible strain (both the magnitude and direction), see Fig. 4.48.

Estimation of the accumulation rate $\mathbf{D}^{\mathrm{acc}} = \mathrm{d}\boldsymbol{\epsilon}^{\mathrm{acc}}/\mathrm{d}N$ due to a bunch (package) of strain cycles $\mathrm{d}N$ of a given strain amplitude and at a given average stress $\mathbf{T}^{\mathrm{av}}$ can be found experimentally. In order to use explicit models we define a cycle as a repeatable sequence of applications and removals of loads. For each state variable $\sqcup$ we define its *average* value $\sqcup^{\mathrm{av}}$ upon a cycle in such way that $\sqcup^{\mathrm{av}}$ is the centre of the smallest sphere that

encompasses all states $\sqcup$ of a given cycle. The average value $\sqcup^{\mathrm{av}}$ should not be mixed up with the *mean* value $\frac{1}{n}\sum_{i=1}^{n}\sqcup^{(i)}$. The amplitude is defined as $\sqcup^{\mathrm{ampl}} = \max \| \sqcup - \sqcup^{\mathrm{av}} \|$. A more elaborated definition of amplitude (including polarization and openness of the strain loop) is proposed in Section 4.4.5.

The recoverable (resilient) part of the deformation is calculated in explicit models in a conventional way (using many strain increments per cycle) in order to estimate the amplitude. Having the amplitude we assume that it remains constant over a number of the following cycles. The permanent (residual) deformation due to packages of cycles is calculated with special empirical formulas.

Numerous explicit constitutive models proposed in the literature [8,22,65,95,112,132,145, 146,189,212,227,228,230,257,261] are usually strongly simplified because cyclic tests are much more laborious than the conventional ones and it is difficult to collect a sufficient amount of experimental data. The authors have often very specific applications and very special kinds of loading in mind, e.g., considering volumetric accumulation, constant average stress $\mathbf{T}^{\mathrm{av}}$, linear amplitudes only (in general the openness and the polarization of strain loop may be of importance). In the following subsections an explicit model presented by Sawicki [213,214] will be extended and implemented to hypoplasticity.

Implicit constitutive models are general-purpose relations which reproduce each single load cycle by many (say 100) small strain increments. The accumulation of stress or strain appears as a by-product of this calculation, resulting from the fact that the loops are not perfectly closed. Implicit strategies require much computation time and magnify systematic errors. For example, 100000 cycles with 100 increments per each cycle increase systematic errors 10^7-times! This requires a constitutive model of unreachable perfection. These as well as some other numerical problems discussed in [166] www.AN , see also Fig. 4.49, speak for the application of an explicit strategy, especially if the number of cycles is large. Therefore, despite obvious advantages of implicit formulations (flexibility, elegance) we have to resort to explicit or so-called *semi-explicit* algorithms. In 'semi-explicit' models the cyclic pseudo-creep[20] procedure is interrupted by so-called *control cycles* calculated implicitly. Such cycles are useful to check the admissibility of the stress state, the overall stability (which may be lost if large pore pressures are generated) and, if necessary, to modify the load amplitude (it may change due to a stress redistribution).

Note that the term *accumulation* is a convenient general notion that expresses both cyclic pseudo-relaxation and cyclic pseudo-creep. In fact both of them are just different manifestations of the same phenomenon. If stress cycles are applied we observe cyclic pseudo-creep and if strain cycles are applied we obtain cyclic pseudo-relaxation. It is thus natural to

[20] We reserve the terms 'creep' and 'relaxation' for spontaneous, i.e. thermally activated phenomena.

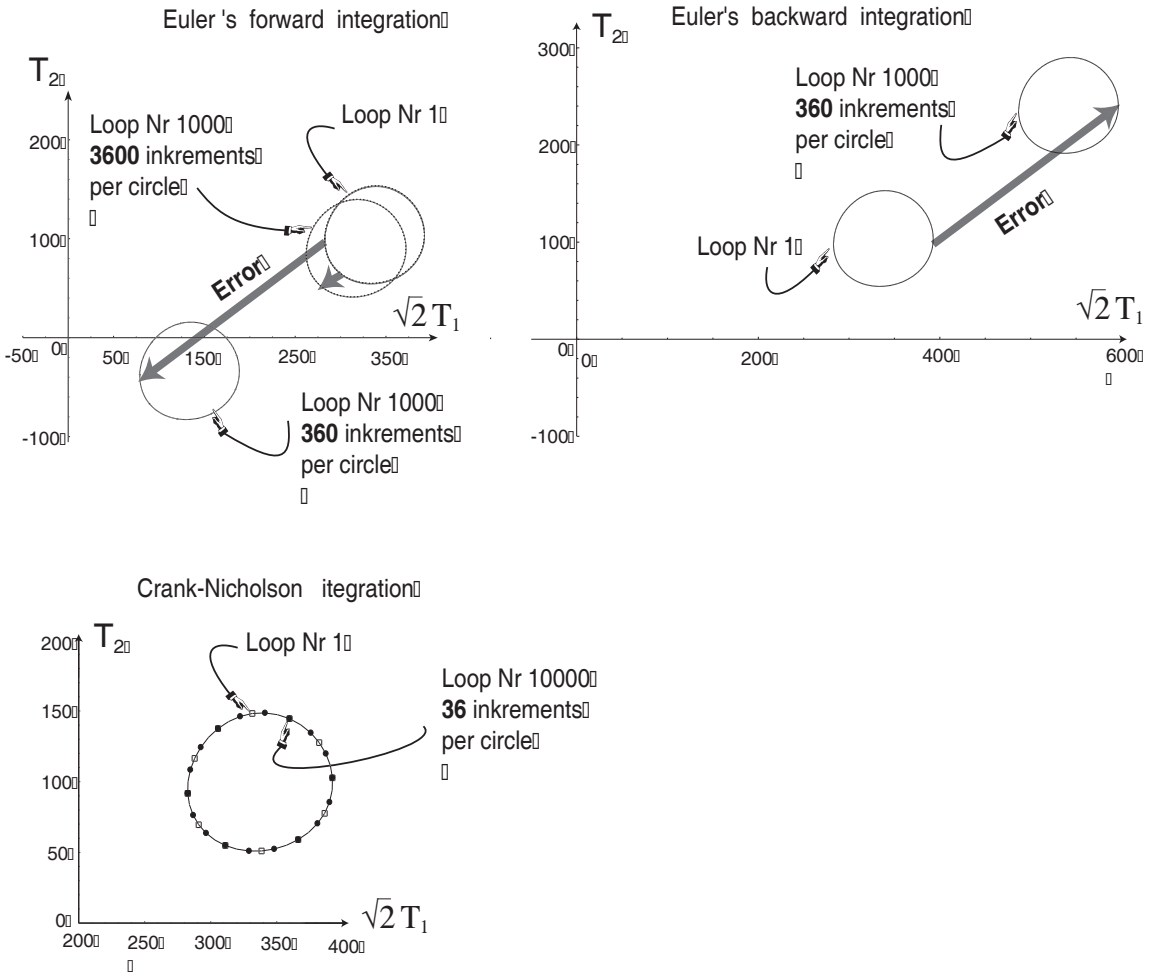

Figure 4.49: Using Euler forward or Euler backward integration scheme produces numerical errors that are accumulated. This 'numerical accumulation' may in some cases exceed the physical one and falsify the results.

speak of accumulation (a physical phenomenon) independently of its appearance in the test, i.e., independently of the technical aspect of how the experiment was controlled. Moreover, many testing devices allow for mixed control so pseudo-relaxation and pseudo-creep occur simultaneously but in different directions.

In saturated and poorly drained soils an immediate settlement occurs due to the deviatoric accumulation only. Instead of volumetric deformation we observe, at first, an increase of pore-water pressure. Later, however, displacements due to volumetric deformation occur (during the consolidation process) and the previously built up pore pressures are dissipated. The increase of pore pressures preceding reconsolidation is a dangerous phenomenon which may reduce considerably the bearing capacity of a foundation and can eventually lead to progressive failure, liquefaction, cyclic mobility etc.

4.4.2 Sawicki's explicit model for cyclic accumulation

Sawicki and Świdziński [213, 214] basing on experimental results from their simple shear device, proposed for the cyclic accumulation of deformation a purely volumetric accumulation rule

$$\epsilon_{ij}^{\mathrm{acc}} = -\frac{1}{3}\epsilon^{\mathrm{acc}\ v}\delta_{ij}, \tag{4.224}$$

in which the volumetric strain was described by a so-called 'universal densification curve'

$$\epsilon^{\mathrm{acc}\ v} = C_1 \ln\left[1 + C_2\tilde{N}\right], \quad \text{with} \quad \tilde{N} = \frac{1}{2}\|\boldsymbol{\epsilon}^{*\ \mathrm{ampl}}\|^2 N\,. \tag{4.225}$$

$C_1(e_0), C_2(e_0)$ are parameters related to the initial void ratio e_0, and $\tilde{N}$ is the number of cycles N scaled with the square of the deviatoric strain amplitude $\frac{1}{4}(\gamma^{\mathrm{ampl}})^2 = \frac{1}{2}\|\boldsymbol{\epsilon}^{*\ \mathrm{ampl}}\|^2$. According to Ko and Scott [115] who performed tests with an isotropic change of stress, the influence of the amplitude of volumetric strain can be neglected. Therefore, in agreement with Sawicki, we always calculate the strain amplitude from the deviatoric deformation, also if the tensorial definition (proposed in Eq. (4.235)) is used.

For fine, medium dense ($I_D = 0.65$) Lubiatowo sand they obtained $C_1 = 0.008970$ and $C_2 = 69400.0$ [213]. Strictly speaking, the original notion of 'densification' proposed by Sawicki [213, 214] is slightly different than the irreversible volumetric strain used in (4.225). However, this simplification preserves all merits of the original formulation.

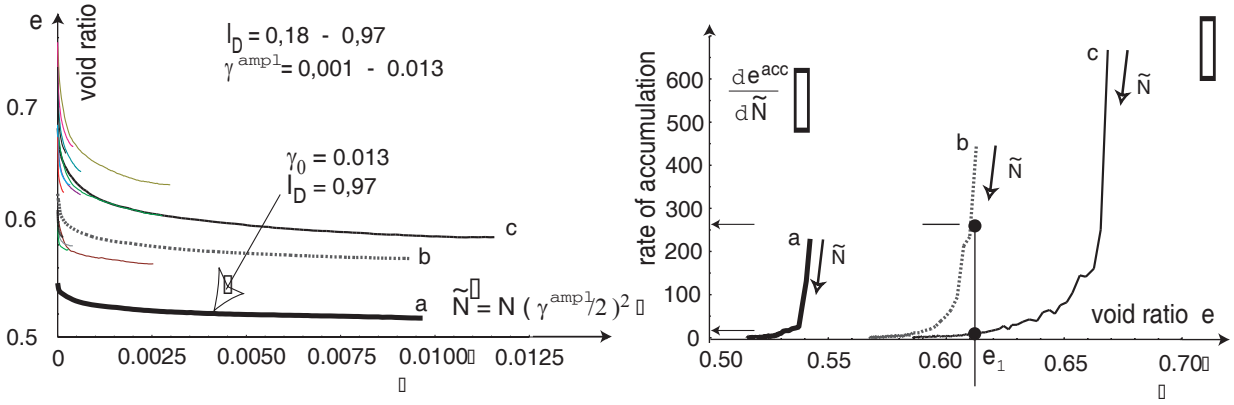

Figure 4.50: Reinterpreted results from [213] demonstrate clearly that the rate of cyclic accumulation of volumetric deformation ($\partial e^{\mathrm{acc}}/\partial\tilde{N}$) in two samples (b) and (c) in the simple shear apparatus may be quite different although the vertical stress, void ratio (e_1) as well as the applied load cycles were identical

The procedure of the explicit algorithm is quite simple:

1. Calculate the initial stress state (from self weight and all dead loads) using an elastic model.

2. Calculate incrementally (implicitly) the first cycle. For this purpose we must apply and then remove all traffic (and similar) loads which are expected to appear repeatedly. The resulting strain path must be memorized for the future evaluation of the strain amplitude at each FE integration point. Elastic, or hyperelastic model (here by Vermeer [255]) can be used. We assume further that this amplitude remains constant over subsequent cycles.

3. Estimate the strain amplitude at each integration point from the stored strain path. The size of the strain path will be needed in the explicit calculation of pseudo-creep.

4. Find the rate of strain accumulation using incremental form of (4.225)

$$\mathbf{D}^{\mathrm{acc}} = \frac{1}{3}\,\mathbf{1}\frac{\partial \epsilon^{\mathrm{acc}\ v}}{\partial N} \tag{4.226}$$

wherein $\mathbf{D}^{\mathrm{acc}} = \dfrac{\partial \boldsymbol{\epsilon}^{\mathrm{acc}}}{\partial \tilde{N}}\dfrac{\partial \tilde{N}}{\partial N} = \dfrac{\partial \boldsymbol{\epsilon}^{\mathrm{acc}}}{\partial \tilde{N}}\dfrac{1}{2}\|\boldsymbol{\epsilon}^{*\ \mathrm{ampl}}\|^2$. One should remark that Sawicki eliminated $\tilde{N}$ from (4.225) combining (4.225) with its rate form. Having the $\tilde{N}$-derivative of (4.225) we may indeed eliminate $\tilde{N}$ as follows

$$\frac{\partial \epsilon^{\mathrm{acc}\ v}}{\partial \tilde{N}} = C_1\frac{C_2}{1+C_2\tilde{N}} = C_1C_2\exp(-\frac{\epsilon^{\mathrm{acc}\ v}}{C_1}). \tag{4.227}$$

This mathematical manipulation, however, does not remove the basic physical problem of the method related to the initial value of $\tilde{N}$ (see discussion below).

5. Find the stress increment due to $\Delta t = \Delta N$

$$\Delta T_{ij} = E_{ijkl}(D_{kl} - D^{\mathrm{acc}}_{kl})\Delta t\ . \tag{4.228}$$

and redistribute the stress in the course of equilibrium iteration, which finally results in settlements/displacements.

Discussion

The advantage of the model lies in its simplicity. The essential phenomenon of volumetric accumulation (especially important for pore pressure generation and soil liquefaction) is well described and the model may be used in both drained and undrained cases as shown in numerous applications to BVPs, e.g. [212–215, 231]. The Miner's rule [154] is obeyed because cycles with large and small amplitudes are all converted to 'normalized' increments $\Delta\tilde{N}$. According to (4.225) a sequence in which they are applied is meaningless because the final result depends only on the sum $\tilde{N}$. In BVPs with slow pore pressure

dissipation the *true rate* ($\mathrm{d}\tilde{N}/\mathrm{d}t$) of application of cycles may become important and so may the sequence packages of cycles.

An interesting problem, not addressed by Sawicki, is the determination of the initial value $\tilde{N}_0$ which, according to (4.226), is the only variable that dictates the rate of accumulation ($\mathrm{d}e/\mathrm{d}\tilde{N}$). As shown in Fig. 4.50 the rate of densification is not unique for a given void ratio e so no correlation between $\tilde{N}_0$ and e is possible. The fact that Sawicki eliminated the global value $\tilde{N}$ using the rate form (4.227) does not eliminate the problem. The question can be re-stated: what is the initial value $\epsilon_0^{\mathrm{acc}\ v}$? Sawicki commences his calculations with $\epsilon_0^{\mathrm{acc}\ v} = 0$ which corresponds to the initial state in the direct shear test from which C_1 and C_2 were found. Therefore we may presume that freshly pluviated state corresponds to $\tilde{N} = 0$ or equivalently to $\epsilon^{\mathrm{acc}\ v} = 0$ in his model. However, dealing with BVPs in situ, one may need initial values $\epsilon_0^{\mathrm{acc}\ v} \neq 0$ and their determination may be troublesome. As demonstrated in Fig. 4.50, two samples (b) and (c) under equal vertical pressure and with the same void ratio e_1 may have quite different rates of accumulation, depending on their history of deformation. In order to determine $\tilde{N}_0$ or $\epsilon_0^{\mathrm{acc}\ v}$ we need some additional characteristics of soil (not only density), responsible for resistance to further densification. This problem is not trivial and some attempts to correlate $\epsilon_0^{\mathrm{acc}\ v}$ with dynamic soil properties are briefly reported in Section 4.4.5.

Considering Fig. 4.50 one may ask if observations from a simple shear apparatus are sufficient to conclude about strong structural effects in repeatedly loaded soil. This apparatus has several defects [26, 27] and it is possible that the slowdown of densification is caused by an increase of horizontal stress components. Unfortunately, these components were not measured in experiments. It is possible that such increase could strengthen the arching of grains and thus hamper the process of densification.

In order to eliminate the uncontrolled increase of horizontal stress, cyclic tests should be performed in a triaxial apparatus. Three such tests are compared in Fig. 4.51. They confirm the observation from the simple shear device that stress and void ratio alone indeed do not suffice to tell the rate of densification per cycle. Samples of the same sand with the same average stress $\mathbf{T} = \mathrm{const}$ and void ratio e may have different rates of densification $\dot{e}$. The fact that a sample was cyclically preloaded considerably decreases the rate of compaction, compared to the one during the first several thousands cycles applied to a freshly pluviated sample of the same density. In the following some modifications to Sawicki's model are proposed in order to account for new experimental observations.

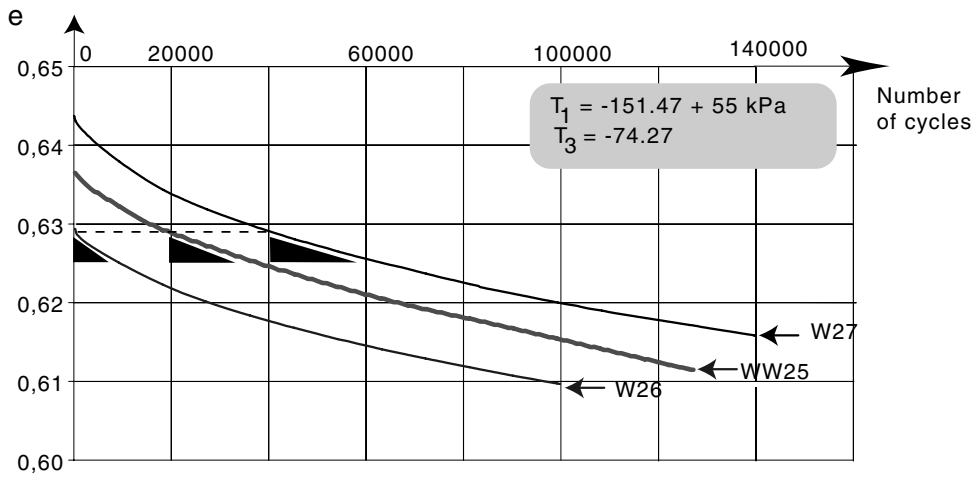

Figure 4.51: Cyclic triaxial tests confirm the observation that stress and void ratio alone are not sufficient to determine the rate of densification. Three good quality 100×200 mm samples: W27, WW25 and W26 of fine ($d_{50} = 0.17$ mm) uniform sand were prepared to three slightly different void ratios e and subjected to a large number of stress cycles. For a given void ratio (e.g. $e = 0.63$) the initially loosest sample W27 (compacted under repeated loading) has a smaller slope (rate of densification) than the initially dense sample W26 (pluviated to have smaller e). In other words, the densification rate at a given e is significantly lower if a sample was cyclically preloaded

4.4.3 A modified Sawicki model

Numerical calculations as well as experimental data from numerous cyclic triaxial tests only partly confirmed the assumptions of the Sawicki's model. In particular the following observations have been made:

1. The rate of strain accumulation $\mathbf{D}^{\mathrm{acc}}$ is not purely volumetric and significant deviatoric accumulation can be observed, see e.g. [228]. Judging by the triaxial compression tests [260], the direction of accumulation is well described by the flow rule taken from the hypoplastic model, viz.

$$\mathbf{D}^{\mathrm{acc}} \sim \mathbf{m} = -\vec{\mathbf{B}}\,, \tag{4.229}$$

see Fig. 4.52. In particular, for $\mathbf{T}^{\mathrm{av}}$ above the critical stress obliquity M_c the void ratio can increase! Therefore the stress path obtained from (4.228) cannot surpass the limit surface in the course of a pseudo-relaxation process. The direction of the accumulation in samples tested in [260] did not depend on the void ratio. However, at the density limit $e = e_d$ densification must be expected to vanish [74]. Incorporation of deviatoric accumulation into FE calculation decisively increases the predicted settlements.

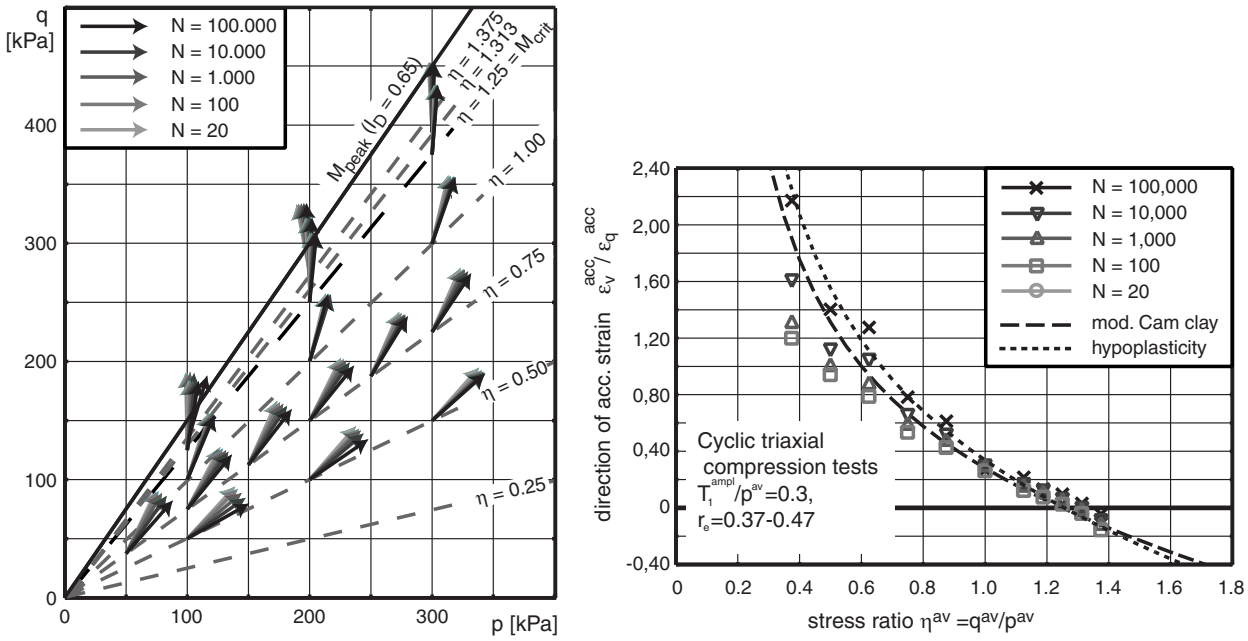

Figure 4.52: Strain ratio $\omega = \operatorname{tr}\mathbf{D}^{\mathrm{acc}}/(\sqrt{\frac{2}{3}}\|\mathbf{D}^{*\mathrm{acc}}\|)$ as a function of average stress inclination $\eta^{\mathrm{av}} = q^{\mathrm{av}}/p^{\mathrm{av}}$ for different numbers of cycles N (all tests at: $p^{\mathrm{av}} = 200$ kPa, $T_1^{\mathrm{ampl}}/p^{\mathrm{av}} = 0.30$, $0.57 \leq I_{D,1} \leq 0.67$), after [260]

2. The accumulation rate depends on the square of the strain amplitude, i.e. it is the accumulation rate and not the number of cycles N what should be scaled by the square of the strain amplitude. We have $\epsilon^{\mathrm{acc}}(n\epsilon^{\mathrm{ampl}}, N \dots) = n^2\epsilon^{\mathrm{acc}}(\epsilon^{\mathrm{ampl}}, N, \dots)$. The function $\epsilon^{\mathrm{acc}}(\tilde{N}, \dots)$ wherein $\tilde{N} = (\gamma^{\mathrm{ampl}})^2 N$ was found to be non-unique in the triaxial tests, see Fig. 4.53a and 4.53b.

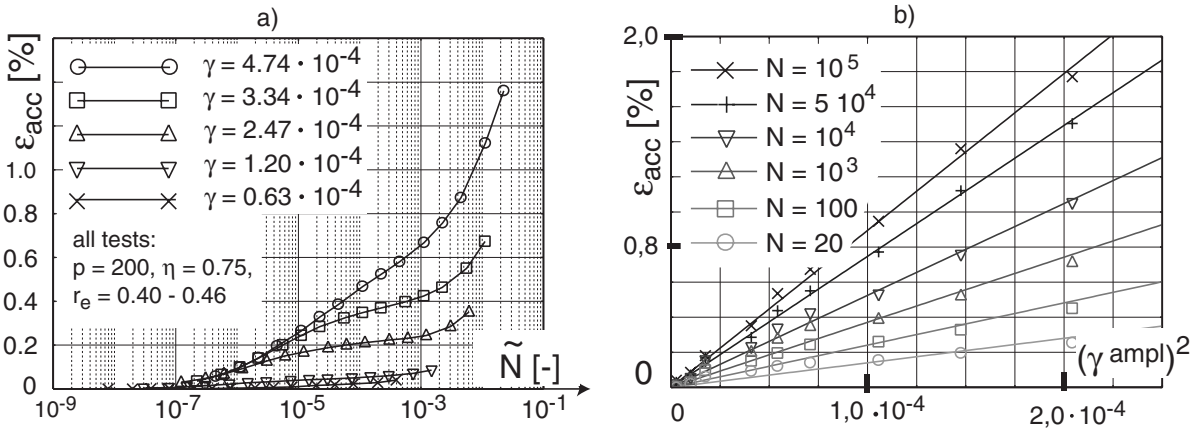

Figure 4.53: (a) Discrepancy from 'universal densification curve' in triaxial tests; (b) Accumulation as a second order homogeneous function of strain amplitude, after [178].

3. The rate of accumulation measured in triaxial tests increases strongly with the stress

ratio $\eta = q/p$, especially if η is close to M_c. This dependence can be described using the the yield function y_{M-N} given in (2.62). Defining

$$\bar{Y} = \frac{Y - 9}{Y_c - 9} \quad \text{with} \quad Y = -\frac{I_1 I_2}{I_3} \quad \text{and} \quad Y_c = \frac{9 - \sin^2\varphi}{1 - \sin^2\varphi} \tag{4.230}$$

the observed accumulation rate increases according to

$$f_Y = \exp(C_4 \bar{Y}^2) \quad \text{with} \quad C_4 \approx 2\,. \tag{4.231}$$

This result is based on about twenty triaxial compression tests and may need modifications if more experimental data is available. In the literature [34, 260] one may find results confirming that the volumetric accumulation depends on stress obliquity.

4. The dependence $\mathbf{D}^{\text{acc}}(p, e)$ of the accumulation rate on pressure p and on void ratio e cannot be described collectively as $\mathbf{D}^{\text{acc}}(r_e)$ using relative density r_e given in (2.41). Keeping r_e = const the rate of cyclic accumulation was observed to be almost proportional to p^{-1} (for $N = 10^5$), i.e. $\mathbf{D}^{acc}$ decreases(!) with p. This means that the critical state line $e_c(p)$ usually described by inclination λ in $e - \log p$ diagram does not apply to pairs (p, e) of identical rate of accumulation [178]

5. Within the scope of the testing program reported in [260] the accumulation does not decrease logarithmically, as in Sawicki's model, but along with

$$f_N \;=\; C_{N1}\;\ln\left(1 \;+\; C_{N2}\;N\right) \;+\; C_{N3}\;N\,. \tag{4.232}$$

Fig. 4.54 shows that the formula for f_N with the additional term $C_{N3}\;N$ sufficiently well approximates the experimental data.

6. The initial stress state should not lie outside a limit cone. Therefore instead of linear elastic estimation of the initial stress one should use the hypoplastic model with intergranular strain as described in Section 4.1. This model can also be used for implicit calculation of the first cycle in order to estimate the amplitude[21]. The amplitudes predicted by hypoplasticity (with intergranular strain extension) were close to the measured ones. An extensive discussion on the amplitude is given in Section 4.4.5. Since the rate and the direction of accumulation strongly depends on stress obliquity $\hat{\mathbf{T}}$ and on the void ratio it is advisable to interrupt cyclic pseudo-creep process and to calculate implicitly the actual strain amplitude. Such implicit calculations are termed 'control cycles'.

[21] Actually the first two cycles should be calculated. The first (so-called irregular) cycle is very much different from all subsequent ones and is not suitable for estimation of the representative strain amplitude. The second cycle (= first regular cycle) provide much more reliable information. The accumulation from implicit calculation of the first two cycles is added to the accumulation from explicit calculation.

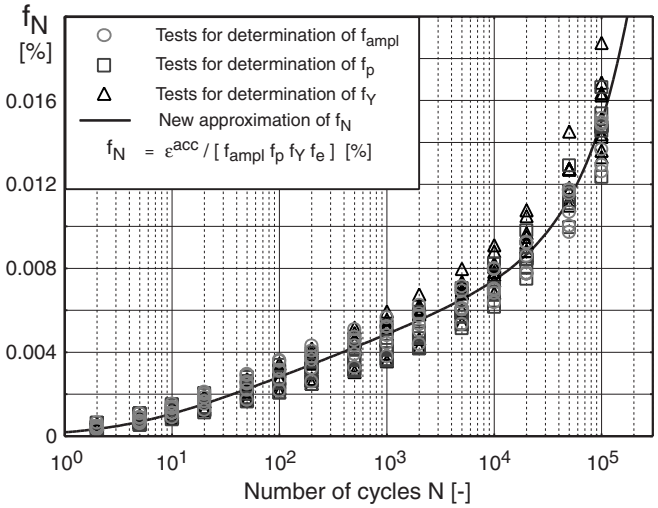

Figure 4.54: Accumulated strain ε^{acc} as a purified function of the number of cycles, i.e. influences of factors f_{ampl}, f_p, f_Y and f_e have been removed.

Function	Material constants	
$f_{\text{ampl}} = \left(\frac{\gamma^{\text{ampl}}}{\gamma^{\text{ampl}}_{\text{ref}}}\right)^2$	$\gamma^{\text{ampl}}_{\text{ref}}$	10^{-4}
$\dot{f}_N = \frac{C_{N1}C_{N2}}{(1 + C_{N2}\ N)} + C_{N3}$	C_{N1}	$8.26 \cdot 10^{-6}$
	C_{N2}	0.240
	C_{N3}	$7.04 \cdot 10^{-5}$
$f_p = \exp\left[-C_p \left(\frac{p^{\text{av}}}{p_{\text{atm}}} - 1\right)\right]$	C_p	0.5
$f_Y = \exp\left(C_Y\ \bar{Y}^{\text{av}}\right)$	C_Y	2.05
$f_e = \begin{cases} 1 & \text{for } e < C_{e2} \\ 1 + C_{e1}\ (e - C_{e2}) & \text{for } e \geq C_{e2} \end{cases}$	C_{e1}	65
	C_{e2}	0.616
$f_\pi = 1 + C_{\pi 1} - \left[1 - (\vec{\mathsf{A}}_\epsilon :: \boldsymbol{\pi})^{C_{\pi 2}}\right]$	$C_{\pi 1}$	5.5
	$C_{\pi 2}$	0.2
$\dot{\pi} = C_{\pi 3}(\vec{\mathsf{A}}_\epsilon - \boldsymbol{\pi})\|\mathsf{A}_\epsilon\|^2$	$C_{\pi 3}$	1250

Table 4.2: Approximation functions for modified explicit accumulation model

Summing up, according to the current laboratory tests [178,260] the rate of accumulation can be approximated as follows

$$\mathbf{D}^{\text{acc}} = \mathbf{m} f_{\text{ampl}}\ \dot{f}_N\ f_p\ f_Y\ f_e\ f_\pi \tag{4.233}$$

The functions $f_{\text{ampl}}, f_N, f_p, f_Y, f_e, f_\pi$ describe the influence of strain amplitude γ^{ampl}, the number of cycles N, the average stress $p^{\text{av}}, \bar{Y}^{\text{av}}$, the void ratio e, the cyclic strain history and the shape of the strain loop. Function f_π is discussed further in this subsection.

Algorithm

The solution algorithm is similar to the one presented in Section 4.4.2.

1. Calculate the initial stress state (from self weight and all dead loads) using the hypoplastic model with intergranular strain.
2. Perform implicitly two first load cycles using the hypoplastic model and with the intergranular strain and recording the strain path of the second one.
3. Estimate the strain amplitude using the strain path
4. Find the accumulation rate $\mathbf{D}^{\mathrm{acc}}$ using the incremental form (4.233)
5. Find the stress increment due to a bunch of $\Delta N = \Delta t$ cycles

$$\Delta \mathbf{T} = \mathsf{L} : (\mathbf{D} - \mathbf{D}^{\mathrm{acc}})\Delta t \tag{4.234}$$

The FE program redistributes stress in the course of equilibrium iteration, which depending on the BVP results in settlements, horizontal displacements or pseudo-relaxation. The Jaumann terms must be added.

Amplitude of strain for multiaxial loading

An important element of explicit description of the accumulation phenomenon is the shape (openness) of the strain cycle. For example, a twirled multiaxial strain loop that encloses some volume in the strain space causes larger accumulation than a one-dimensional cycle of the same *scalar* amplitude. A need of a generalized amplitude definition appears also in fatigue problem for metals, cf. Ekberg [59] and Papadopoulos [188]. In Fig. 4.55a a circular strain path with a diameter (size) $8 \cdot 10^{-3}$ is shown to generate 2.5 times larger accumulation than an uniaxial strain path of the same size. In order to consider the openness and the complexity of the stress loop a novel definition is proposed here. It is assumed to be a fourth rank dyadic tensor that considers the shape and the orientation (polarization) of the strain loop.

Another phenomenon shown in Fig. 4.55b, is a sudden change of the orientation of the plane in which the cycles are performed. It turns out that such change increases the rate of accumulation. This effect is described in the following using a so-called 'back polarization' tensor. The results shown in Fig. 4.55 were obtained from a cyclic multiaxial direct simple shear (CMDSS) device shown in Fig. 4.56. The sample is initially placed in a rubber membrane laterally supported by the aluminium rings. The sample is closed

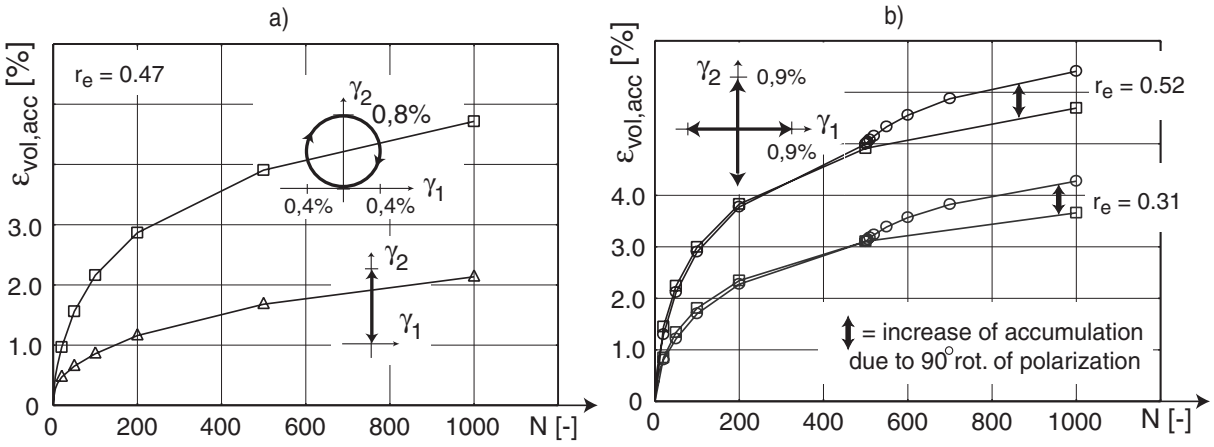

Figure 4.55: Rate of accumulation influenced by a) shape of the strain loop; b) rapid change of polarization, after [178]

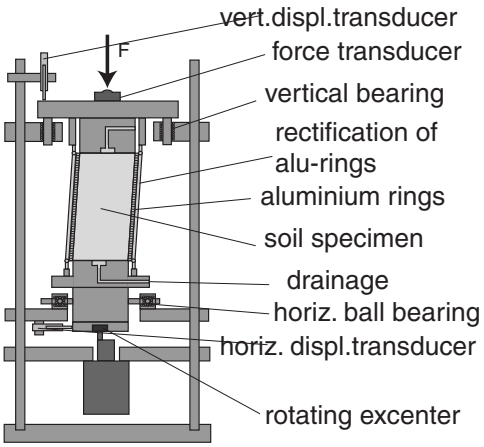

Figure 4.56: Construction of the cyclic multiaxial direct simple shear (CMDSS) device, after [178]

by two end plates and vertically loaded from the top. The upper plate may move only vertically and the lower plate may move horizontally (in both directions). A biaxial shear amplitude, i.e. the movement of the lower plate to both sides, may be chosen using eccentricity of coupling between the plate and an electric engine rotating at 0.5 Hz. The rings are coupled with each other in order to distribute equally the deformation along the height. The accumulation is measured as the settlement of the upper plate.

Uniaxial cycles can be described by $\boldsymbol{\epsilon} = \boldsymbol{\epsilon}^{\mathrm{av}} + \boldsymbol{\epsilon}^{\mathrm{ampl}} f(t)$ where $\boldsymbol{\epsilon}^{\mathrm{ampl}} = \mathrm{const}$ is a kind of tensorial amplitude (a better definition is given below) and $f(t)$ is a scalar parametrization, for example, $f(t) = \sin \omega t$. The multiaxial tensorial amplitude A_ϵ is defined as a combination of spheres that encompass several specially chosen projections of the strain path (loop) in six dimensional strain space.

Suppose that we are given a single strain loop in form of the strain path consisting

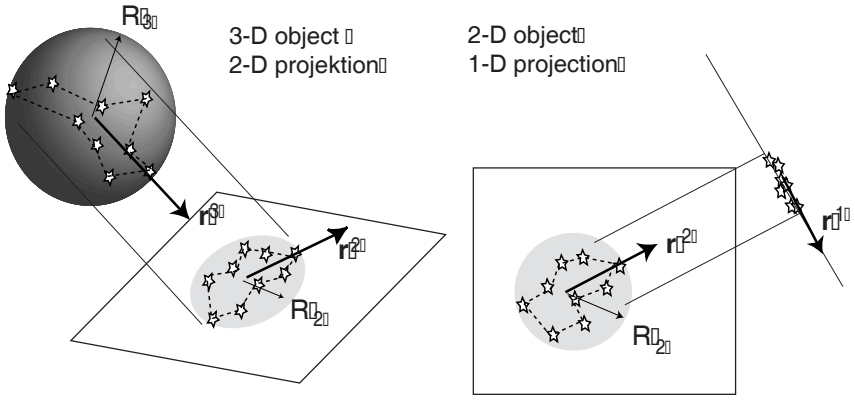

Figure 4.57: The directions $\mathbf{r}_i$ and the sizes R_i of the strain loop amplitude

of a sequence of discrete strain points $\boldsymbol{\epsilon}(t_i)$, $i = 1, \ldots, N$ distributed along the strain loop (this loop need not be closed) at an FE integration point of interest. These strain states lie in a 6-d strain space and may need not be coaxial (so we cannot consider the problem in the space of principal strains). Note that rotation of the principal directions of strain also generates a loop. Since we are interested merely in the strain amplitude, the state at the first point on the strain loop ($i = 1$) may be assumed to be undeformed and the strain tensors may be calculated with respect to this configuration. The strain amplitudes we have in mind are about 0.001 so any definition of strain can be used. The following flow chart demonstrates how to calculate the subsequent projections, their radii and perimeters. The upper index indicate the number of dimensions of the strain space which need to be considered.

1. Calculate the deviatoric projection $\mathbf{e}^5(t_i) = \boldsymbol{\epsilon}(t_i) - \frac{1}{3}\mathbf{1}\mathrm{tr}\,\boldsymbol{\epsilon}(t_i)$ of the strain points $\boldsymbol{\epsilon}(t_i)$. For soils it was observed that only the deviatoric part of strain amplitude influences the process of cyclic relaxation or cyclic creep[22]. The space in which $\mathbf{e}^5(t_i)$-path could be drawn has 5 dimensions because the deviator of symmetric 3×3 tensor has 5 independent components.

2. Calculate the perimeter $P_5 = \sum_{i=1}^{N} \|\mathbf{e}^5(t_i) - \mathbf{e}^5(t_{i-1})\|$ of the loop[23] wherein N denotes the number of strain states (points) used to record the loop.

3. Find the average point $\mathbf{e}^5_{\mathrm{av}}$ and the radius R_5 of the smallest 5-d sphere $\|\mathbf{e}^5 - \mathbf{e}^5_{\mathrm{av}}\| = R_5$ that encompasses the loop[24].

4. Calculate the unit tensor $\mathbf{r}^5$ along the line that connects the average strain $\mathbf{e}^5_{\mathrm{av}}$ with

[22] Usage of the deviatoric portion of strain is not an essential assumption. An analogous procedure can be easily formulated starting from the 6-dimensional strain path $\boldsymbol{\epsilon}^6(t_i)$

[23] Define $\mathbf{e}^5(t_0) = \mathbf{e}^5(t_N)$ to close the loop.

[24] We may do it numerically using $\mathbf{e}_g = \frac{1}{N}\sum_{i=1}^{N} \mathbf{e}^5(t_i)$ as the first approximation of $\mathbf{e}^5_{\mathrm{av}}$.

the most distant point $\mathbf{e}^5(t_i)$ of the loop. Usually there are two equally distant points (antipodes). In case of more than two equally distant points choose anyone of antipodes.

5. Project the loop onto the plane perpendicular to $\mathbf{r}_5$ calculating $\mathbf{e}^4(t_i) = \mathbf{e}^5(t_i) - \mathbf{r}^5 : \mathbf{e}^5(t_i)\mathbf{r}^5$.

6. Find the perimeter $P_4 = \sum_{i=1}^{N} \|\mathbf{e}^4(t_i) - \mathbf{e}^4(t_{i-1})\|$.

7. Find the average point $\mathbf{e}^4_m$ and the radius R_4 of the smallest 4-d sphere $\|\mathbf{e}^4 - \mathbf{e}^4_{\rm av}\| = R_4$ that encompasses the 4-d projection of the loop.

8. Analogously find the unit tensor $\mathbf{r}_4$ and the projection $\mathbf{e}^3(t_i) = \mathbf{e}^4(t_i) - \mathbf{r}^4 : \mathbf{e}^4(t_i)\mathbf{r}^4$. Using the new projection find $R_3, P_3, \mathbf{r}_3$ and then $R_2, P_2, \mathbf{r}^2$ and $R_1, P_1, \mathbf{r}^1$.

Reduction steps from the 3-dimensional path to the 1-dimensional path are shown in Fig. 4.57.

For any D-dimensional sub-space $\mathbf{e}^D$ is preserved in full tensorial (3×3) form. Doing this, the conventional definition of the distance, $R = \sqrt{[e_{ij} - e^{\rm av}_{ij}][e_{ij} - e^{\rm av}_{ij}]}$, remains insensible to the choice of the coordinate system.

After a series of projections a list of amplitudes R_D, perimeters P_D and orientations $\mathbf{r}^D$ is calculated with dimensions $D = 1 \dots 5$. The orientations are all mutually perpendicular $\mathbf{r}^i : \mathbf{r}^j = \delta_{ij}$. The inequalities $R_D \geq R_{D-1}$, $P_D \geq P_{D-1}$ and $P_D \geq 4R_D$ hold. Moreover, if $P_D = 4R_D$ then $R_j = 0$ for all $j < D$. The sense of the orientation $\mathbf{r}^D$ must not enter the definition of the amplitude. Therefore the dyadic products $\mathbf{r}^D\mathbf{r}^D$ are used and their weighted sum:

$$\mathsf{A}_\epsilon = \frac{1}{4}\sum_{D=1}^{5} P_D \mathbf{r}^D\mathbf{r}^D \tag{4.235}$$

is proposed to be the definition of the amplitude. The unit amplitude

$$\vec{\mathsf{A}}_\epsilon = \mathsf{A}_\epsilon / \|\mathsf{A}_\epsilon\| \tag{4.236}$$

is further called *polarization*. Let the package of cycles with the amplitude $\mathsf{A}_\epsilon{}^1$ be directly followed by another one with $\mathsf{A}_\epsilon{}^2$. If $\vec{\mathsf{A}}_\epsilon{}^1 :: \vec{\mathsf{A}}_\epsilon{}^2 = 1$, the polarizations are identical and no additional increase of accumulation rate should appear. However, if $\vec{\mathsf{A}}_\epsilon{}^1 :: \vec{\mathsf{A}}_\epsilon{}^2 = 0$, the polarizations are perpendicular to each other. In such case the rate of accumulation (cyclic creep/relaxation) should be increased.

Function f_π

This section presents the current development of a new model for explicit calculation of cyclic accumulation. It should be considered as a draft proposition to be supported by reliable experimental data in future. As suggested by the experimental observation presented in Figs. 4.63 and 4.64 the deformation history should be described more precisely and cannot be lumped together into a single scalar variable $\tilde{N}_0$. The adaptation to cyclic loading should take into account the anisotropy of soil structure dictated by the polarization of strain during preloading. The degree of adaptation to a given bundle of cycles is proposed to be dependent on back polarization $\boldsymbol{\pi}$ corresponding to the recent value of $\vec{\mathsf{A}}_\epsilon$. It accounts for the the difference between the current and recent polarization of cycles.

The underlying hypothesis is that rapid changes in the polarization go together with an increased accumulation rate. This can be interpreted as a lack of adaptation. Process of adaptation manifests itself as a slow-down of the accumulation $\boldsymbol{\pi} \to \vec{\mathsf{A}}_\epsilon = \text{const}$.

The increased rate of accumulation gradually declines if the applied cycles and the average stress remain constant. This behaviour can be expressed by the following evolution equations:

$$\mathrm{d}\boldsymbol{\pi} \;=\; C_{\pi 3}\left(\vec{\mathsf{A}}_\epsilon - \boldsymbol{\pi}\right)\|\mathsf{A}_\epsilon\|^2 \mathrm{d}N \tag{4.237}$$

The above evolution equation cause that the back polarization tends towards the polarization of current amplitude $\boldsymbol{\pi} \to \vec{A}_\epsilon$ ($C_{\pi 3}$ is positive). If the polarization is fixed over a large number of cycles then $\vec{\mathsf{A}}_\epsilon \approx \boldsymbol{\pi}$, respectively. Let us call the loading at constant average stress and polarization *c-monotonic*.

The increase in the rate of accumulation is proposed to be described by two multipliers f_α and f_π

$$f_\pi \;=\; 1 + C_{\pi 1}\left[1 - (\vec{\mathsf{A}}_\epsilon :: \boldsymbol{\pi})^{C_{\pi 2}}\right] . \tag{4.238}$$

They can be used to increase the rate described in Section 4.4.3. Finally we discuss shortly the determination of the material constants in our hypothetical model. After a long c-monotonic process, according to (4.237) one obtains

$$\vec{\mathsf{A}}_\epsilon \approx \boldsymbol{\pi} \tag{4.239}$$

which means that $f_\pi = 1$ and the c-monotonic accumulation rate (the 'referential' rate) can be used to determine the material constants of the basic model presented in the previous section.

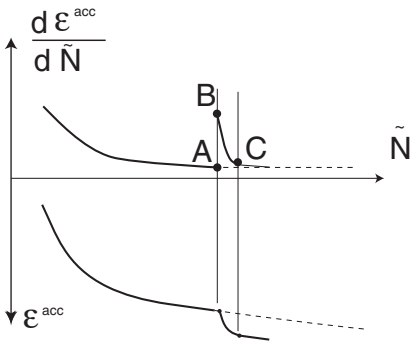

Figure 4.58: Calibration of material constants. Continuation of the c-monotonic loading is shown with a dashed line (referential accumulation curve)

Now, let our c-monotonic process be interrupted by a sudden change in the polarization. Since $\vec{\mathsf{A}}_\epsilon \neq \boldsymbol{\pi}$ we have $f_\pi > 1$ and the rate of accumulation shown in Fig. 4.58 jumps from the point A to B. Knowing the twist of polarization $1 - (\vec{\mathsf{A}}_\epsilon(B) :: \vec{\mathsf{A}}_\epsilon(A))^{C_{\pi 2}}$ we may calculate the constant $C_{\pi 1}$ and $C_{\pi 2}$ comparing the rates of accumulation at A and B. The constant $C_{\pi 3}$ may be found considering the number of cycles $\Delta\tilde{N}$ necessary for the accumulation rate to decline back to the referential value at point C in Fig. 4.58.

A separate problem is to determine the initial back polarization $\boldsymbol{\pi}_0$. A temporary assumption in FE calculation was to use the dyadic product $\boldsymbol{\pi}_0 \approx \vec{\mathbf{h}}\vec{\mathbf{h}}$ of the intergranular strain $\vec{\mathbf{h}}$ known from the implicit calculation of the initial state.

4.4.4 Remarks on the FE implementation

The semi-explicit model has been implemented to the FE-program ABAQUS in a form of a user's material subroutine. An alternative computation algorithm (not requiring ABAQUS) is presented in [166] www.AN . The constitutive model subroutine has three modes of operation:

1. *Implicit mode* passes the control to the conventional hypoplastic constitutive model with intergranular strain. This mode is used to find the initial state equilibrium and to perform irregular cycles.

2. *Recording mode* is also an implicit mode but the strain states the program is going through are memorized for the future calculation of amplitude. Of course only characteristic states need to be written down not tot overload the memory. For this purpose some filtering criteria, e.g. $\vec{\mathbf{e}} : \vec{\Delta\mathbf{e}} > 0.9$ can be used, wherein the deviatoric strain $\mathbf{e} = 0$ at the beginning of the loop and $\Delta\mathbf{e}$ is measured from the recent recorded strain.

3. *Pseudo-creep mode* calculates stress increments explicitly using (4.234) and (4.233). Before the first increment in this mode the amplitude $\mathsf{A}_{epsilon}$ or γ^{ampl} must be calculated.

A vertically loaded strip foundation under $N = 10^5$ load cycles with stress amplitude of about 50% of the static bearing capacity, see [171] www.AN and a pull-out test of a

horizontal plate with $N = 7 \cdot 10^4$ cycles with an amplitude almost reaching the ultimate static load were simulated. In both cases a fine ($d_{50} \approx 0.17$mm) sand at a verry dense state ($I_D \approx 0.9$) was used. In experiments static tests gave about 20% higher ultimate loads than in the calculations, presumably due to the friction at the front and rear glass.

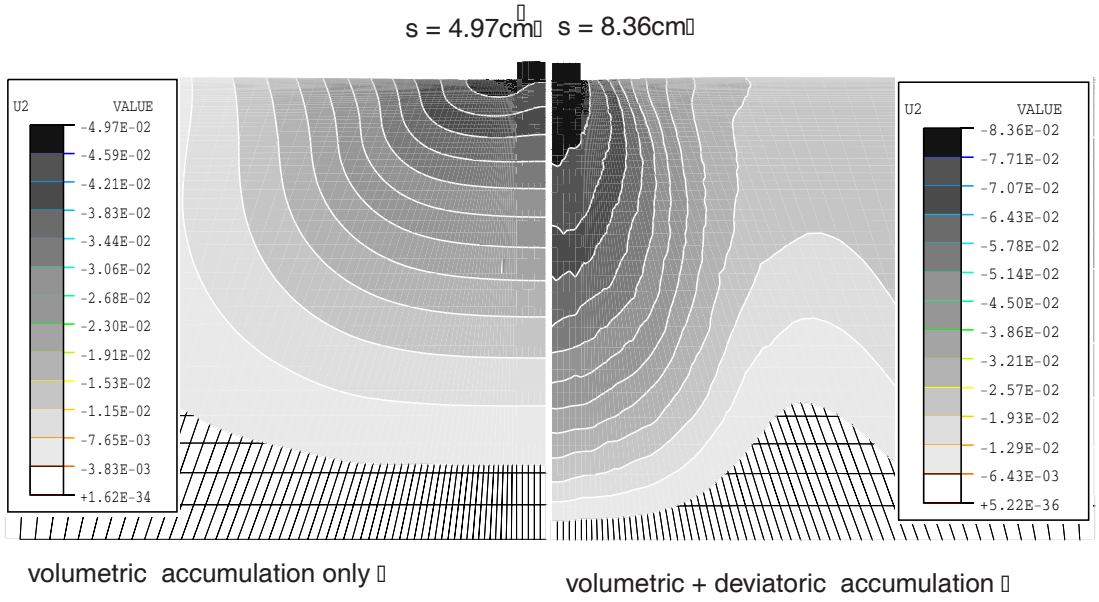

Figure 4.59: Settlement field under a strip foundation. In the centrifuge (200-g) model test the settlement of $s \approx 9$cm (scaled to prototype) was measured

The strip foundation test was performed in the geotechnical centrifuge at 200−g and was calculated in the prototype scale. The plate pull-out test was performed at 1-g in a relatively small plexiglass chest $0.2 \times 0.2 \times 0.4$m.

Details about the material parameters used in the calculation are given by Niemunis [166] www.AN and Wichtmann [259]. An initial $\epsilon_0^{\mathrm{acc}\ v} = 0$ was assumed, which is justified by the fact that the preliminary material element tests as well as the model tests were performed on freshly pluviated sand. The modifications discussed in the previous sections were introduced one by one. The most decisive changes (increase of settlements of the strip foundation and reduction of subsidance of the soil surface in the pull-out test) with respect to the original calculation with Sawicki's model were observed after the deviatoric accumulation had been added. Although quite different amplitude fields γ^{ampl} have been obtained from the reference hyperelastic model on one hand and from the hypoplastic model with intergranular strain on the other, this had surprisingly little influence on the final value of the calculated settlement. A similar study in 1-g model is given in [216].

The SGI "Power Challenge" computer (12 x 194 MHZ IP25 Processors (MIPS R10000)) under IRIX 6.2 (64-Bit UNIX) needed about 3 h CPU time for computation of settlement

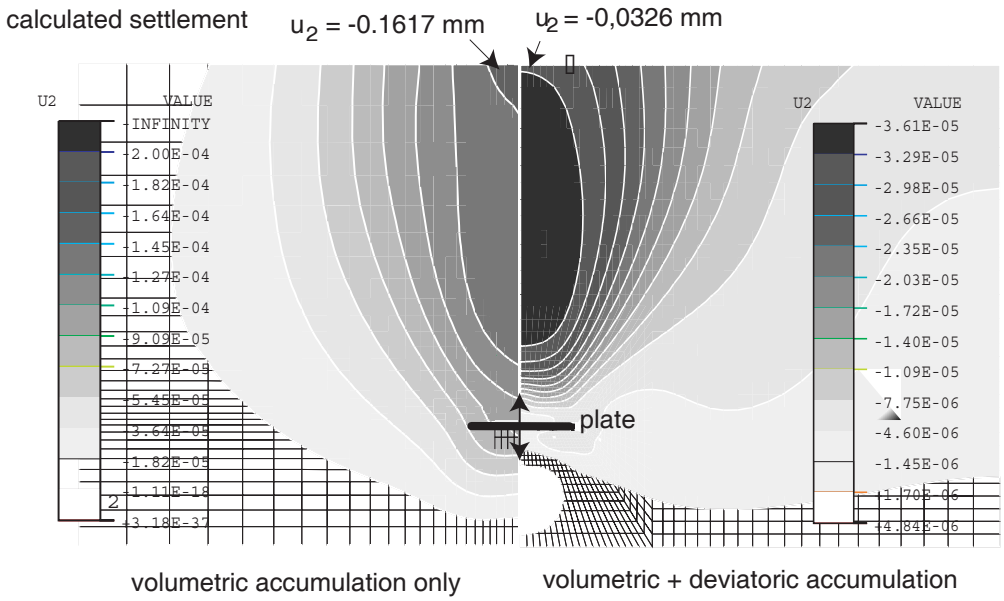

Figure 4.60: Settlement field due to the cyclic pull-out test of an anchor plate ($u_2 < 0$). In the (1-g) experiment a heave $u_2 > 0$ of about 0.3 mm was observed. The discrepancy can be contributed to the friction at the front and rear glass (no perfect plane strain conditions) and to the related arching due to a possible increase in the off-plane stress component. For details see [259]

with hypoplasticity and 1160 CPE8 elements. Analogous elastic computation took about 20 min. The agreement with the experiment test was acceptable.

Mesh dependence

The explicit calculation is mesh sensitive due to the fact that the rate of pseudo-creep is a function of the *square* of the strain amplitude. As an illustration we consider the case of a one-dimensional strain amplitude field $\epsilon^{\text{ampl}} = (1 - x/2)$ for $0 < x < 2$, Fig. 4.61.

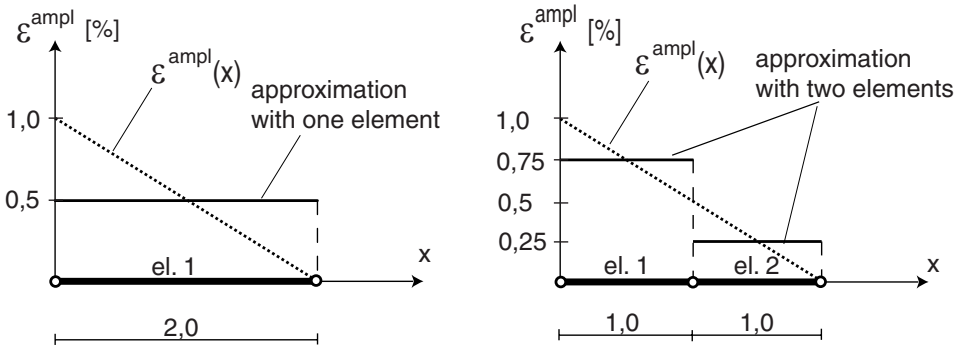

Figure 4.61: Mesh dependence of 'explicit' computation

The conventional settlement Δs is a *linear* function of strain and therefore the number of constant-strain elements (step-like approximation of strain) has little effect on the

integral value Δs. The rate of cyclic accumulation is dependent on the square of the amplitude and thus the approximation of amplitude is improved with the number of constant-strain elements and we obtain different values of settlement. With reference to Fig. 4.61 accumulation

$$\Delta s = \int_0^L C \left(\epsilon^{appr}\right)^2 \mathrm{d}x \tag{4.240}$$

results in displacements $\Delta s^{(1)} = \frac{1}{2}C$ and $\Delta s^{(2)} = \frac{10}{16}C$ for one-element and two-element discretization, respectively. Elements with quadratic shape functions have also been used. For the BVP with the strip foundation the following results were obtained

No	Element type	Nodes	Number of elements	Settlement
1	CPE4	967	905	7,69 cm
2	CPE4	3727	3605	8,33 cm
3	CPE8	947	292	8,19 cm
4	CPE8	3619	1160	7,82 cm

We must conclude that relatively fine meshes should be used for the FE calculation with explicit accumulation models, independently of the element type.

Stain amplitude for dynamic loads

In the algorithms presented in Sections 4.4.2 and 4.4.3 we have assumed quasi-static loads. Of practical interest may be accumulation due to dynamic (harmonic) loads. The strain amplitudes in such case can be found from a dynamic boundary element of finite element analysis. Alternatively, they may be estimated experimentally from the particle velocity v, $\gamma^{\mathrm{ampl}} = v/c$ (note a pitfall described in [164] www.AN), or estimated from the following table, cf. [208]:

Excitation source	Type of wave	Geometrical damping of the amplitude u at the distance r
Point	P,S-wave	$u \sim r^{-1}$
Point	R-wave	$u \sim r^{-0,5}$
Line	P,S-wave	$u \sim r^{-0,5}$
Line	R-wave	$u \sim r^{0}$.

4.4.5 Soil structure effects during cyclic loading

As already mentioned, for an adequate description of cyclic densification a structural state variable seems necessary. Although this research has not succeeded in a fully developed model (as yet), some tentative results might be of interest. The problem was attacked from the experimental and from the theoretical side. Experimentally, we attempted to correlate the degree of cyclic adaptation with the shear wave velocity. Independently, a theoretical framework for explicit accumulation formula was prepared. Both lines of research stimulate each other.

Experimental approach

The influence of soil structure on the process of densification was pointed out by Triantafyllidis and Niemunis [242]. A simple analysis of the spatial stress fluctuations reveals that a process of their smoothing should occur spontaneously (lower energy) and that it should be accompanied by an increase of stiffness as shown (using Herz theory for the contact force) in Fig. 4.62. This observation motivated a series of experiments consisting in resonant column (RC) tests of cyclically preloaded samples.

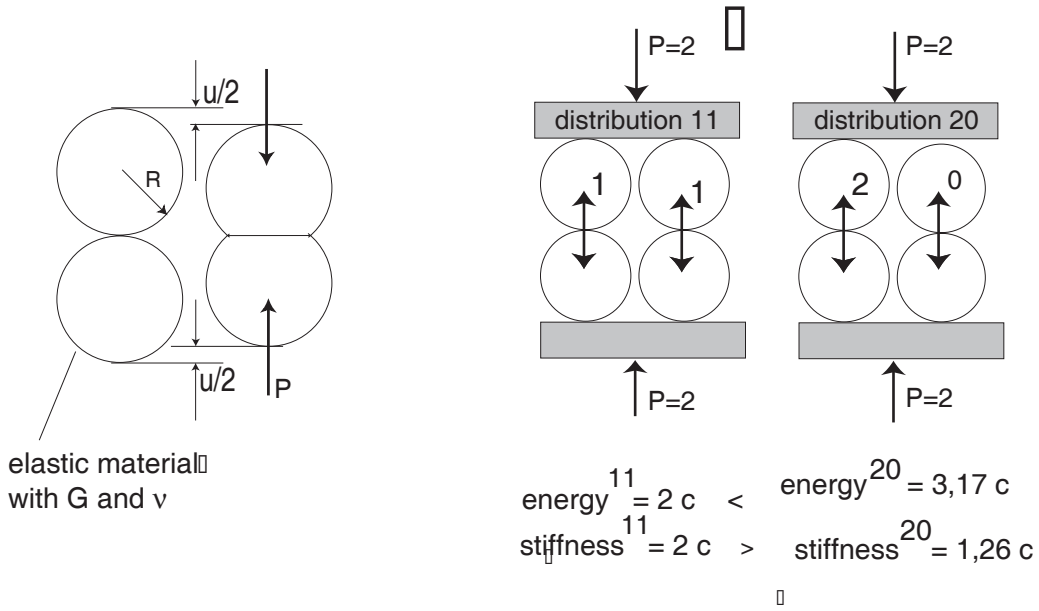

Figure 4.62: The total elastic stiffness should increase and the total elastic energy should decrease if the contact force distribution becomes more uniform. This follows from Herz theory according to which the stiffness of a single contact is $\mathrm{d}P/\mathrm{d}u \sim P^{1/3}$ and the elastic energy is $E = \int_0^P P(u)\mathrm{d}u \sim P^{5/3}$. The total stiffness and the total energy for a pair of grain contacts depend on the distribution of the total force (here, the total force is 2 and the distributions are $2-0$ and $1-1$). Similar results worked out with the statistical analysis and with the Chicago-model [37] of force distribution are presented by Triantafyllidis and Niemunis [242]

The effect of increased resistance to cyclic compaction is similar to the phenomenon of *aging* researched recently by Baxter [16]. Undisturbed, pluviated samples increase their low-strain shear stiffness modulus according to

$$G(t) = G(t_0)\,(1 + N_G \ln(t/t_0)) \tag{4.241}$$

with $t_0 = 1000$ min and $N_G \approx 1 \ldots 12\%$ although the stress and the void ratio are practically unchanged. It is not clear, however, if this increase can be attributed to small movements of grains or to some other physical phenomena like formation of silica-acid gel around grain contacts. Baxter reports a parallel increase in liquefaction resistance up to 75%. The resistance to densification is most likely related to the liquefaction potential. Note that both are not only functions of the void ratio.

The correlation of the initial value $\epsilon_0^{\mathrm{acc}\ v}$ (or $\tilde{N}_0$) with the shear wave velocity from RC-tests [259] is not straightforward. A simple experimental program demonstrated that the dynamic shear modulus is either independent of the adaptation phenomenon or that the scalar measure of cyclic adaptation like $\tilde{N}_0$ is insufficient. Freshly pluviated sand samples of good quality (fine, uniform sand $d_{50} \approx 0.17$mm, $d_{60}/d_{10} \approx 4$) were vertically preloaded with the average stress on the K_0-line and relatively large stress amplitude up to $\varphi_{mob} = 30°$. During $N = 50 \cdot 10^3$ cycles considerable vertical deformations up to 4% were accumulated. The preloaded samples were carefully (under support of vacuum) transported to the RC device and the vertical shear wave velocities were measured. The results shown in Fig. 4.63 do not confirm the expectation that the higher number of cycles can be correlated with the higher dynamic shear moduli.

Contrary to this result, Drnevich and Richart [56] reported that cyclic preloading (or 'prestraining') at relatively low amplitude carried out in the RC-device (RC was used for both preloading and for measurement of the shear wave velocity) resulted in a considerable increase of stiffness, as shown in Fig. 4.64.

The tests similar to the ones in Figs. 4.63 and 4.64 obtained by preloading with cycles of different polarizations were repeated and examined in more detail by Wichtmann [259]. Unfortunately the dependence observed by Drnevich and Richart [56] could be confirmed.

4.5 Partly saturated soils

Partly saturated soil is a ternary mixture of air, water and solid particles. The presence of air generates capillary forces, and this is of importance for many practical geotechnical problems. Spectacular consequences of capillary pressure for the measured displacements

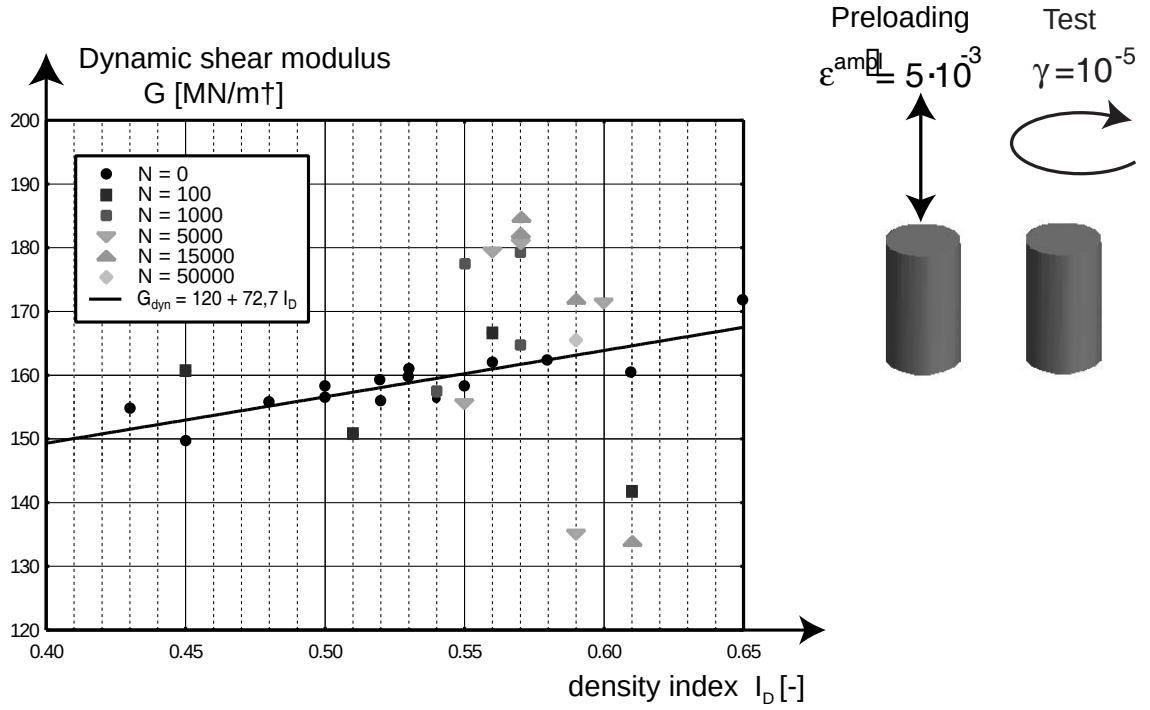

Figure 4.63: Weak correlation between the dynamic modulus G from the RC test and the number of load cycles (preloading) in triaxial apparatus. The intact sample was carefully carried from the triaxial apparatus to the RC-device

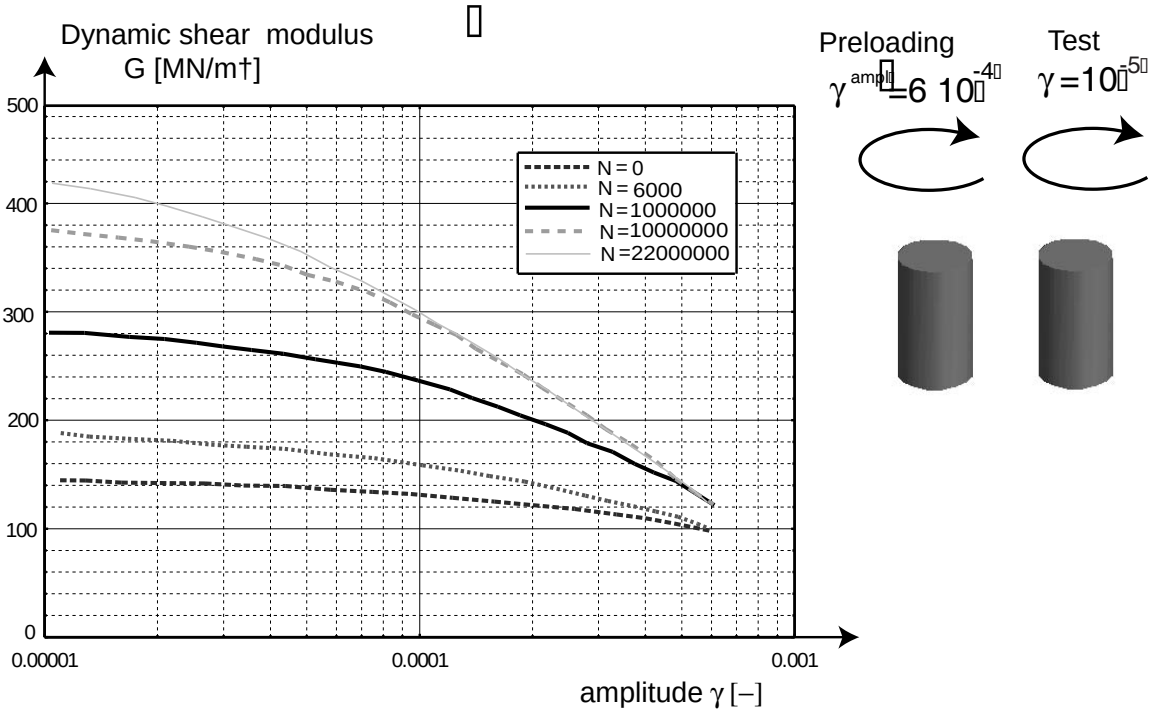

Figure 4.64: Good correlation between dynamic modulus G from RC test and the number/amplitude of cyclic preloading applied in RC, cf. [56]

of a sheet pile wall and for the strut forces supporting a deep excavation were reported by Wolffersdorff [264].

In this section, after a short discussion of physical aspects of capillary effects, an empirical formula for capillary pressure proposed by Gudehus [70] is presented. Its implementation to the hypoplastic constitutive model is described in detail.

4.5.1 Capillarity

The particles (atoms or molecules) at an interface between two substances or between a substance and vacuum have a specific energetic state which is different from the one of particles in the bulk, surrounded from all sides by identical neighbours. Let us denote the interfacial free energy per unit area of the surface between substances (a) and (b) by $\gamma_{a/b}$. The work required to create a new surface $\mathrm{d}A$ is therefore proportional to the increase of surface area, i.e. $\mathrm{d}W = \gamma_{a/b}\mathrm{d}A$. Often $\gamma_{a/b}$ is called surface tension. An air[25]/quarz interface has a higher free energy per unit surface than the water/quarz interface, i.e. $\gamma_{a/s} > \gamma_{w/s}$. Therefore wetting can progress easily in soil against the gravity force. The water head h_c in a capillary pipe of diameter d keeps on climbing (Fig. 4.65a) until the decrease of surface energy $\pi d(\gamma_{a/s}-\gamma_{w/s})\mathrm{d}h$ is compensated by the identical increase of the gravity potential $\frac{1}{4}\pi d^2\rho_w g h_c \mathrm{d}h$. From the comparison we find $h_c\rho_w g = 4(\gamma_{a/s} - \gamma_{w/s})/d$. This value is termed capillary pressure and it is traditionally written as $p_c = h_c\rho_w g = \dfrac{4}{d}\gamma_{w/a}\cos\theta$, wherein $\theta = \arccos\left[\dfrac{\gamma_{a/s} - \gamma_{w/s}}{\gamma_{w/a}}\right]$ denotes the so-called contact angle, Fig. 4.65b. The wetting behaviour corresponds to $\gamma_{a/s} > \gamma_{w/s}$ i.e. to $\theta < \pi/2$. For soils a typical value of $\gamma_{w/a} \approx 73 \cdot 10^{-3}$ N/m (at 20°C) can be assumed.

If the surface particle energy is higher than the bulk particle energy (e.g. fluid) then the substance is shrinking towards a sphere. Otherwise the substance is expanding (like a gas).

The capillary water can climb in the soil skeleton up to the height h_c. In the capillary regime the water is under tension relative to the atmosphere, $u_w < 0$, but the buoyancy forces are acting upwards as usual.

Consider now two fluid drops connected with a pipe with a piston, Fig. 4.65c. Pressures u_1 and u_2 (compression positive) on both sides of the piston may be different. The change of the total surface energy $8\pi\gamma_{w/a}(r_1\mathrm{d}r_1 + r_2\mathrm{d}r_2)$ is equal to the work done over the system or to the minus work done by the system i.e. to $-(u_2 - u_1)\mathrm{d}V$, wherein the change of volume is $\mathrm{d}V = A\mathrm{d}x = 4\pi r_1^2\mathrm{d}r_1 = -4\pi r_2^2\mathrm{d}r_2$, because the drop No 1 is expanding whereas the drop No 2 is shrinking.

[25]We call 'air' the saturated water vapor here.

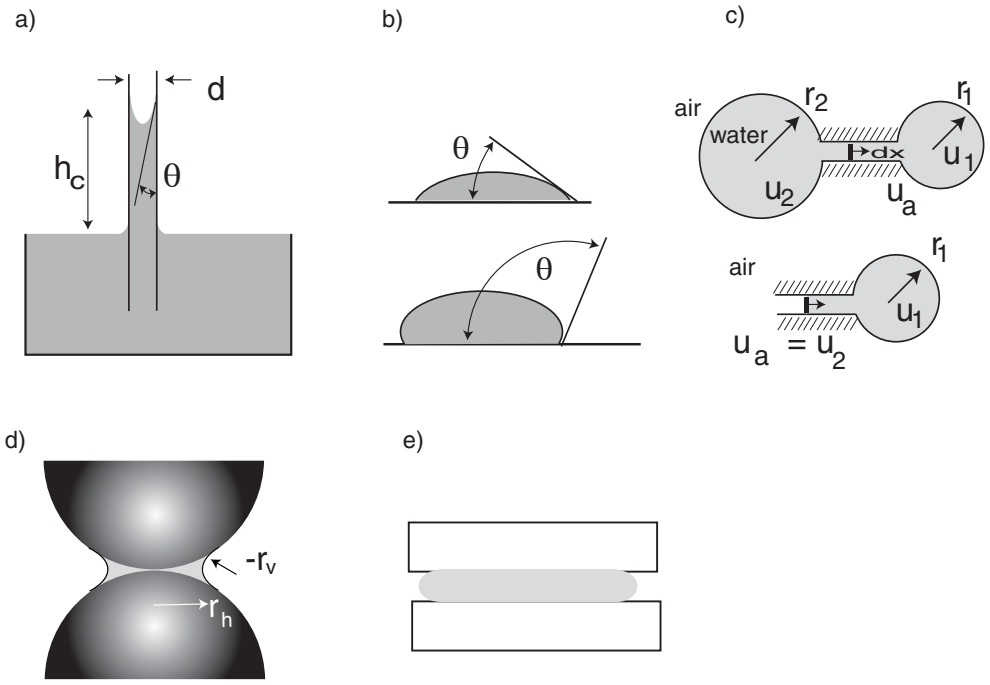

Figure 4.65: a) Capillary pipe, b) contact angle, c) connected two fluid drops, d) capillary water around a grain contact, e) squeezed water film

From the conservation of energy we obtain

$$(u_1 - u_2) = 2\gamma_{w/a}\left(\frac{1}{r_1} - \frac{1}{r_2}\right) \tag{4.242}$$

which in a limit case of $r_2 \to \infty$ and $u_2 \to u_a$ leads to the Laplace[26] equation

$$u_1 - u_a = \frac{2\gamma_{w/a}}{r_1}\,. \tag{4.243}$$

If the air/water contact surface is not spherical one has to consider the following sum of the minimal- and the maximal curvatures

$$u_1 - u_a = \gamma_{w/a}\left(\frac{1}{r_v} + \frac{1}{r_h}\right)\,. \tag{4.244}$$

In the above derivation the radius r is positive if the contact surface watched from the water side is convex. Accordingly, an air bubble in water has a negative radius and thus the air pressure u_a is higher that the water pressure u_w. For a water bridge at a grain contact, Fig. 4.65d, the vertical radius r_v is negative and the horizontal radius r_h is positive. Since $|r_v| < r_h$ the inequality $u_w < u_a$ must hold. Tensile pressure u_w contributes to higher effective (grain-to-grain) stress. An opposite situation with $u_a < u_w$ is depicted in Fig. 4.65e where a thin water film is squeezed between two blocks.

[26] sometimes called Young-Laplace equation

Speaking of air we actually mean water saturated vapor which is in equilibrium with water. A long-lasting situation in which the relative air humidity ψ is lower than 100% is possible only at a relatively large difference $u_a - u_w$ between air and water pressure. The humidity is usually calculated from $\psi = u_a/u_{as}$, wherein u_a denotes vapor pressure and u_{as} is the pressure in which this vapor condenses. The condensation - evaporation equilibrium is governed by the Kelvin's equation

$$u_a - u_w = \frac{RT}{v_{mw}} \ln(1/\psi)\,, \tag{4.245}$$

wherein $R = 8.314$ J / (mol °K) denotes the gas constant, T is the absolute temperature (in °K) and $v_{mw} = 18.015 \cdot 10^{-6}$ m^3/mol is the molar volume of water. For the balance of mass, the departure of humidity ψ from the state of fully saturated vapor $\psi = 100\%$ is negligible because such departure requires large suction $u_a - u_w$. For example, the suction $u_a - u_w = 1$ MPa at 10°C corresponds to the state of equilibrium (i.e. no evaporation or condensation) at $\psi \approx 99.2\%$

Considering water - air interface we assume that water is sufficiently pure so that osmotic pressure need not be considered The water - air interface is semi-permeable: non-permeable for ions and permeable for water particles, so the Kelvin's equation must be supplemented by pressure difference π due to osmosis, compare [75]. The ionic pressure can be estimated using the van't Hoff's equation $\pi = m_i RT$, wherein m_i is molar density of the ions of the solute, $m_i = im$, where the van't Hoff's constant i says how many moles of ions are dissociated from one mole of the solute. For example, from one mole NaCl we get not $i = 2$ but only $i = 1.8$ moles of Na^+ and Cl^- due to 'pairing'. Plants can therefore osmotically imbibe capillary water even at $u_w = -16$ bar.

4.5.2 Effective stress

Depending on the amount of air in the mixture we may distinguish qualitatively between two situations:

- Water fills completely the pores and air is present in form of isolated bubbles. The degree of saturation S lies above a threshold value S_g [70, 75]
- Air forms a system of interconnected channels if the degree of saturation $S < S_g$ is small enough.

In the first case we would intuitively use the concept of effective stress for the solid constituent. Similarly as for fully saturated soil we assume that the effective stress is

relevant for the strength and for the stiffness of the soil skeleton irrespectively of the current pore pressure as long as the compressibility of individual particles [128] due to the pore pressure is negligible. According to Gudehus [75] if gaseous constituent is not interconnected the capillary pressure p_c disappears. This situation is typical for some marine sediments [202]. It pertains also to imperfectly insulated clay samples stored for a longer period. The description of the compressibility of the water/air mixture is discussed in Subsection 4.5.4.

If air forms a system of interconnected channels, the concept of effective stress is less obvious because the grain-to-grain stress induced *from the inside* by capillary forces seems to be qualitatively different from the stress caused by the boundary tractions coming *from the outside*. The difficulties in finding a single effective stress equation were reported already in the fifties and progressively lead to the acceptance of the suction $u_a - u_w (> 0)$ as an additional state variable for the response of a soil skeleton [2].

As an illustration of the problem consider the following micro-mechanic situation. Two identical dry samples are subjected to the same volumetric deformation in two different ways. The first sample is placed in the condensing (cooled) water vapor so the sample becomes partly saturated with an isotropic grain-to-grain stress $\Delta\mathbf{T}^{(c)} = -p_c\mathbf{1}$ induced by the tensed capillary water around the grain contacts. The second sample remains dry and an isotropic effective stress $\Delta\mathbf{T} = -\Delta p\mathbf{1}$ is caused by surface tractions applied at the boundaries. The pressures p_c and Δp are equal because the effective pressures $\Delta\mathbf{T}^{(c)}$ and $\Delta\mathbf{T}$ are equal. We recall that the volumetric deformations in both samples are supposed to be identical so $\Delta\mathbf{T}^{(c)} = \Delta\mathbf{T}$. We may speculate that the stress chains are longer and the spatial fluctuation of stress is larger in the second sample than in the first one. Moreover the partly saturated sample seems to be more robust because of the lateral support of stress chains. All (even peripheral) grain contacts are reinforced. We may therefore expect that the effective pressure due to the internal suction may generate a higher strength than the one due to the external compression, although both produce the same volumetric strain.

Consistently with this interpretation Loret and Khalili [137] recently suggested that the Bishop's [20] extension of Terzaghi's effective stress principle should be supplemented introducing the suction term $(f(u_a - u_w))$ into the equation of the yield surface.

According to Bishop [20], the total stress $\mathbf{T}^{\rm tot}$ (tension positive) and the effective stress $\mathbf{T}$ can be interrelated at a given degree of saturation S by

$$\mathbf{T}^{\rm tot} = \mathbf{T} - [(1-\chi)u_a + \chi u_w]\ \mathbf{1} \quad \text{with} \quad \chi \approx S(2-S) \tag{4.246}$$

Usually, if the gas channels are open and connected with the atmosphere at $u_a \approx 100$ kPa, the total stress in such soil is understood differently than $\mathbf{T}^{\rm tot}$. Actually the stress *applied*

mechanically to skeleton and water is of importance $\mathbf{T}^{\text{tot}} = \mathbf{T}^{\text{tota}} - u_a\ \mathbf{1}$. The atmospheric pressure is already in equilibrium with the air in pores and need not be considered. Hence we use

$$\mathbf{T}^{\text{tota}} = \mathbf{T} + \chi(u_a - u_w)\ \mathbf{1} = \mathbf{T} + p_c\ \mathbf{1} \tag{4.247}$$

wherein the capillary pressure $p_c = \chi(u_a - u_w)$ expresses the grain-to-grain stress *in the soil skeleton* that originates from suction $u_a - u_w$ alone i.e. at $\mathbf{T}^{\text{tot}} = -\ \mathbf{1} \cdot 100$ kPa or at $\mathbf{T}^{\text{tota}} = \mathbf{0}$.

4.5.3 Implementation of capillarity into hypoplasticity

The Bishop's effective stress formula has been combined with hypoplasticity by Gudehus [70]. He postulated a more elaborated expression for the capillary pressure

$$p_c = \lambda_c \frac{\gamma_{a/w}}{d_{50}} \left(\frac{e}{e_{d0}}\right)^{-m_c} S(1-S)^{r_c} \frac{(r_c+1)^{r_c+1}}{r_c^{r_c}} \quad > 0 \tag{4.248}$$

The 'capillary' soil parameters are $1 < \lambda_c < 5$, $3 < m_c < 30$ and $0.3 < r_c < 1$ and were discussed by Mikulitsch and Gudehus [153]. The characteristic void ratio e_{d0} is known already from the reference model. The capillary pressure enters the equation for effective stress via

$$\mathbf{T} = \mathbf{T}^{\text{tota}} - p_c\ \ \mathbf{1}\,. \tag{4.249}$$

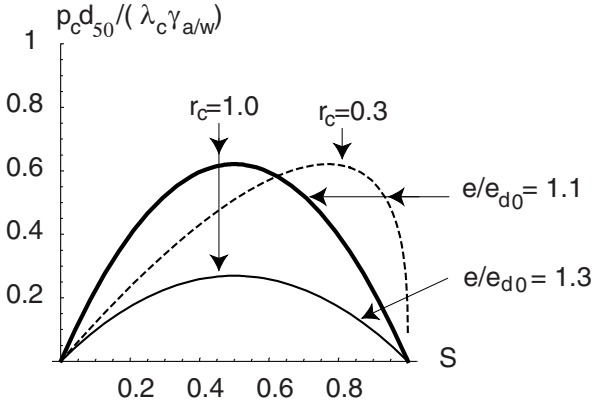

Figure 4.66: Examples of normalized capillary pressure plotted for $m_c = 5$. One can shift the peak value along the S-axis with changing r_c and increase the value of p_c with λ_c. Densification increases p_c

Of course, a positive capillary pressure p_c means a negative isotropic stress, e.g. the effective stress is $\mathbf{T} = -p_c\ \mathbf{1}$ if the total stress vanishes. Having (4.248) we may forget

the pore water pressure u_w and the air pressure u_a and instead of $p_c(u_w, u_a)$ we may think of p_c as of an additional portion of the effective stress which depends on the void ratio e and on the water content w only. Although (4.248) postulates p_c to be a function of the void ratio e and of the degree of saturation S we prefer to use the water content

$$w = m_w/m_s \quad \text{with} \quad S = \frac{w\ \rho_s}{e\ \rho_w} \quad \text{where} \quad \dot{S} = S\left(\frac{\dot{w}}{w} - \frac{\dot{e}}{e}\right) \tag{4.250}$$

because w is not influenced by changes in the void ratio. With the independent state variables

- total stress $\mathbf{T}^{\text{tota}}$
- void ratio e
- water content w

the hypoplastic Equation (2.61) takes the form

$$\overset{\circ}{\mathbf{T}}{}^{\text{tota}} = \mathsf{L} : \mathbf{D} + f_d \mathbf{N}||\mathbf{D}|| + \dot{p}_c\ \mathbf{1}. \tag{4.251}$$

with the rate of capillary pressure added.

Let us express the rate of capillary pressure $\dot{p}_c$ by the rate of void ratio $\dot{e}$ and by the rate of water content $\dot{w}$. The additional variable $\dot{w}$ is assumed to be prescribed by some water transport equations.
From (4.248) we obtain:

$$p_c = C(e/e_{d0})^{-m_c} S(1-S)^{r_c} \quad \text{with} \quad C = \frac{\lambda_c \gamma_{a/w}}{d_{50}} \frac{(r_c+1)^{r_c+1}}{{r_c}^{r_c}}$$

and its rate form

$$\dot{p}_c = p_c \left\{ \frac{-m_c \dot{e}}{e} + \left[\frac{1}{S} - \frac{r_c}{1-S}\right]\left[S\left(\frac{\dot{w}}{w} - \frac{\dot{e}}{e}\right)\right]\right\} \tag{4.252}$$

Let us introduce the following abbreviations

$$A = -\frac{p_c}{e}\left(m_c + \frac{1-S-Sr_c}{(1-S)}\right) \quad \text{and} \quad B = \frac{p_c}{w}\left(\frac{1-S-Sr_c}{(1-S)}\right) \tag{4.253}$$

whereby

$$\dot{p}_c = A\dot{e} + B\dot{w} \quad .$$

Substituting this result into (4.251) we have

$$\overset{\circ}{\mathbf{T}}{}^{\text{tota}} = \mathsf{L} : \mathbf{D} + f_d \mathbf{N}||\mathbf{D}|| + A\ \dot{e}\ \ \mathbf{1} + B\ \dot{w}\ \ \mathbf{1} \tag{4.254}$$

The rate of change of the void ratio in (4.254) can be expressed using the strain rate $\dot{e} = (1+e)\ \mathbf{1} : \mathbf{D}$ and finally the incremental constitutive equation has the form

$$\mathring{\mathbf{T}}^{\text{tota}} = \mathsf{L}^{\text{tota}}\ \mathbf{D} + f_d \mathbf{N}||\mathbf{D}|| + B\dot{w}\ \mathbf{1} \quad \text{with} \quad \mathsf{L}^{\text{tota}} = \mathsf{L} + (1+e)A\ \mathbf{1}\ \mathbf{1} \tag{4.255}$$

We assume that the rate of water content $\dot{w}$ is given and therefore Equation (4.255) can be directly used in FE or in strain-controlled problems. Stress or mixed control tests can be simulated in terms of composite variables using the following solving procedure (notation introduced in Section 3.2.3 is relevant):

1. For the current state defined by $\mathbf{T}^{\text{tota}}, e, w$ calculate S, p_c and the effective stress $\mathbf{T}$. Next compute: $\mathsf{L}^{\text{tota}}(\mathbf{T}, e, p_c, S)$, $\mathbf{N}(\mathbf{T}, e)$, $B(S, p_c, w)$ and $f_d(\mathbf{T}, e)$

2. Write the rate of the capillary pressure in terms of composite stress components $\mathsf{M} :\ \mathbf{1}B\dot{w}$, and modify the *prescribed* components of the stress rate only $\dot{\mathbf{t}}^{\diamond} = \dot{\mathbf{t}} - \mathsf{M} :\ \mathbf{1}B\dot{w}$

3. Solve the hypoplastic equation

$$\dot{\mathbf{t}}^{\diamond} = \bar{\mathsf{L}}^{\text{tota}} : \mathbf{d} + f_d \bar{\mathbf{N}} \sqrt{\mathbf{d}^T : \mathsf{C} : \mathbf{d}} \tag{4.256}$$

   for the missing components of $\dot{\mathbf{t}}^{\diamond}$ and $\mathbf{d}$, cf. Section 3.2.3. After this step all components of $\dot{\mathbf{t}}^{\diamond}$ and $\mathbf{d}$ must be known.

4. Modify *all* components of the stress rate increasing them by the respective components of the composite capillary pressure: $\hat{\dot{\mathbf{t}}} = \hat{\dot{\mathbf{t}}}^{\diamond} + \mathsf{M} :\ \mathbf{1}B\dot{w}$. In this way the prescribed components of stress rate obtain again their original value (which was changed in step 2). The remaining components obtain a contribution from the rate of capillary pressure.

5. Convert the resulting composite rates back to the $\mathring{\mathbf{T}}^{\text{tota}}$ and $\mathbf{D}$ and update $w, e, \mathbf{T}^{\text{tota}}$ and also S and p_c for convenience.

An example of calculation is shown in Fig. 4.67. An initially almost fully saturated sample becomes fully saturated in the course of oedometric compression. Then the sample is dried to $S \approx 10\%$, compressed and wetted again. The irreversible densification due to such drying wetting loop is significant. The reference model with the following 'partly saturated' parameters was used $\lambda_c \gamma_{a/w}/d_{50} = 2000$ kPa, $m_c = 1$, $r_c = 0.7$.

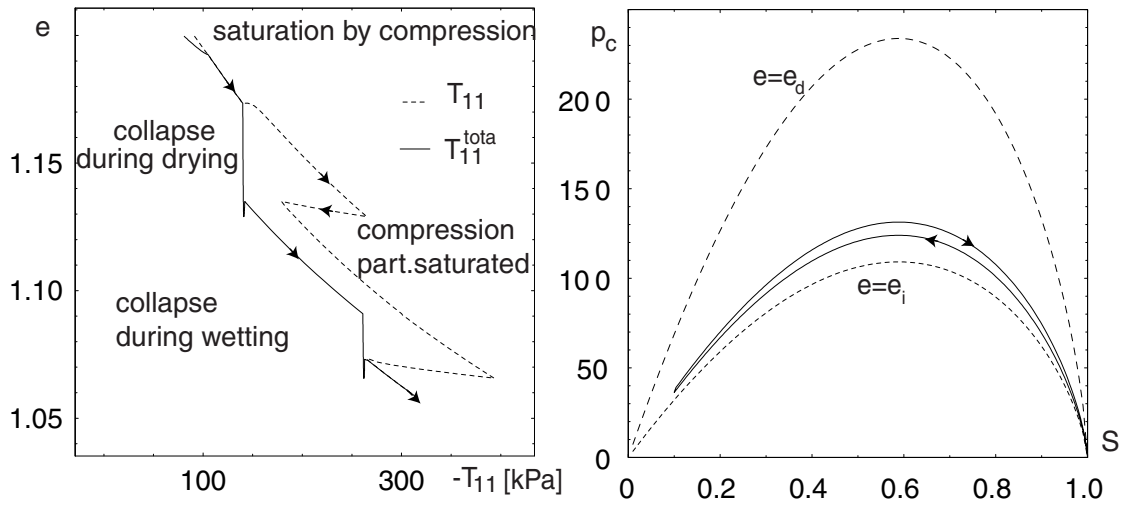

Figure 4.67: Simulation of an oedometric compression test overlaid by a drying/wetting cycle. According to the model, both drying and wetting cause considerable densification. The intergranular strain is not implemented as can be seen from the effective compression line (dashed)

4.5.4 Compressibility of water-air mixture

The soil behaviour close to saturation ($S > S_g$) is shortly discussed. An extensive experimental program with numerous triaxial and oedometric tests was reported by Niemunis [79]. Here, the computational part of this work and some problems related to the compliance of the water-air mixture are discussed.

We derive a formula for a compressibility of water/air mixture for $S > S_g \approx 0.9$ so that the air is present in bubbles but not in interconnected channels. We assume that the gas bubbles are surrounded by water only with the argument that from the energetic point of view water should tends to wet the grains due to $\gamma_{a/s} > \gamma_{w/s}$, cf. Section 4.5.1.

Let us calculate the compression of the air bubbles $\Delta\epsilon^a = -\Delta V_a/V_a$ due to an increase of pore water pressure Δu_w at $V_w = \text{const}$, i.e. the unknown function is $\epsilon^a(u_w)$. For simplicity the wetting-drying hysteresis is neglected.

For the gas bubbles trapped in pore water we assume a constant temperature so the Boyle-Mariotte law (for perfect gas)

$$u_a V_a = \text{const.}(= mRT) \tag{4.257}$$

applies where m is the amount of gas (in moles), $R = 8.314$ J/(mol °K) is the molar gas constant and T is the absolute temperature.

The compressibility of gas following from (4.257) is overlaid by the process of solving of the air bubbles in water that accompanies the increase of gas pressure u_a. Henry's law [60] states that the *volume* of the dissolved air is equal to 2% of the water volume V_w. From

(4.257) we know that this volume $2\%V_w = \text{const} = mRT/u_a$ means that more moles m of air are dissolved in water at larger gas pressure u_a.

Compressibility and solvability of air can be jointly expressed by:

$$u_a(V_a + HV_w) = \text{const.} \tag{4.258}$$

where V_w is the volume of water and $H \approx 0.02$ denotes Henry's constant [60].

The third phenomenon that we consider during compression of water/air mixtures is the decrease of surface energy of air/water interface due to shrinking of the surface of the air bubbles. According to the Young-Laplace law the air pressure u_a inside an air bubble with radius r_a can be found from

$$u_w - u_a = 2\gamma_{a/w}/(-r_a) \tag{4.259}$$

wherein $\gamma_{a/w} \approx 73 \cdot 10^{-3}$ N/m (surface tension water/air at 20° C) and r_a is (made) positive. Let us combine the rate forms of (4.258) and (4.259) assuming spherical bubbles. We write the equations

$$\dot{u}_a(1 + H\frac{V_w}{V_a}) + u_a\frac{\dot{V}_a}{V_a} = 0 \quad \text{and} \quad \dot{u}_a - \dot{u}_w = -2\gamma_{a/w}\frac{\dot{r}_a}{r_a^2} \tag{4.260}$$

from which we eliminate $\dot{u}_a$ and u_a and introduce $\dot{V}_a/V_a = 3\dot{r}_a/r_a$ and an abbreviation $S = V_a/V_w$ to obtain

$$\frac{\partial r_a}{\partial u_w} = \frac{r_a^2(1 + H/S)}{-3r_a u_w - 4\gamma_{a/w} + 2\gamma_{a/w}H/S} \tag{4.261}$$

From this result follows directly the equation for volumetric strain $\dot{\epsilon}^a = -\dot{V}_a/V_a = -3\dot{r}_a/r_a$:

$$\dot{\epsilon}^a = \frac{1}{K_a}\dot{u}_w \quad \text{with} \quad K_a = -\frac{-3r_a u_w - 4\gamma_{a/w} + 2\gamma_{a/w}H/S}{3r_a(1 + H/S)} = -\frac{(u_a - u_w)}{3} + \frac{u_a S}{S + H} \tag{4.262}$$

Let us estimate the radius r_a of a typical air bubble. We assume that the gas bubbles inside a gap between grains join themselves spontaneously because this is energetically advantageous. The total surface energy $\gamma_{a/w}n_b 4\pi r_a^2$ of n_b air bubbles divided by their volume $n_b\frac{4}{3}\pi r_a^3$ yields $3\gamma_{a/w}/r_a$, so the energy decreases if r_a grows. This causes the bubbles to join themselves (coalescence) if they collide. Moreover, in case of (polydisperse) bubbles of different sizes r_a we expect that the small ones are dissolved whereas the large ones grow. Such phenomenon should occur if we agree that the amount of air dissolved in water is governed by the *average* air pressure in the bubbles. According to (4.259)

different radii r_a imply different suction values $u_a - u_w$ and hence, due to the Henry's law, bubbles with high suction should be dissolved.

By these arguments we assume that the number of bubbles per volume V is equal to the number of gaps of the skeleton, i.e. $n_b \approx V/d_{50}^3$, wherein d_{50} denotes the diameter of an average grain. The corresponding pore volume is $Ve/(1+e)$ and a part $1-S$ (S=degree of saturation) of this volume is occupied by air bubbles. Hence the volume of air is $(1-S)Ve/(1+e)$. The radius of an average bubble and the suction (from (4.259)) are:

$$r_a \approx d_{50}\sqrt[3]{\frac{3}{4\pi}\cdot\frac{(1-S)e}{1+e}} \quad \text{and} \quad u_a - u_w = \frac{2\gamma_{a/w}}{d_{50}\sqrt[3]{\frac{3}{4\pi}\cdot\frac{(1-S)e}{1+e}}}, \tag{4.263}$$

respectively. For example, for $S = 0.97$ and $e = 1$ we obtain $r_a \approx 0.15 d_{50}$ and with $\gamma_{a/w} = 73 \cdot 10^{-3}$ N/m and $d_{50} = 10^{-6}$m the value $u_a - u_w = 973$ kPa.

Increasing u_w will cause the difference $u_a - u_w$ also to grow and the value S_a to become smaller. Continuing compression we could arrive at a state where $K_a = 0$ and a spontaneous collapse of bubbles occurs. The instability condition $K_a = 0$ is shown in Fig. 4.68. The critical radius of an imploding bubble, corresponds to $\mathrm{d}r_a/\mathrm{d}u_w = -\infty$ or to

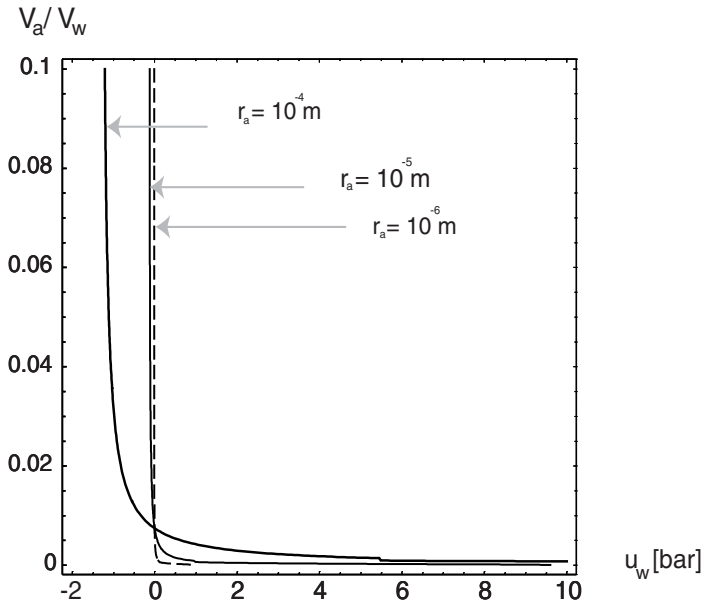

Figure 4.68: Combination of $S = V_a/V_w$ and u_w that may lead to the collapse of bubbles of various radii r_a

$$r_a = \frac{2\gamma_{a/w} H V_w/V_a - 2}{3u_w}\,. \tag{4.264}$$

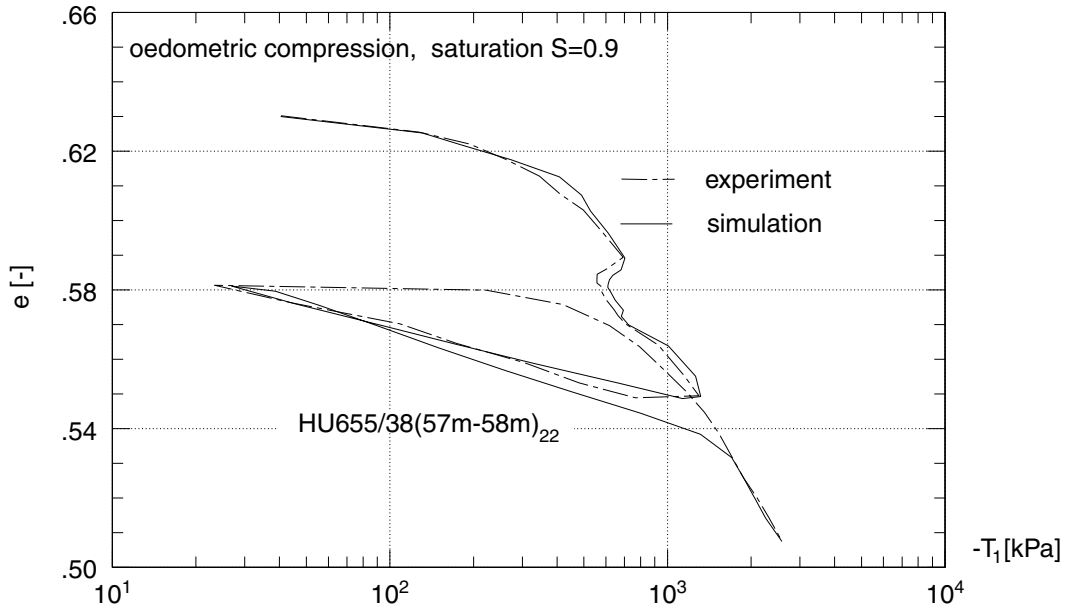

Figure 4.69: Oedometric test of a stiff clay sample. The comparative calculation were performed with the visco-hypoplastic model without intergranular strain. The model in not capable of reproducing the hysteretic unloading-reloading loop. Parameters used in calculation: $D_r = 1.18 \cdot 10^{-5}$[-/s], $\lambda = 0.060$, $\kappa = 0.008$, $I_v = 0.15$, $\phi_c = 12.50°$, $e_0 = 0.63$ $p_e = 270.0$ kPa, $\beta_R = 0.95$, $T_0 = -80.0$ kPa, $k = 1.0 \cdot 10^{-8}$ [m/s], $H = 0.02$, $K_w = 2$ GPa and $S = 0.9$

With $H = 0.02$ we obtain implosion for $V_a/V_w > 0.01$. For example, let $V_a/V_w = 0.5\%$ and $u_w = 100$ kPa, then the critical radius is $r_{a\,crit} = 10^{-6}$ m

The model for partly saturated soil with $S > S_g$ was implemented into a computer code and used for interpretations of triaxial and oedometric tests [79]. For example, Fig. 4.69 shows an example of oedometric compression test in which the transition between reloading and first loading is 'rounded' by the presence of air in water. The collapse of bubbles has not been experimentally confirmed as yet.

Chapter 5

Concluding remarks

A great advantage of the original hypoplastic model was its simplicity. This treatise deals with several shortcomings caused by this simplicity and proposes methods to circumvent the related problems. Most problems are rather subtle and appear in special applications, which causes that readers of this thesis are confronted with many details. The Polish proverb 'diabeł tkwi w szczegółach' (the devil is in the detail) is quite relevant in this context. From the presented analysis it can be concluded that for numerous geotechnical applications the hypoplastic model need and can be improved.

Most of the results should be of practical importance. They may be helpful in choosing the constitutive model because both the virtues and the disadvantages of the hypoplastic model are fairly described. A hypoplastic model can be implemented into an FE code within several hours (ready to use computer code is available in Internet and used without knowing much about the intricacy of the involved equations, e.g.
`http://wwwrz.rz.uni-karlsruhe.de/~gn25/ibf/_hypoplastizitaet/`

This text is addressed to readers who have discovered that something goes wrong in the calculation, some features are absent or poorly simulated. In spite of its long evolution the hypoplastic model is still insufficient in some applications, and some defects have not been removed so far. In such cases a user of the model is forced to become its developer, and the presented practical experience in manipulation of hypoplastic equation may be valuable. Several extensions are ready to use and several suggestions have been given in this thesis. The proposed rearrangement of the fundamental equation has been demonstrated to facilitate changes and refinements.

Bibliography

[1] Adachi T., Oka F.: Constitutive equations for normally consolidated clay based on elasto-viscoplasticity. Soils and Foundations 22: 1982 57–70.

[2] Alonso E., Gens A., Josa A.: A constitutive model for partially saturated soils. Géotechnique 40: 1990 405–430.

[3] Armstrong P., Frederick C.: A mathematical representation of multiaxial Bauschinger effect. Technical Report RD/N/NN 731, C.E.G.B., 1966.

[4] Atkinson J., Richardson D., Stallebrass S.: Effect of recent stress history on the stiffness of overconsolidated soil. Géotechnique 40: 1990 531–540.

[5] Baligh M., Whittle A.: Soil models and design methods. In: Geotechnical Design: Design Methods and Parameters, 1987, conference, Politecnico di Torino.

[6] Banerjee P., Yousif N.: A plasticity model for the mechanical behaviour of anisotropically consolidated clay. International Journal for Numerical and Analytical Methods in Geomechanics 10: 1986 521–541.

[7] Bardet J.: Numerical simulations of the incremental responses of idealized granular materials. International Journal of Plasticity 10: 1994 879–908.

[8] Barksdale R.: Laboratory evaluation of rutting in base course materials. In: Third International Conference on Structural Design of Asphalt Pavements, volume 3, 161–174, 1972.

[9] Bauer E.: Zum mechanischen Verhalten granularer Stoffe unter vorwiegend ödometrischer Beanspruchung. Ph.D. thesis, Insitutes für Boden und Felsmechanik der Universität Karlsruhe (TH), 1992, Heft, Nr. 130.

[10] Bauer E.: Calibration of a comprehensive constitutive equation for granular materials. Soils and Foundations 36: 1996 13–26.

[11] Bauer E.: Condition for embedding Casagrande's critical states into hypoplasticity. Mechanics of Cohesive-Frictional Materials 5: 2000 125–148.

[12] Bauer E., Herle I.: Stationary states in hypoplasticity. In: Constitutive Modelling of Granular Materials (Editor D. Kolymbas), 167–192, Springer, 1999, Horton.

[13] Bažant Z.: Endochronic inelasticity and incremental plasticity. International Journal of Solids and Structures 14: 1978 691–714.

[14] Bažant Z.: Physical argument for nonlocality of mikrocracking damage in a continuum. In: Advances in Continuum Mechanics (Editors O. Brüller, V. Mannl, J. Najar), 238–241, Springer-Verlag, 1991.

[15] Bažant Z., Shieh C.L.: Hysteretic fracturing endochronic theory for concrete. Journal of the Engineering Mechanics Division ASME 106: 1980 921–949.

[16] Baxter C.: An Experimental Study on the Aging of Sands. Phd. thesis, Virginia Polytechnic Institute, Blacksburg, 1999.

[17] Been K., Jefferies M., Hachey J.: The critical state of sands. Géotechnique 41: 1991 365–381.

[18] Benedetto H.D., F. T., Ishihara M.: Time dependent shear deformation characteristics of sand and their constitutive modelling. Soils and Foundations 41: 2001 .

[19] Betten J.: Tensorrechnung für Ingenieure. B.G.Teubner, Stuttgart, 1987.

[20] Bishop A., Henkel D.: The Measurement of Soil Properties in the Triaxial Test. Edward Arnolds, London, 1962.

[21] Borja R.: Generalized creep and stress relaxation model for clays. Journal of the Geotechnical Engineering Division ASCE 118: 1992 1765–1786.

[22] Bouckovalas G., Whitman R., Marr W.: Permanent displacement of sand with cyclic loading. Journal of Geotechnical Engineering 110: 1984 1606–1623.

[23] Brannon R.: Caveats concerning conjugate stress and strain measures for the frame indifferent anisotropic elasticity. Acta Mech 129: 1998 .

[24] Brannon R.: private communication .

[25] Bruhns O.T., Xiao H., Meyers A.: Self-consistent eulerian rate type elasto-plasticity models based upon the logarithmic stress rate. International Journal of Plasticity 15: 1999 479–520.

[26] Budhu M.: Nonuniformities imposed by simple shear apparatus. Canadian Geotechnical Journal 20: 1984 125–137.

[27] Budhu M., Britto A.: Numerical analysis of soils in simple shear devices. Soils and Foundations 27: 1987 31–41.

[28] Butterfield R.: A natural compression law for soils. Géotechnique 29: 1979 .

[29] Casagrande A.: Characteristics of cohesionless soils affecting the stability of earth fills. Journal of Boston Society of Civil Engineers : 1936 1925–1940, contributions to Soil Mechanics.

[30] Chaboche J.: Modelling of ratchetting: evaluation of various approaches. European Journal of Mechanics 13: 1994 501–781.

[31] Chambon R.: Bifurcation analysis for incrementally non linear models, illustration by Cloe models. In: Localization in Geomaterials (Editor R. Chambon), 1996, proc. of 8-th European Autumn School, Aussois, France.

[32] Chambon R.: Stability and bifurcation basic concepts. In: Localization in Geomaterials (Editor R. Chambon), 1996, proc. of 8-th European Autumn School in Aussois, France.

[33] Chambon R., Crochepeyre S.: Daphnis: a model, consistent with CLoE, for the description of post localization behaviour. In: Numerical Models in Geomechanics (Editors Pietruszczak, Pande), 187–191, Balkema, Rotterdam, 1997.

[34] Chang C., Whitman R.: Drained permanent deformation of sand due to cyclic loading. Journal of Geotechnical Engineering 114: 1988 1164–1179.

[35] Christoffersen J., Hutchinson J.: A class of phenomenological corner theories of plasticity. Mechanics and Physics of Solids 27: 1979 465–480.

[36] Chu J., Lo S.C.: Asymptotic behaviour of granular soil in strain path testing. Géotechnique 44: 1994 65–82.

[37] Coppersmith S., Liu C., Majumdar S., Narayan O., Witten T.: A model for force fluctuations in bead packs. Physical Review E 53: 1996 4673–4685.

[38] Crochepeyre S.: Constribution á la modélisation numérique et théorique de la localisation et de la post-localisation dans les géomatériaux. Ph.D. thesis, Universite Joseph Fourier Grenoble I, 1998.

[39] Crochepeyre S., Chambon R.: Daphnis: a new model for the description of post-localization behaviour: Application to sands. Mechanics of cohesive-frictional materials 3: 1998 127–153.

[40] Cundall P., Strack O.: A discrete numerical model for granular assemblies. Géotechnique 29: 1979 47–65.

[41] Dafalias Y.: Bounding surface elastoplasticity-viscoplasticity for particulate cohesive media. In: Deformation and Failure of Granular Materials, 97–107, 1982, proceedings IUTAM Conf., Delft.

[42] Dafalias Y.: Corotational rates for kinematic hardening at large plastic deformations. Journal of Applied Mechanics 50: 1983 561–565.

[43] Dafalias Y.: The plastic spin. Journal of Applied Mechanics 52: 1985 865–871.

[44] Dafalias Y.: Bounding surface plasticity I: Mathematical foundation of hypoplasticity. Journal of Engineering Mechanics 112: 1986 966–987.

[45] Dafalias Y.: Overview of constitutive models used in VELACS. In: Verification of Numerical Procedures for the Analysis of Soil Liquefaction Problems (Editors K. Arulandan, R. Scott), volume 2, 1293–1304, Balkema, 1994, proceedings of the International Conference in Davis, California.

[46] Darve F.: Stability and uniqueness in geomaterials constitutive modelling. In: Localisation and Bifurcation Theory for Soils and Rocks (Editors R. Chambon, J. Desrues, I. Vardoulakis), 1993, proceedings of the Third International Workshop, Grenoble, France.

[47] Darve F., Flavigny E., Meghachou M.: Constitutive modelling and instabilities of soil behaviour. Computers and Geotechnics 17: 1995 203–224.

[48] Darve F., Pal O., Roguiez X.: Material instabilities and bifurcations in granular media. In: Proceedings (Editors Pietruszczak, Pande), 167–173, Balkema, Rotterdam, 1997.

[49] Darve F., Thanopoulos Y.: Description of cyclic behaviour of sands by a non-linear incremental constitutive law. In: Deformation and failure of Granular Materials, 201–212, 1982, proc.IUTAM Conf. in Delft, Holland.

[50] Davis R., Mullenger G.: A rate-type constitutive model for soil with a critical state. International Journal for Numerical and Analytical Methods in Geomechanics 2: 1978 255–282.

[51] Desrues J., Chambon R.: A new rate type constitutive model for geomaterials: Cloe. In: Modern Approaches in Plasticity, 309–324, Elsevier, Holland, 1993, proceedings of Int. Workshop in Horton, Greece.

[52] Desrues J., Chambon R., Mokni M., Mazerolle F.: Void ratio evolution inside shear bands in triaxial sand specimens studied by computed tomography. Géotechnique 46: 1996 529–546.

[53] Doanh T.: Strain response envelope: a complementary tool for evaluating hypoplastic constitutive equations. In: Constitutive Modelling of Granular Materials (Editor D. Kolymbas), 57–106, Springer, 1999, Horton.

[54] Doanh T., Inraim E., Dubujet P., Matiotti R., Herle I.: Static liquification of very loose Hostun RF sand: experiments and modelling. In: Physics and Mechanics of Soil Liquefaction (Editor J. P.V. Lade), 17–28, 1999, proceedings of the Int. Workshop, Baltimore, Maryland,USA.

[55] Dolezalova M.: On overestimation of displacements in numerical calculation of zoned dams. International Journal for Numerical and Analytical Methods in Geomechanics 18: 1994 1–24.

[56] Drnevich V., Richart F.: Dynamic prestraining of dry sand. Journal of Soil Mechanics and Foundations Division : 1970 453–467.

[57] Drucker D.: A definition of stable inelastic material. Journal of Applied Mechanics : 1959 101–106.

[58] Eekelen H. van: Isotropic yield surfaces in three dimensions for use in soil mechanics. International Journal for Numerical and Analytical Methods in Geomechanics 4: 1980 89–101.

[59] Ekberg A.: Rolling contact fatigue of railway wheels. Ph.D. thesis, Chalmers University of Technology, 2000, Solid Mechanics.

[60] Fredlund D., Rahardjo H.: Soil Mechanics for Unsaturated Soils. John Wiley and Sons Inc, New York, 1993.

[61] Gajo A., Wood D.: Severn trent sand: a kinematic hardening constitutive model: q-p formulation. Géotechnique 49: 1999 595–614.

[62] Goldscheider M.: Grenzbedingung und Fliessregel von Sand. Mechanics Research Communications 3: 1976 463–468.

[63] Goldscheider M.: True triaxial tests on dense sand. In: Constitutive Relations for Soils, 11–54, 1982, workshop Grenoble.

[64] Goldscheider M.: Spannungen in Sand bei räumlicher, monotoner Verformung. Ph.D. thesis, Insitut für Boden- und Felsmechanik der Universität Karlsruhe (TH), 1983, Heft Nr. 92.

[65] Gotschol A.: Veränderlich elastisches und plastisches Verhalten nichtbindiger Böden und Schotter unter zyklisch-dynamischer Beanspruchung. Ph.D. thesis, Universität Gh Kassel, 2002.

[66] Green A., Naghdi P.: A general theory of an elastic - plastic continuum. Archive of Rational Mechanics and Analysis 18: 1965 251–281.

[67] Gudehus G.: Stability of saturated granular bodies under cyclic load. In: Plastic and long-term effects in soils (Editor G. Gudehus), Balkema, 1977, DMSR, Karlsruhe.

[68] Gudehus G.: Comparison of some constitutive laws for soils under radially symmetric loading and unloading. In: Numerical Methods in Geomechanics, 1309–1323, Balkema, Rotterdam, 1979, 3-rd International Conference in Aachen.

[69] Gudehus G.: Spontaneous liquefaction of saturated granular bodies. In: Modern Approaches to Plasticity (Editor D. Kolymbas), 691–714, Elsevier, 1992, Workshop in Horton, Greece.

[70] Gudehus G.: A comprehensive concept for non-saturated granular bodies. In: Unsaturated Soils, 1995, 1st Int. Conference, Paris.

[71] Gudehus G.: A comprehensive constitutive equation for granular materials. Soils and Foundations 36: 1996 1–12.

[72] Gudehus G.: Constitutive equations for granulate-fluid mixtures with a pectic constituent. Mechanics of Materials 22: 1996 93–103.

[73] Gudehus G.: Attractors, percolation thresholds and phase limits of granular soils. In: Powder and Grains (Editors Behringer, Jenkins), 169–183, Balkema, 1997.

[74] Gudehus G.: Discussion. In: Workshop "Boden unter fast zyklischer Belastung: Erfahrungen und Forschungsergebnisse", Schriftreihe des Lehrstuhls für Grundbau und Bodenmechanik der RUB (Editor Th. Triantafyllidis), 2000.

[75] Gudehus G.: Grundbautaschenbuch Teil 1, chapter Stoffgesetze für Boden aus physikalischer Sicht, 203–254. Ernst und Sohn, 2000.

[76] Gudehus G.: A visco-hypoplastic constitutive relation for soft soil. Soils and Foundations Submitted to publication.

[77] Gudehus G., Goldscheider M., Winter H.: Mechanical properties of sand and numerical integration methods: some sources of errors and bounds of accuracy. In: Finite elements for geomechanics (Editor G. Gudehus), John Wiley, 1977.

[78] Gudehus G., Hügel H., G. A. Niemunis, Kreuter H.: Entwicklung einer numerischen Methode zur Verformungsberechnung für den Braunkohletagebau. Technical report, Lehrstuhl für Bodenmechanik und Grundbau, Universität Karlsruhe, 1994, 2.Zwischenbericht.

[79] Gudehus G., Niemunis A., Bösinger E.: Bestimmung von Kennwerten für Proben aus den Bohrlöchern HU655 und HU659. Technical report, Lehrstuhl für Bodenmechanik und Grundbau, Universität Karlsruhe, 1996, 3.Zwischenbericht.

[80] Gudehus G., Niemunis A., Karcher C.: Entwicklung einer numerischen Methode zur Verformungsberechnung für den Braunkohletagebau. Technical report, Lehrstuhl für Bodenmechanik und Grundbau, Universität Karlsruhe, 1996, 3.Zwischenbericht.

[81] Herle I.: Hypoplastizität und Granulometrie einfacher Korngerüste. Ph.D. thesis, Insitut für Boden- und Felsmechanik der Universität Karlsruhe, 1997, Nr. 142.

[82] Herle I.: Granulometric limits of hypoplastic models. Task Quarterly 4: 2000 389–408.

[83] Herle I.: Influence of pressure level and stress amplitude on the compaction of granulates. In: Compaction of Soils, Granulates and Powders (Editors D. Kolymbas, W. Fellin), 285–295, Balkema, 2000.

[84] Herle I., Doanh T.: Verification of a hypoplastic model with static liquefaction tests on Hostun rf sand. In: Pre-failure Deformation Characteristics of Geomaterials,, 1999, proc. 2nd Int. Symposium, Torino.

[85] Herle I., Doanh T., Wu W.: Comparison of hypoplastic nad elastoplastic modelling of undrained triaxial tests on loose sand. In: Constitutive Modelling of Granular Materials, Horton 1999 (Editor D. Kolymbas), 335–351, Springer, 2000.

[86] Herle I., Gudehus G.: Determination of parameters of a hypoplastic constitutive model from properties of grain assemblies. Mechanics of Cohesive-Frictional Materials 4: 1999 461–486.

[87] Herle I., Kolymbas D.: Pressure- and density-dependent bifurcation of soils. In: Localization and Bifurcation Theory for Soils and Rocks (Editor H.B. Mühlhaus), A.A.Balkema, 1999, proc. 5th Int. Workshop.

[88] Herrmann H., Luding S.: Modeling granular media on the computer. Continuum Mechanics and Thermodynamics : 1998 189–231.

[89] Hibbitt, Karlsson & Sorensen Inc: Abaqus 5.6 Theory Manual. 1995.

[90] Hill R.: A general theory of uniqueness and stability in elastic-plastic solids. Journal of the Mechanics and Physics of Solids 6: 1958 236–249.

[91] Hill R.: Some basic principles in the mechanics of solids without a natural time. Journal of the Mechanics and Physics of Solids 7: 1959 209–225.

[92] Hill R.: Uniqueness criteria and extremum principles in self-adjoint problems of continuum mechanics. Journal of the Mechanics and Physics of Solids 10: 1962 185–194.

[93] Hill R.: On constitutive inequalities for simple materials - 1. Journal of the Mechanics and Physics of Solids 16: 1968 229–242.

[94] Hill R.: On constitutive inequalities for simple materials - 2. Journal of the Mechanics and Physics of Solids 16: 1968 315–322.

[95] Hornych P., Corte J., Paute J.: tude des déformations permanentes sous chargements répétés de trois graves non traitées. Bulletin de Liaison des Laboratoires des Ponts et Chaussées 77–84.

[96] Hsu S., Jain S., Griffin O.J.: Verification of endochronic theory for nonproportional loading paths. Journal of Engineering Mechanics 117: 1991 .

[97] Huang W.: Hypolplastic modelling of shear localisation in granular materials. Dissertation, Faculty of Civil Engineering, Institute of General Mechanics, Graz University of Technology, Austria, 2000.

[98] Hueckel T.: On effective stress concepts and deformation in clays subjected to environmental loads: Discussion. Canadian Geotechnical Journal 29: 1992 1120–1125.

[99] Hueckel T.: Water-mineral interaction in hygromechanics of clays exposed to environmental loads: a mixture-theory approach. Canadian Geotechnical Journal 29: 1992 1071–1086.

[100] Hueckel T.: Chemo-plasticity of clays subjected to stress and flow of a single contaminant. International Journal for Numerical and Analytical Methods in Geomechanics 21: 1997 43–72.

[101] Hueckel T., Drescher A.: On dilatational effects of inelastic granular media. Archive of Mechanics 27: 1975 157–172.

[102] Hügel H.M.: Prognose von Bodenverformungen. Ph.D. thesis, Insitut für Boden- und Felsmechanik der Universität Karlsruhe, 1995, Nr. 136.

[103] Hvorslev M.: Physical components of the shear strength of saturated clays. In: Shear Strength of Cohesive Soils, 1960, proceedings of ASCE Research Conference, Boulder, Colorado.

[104] Hyodo M., Tanimizu H., Yasufuku N., Murata H.: Undrained cyclic and monotonic triaxial behaviour of saturated loose sand. Soils and Foundations 34: 1994 19–32.

[105] Imai G., Tang Y.X.: A constitutive equation of one-dimensional consolidation derived from inter-connected tests. Soils and Foundations 32: 1992 83–96.

[106] Imposimato S., Nova R.: An investigation of the uniqueness of the incremental response of elastoplastic models for virgin sand. Mechanics of Cohesive-Frictional Materials 3: 1998 65–87.

[107] Jamiolkowski M., Ladd C., Germaine J., Lancellotta R.: New developements in field and laboratory testing of soils. State-of-the-Art Report. In: Soil Mechanics and Foundation Engineering., volume 1, 57–153, 1985, proceedings of the 11th International Conference , San Francisco.

[108] Jardine R.: Some observations on the kinematic nature of soil stiffness. Soils and Foundations 32: 1992 111–124.

[109] Jardine R., Symes M., Burland J.: The measurement of soil stiffness in the triaxial apparatus. Géotechnique 34: 1984 323–340.

[110] Kaliakin V., Dafalias Y.: Theoretical aspects of the elastoplastic-viscoplastic bounding surface model for cohesive soils. Soils and Foundations 30: 1990 11–24.

[111] Karcher C.: Tagebaubedingte Deformationen im Lockergestein. Ph.D. thesis, Institut fr Boden- und Felsmechanik der Universität Karlsruhe, 2002, Heft 160.

[112] Khedr S.: Deformation characteristics of granular base course in flexible pavements. In: Transportation Research Record, volume 1043, 131–138, 1985.

[113] Klein G.: Grundbautaschenbuch Teil 1, chapter Bodendynamik und Erdbeben, 443–495. Ernst und Sohn, 1995.

[114] Klobe B.: Eindimensionale Kompression und Konsolidation und darauf basierende Verfahren zur Setzungsprognose. Ph.D. thesis, Insitutes für Boden und Felsmechanik der Universität Karlsruhe, 1992, Heft Nr 128.

[115] Ko H., Scott R.: Deformation of sand in hydrostatic compression. Journal of Soil Mechanics and Foundations Division 93: 1967 137–156.

[116] Kolymbas D.: Ein nichtlineares viskoplastisches Stoffgesetz für Böden. Ph.D. thesis, Insitut für Boden- und Felsmechanik, Universität Karlsruhe, 1978, Heft 77.

[117] Kolymbas D.: Eine konstitutive Theorie für Boden und andere körmige Stoffe. Ph.D. thesis, Intitut für Boden- und Felsmechanik, Universität Karlsruhe, 1988, Habilitation, Heft 109.

[118] Kolymbas D.: Computer-aided design of constitutive laws. International Journal for Numerical and Analytical Methods in Geomechanics 15: 1991 593 – 604.

[119] Kolymbas D.: An outline of hypoplasticity. Archive of Applied Mechanics 61: 1991 143–151.

[120] Kolymbas D.: Introduction to Hypoplasticity, volume 1 of Advances in Geotechnical Engineering and Tunneling. Balkema, Rotterdam, 2000.

[121] Kolymbas D., Rombach G.: Shear band formation in generalized hypoplasticity. Ingenieur-Archiv 59: 1989 177–186.

[122] Koseki J., Kawakami S., Nagayama H., Sato T.: Change of small strain quasi-elastic deformation properties during undrained cyclic torsional shear and triaxial tests of Toyoura sand. Soils and Foundations 40: 2000 101–110.

[123] Krieg S.: Viskoses Bodenverhalten von Mudden, Seeton und Klei. Ph.D. thesis, Institut für Boden- und Felsmechanik der Universität Karlsruhe, 2000, Heft 150.

[124] Kruyt N., Rothenburg L.: Micromechanical definition of strain tensor for granular materials. Journal of Applied Mechanics 118: 1996 706–711.

[125] Kujawski D., Mroz Z.: A viscoplastic material model and its application to cyclic loading. Acta Mechanica 36: 1980 213–230.

[126] Kutter B., Sathialingam N.: Elastic-viscoplastic modelling of rate-dependent behaviour of clays. Géotechnique 42: 1992 427–441.

[127] Lade P.: Three-dimensional behavior and parameter evaluation for an elasto-plastic model. In: Numerical Models in Geomechanics, 1982, International Symposium in Zürich.

[128] Lade P., De Boer R.: The concept of effective stress for soil concrete and rock. Géotechnique 47: 1997 61–78.

[129] Lade P., Nelson R., Ito Y.: Instability of granular materials with nonassociated flow. Journal of the Geotechnical Engineering Division ASCE 113: 1987 1302–1318.

[130] Landman U., Luedtke W., Burnham N., Colton R.: Atomistic mechanisms and dynamics of adhesion, nanoindentation, and fracture. Science 248: 1990 454–461.

[131] Leinenkugel H.: Deformations- und Festigkeitsverhalten bindiger Erdstoffe. Experimentelle Ergebnisse und ihre physikalische Deutung. Ph.D. thesis, Insitut für Boden- und Felsmechanik, Universität Karlsruhe, 1978, Heft 66.

[132] Lentz R., Baladi G.: Constitutive equation for permanent strain of sand subjected to cyclic loading. In: Transportation Research Record, volume 810, 50–54, 1981.

[133] Lewin P., Burland J.: Stress-probe experiments on saturated normally consolidated clay. Géotechnique 20: 1970 38–56.

[134] Lewis R., Schrefler B.: The finite element method in the static and dynamic deformation and consolidation of porous media. John Wiley and Sons, 1998.

[135] Li X., Dafalias Y.: Dilatancy for cohesionless soils. Géotechnique 50: 2000 449–460.

[136] Loret B.: On the choice of elastic parameters for sand. Short communication. International Journal for Numerical and Analytical Methods in Geomechanics 9: 1985 285–292.

[137] Loret B., Khalili N.: A three-phase model for unsaturated soils. International Journal for Numerical and Analytical Methods in Geomechanics 24: 2000 893–927.

[138] Loret B., Prévost J., Harireche O.: Loss of hyperbolicity in elastic-plastic solids with deviatoric associativity. European Journal of Mechanics 9: 1990 225–231.

[139] Lubarda V.: Elastoplasticity Theory. CRC Press, Boca Raton, 2002.

[140] Luding S.: Die Physik kohäsionsloser granularer Medien. Logos Verlag, Berlin, 1998, Habilitationsschrift.

[141] Maier G., Hueckel T.: Nonassociated and coupled flow rules of elastoplasticity for rock-like materials. International Journal for Roch Mechanics Mining Science and Geomechanical Abstracts 16: 1979 77–92.

[142] Maier T.: Numerische Modellierung der Entfestigung im Rahmen der Hypoplastizität. Schriftenreihe des Lehrstuhls Baugrund-Grundbau, Universität Dortmund, 2002, Heft 24.

[143] Malvern L.E.: Introduction to the Mechanics of a Continuous Medium. Prentice-Hall Series in Engineering of the Physical Sciences, Prentice-Hall, Inc., Englewood Cliffs, New Jersey, 1969.

[144] Mandel J.: Generalisation de la theorie de la plasticite de W.T. Koiter. International Journal of Solids and Structures 273–280.

[145] Marr W., Christian J.: Permanent displacements due to cyclic wave loading. Journal of the Geotechnical Engineering Division ASCE 107: 1981 1129–1149.

[146] Martin G., Finn W., Seed H.: Fundamentals of liquefaction under cyclic loading. Journal of the Geotechnical Engineering Division ASCE 101: 1975 423–439.

[147] Matsui T., Ohara H., Ito T.: Cyclic stress-strain history and shear characteristics of clay. Journal of the Geotechnical Engineering Division ASCE 106.

[148] Matsuoka H., Nakai T.: Stress-strain relationship of soil based on the smp, constitutive equations of soils. In: Speciality Session 9 (Editors S. Murayama, A. Schofield), Japanese Society of Soil Mechanics and Foundation Engineering, 1977, iX ICSMFE, Tokyo.

[149] Matsuoka H., Nakai T.: A new failure for soils in three-dimensional stresses. In: Deformation and Failure of Granular Materials, 253–263, 1982, proc. IUTAM Symp. in Delft.

[150] Matsuoka H., Yao Y.P., Sun D.: The cam-clay models revised by the SMP criterion. Soils and Foundations 39: 1999 81–95.

[151] Mear M.E., Hutchinson J.W.: Influence of yield surface curvature on flow localization in dilatant plasticity,. Mechanics of Materials 4: 1985 395–407.

[152] Mesri G., Choi Y.: The uniqueness of the end-of-primary (eop) void ratio-effective stress relationship. In: Soil Mechanics and Foundation Engineering, volume 2, 587–590, 1985, proceedings of the 11th International Conference in San Francisco, USA.

[153] Mikulitsch W., Gudehus G.: Uniaxial tension, biaxial loading and wetting tests on loess. In: Unsaturated Soils, 1995, proceedings of the 1-st International Conference in Paris, France.

[154] Miner M.: Cumulative damage in fatigue transactions. Journal of the Engineering Mechanics Division ASME 67: 1945 .

[155] Mitchell J.: Fundamentals of soil behaviour (2-nd ed.). John Wiley and Sons, 1993.

[156] Mróz Z.: On hypoelasticity and plasticity approaches to constitutive modelling of inelastic behaviour of soils. International Journal for Numerical and Analytical Methods in Geomechanics 4: 1980 45–55.

[157] Mróz Z., Niemunis A.: On the description of deformation anisotropy of materials. In: Yielding, Damage and Failure of Anisotropic Solids (Editor J. Boehler), 171–186, 1987, proceedings of IUTAM Symposium in Grenoble, France.

[158] Mróz Z., Norris V.: Elastoplastic and viscoplastic constitutive models for soil with application to cyclic loading. Soil mechanics-transient and cyclic loads. In: Soil Mechanics - Transient and Cyclic Loads. Constitutive Relations and Numerical Treatment. (Editors G. Pande, O. Zienkiewicz), 173–218, John Wiley and Sons, 1982.

[159] Mühlhaus H.B.: Berücksichtigung von Inhomogenitäten im Gebirge im Rahmen einer Kontinuumstheorie. Ph.D. thesis, Insitut für Boden- und Felsmechanik der Universität Karlsruhe, 1987, Heft Nr. 106.

[160] Müllerschön H.: Spannungs-Verformungsverhalten granularer Materialien am Beispiel von Berliner Sand. Ph.D. thesis, Universität Stuttgat, 2000, Institut für Mechanik.

[161] Needleman A., Tvergaard V.: Analyses of plastic flow localization in metals. Applied Mechanics Reviews 45: 1992 S2–S18.

[162] Niemunis A.: Hypoplasticity vs. elasto-plasticity, selected topics. In: Modern Approaches to Plasticity (Editor D. Kolymbas), 277–308, Balkema, Rotterdam, 1992, proc. of the Conference in Horton, Greece.

[163] Niemunis A.: Viscoplastic 1-d model for soils. In: Geotechnika w Inżynierii Wodnej i Lądowej (Editors B. Zadroga, Z. Sikora, A. Bolt), 1994, materały Jubileuszowej Sesji Naukowej Profesora E. Dembickiego, Gdańsk (in Polish).

[164] Niemunis A.: On the estimation of the amplitude of shear strain from measurements in situ. Soil Dynamics and Earthquake Engineering 14: 1995 1–3.

[165] Niemunis A.: A visco-plastic model for clay and its FE-implementation. In: Resultats Recents en Mechanique des Sols et des Roches (Editors E. Dembicki, W. Cichy, L. Bałachowski), 151–162, Politechnika Gdańska, 1996, xI Colloque Franco-Polonais, Gdańsk.

[166] Niemunis A.: Akkumulation der Verformung infolge zyklischer Belastung des Bodens - numerische Strategien. In: Boden unter fast zyklischer Belastung: Erfahrungen und Forschungsergebnisse (Editor Th. Triantafyllidis), volume 32, 1–20, Lehrstuhl für Grundbau und Bodenmechanik der Ruhr-Universität Bochum, 2000.

[167] Niemunis A.: Über die Anwendung der Kontinuumstheorie auf bodenmechanische Probleme. Technical report, Ruhr-Universität Bochum, Inst. f. Grundbau u. Bodenmechanik, 2002, Skript.

[168] Niemunis A.: Anisotropic effects in hypoplasticity. In: Deformation Characteristics in Geomaterials (Editor H. Benedetto), Swets and Zeitlinger, 2003, accepted for publication.

[169] Niemunis A., Cudny M.: On hyperelasticity for clays. Computers and Geotechnics 23: 1998 221–236.

[170] Niemunis A., Cudny M.: O teorii sprężystości w modelowaniu gruntów spoistych. In: "Geotechnika w Budownictwie i Inżynierii Środowiska" poświęconej 47-leciu pracy naukowej i 70-leciu urodzin Profesora Eugeniusza Dembickiego (Editor B. Zadroga), Politechnika Gdańska, 2000.

[171] Niemunis A., Helm J.: Settlement of a strip foundation due to cyclic loading. centrifuge model and FE-calculation. In: Soils Mechanics and Geotechnical Engineering, 761–764, Balkema, 2001, proceedings of 15-th International Conference in Istambul, Turkey.

[172] Niemunis A., Herle I.: Hypoplastic model for cohesionless soils with elastic strain range. Mechanics of Cohesive-Frictional Materials 2: 1997 279–299.

[173] Niemunis A., Karcher C., Theile T.: An averaging procedure for layered materials. International Journal for Numerical and Analytical Methods in Geomechanics 24: 2000 837–851.

[174] Niemunis A., Krieg S.: Viscous behaviour of soil under oedometric conditions. Canadian Geotechnical Journal 33: 1996 159–168.

[175] Niemunis A., Maier T.: A finite element for gradient hypoplasticity. Computers and Geotechnics In preparation.

[176] Niemunis A., Nübel K., Karcher C.: The consistency conditions for density limits of hypoplastic constitutive law. Task Quarterly 4: 2000 412–420, publications of TASK, Gdańsk.

[177] Niemunis A., Triantafyllidis T.: Liapunov instability of hypoplasticity. Soil Dynamics and Earthquake Engineering Accepted for publication.

[178] Niemunis A., Wichtmann T., Triantafyllidis T.: Compaction of freshly pluviated granulates under uniaxial and multiaxial cyclic loading. In: XIIIth European Conference On Soil Mechanics and Geotechnical Engineering: Geotechnical problems with man-made and man-influenced grounds, 2003, prag, accepted for publication.

[179] Norton F.: The Creep of Steel at High Temperatures. Mc Graw Hill Book Company, Inc., New York., 1929.

[180] Nova R.: Controllability of the incremental response of soil specimens subjected to arbitrary loading programmes. Journal of the Mechanical Behaviour of Materials 5.

[181] Nübel K.: Experimental and Numerical Investigation of Shear Localization in Granular Material. Ph.D. thesis, Institut fr̈ Boden- und Felsmechanik der Universität Karlsruhe, 2002, Heft 159.

[182] Nübel K., Karcher C.: FE simulations of granular material with a given frequency distribution of voids as initial condition. Granular Mattter 1: 1998 105–112.

[183] Oda M., Iwashita K.: Mechanics of Granular Materials. Balkema, Rotterdam, 1999.

[184] Oka F., Adachi T., Okano Y.: Two-dimensional consolidation analysis using an elasto-viscoplastic constitutive equation. International Journal for Numerical and Analytical Methods in Geomechanics 10: 1986 1–16.

[185] Olszak W., Perzyna P.: The constitutive equations of the flow theory for a nonstationary yield condition. In: Applied Mechanics, 545–553, 1966, proceedings of the 11th International Congress.

[186] Osinov V., Gudehus G.: Plane shear waves and loss of stability in a saturated granular body. Mechanics of Cohesive-Frictional Materials 1: 1996 25–44.

[187] Osinov V., Loukachev I.: Settlement of liquified sand after a strong earthquake. In: Compaction of Soils, Granulates and Powders (Editors D. Kolymbas, W. Fellin), 297–307, Balkema, 2000.

[188] Papadopoulos I.: A new criterion of fatigue strength for out-of-phase bending and torsion of hard metals. International Journal of Fatigue 16: 1994 377–384.

[189] Paute J., Jouve P., Ragneau E.: Modèle de calcul pour le dimensionnement des chaussées souples. Bulletin de Liaison des Laboratoires des Ponts et Chaussées 21–36.

[190] Petryk H.: On the second-order work in plasticity. Acta Mechanica 43: 1991 377–397.

[191] Petryk H.: Theory of bifurcation and instability in time-dependent plasticity. In: CISM Lecture Notes No. 327 (Editor Q. Nguyen), 1–58, Springer, 1991.

[192] Petryk H.: On stability of time-independent materials at finite strain. In: Finite Inelastic Deformations - Theory and Aplications (Editors D. Besdo, E. Stein), Springer Verlag, 1992, iUTAM Symposium, Hannover 1991.

[193] Petryk H.: Theory of material instability in incrementally nonlinear plasticity. In: Material Instabilities in Elastic and Plastic Solids (Editor H. Petryk), 261–331, Springer Verlag, 2000, courses and lectures No 414 - International centre for mechanical science.

[194] Pradhan T.: Modelling of shear deformation of geomaterials identification of material properties. In: Proc. Pre-failure deformation of Geomaterials (Editors Shibuya, Mitachi, Miura), 1139–1154, Balkema Rotterdam, 1995, general report.

[195] Pradhan T., Tatsuoka F., Sato Y.: Experimental stress-dilatancy relations of sand subjected to cyclic loading. Soils and Foundations 29: 1989 45–64.

[196] Prisco C.D., Imposimato S.: The influence of time derivative on the mechanical behaviour of loose sands. In: Constitutive Modelling of Granular Materials (Editor D. Kolymbas), 303–318, Springer, 1999, Horton.

[197] Prisco C.D., Nova R.: Stability problems related to static liquefaction of loose sand. In: Localisation and Bifurcation Theory for Soils and Rocks (Editors R. Chambon,

J. Desrues, I. Vardoulakis), 1993, proceedings of the Third International Workshop in Grenoble, France.

[198] Prisco C.D., Nova R., Lanier J.: A mixed isotropic hardening constitutive law for sand. In: Modern Approaches to Plasticity (Editor D. Kolymbas), Elsevier, 1993, workshop in Horton, Greece.

[199] Puzrin M., Burland J.: Non-linear model of small-strain behaviour of soils. Géotechnique 48: 1998 217–233.

[200] Raffel M., Willert C., Kompenhans J.: Particle image velocimetry. A practical guide. Springer Verlag, 1998.

[201] Raju V.: Spontane Verflüssigung lockerer granularer Körper - Phänomene, Ursachen, Vermeidung. Ph.D. thesis, Institut für Boden- und Felsmechanik der Univ. Karlsruhe, 1994, Heft 134.

[202] Rau G., R.C. C.: Triaxial testing of marine sediments with high gas contents. In: Advanced Triaxial Testing of Soil and Rock (STP 977) (Editor M.S. R.T. Donaghe R.C. Chaney), 338–351, ASTM, 1988.

[203] Rice J., Rudnicki J.W.: A note on some features of the theory of localization of deformation. International Journal of Solids and Structures 16: 1980 597–605.

[204] Rivlin R.: Some comments on the endochronic theory of plasticity. International Journal of Solids and Structures 17: 1981 231–248.

[205] Romano M.: A continuum theory for granular media with a critical state. Acta Mechanica 20: 1974 1011–1028.

[206] Roscoe K., Burland J.: On the generalized stress-strain behaviour of wet clays. In: Engineering plasticity (Editors J. Heyman, F. Leckie), Cambridge University Press, 1968.

[207] Rowe P.: The stress-dilatancy relation for static equilibrium of an assembly of particles in contact. Proceedings of the Royal Society of London 269: 1962 500–527.

[208] Rücker W.: Schwingungsausbreitung im Untergrund. Bautechnik 66: 1989 .

[209] Rudnicki J., Rice J.R.: Conditions for the localization of deformation in pressure-sensitive dilatant materials. Journal of the Mechanics and Physics of Solids 23: 1975 371–394.

[210] Sagaseta G., Cuellar V., Pastor M.: Cyclic loading. In: Deformation of soils and displacements of structures, volume 3, 981–999, 1991, proceedings of the 10-th ECSMFE in Firenze, Italy.

[211] Sandler I.: On the uniquness and stability of endochronic theories of material behaviour. Journal of Applied Mechanics 45: 1978 263–266.

[212] Sawicki A.: An engineering model for compaction of sand under cyclic loading. Engineering Transactions 35: 1987 677–693.

[213] Sawicki A.: Mechanika gruntów dla obciążen cyklicznych. Wydawnictwo IBW PAN, Gdańsk, 1991.

[214] Sawicki A., Świdziński W.: Mechanics of sandy subsoil subjected to cyclic loadings. International Journal for Numerical and Analytical Methods in Geomechanics 13: 1989 511–529.

[215] Sawicki A., Świdziński W.: Compaction beneath a flexible pavement due to traffic. Journal of the Geotechnical Engineering Division ASCE 116: 1998 1738–1743.

[216] Sawicki A., Świdziński W., Zadroga B.: Settlement of shallow foundations due to cyclic vertical force. Soils and Foundations 38: 1998 35–43.

[217] Schofield A., Wroth C.: Critical state soil mechanics. Mc Graw Hill, London, 1968.

[218] Sekiguchi H.: Constitutive laws of soils. Macrometric approaches - static-intrinsically time dependent. In: Discussion Session, 1985, proceedings of the 11th ICSMFE, San Francisco, USA.

[219] Sikora Z.: Hypoplastic flow of granular materials. Ph.D. thesis, Insitut für Boden- und Felsmechanik der Universität Karlsruhe, 1992, Heft Nr. 123.

[220] Simo J., Hughes T.: Computational Inelasticity. Springer, 1998.

[221] Simpson B.: Retaining structures: displacement and design. Géotechnique 42: 1992 541–576.

[222] Simpson B.: Engineering needs. In: Preprints of 2. Int. Symp. on Pre-failure Deformations Characteristics of Geomaterials (Editors M. Jamiolkowski, R. Lancellotta, D.L. Presti), 142–158, 1999, IS Torino.

[223] Smith D.: An introduction to continuum mechanics after Truesdell and Noll. Kluwer Academic Publishers, Dordrecht, 1993.

[224] Sobotka Z.: Rheology of Materials and Engineering Structures. Academia, Prague, 1984.

[225] Stallebrass E.: Modelling of the effect of recent stress history on the deformation of overconsolidated soils. Ph.D. thesis, The City University, 1990.

[226] Stutz A.: Comportment elasto-plastique des milieux granularien. In: Foundation of Plasticity (Editors Noordoff, Leyden), 33–49, 1973.

[227] Suiker A.: Fatigue Behaviour of Granular Materials. Technical Report 7-98-119-3, Delft University of Technology, Faculty of Civil Engineering, 1998.

[228] Suiker A.: Static and cyclic loading experiments on non-cohesive granular materials. Technical Report 1-99-DUT-1, Delft University of Technology, Faculty of Civil Engineering, 1999.

[229] Suklje L.: Rheological Aspects of Soil Mechanics. Wiley-Interscience, London/ New York/ Sydney/ Toronto, 1969.

[230] Sweere G.: Unbound granular bases for roads. Ph.D. thesis, Delft University of Technology, Netherlands, 1990.

[231] Świniański J., Sawicki A.: A model of soil-pile interaction due to cyclic loading. Canadian Geotechnical Journal 28: 1991 11–19.

[232] Tamagnini C., Viggiani G., Chambon R.: A review of two different approaches to hypoplasticity. In: Constitutive Modelling of Granular Materials (Editor D. Kolymbas), 107–144, Springer, 1999, Workshop in Horton, Greece.

[233] Taylor D., Merchant W.: A theory of clay consolidation accounting for secondary compression. Journal of Mathematical Physics 19: 1940 167–185.

[234] Tejchman J.: Scherzonenbildung und Verspannungseffekte in Granulaten unter Berücksichtigung von Korndrehungen. Ph.D. thesis, Insitut für Boden- und Felsmechanik der Universität Karlsruhe, 1989, Heft Nr. 117.

[235] Tejchman J.: Modelling of shear localisation and autogeneous dynamic effects in granular bodies. Ph.D. thesis, Institut für Boden- und Felsmechanik der Universität Karlsruhe, 1997, Heft Nr. 140.

[236] Terzaghi K.: Erdbaumechanik auf bodenphysikalischer Grundlage. Franz Deuticke, Leipzig und Wien, 1925.

[237] Thornton C.: On the relationship between the modulus of particulate media and the surface energy of the constituent particles. Journal of Physics D.: Applied Physics 26: 1993 1587–1591.

[238] Thornton C.: Micromechanics of elastic sphere asemblies during 3D shear. Mechanics and Statistical Physics of Particulate Materials. Technical Report 9, Institute of Mechanics and Materials Univeristy of California, San Diego, 1994.

[239] Toki S., Tatsuoka F., Miura S., Yoshimi Y., Yasuda S., Makihara Y.: Cyclic undrained triaxial strength of sand by a cooperative test program. Soils and Foundations 26: 1986 117–128.

[240] Topolnicki M.: Observed stress-strain behaviour of remoulded saturated clay and examination of two constitutive models. Ph.D. thesis, Institut für Boden- und Felsmechanik der Universität Karlsruhe, 1987, Heft Nr 107 (habilitation).

[241] Topolnicki M., Gudehus G., Mazurkiewicz B.: Observed stress-strain behaviour of remoulded saturated clay under plane strain conditions. Géotechnique 40: 1990 155–187.

[242] Triantafyllidis T., Niemunis A.: Offene Fragen zur Modellierung des zyklischen Verhaltens von nichtbindigen Böden. In: "Boden unter fast zyklischer Belastung: Erfahrungen und Forschungsergebnisse" (Editor Th. Triantafyllidis), 109–134, Lehrstuhl für Grundbau und Bodenmechanik, Ruhr-Universität Bochum, 2000, Heft 32.

[243] Truesdell C., Noll W.: The non-linear field theories of mechanics. In: Encyclopedia of Physics (Editor S. Flügge), volume III/3, Springer Verlag, 1965.

[244] Truesdell C., Toupin R.: Principles of classical mechanics and field theory. In: Encyclopedia of Physics (Editor S. Flügge), volume III/1, Springer Verlag, 1965, 1960.

[245] Vaid Y., Sivathayalan S., Stedman D.: Influence of specimen-reconstituting method on the undrained response of sand. Geotechnical Testing Journal 22: 1999 187–195.

[246] Valanis K.: An endochronic geomechanical model for soils. In: Deformation and Failure of Granular Materials, 159–165, 1982, proceedings of the IUTAM Conference, Delft.

[247] Valanis K., Chau-Fei L.: Some recent developments of the endochronic theory with applications. Nuclear Engineering and Design 69: 1982 327–344.

[248] Valanis K., Peters J.: An endochronic plasticity theory with shear-volumetric coupling. International Journal for Numerical and Analytical Methods in Geomechanics 15: 1991 77–102.

[249] Valanis K.C.: A theory of viscoplasticity without a yield surface, Part I. General theory. Arch. Mech 23: 1971 517–533.

[250] Valanis K.C.: A theory of viscoplasticity without a yield surface, Part II. Application. Arch. Mech 23: 1971 535–551.

[251] Valanis K.C., Lee C.F.: Endochronic theory of cyclic plasticity with applications. Journal of Applied Mechanics 51: 1984 367–374.

[252] Vardoulakis I.: Scherfugenbildung in Sandkörpern als Verzweigungsproblem. Ph.D. thesis, Institut für Boden- und Felsmechanik der Universität Karlsruhe, 1977, Heft Nr 70.

[253] Vardoulakis I.G., Graf B.: Imperfection sensitivity of the biaxial test on dry sand. In: IUTAM Conference on deformation and failure analysis of granular materials (Editors P.A. Vermeer, H. Luger), 485–491, Balkema, 1982.

[254] Vardoulakis I.G., Sulem J.: Bifurcation Analysis in Geomechanics. Blackie Academic and Professional, Glasgow, 1995.

[255] Vermeer P.: A five constant model unifying well established concepts. In: Constit. Relat. for Soils, 175–198, Balkema, Holland, 1982, proceedings of the International Workshop in Grenoble.

[256] Vermeer P.: Upgrading of soil models by Hencky's deformation theory of plasticity. In: Modern Approaches to Plasticity (Editor D. Kolymbas), 71–82, Elsevier, 1992, proc. of Conference in Horton, Greece.

[257] Vuong B.: Evaluation of back-calculation and performance models using a full scale granular pavement tested with the accelerated loading facility (alf). In: Proceedings 4 th International Conference on the Bearing Capacity of Roads and Airfields, Minneapolis, 183–197, 1994.

[258] Wang C.C.: On a general representation theorem for constitutive relations. Archive of Rational Mechanics and Analysis 40: 1968 1–25.

[259] Wichtmann T.: Prognose von Verdichtbarkeit des Sandes infolge zyklischer Belastung. Master's thesis, Lehrstuhl für Grundbau und Bodenmechanik, Ruhr-Universität Bochum, 2000.

[260] Wichtmann T., Niemunis A., Triantafyllidis T.: Accumulation of strain in sand due to cyclic loading under drained triaxial conditions. Geotechnical Testing Journal Submitted for publication.

[261] Wolff H., Visser A.: Incorporating elasto-plasticity in granular layer pavement design. In: Proceedings of Institution of Civil Engineers Transport, volume 105, 259–272, 1994.

[262] Wolffersdorf P.A.v.: Verformungsprognosen für Stützkonstruktionen. Ph.D. thesis, Insitut für Boden- und Felsmechanik der Universität Karlsruhe, 1997, Habilitationschrift, Heft Nr. 141.

[263] Wolffersdorff P.A.v.: Probebelastung zur Baugrundtagung 1990: Bodendaten. Geotechnik 1: 1990 44–46.

[264] Wolffersdorff P.A.v.: Feldversuch an einer Spundwand in Sandboden: Versuchsergebnisse und Prognosen. Geotechnik 17: 1994 73–83.

[265] Wolffersdorff P.A.v.: A hypoplastic relation for granular materials with a predefined limit state surface. Mechanics of Cohesive-Frictional Materials 1: 1996 251–271.

[266] Wu W.: Hypoplastizität als mathematisches Modell zum mechanischen Verhalten von Böden und Schüttstoffen. Ph.D. thesis, Institut für Boden- und Felsmechanik der Universität Karlsruhe, 1992, Heft 129.

[267] Wu W.: Non-linear analysis of shear band formation in sand. International Journal for Numerical and Analytical Methods in Geomechanics 24: 2000 245–263.

[268] Wu W., Bauer E.: A hypoplastic constitutive model for barotropy and pyknotropy of granular materials. In: Modern Approaches in Plasticity (Editor D. Kolymbas), 225–258, Elsevier, 1993, Workshop in Horton, Greece.

[269] Wu W., Bauer E.: A simple hypoplastic constitutive model for sand. International Journal for Numerical and Analytical Methods in Geomechanics 16: 1994 .

[270] Wu W., Bauer E., Kolymbas D.: Hypoplastic constitutive model with critical state for granular materials. Mechanics of Materials 23: 1996 45–69.

[271] Wu W., Kolymbas D.: Numerical testing of the stability criterion for hypoplastic constitutive equations. Mechanics of Materials 9: 1990 245–253.

[272] Wu W., Niemunis A.: Beyond invertibility surface in granular materials. In: Localisation and Bifurcation Theory for Soils and Rocks (Editors R. Chambon, J. Desrues,

I. Vardoulakis), 113–126, 1994, proceedings of the 3rd International Workshop in Aussois, France.

[273] Wu W., Niemunis A.: Failure criterion, flow rule and dissipation function derived from hypoplasticity. Mechanics of Cohesive-Frictional Materials 1: 1996 145–163.

[274] Wu W., Niemunis A.: Beyond failure in granular materials. International Journal for Numerical and Analytical Methods in Geomechanics 21: 1997 153–174.

[275] Wu W., Sikora Z.: Localized bifurcation in hypoplasticity. Proceedings of the Royal Society of London 29: 1991 195–201.

[276] Wu W., Sikora Z.: Localized bifurcation in hypoplasticity. International Journal of Engineering Science 29: 1991 195–201.

[277] Xiao H.: private communication .

[278] Yin J.H., Graham J.: Viscous-elastic-plastic modelling of one-dimensional time-dependent behaviour of clays. Canadian Geotechnical Journal 26: 1989 199–209.

[279] Yin J.H., Graham J.: Equivalent times and one-dimensional elastic viscoplastic modelling of time-dependent stress-strain behaviour of clays. Canadian Geotechnical Journal 31: 1994 42–52.

[280] Yoshimine M., Ishihara K., Vargas W.: Effects of principal stress direction and intermediate principal stress on undrained shear behaviour of sand. Soils and Foundations 38: 1998 179–188.

[281] Yoshizawa H., Y.-L. C., Israelachvili J.: Fundamental mechanisms of interfacial friction. 1. Relation between adhesion and friction. J. Physical Chemistry 97: 1993 4128–4140.

[282] Zienkiewicz O., Cormeau I.: Visco-plasticity - plasticity and creep in elastic solids - a unified numerical solution approach. International Journal for Numerical Methods in Engineering 8: 1974 821–845.

[283] Zlatovic S., Ishihara K.: Normalized behaviour of very loose non-plastic soils: effect of fabric. Soils and Foundations 37: 1997 47–56.

[284] Zou Y.: Der Einflußdes gebundenen Wassers auf die Leitfähigkeit und die mechnischen Eigenschaften feinkörniger Böden. Ph.D. thesis, Institut für Boden- und Felsmechanik der Universität Karlsruhe, 1998, Heft 144.

SCHRIFTENREIHE DES LEHRSTUHLS FÜR GRUNDBAU UND BODENMECHANIK DER RUHR-UNIVERSITÄT BOCHUM

Herausgeber: H.L. Jessberger

HEFT NR.		
1	(1979)	**Hans Ludwig Jessberger** Grundbau und Bodenmechanik an der Ruhr-Universität Bochum
2	(1978)	**Joachim Klein** Nichtlineares Kriechen von künstlich gefrorenem Emschermergel
3	(1979)	**Heinz-Joachim Gödecke** Die Dynamische Intensivverdichtung wenig wasserdurchlässiger Böden
4	(1979)	**Poul V. Lade** Three Dimensional Stress-Strain Behaviour and Modeling of Soils
5	(1979)	**Roland Pusch** Creep of soils
6	(1983)	**Norbert Diekmann** Zeitabhängiges, nichtlineares Spannungs-Verformungsverhalten von gefrorenem Schluff unter triaxialer Belastung
7	(1984)	**Rudolf Dörr** Zeitabhängiges Setzungsverhalten von Gründungen in Schnee, Firn und Eis der Antarktis am Beispiel der deutschen Georg-von-Neumayer- und Filchner-Station
8	(1984)	**Ulrich Güttler** Beurteilung des Steifigkeits- und Nachverdichtungsverhaltens von ungebundenen Mineralstoffen
9	(1986)	**Peter Jordan** Einfluß der Belastungsfrequenz und der partiellen Entwässerungsmöglichkeiten auf die Verflüssigung von Feinsand
10	(1986)	**Eugen Makowski** Modellierung der künstlichen Bodenvereisung im grundwasserdurchströmten Untergrund mit der Methode der finiten Elemente

11	(1986)	**Reinhard A. Beine** Verdichtungswirkung der Fallmasse auf Lastausbreitung in nicht-bindigem Boden bei der Dynamischen Intensivverdichtung
12	(1986)	**Wolfgang Ebel** Einfluß des Spannungspfades auf das Spannungs-Verformungsverhalten von gefrorenem Schluff im Hinblick auf die Berechnung von Gefrierschächten
13	(1987)	**Uwe Stoffers** Berechnungen und Zentrifugen-Modellversuche zur Verformungsabhängigkeit der Ausbaubeanspruchung von Tunnelausbauten in Lockergestein
14	(1988)	**Gerhard Thiel** Steifigkeit und Dämpfung von wassergesättigtem Feinsand unter Erdbebenbelastung
15	(1991)	**Mahmud Thaher** Tragverhalten von Pfahl-Platten-Gründungen im bindigen Baugrund, Berechnungsmodelle und Zentrifugen-Modellversuche
16	(1992)	**Rainer Scherbeck** Geotechnisches Verhalten mineralischer Deponieabdichtungsschichten bei ungleichförmiger Verformungswirkung
17	(1992)	**Martin M. Bizialiele** Torsional Cyclic Loading Response of a Single Pile in Sand
18	(1993)	**Michael Kotthaus** Zum Tragverhalten von horizontal belasteten Pfahlreihen aus langen Pfählen in Sand
19	(1993)	**Ulrich Mann** Stofftransport durch mineralische Deponieabdichtungen: Versuchsmethodik und Berechnungsverfahren
20	(1992)	**Festschrift anläßlich des 60. Geburtstages von Prof. Dr.-Ing. H. L. Jessberger** 20 Jahre Grundbau und Bodenmechanik an der Ruhr-Universität Bochum
21	(1993)	**Stephan Demmert** Analyse des Emissionsverhaltens einer Kombinationsabdichtung im Rahmen der Risikobetrachtung von Abfalldeponien
22	(1994)	**Diethard König** Beanspruchung von Tunnel- und Schachtausbauten in kohäsionslosem Locker-

gestein unter Berücksichtigung der Verformung im Boden

23 (1995) **Thomas Neteler**
Bewertungsmodell für die nutzungsbezogene Auswahl von Verfahren zur Altlastensanierung

24 (1995) **Ralph Kockel**
Scherfestigkeit von Mischabfall im Hinblick auf die Standsicherheit von Deponien

25 (1996) **Jan Laue**
Zur Setzung von Flachfundamenten auf Sand unter wiederholten Lastereignissen

26 (1996) **Gunnar Heibrock**
Zur Rißbildung durch Austrocknung in mineralischen Abdichtungsschichten an der Basis von Deponien

27 (1996) **Thomas Siemer**
Zentrifugen-Modellversuche zur dynamischen Wechselwirkung zwischen Bauwerken und Baugrund infolge stoßartiger Belastung

28 1996) **Viswanadham V. S. Bhamidipati**
Geosynthetic Reinforced Mineral Sealing Layers of Landfills

29 (1997) **Frank Trappmann**
Abschätzung von technischem Risiko und Energiebedarf bei Sanierungsmaßnahmen für Altlasten

30 (1997) **Andre Schürmann**
Zum Erddruck auf unverankerte flexible Verbauwände

31 (1997) **Jessberger, H. L. (Herausgeber)**
Environment Geotechnics, Report of ISSMGE Technical Committee TC 5 on Environmental Geotechnics
(www.gub.ruhr-uni-bochum.de/tc5)

Herausgeber: Th. Triantafyllidis

HEFT NR.

32	(2000)	**Triantafyllidis, Th. (Herausgeber)** Workshop "Boden unter fast zyklischer Belastung: Erfahrung und Forschungsergebnisse. Bochum April 2000
33	(2002)	**Christof Gehle** Bruch- und Scherverhalten von Gesteinstrennflächen mit dazwischenliegenden Materialbrücken
34	(2003)	**Andrzej Niemunis** Extended hypoplastic models for soils